

AD-A264 160



ION PAGE

Form Approved
OMB No. 0704-0188



average 1 hour per response, including the time for reviewing instructions, searching existing data sources, gathering the collection of information. Send comments regarding this burden estimate or any other aspect of this collection of information, including suggestions for reducing this burden, to Washington Headquarters Services, Directorate for Information Operations and Reports, 1215 Jefferson Davis Highway, Suite 1204, Arlington, VA 22202-4302, and to the Office of Management and Budget, Paperwork Reduction Project (0704-0188), Washington, DC 20503.

1. AGENCY USE ONLY (Leave blank)		2. REPORT DATE December 1992	3. REPORT TYPE AND DATES COVERED Technical Report	
4. TITLE AND SUBTITLE Evaluation of Lateral Strength and Deflection for Cracked Unreinforced Masonry Walls			5. FUNDING NUMBERS DAAL03-87-K-0006	
6. AUTHOR(S) Weijia Xu & Daniel P. Abrams				
7. PERFORMING ORGANIZATION NAME(S) AND ADDRESS(ES) Advanced Construction Technology Center University of Illinois at Urbana-Champaign Department of Civil Engineering 205 N. Mathews Ave., MC - 250 Urbana, IL 61801			8. PERFORMING ORGANIZATION REPORT NUMBER ACTC Document #92-26-11	
9. SPONSORING/MONITORING AGENCY NAME(S) AND ADDRESS(ES) U.S. Army Research Office P.O. Box 12211 Triangle Park, NC 27709-2211			10. SPONSORING/MONITORING AGENCY REPORT NUMBER ARO 24605.163-EG-U1R	
11. SUPPLEMENTARY NOTES The view, opinions and/or findings contained in this report are those of the author(s) and should not be construed as an official Department of the Army position, policy, or decision, unless so designated by other documentation.				
12a. DISTRIBUTION/AVAILABILITY STATEMENT Approved for public release; distribution unlimited.			12b. DISTRIBUTION CODE	
13. ABSTRACT (Maximum 200 words) An analytical model for lateral strength and deflection of cracked unreinforced masonry walls is developed. Post cracked behavior is considered by neglecting shear transfer across cracked masonry. Based on shear and normal stress distributions derived with the model, possible failure modes are examined. Effects of cracking are considered by modifying conventional expressions for lateral deflection with shear and flexural deformation amplifying factors. The feasibility of the evaluation procedure is verified through correlation with the results of experimental work done by others. Based on a series of computations using the model, tables are generated for estimating lateral strength in terms of different material parameters, amounts of vertical compressive stress, and wall length-to-height aspect ratios.				
14. SUBJECT TERMS			15. NUMBER OF PAGES 177	
			16. PRICE CODE	
17. SECURITY CLASSIFICATION OF REPORT UNCLASSIFIED	18. SECURITY CLASSIFICATION OF THIS PAGE UNCLASSIFIED	19. SECURITY CLASSIFICATION OF ABSTRACT UNCLASSIFIED	20. LIMITATION OF ABSTRACT UL	

DTIC
SELECTED
MAY 06 1993

93 5 05 03 9

93-09746



189P1

Technical Report

This is a Technical Report, Document #92-26-11, for the Advanced Construction Technology Center Project titled *NDE of Masonry Buildings*, Project #26. Professor D.P. Abrams is the project investigator. The reproduction is provided for other researchers, particularly those researchers in Army Laboratories interested in this work.

Accession For	
NTIS CRA&I	<input checked="" type="checkbox"/>
DTIC TAB	<input type="checkbox"/>
Unannounced	<input type="checkbox"/>
Justification	
By	
Distribution /	
Availability Codes	
Dist	Avail and/or Special
A-1	

ABSTRACT**EVALUATION OF LATERAL STRENGTH AND DEFLECTION FOR
CRACKED UNREINFORCED MASONRY WALLS**

by

Weijia Xu and Daniel P. Abrams

Department of Civil Engineering
University of Illinois at Urbana-Champaign, 1992

An analytical model for lateral strength and deflection of cracked unreinforced masonry walls is developed. Post cracked behavior is considered by neglecting shear transfer across cracked masonry. Based on shear and normal stress distributions derived with the model, possible failure modes are examined. Effects of cracking are considered by modifying conventional expressions for lateral deflection with shear and flexural deformation amplifying factors. The feasibility of the evaluation procedure is verified through correlation with the results of experimental work done by others. Based on a series of computations using the model, tables are generated for estimating lateral strength in terms of different material parameters, amounts of vertical compressive stress, and wall length-to-height aspect ratios.



ACKNOWLEDGMENTS

The authors would like to thank Profs. W. C. Schnobrich, W. L. Gamble, and G. R. Gurfinkel for serving on the thesis committee of the first author. Their critical and constructive suggestions were found to be quite helpful.

Colleagues Arturo Tena-Colunga, Richard Angel and Nirav Shah are thanked for their interest in the research and their friendship. The first author would like to thank her parents for their support and encouragement, and her husband, Ruofei, for his support, patience, understanding, and assistance.

This research was supported by the U.S. Army Research Office as part of the program of the University of Illinois at Urbana-Champaign Advanced Construction Technology Center. Professor Joseph Murtha, ACTC Director, is thanked for his support of the research project.



TABLE OF CONTENTS

CHAPTER	Page
1 INTRODUCTION	1
1.1 General	1
1.2 Review of Previous Work	3
1.3 Shear Strength Evaluation Method and Uniqueness of Study	5
1.4 Object and Scope of Research	7
1.5 Summary of Notations	8
2 ANALYSIS OF STRESS DISTRIBUTIONS FOR CRACKED WALLS	11
2.1 Introduction	11
2.2 Assumptions Used for Stress Analytical Model	12
2.2.1 Formation of the "Dead Zone"	12
2.2.2 Material Behavior	14
2.2.3 Distribution of Vertical Stress	16
2.3 Stress Field Derivation	17
2.3.1 Basis of Elasticity Theory	17
2.3.2 Stress Distribution Formulation	18
2.4 Analysis of Stress Distribution for a Sample Wall	21
2.4.1 Calculated Vertical and Shear Stress Distributions ...	21
2.4.2 Finite Element Stress Distributions	22
2.4.3 Correlations of Calculated Stress Distributions with Results of Finite Element Analysis	23
3 ANALYSIS OF LATERAL STRENGTH FOR CRACKED WALLS	24
3.1 Introduction	24

3.2	Failure Modes	25
3.2.1	Flexural Cracking	25
3.2.2	Sliding Shear along Mortar Bed Joint	25
3.2.3	Diagonal Compressive Splitting	26
3.2.4	Diagonal Tension Cracking	27
3.3	Failure Criteria	27
3.3.1	Flexural Cracking	27
3.3.2	Shear Sliding	28
3.3.3	Compressive Splitting Failure	29
3.3.4	Diagonal Tension Cracking	31
3.4	Analytical Procedure for Estimating Lateral Strength	31
3.4.1	Shear Stress Redistribution after Shear Sliding	31
3.4.2	Strategy for Estimating Lateral Strength	33
3.4.3	Strength Analysis Procedure	34
3.4.4	Results of A Sample Strength Estimate	36
4	MATERIAL PARAMETER SENSITIVITY STUDIES	38
4.1	Introduction	38
4.2	Flexural Tensile Strength	38
4.3	Compressive Strength	40
4.4	Coefficient of Friction and Cohesion	41
4.5	Diagonal Tension Strength	43
5	SIMPLIFIED EVALUATION METHOD FOR LATERAL STRENGTH OF CRACKED WALLS	45
5.1	Introduction	45
5.2	Strength Tables	46
5.3	Evaluation Procedure for Lateral Capacity of Cracked Walls	48

6	ANALYSIS OF LATERAL DEFLECTIONS FOR CRACKED WALLS	50
6.1	Introduction	50
6.2	Derivation of Deflection Calculation Formula	51
6.2.1	Review of Principle of Virtual Work	51
6.2.2	Lateral Deflection Formulation	52
6.3	Flexural and Shear Deflection Amplifying Factor α and β ..	58
6.3.1	Sensitivity Study of Flexural Tensile Strength f_t and Thickness t	58
6.3.2	Example of α and β Curves	60
6.4	Comparison of Proposed Method with Conventional Method	61
7	CORRELATION BETWEEN PROPOSED METHOD AND EXPERIMENTAL WORK	63
7.1	Introduction	63
7.2	Walls Tested with Monotonically Increasing Loads	64
7.2.1	Review of Experimental Work	64
7.2.2	Comparison of the Results from Experimental Work and Proposed Method	65
7.3	Walls Tested with Cyclic Loads	66
7.3.1	Behavior of Walls Subjected to Cyclic Forces	66
7.3.2	Comparison of the Lateral Capacity from Experimental Work and Proposed Method	68
8	SUMMARY AND CONCLUSIONS	70
8.1	Summary	70
8.2	Conclusions	72
8.3	Recommendations for Further Research	73

REFERENCES	74
TABLES	78
FIGURES	83
APPENDIX A	122
APPENDIX B	153

LIST OF TABLES

Table	Page
6.1 Comparison of Lateral Deflections Calculated by the Proposed Method and Conventional Method	79
7.1 Summary of Wall Test Specimen Subjected to Monotonically Loads	80
7.2 Calculated Lateral Capacity of the Test Walls	80
7.3 Comparison Between the Predicted and Measured Lateral Strength	81
7.4 Comparison Between the Predicted and Measured Maximum Lateral Deflection	81
7.5 Summary of Wall Test Specimen Subjected to Cyclic Loads .	82
7.6 Comparison Between the Predicted and Measured Lateral Capacities	82



LIST OF FIGURES

Figure	Page
1.1 Summary of Measured Top Level Displacement of the Test Walls Versus Shear Stress	84
1.2 Comparison Between In Situ Shear Strength Estimates and Measured Ultimates Shear Strength of Test Walls	85
1.3 Final Crack Patterns of a Typical Test Wall after Failure	86
2.1 Free Body Diagram of a Wall with " Dead Zone " Resulting from Flexural Tension Cracking	87
2.2 Stress-Strain Relation for Brick and Mortar	88
2.3 Recorded Stress-Strain Curves for Prisms	88
2.4 Vertical Stress Distribution at Mid-height of a Wall for different l/h Ratios	89
2.5 Comparison of Different Vertical Stress Distribution	90
2.6 Stress Element	90
2.7 Contours of Vertical Compressive Stress (psi)	91
2.8 Contours of Shear Stress (psi)	91
2.9 FInite Element Mesh for Stress Analysis	92
2.10 Contours of Shear Stress (psi)	93
2.11 Contours of Vertical Compressive Stress (psi)	93
2.12 Shear and Vertical Stress Distribution at Given Height of the Wall	94
2.13 Shear and Vertical Stress Distribution at Given Height of the Wall	95
3.1 Failure Modes	96
3.2 Typical Load-Deflection Relation for Flexural	

	Cracking Failure Mode	97
3.3	Typical Load-Deflection Behavior for Cracked Wall	97
3.4	Shear Sliding Failure Criterion	98
3.5	A Sample Wall for Shear Sliding Index	98
3.6	Contour of Shear Sliding Index	99
3.7	Masonry Element and Corresponding Failure Criteria	100
3.8	Failure Surface for Diagonal Tension Cracking Mode	101
3.9	Shear Transfer across Stair-Stepped Crack	101
3.10	Stress-Strain Relation for Shear after Sliding	102
3.11	Example of the Shear Stress Distribution after Sliding	102
3.12	Analytical Procedure for Unreinforced Masonry Cracked Wall	103
3.13	A typical Screen Display of Cracking Development in a Wall	104
3.14	Shear Strength Versus Vertical Compressive Stress for Different l/h Ratios	105
4.1	Influence of Flexural Tensile Strength on Shear Strength	106
4.2	Influence of Compressive Strength on Shear Strength	106
4.3	Influence of Frictional Coefficient on Shear Strength	107
4.4	Influence of Cohesion on Shear Strength	107
4.5	Influence of Diagonal Tension Strength on Shear Strength ...	108
6.1	Virtual Work System for Derivation of Displacement Formula	109
6.2	Shear Deformation Diagram	109
6.3	Flexural Deflection Amplifying Factor α vs. Stress Ratio (for Flexural Tensile Strength 50 psi and 100 psi)	110

6.4	Shear Deflection Amplifying Factor β vs. Stress Ratio (for Flexural Tensile Strength 50 psi and 100 psi)	111
6.5	Flexural Deflection Amplifying Factor α vs. Stress Ratio (for Thickness 8 and 16 inch)	112
6.6	Shear Deflection Amplifying Factor β vs. Stress Ratio (for Thickness 8 and 16 inch)	113
6.7	α and β vs. Stress Ratio for Different l/h Ratios	114
6.8	Comparison of Deflections between the Proposed Method and the Conventional Method	115
6.9	Comparison of Deflections between the Proposed Method and the Conventional Method	116
7.1	Displacement Transducer Arrangement for Test Walls	117
7.2	Comparison of the Deflections between the Experimental and the Proposed Method	118
7.3	Comparison of the Deflections between the Experimental and the Proposed Method	119
7.4	Comparison of the Deflections between the Experimental and the Proposed Method	120
7.5	Observed Crack Pattern for Wall 1	121
7.6	Observed Crack Pattern for Wall 2	121



CHAPTER 1

INTRODUCTION

1.1 General

Unreinforced masonry buildings constitute a large portion of the urban infrastructure. Traditionally, they have been constructed to satisfy the demands of function, economy and esthetics. Since they were unreinforced and built with little or no consideration with regard to possible earthquake or strong wind loads, their shear resistance to lateral forces has been a major concern.

It is important to recognize that many of masonry buildings were originally designed with excessive conservatism. Building code specifications usually carry large safety factors because of the uncertainty in defining material properties. Insitu measurement of actual properties can reduce the conservatism, and strengthening or demolition may be precluded. Currently, a number of nondestructive techniques have been developed for masonry, such as wave velocity tests (either ultrasonic or sonic test), the flat-jack test and the in-place shear test (22, 23). These methods may be used to determine insitu material strength, or structural condition. To reduce the number and cost of measurements, the test data must be extrapolated rationally. Thus, the integrity of a structure system may be evaluated with confidence at a reasonable cost.

To evaluate the performance of an unreinforced masonry building under wind or earthquake force, a fundamental failure theory for estimating shear strength of its components is required. An essential part of this failure theory is an understanding of the behavior of unreinforced masonry building components after cracking. It is a common conception to believe that an unreinforced masonry wall or pier cannot resist further lateral force after it cracks in flexure or shear. These concerns are related to a per-

ceived brittle behavior for unreinforced masonry. " Building Code Requirements for Masonry Structures and Specifications for Masonry Structures" (ACI 530-88/ASCE 5-88) (6), gives allowable flexural tensile stresses only for the case of out-of-plane loading. No values are given in the Code for in-plane loading of shear walls. According to the ACI - ASCE 530 Commentary (8), flexural tension in walls should be carried by reinforcement from in-plane bending. It appears as if in-plane flexural tensile strength for unreinforced masonry walls should be totally neglected. This lack of understanding is also reflected by the low values of allowable tensile stress for in-plane loading permitted by Chapter 24 of the 1991 " Uniform Building Code" (9).

The experimental work at the University of Illinois at Urbana-Champaign has (14) shown that there can be substantial lateral strength after flexural cracking of an in-plane wall because of the shifting of the vertical force resultant at the wall base. The limit in flexure strength then becomes the compressive stress at the toe, or shear sliding along mortar bed joints. Another important experimental observation is that if diagonal tensile cracking does not extend through to the toe, it may not result in failure of a wall (39). It can be concluded that from these experimental results, an unreinforced masonry wall may have substantial deformation capacity past cracking as the neutral axis gradually shifts with increasing lateral force (Fig. 1.1). This nonlinear behavior implies that an existing unreinforced masonry wall may resist much more lateral force than that associated with initial cracking. Furthermore, unreinforced masonry elements may possess a considerable amount of inelastic deformation capacity. Thus, the lateral strength of a building system will be limited to the sum of the strengths of all elements rather than the strength of the first one to crack.

1.2 Review of Previous Work

In recent years, there has been considerable research related to in-plane behavior of masonry walls. Past research has consisted of both experimental and theoretical analyses, with particular emphasis on behavior of walls subjected to varying combinations of lateral and vertical compressive forces. Previously developed analytical models used to simulate the in-plane behavior of masonry are reviewed here. The discussion is only related to in-plane failure. Studies related to out-of-plane loading have been excluded from the review, because they are not relevant to this study.

Many researchers have extensively investigated the failure of masonry under uniaxial compression, combined shear and compression, and tension. Development of general failure criteria for masonry has been limited because of the lack of experimental data. However, a few have been postulated. Yokel and Fattal (45) considered three failure hypotheses for splitting, and one hypothesis for joint separation, based on their experiments. To define failure under biaxial stress, Page et al. (33) developed a three-dimensional failure surface in terms of the two principal stresses and their orientation to the bed joint. They derived analytically the failure surface for tension-tension principal stress region and determined experimentally a failure surface for masonry subjected to two compressive principal stresses. Essawy and Drysdale (16) applied the composite material strength theories to masonry and proposed a macroscopic biaxial failure criterion for masonry assemblages in the transverse failure mode. Ganz and Thurlimann (17) presented a failure surface in terms of the normal stresses parallel and perpendicular to the bed joint and the shear stress on the bed joint. They defined the failure surface by four separate stress functions corresponding to four distinct failure modes. Mann and Muller (27) proposed a failure envelope for masonry which was

derived from different failure criteria, and was based on a highly questionable stress distribution within the masonry assemblage.

Lateral loading on a masonry wall can produce both diagonal cracking failure and horizontal bed joint shear sliding failure. In the analysis of unreinforced masonry structures, a particular concern is the bed joint resistance. Atkinson et al. (5) investigated the shear strength and deformation behavior of unreinforced brick masonry for different clay units, mortar types and thickness of both existing buildings and new construction. Their tests conducted in the laboratory provide valuable data on the shear load displacement response of masonry bed joint during cyclic loading. These results permit the development of a constitutive relation for masonry bed joint shear behavior. Ridlington and Ghazall (36) proposed a shear failure hypothesis for a masonry joint. It was stated that shear failure was initiated by joint slip at lower precompression stresses, but with higher stress level, tensile failure in mortar started first. Their test and finite element analysis results are shown to support this failure hypothesis.

With the increasing application of the finite element method, various attempts have been made to model the in-plane behavior of masonry. By using an iterating, incremental finite element computer program, Page (30, 32, 34) studied the influence of masonry material properties, wall geometry and the method of load application on the performance of brick masonry shear walls. For a given set of parameters, a total of 132 analyses were performed to simulate a complete racking test. These tests involved walls subjected to vertical and horizontal shear load on the top. It is shown that the variations in the masonry bond and compressive strength can drastically influence the resulting failure criterion expressed in terms of average normal and shear stress on the bed joint. To be fully representative, a failure criterion should include the effects of material parameters, wall geometry and boundary conditions on the shear strength.

1.3 Shear Strength Evaluation Method and Uniqueness of Study

Shear strength of an existing masonry building depends on the amount and type of materials, and the quality of workmanship during construction. The most commonly used insitu measurement technique for the shear strength is the in-place shear test. The test consists of replacing a brick with a hydraulic jack that pushes the adjacent brick until it slides (the mortar head joint on the opposite side of the adjacent brick is also removed). The shear stress is then calculated as the shove force divided by the area of mortar in contact with the brick. Currently, wall strength is extrapolated by integrating shove test results across the gross area of a wall or pier. Based on the limitation that flexural tensile stress is less than tensile strength, so that section will be uncracked and shear stress may be assumed across entire cross section. The guidelines " Seismic Strengthening Provisions for Unreinforced Masonry Bearing Wall Buildings " recently prepared by SEAOC evaluates wall shear strength with the following equation (44):

$$V_a = 0.1V_t + 0.15\frac{P_D}{A} \quad (1.1)$$

Where V_a is allowable shear stress, V_t is the value that is exceeded by 80 percent of all of the test values corresponding to zero normal stress, P_D is vertical force and A is the area of unreinforced masonry wall or pier. This allowable stress equation is based on the following strength equation:

$$V_a = \frac{0.75\left(0.75V_t + \frac{P_D}{A}\right)}{1.5} \quad (1.2)$$

An understrength factor equal to 0.75 is assumed along with a correction factor of 0.75 for the effect of the collar joint and a factor of 1/1.5 to convert average stress

to critical stress at the center of section. If a factor of 1/3.75 is considered to convert from ultimate to working stress, the first equation will be obtained.

A previous experiment at the University of Illinois at Urbana – Champaign (14) has shown that for higher lateral strength, post – cracking effects should be considered, and then shear stress must be checked with cracked element. However, measured shear stress from the in – place shear test can be three or more times the measured ultimate shear strength of a wall, if the wall cracks (Fig.1.2). The basic problem is that the NDE method defines the shear strength at a point or local area rather than across the surface of a wall. Furthermore, vertical compressive stress and wall aspect ratio are not considered. Effects of cracking and variable axial compressive stress can make this global – local extrapolation difficult. To consider the post – cracking effects, what is needed is a methodology for estimating the total lateral resisting force of a cracked wall from results of the in – place shear test. To do this, an analytical model needs to be developed that considers the variation in shear and normal stress across a wall surface as influenced by cracking.

A further improvement for evaluation technology would be to recognize that sliding shear failure (as measured with the in – place shear test) may not in all cases limit the lateral strength of a wall loaded within its plane. The series of full – scale walls tested at Illinois (14) demonstrated that there may be a few kinds of distress in a wall when it is subjected to vertical and lateral load. They are flexural cracking, shear sliding along mortar bed joints, diagonal tension cracking and compressive splitting. The typical cracking patterns in a wall are shown in Fig. 1.3. The location of the first crack, and the subsequent failure of the wall, depend on the material properties, wall geometry and the ratio of vertical load to lateral load. Obviously, different cracking may exist in a wall when it fails. Thus, evaluation of lateral strength for a wall must consider all of these possible cracking patterns.

The present study is unique in that firstly the developed evaluation methodology is based on the consideration of post cracked behavior, and secondly that nondestructive measurements are not simply applied uniformly across a wall, but with an eye towards a point or local area. In this way, the variation of shear and normal stress resulting from the cracking needs to be considered. Additionally, this methodology also accounts for different combinations of vertical stress and wall aspect ratio. In particular, shear strength from the developed methodology is based on the analysis of all possible failure modes for an unreinforced masonry wall. Thus, the developed methodology can be used to correlate NDE measurements with estimates of wall strength.

1.4 Object and Scope of Research

The object of this study is to develop an evaluation methodology for estimating lateral strength and deflection of unreinforced masonry walls or piers of any length-to-height aspect ratio, or subjected to any amount of vertical compressive stress. The scope of the research will entail:

- (1) Development of an analytical formulation for the distribution of shear and normal stress in terms of wall dimension, vertical compressive stress, and flexural tensile strength. These stress fields will be based on the extent of flexural cracking.
- (2) Use of the proposed stress fields to develop the analytical procedure for evaluating lateral strength considering cracking. The proposed procedure will be applicable to walls whose strengths are limited by flexural cracking, mortar joint sliding, compressive splitting and diagonal tension. Material information needed for input to the methodology will be based on nondestructive tests which are either presently available, or from later tests.

- (3) Derivation of an expression for lateral deflection based on the developed stress field. The proposed expression will be related to the length-to-height aspect ratio, level of vertical compressive stress and flexural tensile strength.
- (4) Verification of the proposed methodology for lateral strength and deflection by correlating with the previous experimental results of a series of full scale masonry walls.
- (5) Investigation of the effect of the different parameters on the lateral strength and deflection. Particularly, considered are aspect ratio (l/h), sliding cohesion and friction coefficient, compressive strength, diagonal tension strength and flexural tension strength.
- (6) Development of strength tables corresponding to different aspect ratios (l/h), vertical compressive stress and different material parameters, so that the current research results can be used directly in engineering practice.

1.5 Summary of Notations

A summary of frequently used symbols in the text is presented below:

- a = effective length of a wall;
- A = section area of a wall;
- B = parameter used in the deflection expression;
- C = parameter used in the deflection expression;
- d = uncracked length at the base of a wall;
- D = parameter used in the deflection expression;
- E = modulus of elasticity;
- f_{mx} = masonry compressive strength parallel to the bed joint;

- f_{my} = masonry compressive strength normal to the bed joint;
- f_t = flexural tensile strength;
- F = parameter used in the deflection expression;
- F_x = x component of the body force;
- F_y = y component of the body force;
- G = shear modulus;
- h = the height of a wall;
- I = moment of inertia;
- K = parameter used in the deflection expression;
- l = the length of a wall;
- M = moment acting on any section of a wall;
- \bar{M} = moment resulting from virtual force;
- P = vertical force acting on the top of a wall;
- SUBV = shear force resisted by the sliding region of a section;
- S_{ind} = shear sliding index;
- t = the thickness of a wall;
- V = horizontal shear force;
- V_r = shear force resisted by the unsliding region of a section;
- W_e = external virtual work;
- W_i = internal virtual work;
- x = a distance from the left edge of a wall;
- y = a distance from the top of a wall;

- y_0 = the ordinate to define the top of the "dead zone";
- α = flexural deflection amplifying factor;
- β = shear deflection amplifying factor;
- γ = shear strain;
- γ_0 = average shear strain across a particular section;
- θ = the ratio of cracked length at base over the height of "dead zone";
- σ_0 = diagonal tension strength;
- σ_x = x component of normal stress;
- σ_y = y component of normal stress;
- σ_v = vertical compressive stress on the top of a wall;
- τ = shear stress;
- $\bar{\tau}$ = shear stress resulting from virtual force;
- τ_0 = cohesion;
- μ = coefficient of friction;
- Δ_s = top-level flexural deflection;
- Δ_m = top-level shear deflection.

CHAPTER 2

ANALYSIS OF STRESS DISTRIBUTIONS FOR CRACKED WALLS

2.1 Introduction

As shown in Fig. 1.1, unreinforced masonry walls exhibit a highly nonlinear behavior after cracking. If post-cracking behavior is considered, then maximum shear stress must be calculated based on the uncracked portion of a wall. The distributed normal stress varies with the state of cracking, and thus the potential for sliding along a bed joint becomes unclear. Without a proper theory to describe these phenomena, it is impossible to evaluate the in-plane shear resistance of a wall past cracking. Thus, simple linear elastic models have to be used that result in much smaller estimates of lateral force capacity. It is important to recognize the effects of cracking on the distribution of normal and shear stress. Moreover, analysis for the strength must be nonlinear because of cracking, although elastic material behavior may be assumed for those portions of a wall in compression.

The analytical model for shear and normal stress distributions developed in this chapter is related to the effects of cracking. It is assumed that once a portion of a wall cracks, it is no longer useful in resisting shear. The cracked portion is represented by a triangular region called a "dead zone", as in Fig. 2.1. To define the size of the dead zone, the cracking initiation and propagation are considered. With increasing lateral forces, cracks continue to propagate, and thus stresses have to be redistributed across a progressively shorter length of a section. This model neglects shear transfer across all masonry that is cracked. Closed-form expressions are derived for normal and shear stress at any location within the plane of a cracked wall. In order to verify the accuracy and applicability of the analytical model, calculated stress distributions for a sample

wall from the proposed model are presented and compared with the results of finite element analyses. Good correlation is demonstrated by these comparisons.

2.2 Assumptions Used for Stress Analytical Model

2.2.1 Formation of the "Dead Zone"

Before proceeding to develop the stress formulation related to cracking effects, it is important to state assumptions necessary for the derivation. Cracking is the most important phenomenon for nonlinear behavior of unreinforced masonry. Correspondingly, cracking effects imposes the most significant impact on the strength of a wall.

Masonry flexural tensile strength is low relative to the compressive strength. The first crack usually initiates at the heel of a wall. With increasing lateral force, flexural cracking progresses, and the effective cross sectional area reduces at the wall base. The "dead zone" is termed for the portion of a wall where tensile stress exceeds flexural tensile strength, as shown in Fig. 2.1. The size of the growing dead zone is defined as the lateral force is increased and flexural cracking extends across the wall. A cantilevered shear wall becomes a nonprismatic element with the formation of dead zone. It is evident that the analysis based on this model has to be nonlinear no matter how the material behavior is considered.

In Fig. 2.1, the length of the uncracked zone at the base is expressed in terms of parameter d . It is derived by setting the net tensile stress (the difference between flexural tension and vertical compressive stress) equal to the tensile strength f_t . The special case has to be considered first when f_t is equal to zero. Obviously, if horizontal shear forces, V , are small enough so that cracking will not occur at the base, d is simply equal to the full length of wall, l , (Eq. 2.1). When forces that are large enough to crack a wall, the distance d will be a fraction of the overall length as obtained by Eq. 2.2. This

equation simply states that the centroid of the vertical force resultant will be located at a distance equal to one-third of the d distance from the compression toe, or the eccentricity will be half the wall length minus this distance.

$$\text{if } f_t = 0 \text{ and } V < \frac{Pl}{6h} \text{ then } d = l \quad (2.1)$$

$$\text{if } f_t = 0 \text{ and } V \geq \frac{Pl}{6h} \text{ then } d = \frac{3l}{2} - \frac{3Vh}{P} \quad (2.2)$$

When the flexural tensile stress, f_t , is some finite amount, expressions for the uncracked distance at the base, d , can be determined by using the same logic. Without cracking, d is still the full length of a wall (Eq. 2.3). When lateral force is larger than the cracking load, flexural and axial stress have to be distributed on decreasing uncracked length. The cracking will be continuously caused by the tensile stress on the base of a wall equal to or larger than flexural tensile strength (Eq. 2.4). Based on this idea, the uncracked length d can be derived as Eq. 2.5.

$$\text{if } f_t > 0 \text{ and } V < \left(f_t + \frac{P}{l_t}\right) \frac{tl^2}{6h} \text{ then } d = l \quad (2.3)$$

$$\text{if } f_t > 0 \text{ and } V \geq \left(f_t + \frac{P}{l_t}\right) \frac{tl^2}{6h} \text{ then}$$

$$f_t = \left(\frac{6}{td^2}\right) \left(hV - P \frac{(l-d)}{2}\right) - \frac{P}{td} \quad (2.4)$$

$$d = \frac{P}{f_t} - \sqrt{\left(\frac{P}{f_t}\right)^2 - \frac{3Pl - 6hV}{f_t}} \quad (2.5)$$

The top of the dead zone is defined as the point where flexural stress is equal to zero. It is located in terms of the y_0 dimension which is determined by equating flexural and axial stresses at that level of the wall (Eq. 2.6). Thus, there is no flexural tensile stress to cause cracking for any section higher than the level defined by y_0 .

$$y_0 = \frac{Pl}{6V} \quad (2.6)$$

A straight line is then drawn defining the triangular portion of the wall which is assumed to be ineffective in resisting shear, or otherwise known as the dead zone. The effective length of the wall at any distance y from the top (where y exceeds y_0) is given by Equation (2.7).

$$a(y) = l - (y - y_0)\theta \quad \text{where} \quad \theta = \frac{c}{h - y_0} \quad (2.7)$$

With increasing lateral force, both values, the uncracked zone at the base, d , and the ordinate to define the top of the dead zone, y_0 , are decreasing. In effect, the size of the dead zone is continuously enlarged and the effective section area to resist shear is reduced. Though masonry may still be linear where in compression, behavior of the wall is highly nonlinear.

2.2.2 Material Behavior

Masonry is composed of two materials with distinct properties: soft mortar and stiff clay units. As a composite material, it is brittle and weak in tension, but has high strength in compression. How to consider its behavior under monotonically increasing compressive forces is the basis of this stress distribution formulation.

Researchers have long been aware that deformation characteristics of brick and mortar are different. The stress-strain relations of relative soft mortar and stiff brick are depicted in Fig. 2.2. The behavior of masonry under compressive force has been the

subject of experimental and theoretical studies. It is general accepted that under uniaxial loading, masonry failure initiates in brick units under a condition of bilateral tension coupled with axial compression, associated with the triaxial compression stress state in mortar. Attempts have been made to rationalize this mode of failure by Hilsdorf, and Francis et al. (19). McNary and Abrams (26) extended this work by investigating the strength and deformation of clay-unit masonry under uniaxial concentric compressive force. Their results reveal that the relation between the stress and strain becomes increasing nonlinear as mortar strength decreases. Drysdale and Guo (12) recently proposed an elastoplastic constitutive model to determine the compressive strength for concrete block masonry. Page (30) has developed an analytical model which considered masonry to be assemblage of elastic bricks separated by mortar joints with non-linear deformation characteristics. This model can simulate the stress redistribution after joint failure but cannot predict a composite failure related both brick and joint. A few researchers assumed idealized parabolic stress-strain relations under uniaxial compression or biaxial compression-compression stress states in their studies. Obviously, the lack of representative material models has been a main problem encountered by most of the researchers in the past.

As a number of different types of mortar and units are used in masonry construction, it is difficult to specify a generally valid stress-strain relation for compressive behavior. The nonlinear behavior of masonry is caused by two major effects: progressive failure resulted from cracking and non-linear material characteristics of the masonry constituents. Since flexural tensile strength is relative low, flexural cracking may occur at a very low lateral force. This flexural cracking will result in a substantial stress redistribution and progressive local failure. In this case, therefore, the cause of non-linear behavior will be predominantly cracking rather than material non-linearity. On the other hand, the results of prism tests at the University of Illinois (14) reveal that for

brick masonry, the stress–strain relation is almost linear until the final stage of failure, which is shown in Fig.2.3. Therefore, a simple linear stress–strain relation for compression is assumed for the analytical model to follow.

2.2.3 Distribution of Vertical Stress

It is assumed that at the top of a wall, vertical stress is distributed uniformly along the entire length. When subjected to lateral force, the vertical stress distribution will vary along the wall length, to various extents depending on the elevation of the particular section. There are three factors to affect the distribution of vertical stress: the amount of vertical compressive stress, length–to–height (l/h) aspect ratio of a wall and material behavior. Even if a linear stress–strain relation is assumed, the stress distribution may become nonlinear because of the shear deformation even at the elastic stage if the aspect ratio l/h is relatively large.

Vertical stress distributions at mid–height of a wall are shown in Fig. 2.4 for walls with different aspect ratios (l/h): 0.5, 2.0 and 5.0. Clearly, the vertical compressive stresses at any elevation are composed of two parts: stress σ_1 caused by lateral forces and uniform compressive stress σ_2 . In the figures, solid and dotted lines represent the results of finite element analyses and beam theory approach. It is noted that the distributions of vertical stresses from FEM are more linear for a slender wall than for a stocky wall. Thus, the results from both approaches are very close as shown in the figure for a slender wall. The reason is that a plane section assumption used in beam theory approach is based on the idea of linear strain distribution and neglecting the shear deformation. However, the stress distribution of a stocky wall is not in harmony with the plane section assumption because of larger shear deformation.

There are different ways to make simplifications to approximate actual stress distributions, which depend on the degree of accuracy required versus the simplicity de-

sired in practice. It is necessary to point out that no matter how vertical stress is distributed, the vertical resultant force will not vary because of statical equilibrium. However, different stress distributions will affect the arm, e , as shown in Fig. 2.7. For relatively smaller aspect ratios, the difference in lever arm is small. To simplify the problem and put emphasis on investigation of cracking effects, the beam theory is used to define the vertical stress distribution and limit the maximum applicable aspect ratio (l/h) for the current analytical model.

2.3 Stress Field Derivation

2.3.1 Basis of Elasticity Theory

Structural mechanics of an in-plane wall are reduced to a plane stress problem (43). As shown in Fig.2.6, σ_x , σ_y , τ_{xy} and τ_{yx} which are functions of x and y , do not vary through the thickness. All other stress components are assumed to be zero. F_x and F_y are the x and y components of the body force per unit volume. Since the size of differential element is infinitesimally small, the stress components may be considered to be distributed uniformly over each face. In the figure, a single vector represents the mean stress value applied at the center of each face.

For an element of unit thickness, the following differential equations of equilibrium can be expressed:

$$\frac{d\sigma_x}{dx} - \frac{d\tau_{xy}}{dy} = 0 \quad (2.8)$$

$$\frac{d\tau_{xy}}{dx} - \frac{d\sigma_y}{dy} = 0 \quad (2.9)$$

Compressive normal forces are defined as positive and the body forces are neglected. Equations (2.10) and (2.11) can be integrated resulting in Equations (2.10), (2.11) and (2.12).

$$\tau_{xy} = \int \left(\frac{d\sigma_y}{dy} \right) dx = \int \left(\frac{d\sigma_x}{dx} \right) dy \quad (2.10)$$

$$\sigma_x = \int \left(\frac{d\tau_{xy}}{dy} \right) dx \quad (2.11)$$

$$\sigma_y = \int \left(\frac{d\tau_{xy}}{dx} \right) dy \quad (2.12)$$

If one of the three stress components σ_x , σ_y and τ_{xy} is assumed, and the certain boundary conditions are prescribed, the other two stress components can be obtained from these integration equations.

2.3.2 Stress Distribution Formulation

Based on the assumptions discussed before, by using principles of mechanics, an analytical formulation for normal and shear stress distribution in a cracked wall can be derived. The moment acting on any cracked section a distance y from the top of a wall (Fig. 2.1) is given by Equation (2.13).

$$M(y) = Vy - P(y - y_0) \frac{\theta}{2} \quad \text{for } y > y_0 \quad (2.13)$$

The vertical stress can easily be derived by using a beam theory approach. Shear and horizontal normal stresses then can be determined by integrating differential stresses across the effective section. For the upper portion of a wall (where y is less than y_0) no cracking will exist, and stresses are the same as these for an uncracked wall (Eqs. 2.14, 2.15 and 2.16).

for $y \leq y_0$

$$\sigma_y = \frac{P}{lt} + \frac{Vy}{I} \left(\frac{l}{2} - x \right) \quad \text{where } I = \frac{tl^3}{12} \quad (2.14)$$

$$\sigma_x = 0 \quad (2.15)$$

$$\tau_{xy} = \frac{V}{2I} \left[\left(\frac{l}{2} \right)^2 - \left(x - \frac{l}{2} \right)^2 \right] \quad (2.16)$$

For the lower portion of a wall (where y is greater than y_0), cracking will limit the size of the effective section. Normal and shear stresses are derived considering this reduction in section to give the expressions in Eqs. (2.17, 2.18 and 2.19).

for $y > y_0$

$$\sigma_y = \frac{P}{at} + \frac{M}{I} \left(\frac{a}{2} - x \right) \quad \text{where } I = \frac{ta^3}{12} \quad (2.17)$$

$$\sigma_x = \frac{1}{2I} \left\{ \frac{x^2}{2} \left[4\theta V - \frac{5}{3} P\theta^2 + \frac{6\theta^2 M}{a} \right] - \frac{x^3}{3} \left[\frac{6\theta}{a} \left(V - \frac{P\theta}{2} \right) + \frac{12\theta^2 M}{a^2} \right] \right\} \quad (2.18)$$

$$\tau_{xy} = \frac{1}{2I} \left[x \left(Va + 2M\theta - \frac{P\theta a}{3} \right) - x^2 \left(V - \frac{P\theta}{2} + \frac{3M\theta}{a} \right) \right] \quad (2.19)$$

The above stress distribution equations must satisfy the following boundary conditions and external equilibrium equations. For the upper portion of a wall, the left and right edge free from load, i.e.

$$\sigma_x = 0 \quad \tau_{xy} = 0 \quad x = 0 \quad \text{and} \quad x = l \quad (2.20)$$

For the lower portion of a wall, the boundary condition at the left edge is the same as that on the upper portion. On the edge of the "dead zone", the resultant forces in the x and y direction should be equal to zero.

$$\sigma_x = 0 \quad \tau_{xy} = 0 \quad x = 0 \quad (2.21)$$

$$\sigma_y \theta - \tau_{xy} = 0 \quad \tau_{xy} \theta - \sigma_x = 0 \quad x = a \quad (2.22)$$

The integration of vertical stresses at any given section must be equal to a resultant vertical force P on the top of a wall, similarly, the integration of shear stresses must be equal to the applied lateral load V.

$$\int_0^l \sigma_y dx = P \quad \text{or} \quad \int_0^a \sigma_y dx = P \quad (2.23)$$

$$\int_0^l \tau_{xy} dx = V \quad \text{or} \quad \int_0^a \tau_{xy} dx = V \quad (2.24)$$

2.4 Analysis of Stress Distribution for A Sample Wall

2.4.1 Calculated Vertical and Shear Stress Distributions

The nonlinear computational model is used to calculate stress distributions for a sample wall having the same dimensions as one of the laboratory test specimens (14). The sample wall was 72 inch high by 114 inch long, and 17 inch thick. It was subjected to a uniform vertical compressive stress of 143 psi at the top and an ultimate horizontal load equal to 162 kips.

Calculated vertical compressive stresses which are based on the expressions presented in the last section are shown with a contour mapping across the plane of the wall in Fig. 2.7. The dead zone considered by the model is evident by the larger triangular portion that extends more than 60% across the wall base, and over half of the wall height. It is also apparent that the model represents the distribution of compressive stress as uniform along the top, and linearly distributed along the base with the peak stress at the toe of the wall. Though compressive stresses are highly concentrated near the toe, they tend to disperse above the base at approximately 20% of the wall height.

The analytical model is also used to plot contours of shear stress (Fig. 2.8). At the top of the wall which is uncracked, it is evident that shear stress varies parabolically across the wall length. At the base of the wall, shear stress is concentrated within 40% of the wall length towards the toe. This is a direct result of the dead zone which can be detected by the triangular area towards the right hand side that attracts no shear stress. Because of effects of flexural cracking, peak shear stress is many times the average shear stress. The contour map reveals a maximum shear stress equal to 340 psi which is located near the center of the compressed zone at the base. The value is nearly four times the average shear stress.

2.4.2 Finite Element Stress Distributions

An elastic finite element analysis is used to calculate the stress distribution for the same sample wall used in the last section. The same value of vertical compressive stress 143 psi is used. The modulus of elasticity and Poisson's ratio are adopted from the test results for the same wall, which are 505,500 psi and 0.3 respectively (14). The uncracked length at base is calculated by Equation (2.5). Then the x and y translations are restrained for the uncracked portion, and the cracked portion is simulated by unrestrained degrees of freedom. A total of 456 four node, isoparametric plane stress elements are used. The finite element mesh is shown in Fig. 2.9. The same lateral load as used before is applied at the top of the wall using a parabolic distribution of shear stress. The analysis was performed by running the program FINITE on an Apollo workstation. The data post-processing was carried out by the program PATRAN, from which stress contours were obtained.

Contours of shear and vertical compressive stress from the finite element analysis are shown in Fig. 2.10 and Fig. 2.11. It is evident that these contours are very similar to those estimated by using the proposed analytical model. It has been noted that the shear stress is distributed parabolically across the length of the wall, except at the toe and crack tip where the stress concentrations resulting from the geometrical singularity occur. The largest vertical compressive stress is at the toe. The tendency for the stress to disperse along the effective length of the wall (as seen in Fig. 2.7) is again dominant. Comparisons of stresses at the same location between analytical model and finite element analyses will be discussed in the next section.

2.4.3 Correlations of Calculated Stress Distributions with Results of Finite Element Analysis

In order to demonstrate the applicability of the presented stress distribution formulation, the shear and vertical compressive stress distributions at the same elevation are shown in Fig. 2.12 and 2.13, for computed results using the analytical model and the finite element analysis. Two typical levels are selected: one is near the top and another is close to the base.

Near the top of the wall ($y = 6$ inch, Fig. 2.12), shear and vertical stress are distributed parabolically and linearly. The calculated stress distributions are very close to those computed with the FEM.

Close to the base of the wall ($y = 60$ inch, Fig. 2.13), two vertical stress distributions are still very close. The peak stress by either model varies by only 5 percent. It is indicated that the linear vertical stress distribution is generally reasonable, and of acceptable accuracy when the length–height aspect ratio is relatively low (such as the sample wall with l/h equal to 1.58). However, a larger discrepancy can be found on the shear stress distribution. According to the analytical model, shear stresses are distributed on the uncracked portion because of the dead zone effect, which results in the increasing of maximum shear stress rapidly. The difference of both maximum values is about 30 percent. The results from the analytical model is larger than that from the FEM analysis, which is on the safe side for a strength analysis. The negative values for both shear and vertical stress shown in Fig. 2.13 are a result of maintaining equilibrium on the edge of the triangular dead zone. Even with this discrepancy, the analytical model considering the cracking effect is still able to capture the stress distribution reasonably, but with a simple formulation.

CHAPTER 3

ANALYSIS OF LATERAL STRENGTH FOR CRACKED WALLS

3.1 Introduction

An important consideration in the evaluation of a masonry building is the ability of the structure to withstand lateral forces induced by earthquake or wind loads. Most masonry buildings are basically wall structures whose resistance to lateral loads is predominantly a function of the in-plane shear capacity of the walls. Because of the significance of the wall element, it is important to evaluate its lateral strength accurately. Thus, an analytical procedure for estimating lateral strength of unreinforced masonry walls in shear needs to be developed. Consequently, the developed analytical procedure can then be used for making rational estimates of lateral strength in terms of non-destructive measurements.

Ultimate shear strength of a cracked wall is defined herein to be the maximum in-plane lateral force divided by the gross sectional area. For an unreinforced masonry wall, the nonlinear behavior can be attributed to significant stress redistribution that occurs during loading beyond initial cracking if the material nonlinearity of masonry itself is neglected. From previous experimental work (Fig. 1.3), it has been observed that different cracking patterns may occur, such as flexural cracking, shear sliding and diagonal splitting. From laboratory tests of many different masonry wall specimens, it has been found that the post cracking-behavior of a wall depends on the wall geometry, external forces and material parameters. In most cases, the failure mode cannot be attributed to a single phenomenon such as shear sliding along a bed joint, flexural or diagonal cracking, even though a specific action may have precipitated the failure sequence. A combination of various modes may need to be consider to estimate lateral

strength. It is necessary to distinguish each failure mode, consider all of the possible cracking patterns, and check the final critical condition when estimating lateral strength of a cracked wall.

In this chapter, different types of specific failure modes will be discussed first, then failure criterion corresponding to respective failure modes will be introduced. Based on these criteria, a general description of the analytical procedure for lateral strength is presented. Then, the procedure will be used to develop a relation between lateral strength and vertical compressive stress in terms of length-to-height aspect ratio.

3.2 Failure Modes

3.2.1 Flexural Cracking

As discussed in the last chapter, the *flexural tension strength normal to the bed joints* is an important parameter in terms of the shear strength of a wall because of the effects of flexural cracking on the distribution of shear and normal stress. However, flexural tension strength can play an even more important role for tall, slender walls with relatively light amount of vertical compressive stress. For this category of wall, flexure cracking quickly extends towards the toe and causes overturning with little or no visible damage in a wall. Thus, the wall will fail in flexure rather than shear, and demonstrate brittle behavior in general. In this failure mode, the flexural tension strength will be related directly to the amount of lateral force that a wall can resist. This failure mode is shown in Fig. 3.1a.

3.2.2 Sliding Shear along Mortar Bed Joint

One of the possible shear failure modes is shear sliding along a mortar bed joint. It is initiated by bed joint slip at a location with low vertical compressive stress and high

shear stress. The particular concern for this type of failure is that bed joint shear resistance is related to the combination of bond shear strength and frictional force between the brick and mortar. The strength defined by the combination of the two material parameters makes it difficult to identify a specific failure location within the plane of a wall. The point of maximum shear stress may not necessarily be the most likely location for sliding along bed joints to occur because vertical compressive stress, and thus, frictional forces may be relatively higher at that location. On the other hand, if sliding is limited to only a local region, it may not limit the lateral strength. The remainder of the wall can resist further lateral force if the wall is relatively stocky. This implies that sliding initiation, and the final failure, may occur at different shear stress levels. In this study, it is assumed that sliding failure is related to sliding extending the full width of a section. It usually occurs for a wall with a moderate length-to-height aspect ratio, as is shown in Fig. 3.1c.

3.2.3 Diagonal Compressive Splitting

Diagonal compressive splitting is a common failure mode for an in-plane wall subjected to vertical compressive stress and shear stress. If the length of a wall is large relative to its height, and vertical compressive stress is high, it may be the case that its shear strength could be governed by the strength of a diagonal compressive strut. After flexural cracking and possible local shear sliding, the total shear force may have to be redistributed to the reduced effective section as the resultant of vertical forces shifts towards the toe. The redistribution of shear and normal stress in the decreased length results in an increase in vertical compressive stress and the shear stress in the compression region. Consequently, the principal diagonal compressive stress will increase because of this stress redistribution, which leads to diagonal splitting or toe crushing of the masonry. This condition is shown in Fig. 3.1b.

3.2.4 Diagonal Tension Cracking

The shear strength of an unreinforced masonry wall may be limited by diagonal tension rather than shear sliding. There are two kinds of diagonal tension cracking: diagonally stepped debonding and diagonal splitting. The former is a result of relatively weak mortar and strong units, and low vertical compressive stress. The latter is for the case of strong mortar, weak units and high vertical compressive stress. Whether initial diagonal cracking induces failure depends on the wall length-to-height aspect ratio. Experimental work has shown that (39), a relatively stocky wall may continue to resist shear force if initial diagonal cracks have not extended to the toe. In this study, diagonal tension failure is defined as the condition when diagonal cracks propagate to the toe. In this case all available shear strength has been lost, as the two segments produced by cracking tend to separate. This type of failure mode is depicted in Fig. 3.1d.

3.3 Failure Criteria

3.3.1 Flexural Cracking

With increasing lateral force, flexural cracks will propagate towards the toe, if behavior of an unreinforced wall is predominantly flexure. For each force increment, it is necessary to check if flexural tensile stress at the wall base has exceeded the flexural tensile strength. When it does, flexural cracks develop and start to propagate along the base. Thus, a flexural-cracking failure is defined when cracks have extended all the way to the toe and overturning results prior to other failures. The cracking criterion is given by:

$$\sigma_y \leq f_t \quad (3.1)$$

Where α_y is the tension stress at the base of a wall which is normal to the bed joint, and f_t is the flexural tensile strength determined from the test result. The typical load–deflection relation for flexural cracking failure mode is shown in Fig. 3.2. The length–to–height aspect ratio (l/h) for this wall is 0.5, and the vertical compressive stress is 50 psi. From the figure, it is evident that before flexural cracking initiates, the force–deflection relation is linear. Once cracks form at base, a nonlinear relation is observed with increasing lateral force. When the crack extends near the toe, the deflection can be as large as six times that at initial flexural cracking. Finally, when the crack reaches the toe, the wall overturns and the deflection continues increasing with no increase in force. It can be inferred that for a flexural cracking failure, the flexural tensile strength f_t heavily affects the force–deflection behavior and is directly related to the ultimate strength of a specific wall.

3.3.2 Shear Sliding

It has been shown in previous experimental work (14), that the sliding along the bed joint at the local region of a wall resulted in a subsequent transfer of shear stress to the toe region, which lead to a sudden increase in principal compressive and tensile stress. It can be concluded that after local sliding, a wall still has capacity to resist further lateral forces. This typical load–deflection behavior is demonstrated in Fig. 3.3. Thus, sliding failure in the analysis is considered as sliding developing across a full width of section. Since masonry is composed of brick and mortar, it can be considered as a frictional material. According to the Mohr–Coulomb shear friction relationship, the bed joint shear sliding criterion will be defined as:

$$\tau \leq \tau_0 + \mu\sigma_y \quad (3.2)$$

Where τ_0 is the cohesion and μ is the coefficient of friction, both values can be obtained from in-place shear test results. The parameters, τ and σ_y , are shear and vertical compressive stress, respectively. This criterion is depicted in Figure 3.4.

Before estimating shear strength of a wall, the possible sliding region needs to be identified. The shear sliding index is then defined to identify the most vulnerable point on the wall with respect to shear sliding. It is defined as follows:

$$S_{ind} = \frac{\tau}{\tau_0 + \mu\sigma_y} \quad (3.3)$$

In this equation, it is clear that if the shear stress, τ , at a specific location is equal to the shear capacity defined by equation (3.2), then the shear index will be equal to 1.0. In such case, sliding will occur at the particular coordinate where the index reaches unity. A sample wall that has the same dimensions and loading condition as the tested wall is shown in Fig. 3.5 (14). The contour mapping of shear sliding index for this wall is shown in Fig. 3.6. The cohesion value has been assumed as 150 psi, and the coefficient of friction equal to 0.75. These values are close to those obtained from the in-place shear test for the same wall. The contour for an index value of 1.0 suggests that sliding should occur along a bed joint near the central portion of the wall. In these regions, shear stress usually is high and normal stress is somewhat low. This phenomenon was confirmed by test results.

3.3.3 Compressive Splitting Failure

Masonry is a material that exhibits distinct directional dependent properties because of the influence of the bed joint acting as a plane of weakness. From most experimental results, it has been shown that the strength of masonry is very much dependent on the orientation of the joints to the local stress. Thus, a three dimensional failure sur-

face is necessary to define failure under biaxial stress (33). This can be achieved by expressing the criterion either in terms of two principal stresses with the orientation to the bed joint ($\sigma_1, \sigma_2, \theta$), or in terms of a stress state related to the bed joint consisting of a normal stress σ_n , a parallel stress σ_p and a shear stress τ . A masonry element with biaxial compression stress state, and the failure surface corresponding to different failure criteria are shown in Fig 3.7 (18). The following failure criterion is used to relate shear strength to biaxial compressive stress and strengths:

$$\tau^2 \leq (f_{mx} - \sigma_x)(f_{my} - \sigma_y) \quad (3.4)$$

Where f_{mx} and f_{my} are masonry compressive strength parallel and normal to the bed joint respectively.

The value of f_{my} can be obtained from prism test and f_{mx} usually is assumed as a certain ratio of f_{my} since it is usually much lower than f_{my} . The value of σ_x and σ_y are the compressive stresses parallel and normal to the bed joint. This criterion is based on the assumption that a constant limit f_{mx} is the maximum compressive stress, which is on safe side for all different principal stress directions.

A special case for compressive splitting failure is toe crushing. From the stress analytical formulation presented in Chapter 2 (Eq. 2.17, 2.18 and 2.19), shear stress, τ , and normal stress, σ_x , at the toe both equal zero. Then, equation (3.4) is simplified to:

$$\sigma_y \leq f_{my} \quad (3.5)$$

This equation indicates that when vertical compressive stress at the toe is larger than compressive strength, then toe crushing will occur.

3.3.4 Diagonal Tension Cracking

Diagonal tension cracks are not accompanied by heavy spalling, popping or the projection of fragments away from the wall, as typically occurs with a compression failure. Diagonal cracking occurs when the principal diagonal tensile stress reaches the prescribed diagonal tension strength. Accordingly, the crack criterion can be derived by using Mohr's circle to determine the amount of diagonal tension at a point. Then, equation for the controlling principal tensile stress can be written as follows (16):

$$\left(\frac{\tau}{\sigma_0}\right) = \left(1 - \frac{\sigma_x}{\sigma_0}\right)\left(1 - \frac{\sigma_y}{\sigma_0}\right) \quad (3.6)$$

Where σ_0 is the diagonal tension strength, which has to be either assumed or inferred from results of diagonal splitting test (ASTM Specification E519-81). Presently, there is no nondestructive technique available for measuring diagonal tension strength. The failure surface for diagonal tension cracking is shown in Figure 3.8.

3.4 Analytical Procedure for Estimating Lateral Strength

3.4.1 Shear Stress Redistribution after Shear Sliding

It was mentioned in Section 3.2.2 that shear sliding along a mortar bed joint may not result in failure of a wall. Since there is a lack of experimental data to quantitatively represent the shear strength along the bed joint after sliding, it is assumed that if shear sliding has occurred at any location, cohesion between brick and mortar interface will no longer exist. In effect, the shear strength to resist sliding at that point drops down to the pure frictional components. According to the equation (3.2), the shear strength then is equal to frictional part, i.e., $\mu\sigma_y$. Recent laboratory tests (2) have shown that even

for a stair-stepped diagonal crack, when head joints opened considerably, the bed joint remained closed (Fig. 3.9). This behavior is attributed to the frictional force acting on the bed joints. The friction is a result of the compressive stress, and plays an important role for the post-cracking behavior. This typical shear-displacement relation is shown in Fig. 3.10 (29). To consider this behavior, shear stress should be redistributed again on the section where sliding has occurred.

The total lateral force resisted by a section will be divided into two parts: $SUBV$, resisted by the sliding region, and V_r , resisted by the remaining portion of the section. The shear force acting on sliding region is easy to obtain since its capacity is restricted to the pure frictional force, which is given by equation (3.7). The shear sliding region is assumed to occur between two points x_0 and x_1 . Consequently, the region without sliding resists the remainder of lateral force as indicated in equation (3.8). Thus, the shear stress distribution will be defined as equation (3.9):

$$SUBV = t \int_{x_0}^{x_1} \mu \sigma_y dx \quad (3.7)$$

$$V_r = V - SUBV \quad (3.8)$$

$$\tau(x,y) = \begin{cases} f(V_r) & x < x_0 \\ \mu \sigma_y & x_0 \leq x \leq x_1 \\ f(V_r) & x_1 < x \end{cases} \quad (3.9)$$

The function $f(V_r)$ in equation (3.9) will be the same as the equation (2.19) or equation (2.16), except that V_r substitutes for V in the equations.

A typical shear stress distribution after sliding is shown in Fig. 3.11. The length of a wall for this sample is 144 inches. The uncracked length shown in the figure is the

decreased effective length resulting from flexural cracking under a given lateral force. Sliding has occurred at the section near mid-height. Initial sliding occurs at the central portion of the section, and extends from the length of 40 to 50 inches. The shear stress has been redistributed according to Eq. 3.9. At the place with sliding, shear stress is decreased to just the frictional component. This is shown in the figure with the straight-line distribution which is the same as the distribution of normal stress. The redistribution results in a migration of the peak shear stress towards the toe, and precipitates a compressive splitting failure.

3.4.2 Strategy for Estimating Lateral Strength

Experimental results have demonstrated that unreinforced walls may have a long life after cracking (Fig. 1.1). Flexural cracking observed at the heel region occurred at a load of 60% of the ultimate load (14). First diagonal tension cracking occurred as a lateral load of approximately 62% of the ultimate lateral load (39). This observed behavior suggests that lateral strength is very much a function of the post-cracking behavior. By considering all possible crack patterns, the ultimate limit state can be determined according to the failure criteria presented in the previous sections. These criteria will be implemented to develop the analytical procedure.

As discussed in Chapter 2, initiation of the first crack will play an important role on the subsequent behavior of a wall, since it results in a substantial redistribution of normal and shear stresses. After initial cracking has occurred, further lateral strength can be developed even though the effective section area to resist shear is decreasing. Thus, when strength of a wall under lateral force is considered, the first step is to define the cracking load and determine the size of the cracked "dead zone". Equations (3.1) are used to check the initiation of cracking. If flexural tension strength is relatively high, sliding or compressive splitting may occur before flexural tension cracking occurs. In

this special case, normal and shear stresses are distributed throughout the whole section.

When stresses are distributed on a decreasing area, for each increment of lateral force, cracks propagate further which causes enlarging of the dead zone. If cracking has reached to the toe, a wall will fail in either a flexural cracking mode or a diagonal cracking mode. On the other hand, if flexure results in decreasing of the effective shear area and first sliding occurs, then shear stress on the sliding section has to be redistributed according to the concept presented in the last section. With increasing lateral force, the potential for sliding, diagonal tension cracking and possible compressive splitting should be checked. The lateral force at which one of these failures occurs will be the capacity of a wall.

3.4.3 Strength Analysis Procedure

Based on the discussion in the last section, the analytical procedure can be schematically described in the flow diagram shown in the Fig. 3.12. For a typical wall, the method of solution may be summarized as follows:

1. Identify necessary parameters:
 - (a) wall dimension;
 - (b) vertical compressive stress;
 - (c) flexural tensile strength;
 - (d) diagonal tension strength;
 - (e) compressive strength;
 - (f) coefficient of cohesion;
 - (g) coefficient of friction.

2. Check if flexural crack occurs at the heel of a wall.
3. Define the crack zone size.
4. Redistribute normal and shear stress on effective length of a wall.
5. Determine if flexural cracking propagates to the toe.
6. Check if shear sliding occurs.
7. Redistribute shear stress on the section with shear sliding.
8. Check if shear sliding extends throughout the section.
8. Check if diagonal tension crack occurs.
9. Check if diagonal splitting or toe crushing occurs.
10. Determine if a wall has failed under given load increment. If not true, increase lateral load and return to step 3.
11. If a wall fails in one of the failure modes as defined in the previous section, the analysis is concluded. The following parameters should be noted:
 - (a) maximum lateral force;
 - (b) coordinate of the failure point;
 - (c) lateral strength;
 - (d) vertical compressive stress applied at top of a wall;
 - (e) bottom uncracked length.

With the analytical procedure presented above, a computer program has been developed to estimate lateral strength of unreinforced masonry walls for given material parameters, wall dimensions and vertical compressive stresses. The program named LATS was written in the Fortran language and can be run on a personal computer. As lateral force is increased, the dead zone grows which is shown graphically on the screen.

In addition, any cracking point is shown which may be a result of sliding, diagonal tension or compressive splitting.

The program LATS is listed in Appendix B. An example of a screen display is shown in Fig. 3.13. The material parameters used for this display are: (a) flexural tensile strength of 100 psi, (b) cohesion of 100 psi, (c) frictional coefficient of 0.6, (d) compressive strength of 1000 psi, (e) diagonal tension strength of 150 psi. The length-to-height ratio of the wall is 2.0. The vertical compressive stress applied at the top of the wall is 130 psi. In the figure, the wall was discretized using a mesh of 6 inches long by 4 inches high. The stresses were calculated at each cross point of the mesh. Shear sliding is represented by the symbol of cross, and the location of diagonal splitting is indicated by the symbol of circle. The dead zone resulting from the flexural cracking is shown by the shaded triangular area. For the diagonal tension cracking (was not shown in this figure), a straight line along the cracking direction will be shown on the screen. With this type of screen display, it is helpful to understand the behavior of a wall under increasing lateral force.

3.4.4 Results of A Sample Strength Estimate

By using program LATS, a relation can be plotted between the shear strength and vertical compressive stress applied at the top of a wall. This relation is referred to as a " strength curve". A typical set of strength curves for various wall aspect ratios are shown in Fig. 3.14. This figure gives the strengths of walls with the same material parameters and a typical range of length-to-height aspect ratios from 0.5 to 2.5. The material parameters used to construct this set of curves are: (a) flexural tensile strength of 80 psi, (b) compressive strength of 3000psi, (c) diagonal tension strength of 250 psi, (d) cohesion of 80psi, (e) frictional coefficient of 0.7. Three types of failure modes are presented in this figure: flexural cracking (A), shear sliding (B) and compressive

splitting (C). Other failure modes such as diagonal tension cracking would also be represented on such a strength curve, if material parameters were varied.

It is observed from this typical set of strength curves, that for slender, square and stocky walls (l/h ratio of 0.5, 1.0 and 2.5), the failure modes are either flexural cracking or diagonal splitting within the range of designated vertical compressive stress. The different aspect ratios result in the change of failure mode from flexural to compressive splitting at different vertical compressive stress. A slender wall, even with high vertical compressive stress, may still fail in flexure because flexural cracking progresses quickly towards the toe. However, for a stocky wall the failure is primarily a result of compressive splitting. This is attributed to the higher principal compressive stress at the toe resulting from the redistribution of the stresses because of flexural cracking or local sliding. For those walls with aspect ratio, l/h between to 1.5 and 2.0, it is likely that a sliding failure will occur when vertical compressive stress is relatively low. The higher the l/h ratio, the lower the likelihood to have a sliding failure, because sliding may not extend toward the toe.

For any given material parameters, external forces and wall aspect ratio, the strength curves presented in this section can be constructed. The uniqueness of this type of strength curves is that it directly relates to the average shear stress and vertical compressive stress on top of a wall based on the checking of the strength at local area. These curves are obtained in terms of the variation of stresses with consideration of cracking effects, which make the global-local strength extrapolation possible. Additionally, they demonstrate reasonably well the possible failure mode, and the effect of aspect ratio l/h on the shear strength. By using the proposed analytical procedure, once this type of strength curve is given, it is convenient to estimate the lateral strength of a cracked wall.

CHAPTER 4

MATERIAL PARAMETER SENSITIVITY STUDIES

4.1 Introduction

As has been discussed before, failure of an unreinforced masonry in-plane wall may be a result of a few different cracking modes. The limit state depends on the values of different material parameters. In order to understand the effects of different material parameters on the lateral strength, it is necessary to run parametric studies based on the analytical procedure developed in Chapter 3.

In this chapter, by using the proposed procedure for lateral strength, the sensitivity of shear strength on five parameters are investigated. These parameters are: flexural tensile strength, compressive strength, coefficient of friction, cohesion and diagonal tension strength.

4.2 Flexural Tensile Strength

It has been discussed before that flexural tensile strength is directly related to the lateral strength of a slender wall with light amounts of vertical compressive stress. Tensile stress at the base of a wall simply causes the observed bed-joint cracks and inhibits the ability to resist shear. It may be recalled from Chapter 2 that the growth of the dead zone is governed by flexural tensile strength. Therefore, it is of interest to examine the effects of flexural tensile strength on lateral capacity, so that good estimates can be provided when considering post-cracking behavior of a wall.

The nominal shear stress at which an unreinforced masonry wall will crack in flexure is given by the following equation:

$$\tau = \frac{1}{6} \left(\frac{l}{h} \right) (f_t + \sigma_v) \quad (4.1)$$

Here σ_v is the vertical compressive stress applied at the top of a wall. It is evident that for a given vertical stress and wall aspect ratio, the flexural tensile strength has a major influence on the lateral stress that initiates cracking. However, once a wall cracks, the most noticeable effect is on the expansion of the cracked zone.

In order to investigate the importance of the flexural tensile strength, relations between lateral strength and vertical compressive stress are constructed for a wall with an aspect ratio of 1.5, compressive strength of 3000 psi, diagonal tension strength of 250 psi, cohesion of 80 psi and frictional coefficient of 0.7. The only variable in this parametric study is the flexural tensile strength with the value of 10psi, 50 psi and 100 psi. Three strength curves are shown in Fig. 4.1. Obviously, with increasing flexural tensile strength, the lateral load for cracking increases. The failure mode changes from flexural cracking to sliding failure at a vertical compressive stress equal to 50 psi, and then to a compression failure at 140 psi for all three curves. As can be seen from the figure, for flexural cracking failure, flexural tensile strength directly affects the shear strength under the same vertical compressive stress.

It has been defined in Chapter 3 that a flexural cracking failure occurs when flexural cracks extend to the toe without or with little other damage in a wall. This failure mode can be considered as the overturning of a wall. According to statics, the overturning of a wall can be checked by following equation:

$$\tau = \frac{\sigma_v}{2} \left(\frac{l}{h} \right) \quad (4.2)$$

This equation is not related to the flexural tensile strength of a wall. It is a common conception that if no cracks occur, overturning is impossible. Therefore, when checking flexural cracking failure, it is necessary first to calculate the cracking strength by using equation (4.1). If the overturning strength from equation (4.2) is larger than the cracking strength, a wall has the ability to resist further lateral force, until cracking occurs throughout the base. In this case, equation (4.2) can be directly used to determine the lateral strength. Otherwise, cracking strength will be the limit of a wall for flexural cracking mode.

Generally, the higher the flexural tensile strength the higher the shear capacity for flexural cracking failure. It has been noted that, when vertical compressive stress is larger than 30 psi and less than 50 psi, the strengths for walls with flexural tensile strengths of 10 psi and 50 psi are the same even if both fail in a flexural cracking mode. The reason is that both strengths are limited by equation (4.2). However, for a wall with flexural tensile strength of 100 psi, the shear strength is limited by the cracking strength within the given vertical compressive stress range. It results in a higher strength than that of walls with lower flexural tensile strength.

When vertical compressive stress is larger than 50 psi, and a wall fails in other failure modes, the three strength curves are identical. It indicates that the ultimate strength does not rely on flexural tensile strength, although the effective area for shear varies with different flexural tensile strength. This observation suggests that the effect of flexural tensile strength on shear capacity of a wall can be neglected, unless a wall fails in flexural cracking mode.

4.3 Compressive Strength

Uniaxial compressive strength of masonry is an important parameter for the shear strength because it is directly related to the failure of a wall. To illustrate its effect, the

strength curves for walls with aspect ratio, (l/h) , 1.5 are presented in Fig. 4.2. The material parameters used to plot these curves are: flexural tensile strength of 80 psi, cohesion of 150 psi, frictional coefficient of 0.7 and diagonal tension strength of 250 psi. The reason to chose these specific values is to attempt to include as few as possible failure modes other than compression failure. Three different values of compressive strength are used f'_m : 1000 psi, 2000 psi, 3000psi. As shown in Fig. 4.2, only two failure modes for this combination of parameters: flexural cracking failure and compression failure.

From Fig. 4.2, It has been noted that within the range of flexural cracking which is between the vertical compressive stress of 0 to 40 psi , the strength indicated by the three curves are identical. When the vertical compressive stress is larger than 40 psi, the difference between the curves with f'_m of 1000 psi and the other two curves are obvious, since strength is a result of compression failure.

The variation in masonry compressive strength significantly influences the part of the curves for compression failure. The initial portion of the curves, that are governed by flexural cracking, is not related to the compressive strength. Clearly, shear strength is dominated by the compressive strength only for the compression failure mode. This also can be inferred from the failure criteria presented in Section 3.3.3 for compression failure, since the only material parameter affecting the shear strength is the compressive strength f'_m . In consequence, if a wall does not fail in compression, the shear strength does not depends on its compressive strength.

4.4 Coefficient of Friction and Cohesion

The value of the coefficient of friction depends on the type of mortar and the type of unit. According to the Coulomb failure criterion, the frictional force is part of the strength to resist shear sliding. As mentioned in Section 3.2.2, the shear sliding failure is defined as the case when sliding occurs throughout the entire section. This limit state

is difficult to reach unless both values of cohesion and coefficient of friction are very low. In most failure cases, a compression failure may be preceded by sliding at some local region. If compressive strength is relatively low, differences of frictional coefficient only results in variation in the length over which sliding occurs. Thus, the lateral strength is predominantly governed by compressive strength.

To investigate the effect of coefficient of friction on shear strength, the strength curves for the same aspect ratio (l/h) as used in Fig 4.1 and 4.2 are given in the Fig.4.3. The material parameters used in the figure are: flexural tensile strength of 80 psi, compressive strength of 3000 psi, diagonal tension strength of 250 psi, and cohesion of 80 psi. The coefficient of friction is varied from 0.5, 0.7, to 0.9.

As can be seen from the figure, within the given range of vertical compressive stress from 0 to 250 psi, the difference in strength caused by the coefficient of friction is very small even for the sliding failure mode. The sliding failure mode occurs at a vertical compressive stress of 40 psi for the curve with the coefficient of friction of 0.5, and occurs at 70 psi of vertical compressive stress for the curve with the value of 0.7. However, for the curve with a value of 0.9, the sliding failure mode does not occur until a vertical compressive stress equal to 120 psi. This finding reflects the common sense understanding that a wall with a low coefficient of friction tends to fail in sliding. As shown in the figure, when the vertical compressive is lower than 50 psi and higher than 230 psi, the three curves are identical. This suggests that when failure is not a result of shear sliding, lateral strengths are not related to coefficient of friction.

Cohesion is the part of shear strength that is related to the bonding between mortar and units. The strength curves shown in the Fig. 4.4 are based on the same material parameters as used in Fig.4.3 except that the coefficient of friction is constant at 0.5, and the value of cohesion has been varied from 100psi, 150psi to 200psi. The three curves are almost identical for different values of cohesion coefficient. For a curve

based on a 100 psi value, sliding failure mode occurs at 60 psi of vertical compressive stress and continues until 230 psi. But when a cohesion coefficient of 200 psi is assumed, sliding failure mode starts at 100 psi of vertical compressive stress. The small difference of the strengths can be seen in the range of vertical compressive stress between 60 psi and 230 psi, since within this range of vertical compressive stress the failure modes are shear sliding.

Based on above discussions, it can be concluded that different coefficients of friction and cohesion may result in sliding at different vertical stress levels. However, variations in both values are not significant on lateral strength for walls failing exclusively by sliding. It would be desirable to study further effects of friction and cohesion when lateral strength is limited by shear sliding.

4.5 Diagonal Tension Strength

A diagonal tension failure is distinguished by cracks passing through the units and the mortar joints or by stepped cracks occurring mostly along the mortar bed and head joints. Currently, there is no nondestructive method available to obtain insitu diagonal tension strength. A value can be inferred from a diagonal splitting test if wall samples are available.

To demonstrate the importance of diagonal tension strength, three strength curves are plotted using different values of σ_0 : 50 psi, 100psi and 150 psi (Fig.4.5). The wall aspect ratio is the same as that used in the last section. The material parameters used are: cohesion 150 psi, coefficient of friction 0.7, flexural tensile strength 150 psi and compressive strength 4000psi.

Since diagonal tension strength is related only to the diagonal tension failure mode, its influence is only for the range of diagonal tension failure. It can be seen from Fig. 4.5 that diagonal tension strength strongly affects the shear strength when a wall

fails in diagonal tension mode. A wall with diagonal tension strength of 50 psi fails in a diagonal tension mode for any value of vertical compressive stress. When diagonal tension strength is increased to 100 psi, the wall fails in diagonal tension at 150 psi of vertical compressive stress. When strength is increased to 150 psi, the wall fails in a diagonal tension mode at 220 psi of vertical compressive stress. It is also shown in the figure that, when the failure mode changes to diagonal tension, the increase of vertical compressive stress has but slight influence on the shear strength

Based on this figure, it can be concluded that diagonal tension strength has a significant influence on ultimate lateral strength, if a wall fails in diagonal tension cracking mode.

CHAPTER 5

SIMPLIFIED EVALUATION METHOD FOR LATERAL STRENGTH OF CRACKED WALLS

5.1 Introduction

An analytical procedure for estimating lateral strength of an unreinforced masonry cracked wall has been presented in Chapter 3. The significance of this evaluation procedure is that the in-plane lateral capacity of an unreinforced masonry wall can be estimated by considering the post cracked behavior.

The proposed procedure developed in this study has accounted for all possible failure modes for an unreinforced masonry in-plane wall. It can provide the entire history of cracking development, though the major concern for structural evaluation is simply peak lateral strength. Lateral capacity can be estimated without considering the particular evolution of cracks. One use of the analytical procedure presented in this study is as a vehicle by which to develop a simple and rational approach for use in engineering practice.

In order to estimate lateral strength, it is desired to have a simplified method that accounts for the cracking effect. The aim of this chapter is to present a simplified evaluation approach, so that current research results can be directly used in engineering practice.

In this chapter, a strength table corresponding to different length-to-height aspect ratios and different material parameters is presented. Then, the evaluation procedure for estimating lateral capacity based on the strength table is introduced. Finally, an example using the presented strength table is illustrated.

5.2 Strength Tables

Since the lateral strength of an in-plane wall is related to several material parameters and to different aspect ratios, it is difficult to represent the strength by a single expression or empirical equation. Using the strength analytical procedure developed in this study, the lateral strengths have been calculated corresponding to various parameters. By tabulating these calculated results, a strength table has been constructed, which is presented in Appendix A. The listed values in each sub-table is the average shear stress with the unit of psi.

This strength table is related to all parameters affecting the lateral strength of an in-plane wall, such as compressive strength f'_m , diagonal tension strength σ_0 , cohesion τ_0 and coefficient of friction μ . As discussed in Chapter 4, the effect of flexural tensile strength can be neglected except when a wall fails in the flexural cracking mode. Thus, the flexural tensile strength of 50 psi is kept constant throughout the construction of this table. All selected material parameters are within the range of those commonly used in masonry construction. The range of wall aspect ratios listed in the table is from 0.5 to 5.0. The compressive strength varies from 1000 psi to 5000 psi, and the diagonal tension strengths range from 50 psi to 250 psi. Values of cohesion are taken as 100 psi, 200 psi and 300 psi, and the coefficient of friction varies from 0.4 to 1.0. The vertical compressive stress ranges from 50 to 250 psi. Thus, each sub-table corresponds to a specific combination of material parameters with different aspect ratios and different vertical compressive stresses.

To discuss the feature of the strength table, a simple entry of the table is presented here:

$$f'_m = 5000 \text{ psi} \quad \sigma_0 = 100 \text{ psi} \quad \tau_0 = 200 \text{ psi} \quad \mu = 0.8$$

l/h	σ_v	50	100	150	200	250
0.5		12.7	25.1	37.5	50.2	61.9
1.0		25.1	50.1	75.0	99.9	120.9
2.0		50.1	93.1	104.0	113.9	123.1
3.0		74.3	94.3	105.6	115.6	124.7
4.0		91.9	100.6	108.5	116.5	124.9
5.0		104.5	112.5	118.7	124.5	130.0

For example, if the vertical stress is 100 psi and the aspect ratio is 2.0, then the average shear stress is 93.1 psi. The ultimate lateral capacity of the wall is calculated as 93.1 psi times gross area of the wall.

It should be noted from the table that for different material parameter combinations, some of the strengths listed in the different sub-tables are the same. It may be recalled that from Chapter 4, that the specific failure mode is only related to the associated parameter, the change of the other parameters will not influence the strength limited by that specific failure mode. Thus, the same strengths may be obtained from different sub-tables, if they result from the same failure mode that is unrelated to the varying material parameters.

It is necessary to point out that strength values listed in the table are limited by the shear sliding criterion. Experimental work (14) has shown that the nominal average shear stress of a cracked wall is lower than the strength defined by the in-place shear

test. In this study, the shear sliding failure is defined as the shear sliding extending throughout the section. When the shear sliding occurs only in the central portion of a wall that has relatively high compressive strength or large aspect ratio, the lateral strength may reach the value defined by shear sliding criterion. This special case indicates that all masonry on top of a wall may slide under this lateral force level. Consequently, the wall must lose all capacity to resist further lateral force. This strength limitation has been reflected in the table by the same strength in the same sub-table for different aspect ratios.

Generally, the higher the vertical compressive stress and the larger the aspect ratio are, the higher the shear strength is. This common sense understanding is confirmed with the maximum table value corresponds to the highest vertical compressive stress and the largest aspect ratio in each sub-table. However, it is still possible to have higher strength with the lower vertical compressive stress, because the strength may be limited by different failure modes governed by different material parameters.

5.3 Evaluation Procedure for Lateral Capacity of Cracked Walls

Based on the strength table presented here, when the material parameters, vertical compressive stress and aspect ratio are known, the lateral strength can be obtained quite easily. The advantage of this strength table is evident. It provides rational results with simple and convenient approach.

By using the strength table, the procedure for estimating the lateral capacity of a wall is stated as follows:

- 1) Calculate the vertical compressive stress from the gravity load applied to a wall.
- 2) Calculate the length-to-height aspect ratio of a wall.

- 3) According to the prescribed material parameters, enter the table and find the value associated with the calculated aspect ratio and vertical compressive stress.
- 4) Determine the lateral capacity with the strength from the table times gross section area.

Based on the above procedure, an example to use strength table is presented:

Determine the lateral strength for an unreinforced 7.63 inch brick wall that is 144 inch long, by 72 inch high. The vertical load applied at the top of the wall is 110 kips. The material parameters are given as follows:

$$f'_m = 2000 \text{ psi}, \sigma_0 = 100 \text{ psi}, \tau_0 = 200 \text{ psi}, \mu = 0.4$$

Solution:

- 1) Determine vertical compressive stress:

$$\sigma_v = \frac{110,000}{144 \times 7.63} = 100 \text{ psi}$$

- 2) Calculate aspect ratio:

$$\frac{l}{h} = \frac{144}{72} = 2.0$$

- 3) Enter body of the table with given material parameters:

$$\tau_{\max} = 93.1 \text{ psi}$$

- 4) Calculate lateral capacity:

$$V_{\max} = \frac{93.1 \times (144 \times 7.63)}{1000} = 102 \text{ kips}$$

CHAPTER 6

ANALYSIS OF LATERAL DEFLECTIONS FOR CRACKED WALLS

6.1 Introduction

An important concern for structural evaluation is the amount that a wall will deflect. Even though unreinforced masonry walls may be quite stiff if uncracked, it is necessary to check deflection when they are cracked. From previous experimental results (Fig.1.1), it was observed that the initial stiffness of an unreinforced masonry wall was reduced with the initiation of flexural cracking. The rate of deflection increased with the increase of lateral load when flexural cracks started to open. Then the lateral stiffness was continuously reduced, because only the uncracked portion of the cross section remained effective. It is evident that, if a wall still has the potential for residual strength after cracking, then, estimates of deflections must be based on the post-cracked state.

The lateral top-level deflection of an in-plane wall consists of two parts: shear deformation and flexural deformation. For different aspect ratios, the relative amounts of shear and flexural deformation will vary as a result of the amount of lateral force and the vertical compressive stress. The shear strain will vary with the change of the section size towards the base. According to the assumption that masonry is linear in compression, once the region of cracking is defined, shear and flexural deflection can be calculated separately, and then summed to give the total deflection.

The purpose of this chapter is to present a calculation method for determining lateral deflection of cracked walls. The comparison of conventional approaches for calculating lateral deflection with the method presented in this chapter is worthwhile, since these comparisons can provide additional information about the cracking effect on structural stiffness.

6.2 Derivation of Deflection Calculation Formula

6.2.1 Review of Principle of Virtual Work

The principle of virtual work has been proved very powerful as a technique for calculating structural displacements, since it is independent of the type of deformation and whether the material follows Hook's law or not. One assumption of virtual work is that the displacement is sufficiently small so that the changes in the geometry of the body are negligible and the original undeformed configuration can be used in setting up the equations for the system. This suggests that any nonlinearity in the compatibility of strain and displacement can be neglected (7). The specific basis of the method of virtual work used to compute deflection is the principle of virtual work for a deformable body. It can be stated that: the external virtual work W_e done by a system of virtual forces acting on any structure is equal to the internal work of deformation W_i . It can be represented by the following expression:

$$W_e = W_i \quad (6.1)$$

In this instance, a deformable body must be in equilibrium and remain in equilibrium throughout a small and compatible deformation for a virtual force system. An appropriate expression for W_e and W_i must be developed according to the different type of deformations. Selecting a suitable virtual force system is required so that the desired deflection components can be computed.

The lateral deflection evaluation method derived in this chapter is based on the principle of virtual work. The stress expressions presented in Chapter 2 are used to evaluate the internal and external virtual work. In the following section the derivation scheme for calculating deflection is described.

6.2.2 Lateral Deflection Formulation

The stress field described in Chapter 2 satisfies the equations of equilibrium and boundary conditions, which is able to develop both internal and external work with the use of the principle of virtual work. The current analytical approach for lateral deflection considers the post-cracking behavior of a masonry wall and separately accounts for the deflection caused by flexure and shear. The basic strategy for developing a deflection calculation method is to include the moment and shear in a virtual work system and construct the formulation by summing up both shear and flexural deformations.

The real and auxiliary structure used here are shown in Fig. 6.1, in which \bar{M} and $\bar{\tau}$ are the virtual force, and M and τ are the real force. The dead zone caused by cracking is depicted by a dotted line on the wall. Then the moment in both structures are expressed as follows:

$$y \leq y_0 \quad M = Vy \quad (6.2)$$

$$\bar{M} = (1)y \quad (6.3)$$

$$y > y_0 \quad M = Vy - P(y - y_0)\frac{\theta}{2} \quad (2.15)$$

$$\bar{M} = (1)y \quad (6.4)$$

The shear stress in the real structure, τ , and the auxiliary structure, $\bar{\tau}$ are:

In the lower cracked portion of a wall, the shear stress is distributed in a decreased effective length. To consider the top-level deflection, it is necessary to define the aver-

$$y \leq y_0$$

$$\tau = \frac{V}{2I}(lx - x^2) \quad (2.18)$$

$$\bar{\tau} = \frac{1}{2I}(lx - x^2) \quad (6.5)$$

$$y > y_0$$

$$\tau = \frac{1}{2I} \left[x \left(Va + 2M\theta - \frac{P\theta a}{3} \right) - x^2 \left(V - \frac{P\theta}{2} + \frac{3M\theta}{a} \right) \right] \quad (2.21)$$

$$\bar{\tau} = \frac{1}{2I} \left[x(a + 2y\theta) - x^2 \left(1 + \frac{3y\theta}{a} \right) \right] \quad (6.6)$$

age shear strain across a particular section. For the element shown in Fig. 6.2, the external and internal work caused by the shear force will be:

$$dW_e = \bar{V}\gamma_0 dy \quad (6.7)$$

$$dW_i = (\bar{\tau} dA)(\gamma dy) \quad (6.8)$$

since $dW_e = dW_i \quad \bar{V} = 1 \quad (6.9)$

thus, $\gamma_0 = \int \bar{\tau} \gamma dA \quad (6.10)$

Assuming shear strain to be directly related to shear stress by the shear modulus, G , then,

$$\gamma = \frac{\tau}{G} \quad (6.11)$$

Substituting equation (6.11) into (6.10), gives the average shear strain across a particular section:

$$\gamma_0 = \int \bar{\tau} \frac{t}{G} dx \quad (6.12)$$

The deflection caused by shear will have different expressions for the upper uncracked portion and the lower cracked portion because of the different shear stress expressions. The top-level shear deflection, Δ_s , will be the sum of the shear deformation along the height of a wall. It consists of two parts : Δ_{s1} , from the uncracked portion, Δ_{s2} from the cracked portion. Then, the expression for Δ_s is given:

$$\Delta_s = \Delta_{s1} + \Delta_{s2} = \int_0^{y_0} \gamma_0 dy + \int_{y_0}^h \gamma_0 dy \quad (6.13)$$

The further expansion will result in the following expression for shear deflection:

$$\begin{aligned} \Delta_s &= \Delta_{s1} + \Delta_{s2} \\ &= \frac{t}{G} \left[\int_0^{y_0} \int_0^l \bar{\tau} dx dy + \int_{y_0}^h \int_0^a \bar{\tau} dx dy \right] \end{aligned} \quad (6.14)$$

Substituting shear stress expressions presented in this section into the above equation, terms for deflections Δ_{s1} and Δ_{s2} can be determined.

$$\Delta_{s1} = \frac{1 \cdot 2Vy_0}{GA} \quad (6.15)$$

$$\begin{aligned} \Delta_{s2} = \frac{1}{Gt} & \left[\left(\frac{-1}{a} \right) \frac{9P\theta y_0}{10} + \left(\frac{y}{a} \right) \left(-18 \frac{V}{5} + 13P \frac{\theta}{10} \right) + \left(\frac{y}{a^2} \right) \frac{6P\theta^2 y_0}{5} \right. \\ & \left. + \left(\frac{y^2}{a^2} \right) \left(12\theta \frac{V}{5} - 6P \frac{\theta^2}{5} \right) + \ln a \left(7 \frac{P}{5} - 24 \frac{V}{5\theta} \right) \right]_{\text{h}}^{y_0} \quad (6.16) \end{aligned}$$

Similarly, the flexural deflection is derived as follows:

$$\begin{aligned} \Delta_m &= \Delta_{m1} + \Delta_{m2} \\ &= \frac{1}{EI} \int_0^{y_0} M\bar{M} dy + \frac{1}{E} \int_{y_0}^h \frac{M\bar{M}}{I} dy \quad (6.17) \end{aligned}$$

By using the moment expressions for real and auxiliary structures, the flexural deflection Δ_{m1} and Δ_{m2} can be deduced to:

$$\Delta_{m1} = \frac{Vy_0^3}{3EI} \quad (6.18)$$

$$\begin{aligned} \Delta_{m2} = \frac{1}{Et} & \left[\left(\frac{1}{a} \right) \left(-\frac{3Py_0}{\theta} \right) - \left(\frac{y}{a} \right) \left(12 \frac{V}{\theta^2} - 6 \frac{P}{\theta} \right) + \left(\frac{y}{a^2} \right) 3Py_0 \right. \\ & \left. + \left(\frac{y^2}{a^2} \right) \left(6 \frac{V}{\theta} - 3P \right) - \ln a \left(\frac{12V - 6P\theta}{\theta^3} \right) \right]_{\text{h}}^{y_0} \quad (6.19) \end{aligned}$$

The following parameters are defined to simplify the expressions integrated from equations (6.17) and (6.19).

$$K = \frac{1}{(l - \theta (h - y_0))} - \frac{1}{l} \quad (6.20)$$

$$B = \frac{h}{(l - \theta (h - y_0))} - \frac{y_0}{l} \quad (6.21)$$

$$C = \frac{h}{(l - \theta (h - y_0))^2} - \frac{y_0}{l^2} \quad (6.22)$$

$$D = \frac{h^2}{(l - \theta (h - y_0))^2} - \left(\frac{y_0}{l}\right)^2 \quad (6.23)$$

$$F = \ln(l - \theta (h - y_0)) - \ln(l) \quad (6.24)$$

The total lateral deflection at the top of a wall is the sum of flexural and shear distortion in both the uncracked and cracked zones.

$$\begin{aligned} \Delta &= \Delta_{m1} + \Delta_{s1} + \Delta_{m2} + \Delta_{s2} \\ &= V \frac{y_0^3}{3EI} + 1.2V \frac{y_0}{GA} + K \left[\frac{1}{Et} \left(-3P \frac{y_0}{\theta} \right) + \frac{1}{Gt} \left(-9P\theta \frac{y_0}{10} \right) \right] \\ &+ B \left[\frac{1}{Et} \left(6 \frac{P}{\theta} - 12 \frac{V}{\theta^2} \right) + \frac{1}{Gt} \left(13P \frac{\theta}{10} - 18 \frac{V}{5} \right) \right] \\ &+ C \left[\frac{1}{Et} (3Py_0) + \frac{1}{Gt} \left(6Py_0 \frac{\theta^2}{5} \right) \right] \\ &+ D \left[\frac{1}{Et} \left(6 \frac{V}{\theta} - 3P \right) + \frac{1}{Gt} \left(12\theta \frac{V}{5} - 6P \frac{\theta^2}{5} \right) \right] \\ &+ F \left[\frac{1}{Et} \left(\frac{6P\theta - 12V}{\theta^3} \right) + \frac{1}{Gt} \left(7 \frac{P}{5} - 24 \frac{V}{5\theta} \right) \right] \end{aligned} \quad (6.25)$$

From Eq. (6.25), it is clear that the lateral deflection for a specific lateral force is related to the wall aspect ratio and material parameter. The θ shown in above expression is the angle of the cracked zone which has been discussed in Section 2.2.1. Its value refers to the size of the dead zone which is directly affected by flexural tensile strength. To simplify the above expression, the following two parameters are defined:

$$\alpha = \frac{\Delta_{m2}}{\frac{V(h^3 - y_0^3)}{3EI}} \quad (6.26)$$

$$\beta = \frac{\Delta_{s2}}{\frac{1.2V(h - y_0)}{GA}} \quad (6.27)$$

Then lateral deflection is expressed as:

$$\Delta = \frac{Vy_0^3}{3EI} + V \frac{(h^3 - y_0^3)}{3EI} \alpha + \frac{1.2Vy_0}{GA} + 1.2V \frac{(h - y_0)}{GA} \beta \quad (6.28)$$

where E and G are Young's modulus and the shear modulus of the masonry, and I, A and h are the moment of inertia, shear area and the height of the wall, respectively.

The parameters α and β are functions of six parameters

$$\alpha = \alpha (P, V, l, t, h, f_t) \quad (6.29)$$

$$\beta = \beta (P, V, l, t, h, f_t) \quad (6.30)$$

where P and V are vertical and lateral force applied at the top of a wall, f_t is flexural tensile strength, and l, h, t are the length, height and the thickness of a wall, respectively. The term α and β are designated as flexural and shear deflection amplifying factors. The notable feature in Eq. (6.28) is that the cracking effect is considered by

factors α and β . This expression adequately characterizes the post-cracking behavior of a wall and can be expected to give sufficient information about deflection caused by cracking. It is easy to understand and accept since it is still based on fundamental approach. Thus, the basis to estimate lateral deflection with considering post-cracking behavior is to determine the values of both factors, α and β . They are functions of six parameters related to wall geometry, vertical and horizontal force, and flexural tensile strength. In engineering practice, it is desired to have the simplest methodology as possible, and still provide the best representation of the initial expressions. In the following section, both factors α and β will be discussed in detail to investigate how cracking affects their values.

6.3 Flexural and Shear Deflection Amplifying Factor α and β

6.3.1 Sensitivity Study of Flexural Tensile Strength f_t and Thickness t

As presented in the last section, the deflection can be expressed with a conventional formula modified to include the cracking effect by the terms, α and β . However, the formulas for α and β may be cumbersome for general use, and may be difficult to interpret in terms of the various parameters. The stiffness of a wall after cracking is directly related to its effective area, which obviously depends on the lateral force, vertical compressive stress and wall aspect ratio. Among six parameters as presented in the last section, α and β may be insensitive to the wall thickness, t , and flexural tensile strength, f_t . To determine the effect of thickness and flexural tensile strength on α and β values, a sensitivity study was done that is discussed below..

Based on the expressions for α and β , for given aspect ratios and maximum lateral forces, the numerical analyses are performed with two parts: using the same thickness but different flexural tensile strength, and using the same flexural tensile strength but

different thickness. The typical thickness values used in the studies are 8 and 16 inches, which are nominal values for two wythes and four wythes of normal size brick. Values for flexural tensile strength are taken to be 50 psi and 100 psi. Assumed aspect ratios represent a typical slender wall ($l/h = 0.5$) and a stocky wall ($l/h = 2.5$). Since the shear-to-normal stress ratio is interesting here, for the convenience, the constant 100 psi vertical compressive stress is used throughout the analyses. Representative curves showing relation between α and β and the ratio of τ/σ_v are shown in Fig. 6.3 to 6.6. To examine the interaction of flexural tensile strength and thickness, each figure includes two sub-plots based on different values of flexural tensile strength or thickness.

Without cracking, both α and β are equal to unity. After cracking, there is a difference in values of α and β for different values of flexural tensile strength. However, this difference decreases rapidly with increasing shear stress. For the larger aspect ratio ($l/h = 2.5$), when lateral force is 20% higher than the cracking load, the values of α and β with higher flexural tensile strength gets very close to those with lower flexural tensile strength. But, for the lower aspect ratio ($l/h = 0.5$), they are almost identical with different flexural tensile strength when the lateral force is 5% higher than the cracking load. From the experimental results presented before (14), the cracks were observed at 60% of the ultimate load and the lateral deflections at ultimate were 15 times that at initial flexural cracking. Thus, the influence of flexural tensile strength on both α and β values can be neglected, since it is not significant on the calculation of the lateral deflection for a cracked wall.

As shown in the Fig. 6.5 and 6.6, α and β have almost the same value for different thickness. For both α and β , plots are the same for stress ratios corresponding to a cracking initiation and beyond at a given thickness of 8 and 16 inches.

From the figures presented here, it has been noted that the effects of flexural tensile strength and thickness have no interaction. By using different flexural tensile

strengths of 50 and 100 psi, the effects of thickness are the same. On the other hand, it is difficult to perceive differences in the curves of α and β with different thicknesses of 8 and 16 inch. The conclusion from the observation, is that the expressions for α and β can be simplified by neglecting secondary effects of both thickness and flexural tensile strength.

6.3.2 Example of α and β Curves

Based on the above discussions, Fig.6.7 represents a relation of α and β values with the ratio of shear to vertical compressive stress. Having eliminated the effects of flexural tensile strength and the thickness, only four parameters (vertical force, P, lateral force, V, length, l, height, h) are relevant to this figure. Both terms have been determined from their exact expressions and are plotted versus stress ratio (τ/α_v) for different aspect ratios. Thus, four parameters affecting their values are included in this plot. It is shown that when the aspect ratio is small ($l/h = 0.5$), both α and β are very close. However, with larger aspect ratios, the difference between α and β increases. This reflects the common sense understanding that for a relative stocky wall, the lateral deflection is heavily dependent on the shear deformation, but for a slender wall, both shear and flexural deformation affect its lateral deflection. By using this figure, values of α and β can be obtained directly for a given wall geometry and stress ratio. This single plot can therefore suffice for defining α and β values for walls of all aspect ratios and stress ratios.

6.4 Comparison of Proposed Method with Conventional Method

The purpose of the proposed method presented in this chapter is to provide a reliable estimate of the lateral deflection of a cracked masonry wall element. It is of interest to examine the correlation between the proposed method and the current common-

ly used method for calculating lateral deflection. Although the proposed method can be expected to provide good estimates of lateral deflection, the conventional method can produce estimates from relatively simple input parameters.

The commonly used method for lateral deflection is defined by the following equation:

$$\Delta = V \frac{h^3}{3EI} + 1.2V \frac{h}{GA} \quad (6.31)$$

This equation is based on the assumption that the rotation at the top is free, but is restrained fully at the bottom. The flexibility of a wall is defined by both flexural and shear distortions. The obvious difference between the equation and the proposed method is that the equation considers the whole section as the effective area, and the cracking effects have not been included.

To study the difference in deflections, using this conventional equation and the method presented in this chapter, four different aspect ratios from 0.5 to 2.0 have been considered. Force–deflection relations are shown in Fig. 6.8 and Fig. 6.9. These curves have been plotted up to a lateral force equal to 1.5 times the cracking load. Each wall is subjected to the same vertical compressive stress of 100 psi. Flexural tensile strength is kept constant at 70 psi, and a thickness of all walls is 8 inches. A shear modulus equal to 202,000 psi, and a elasticity modulus equal to 505,000 psi are used throughout the analysis.

Clearly, before cracking, the two methods give the same results. However, after cracking, with increasing lateral force, the deflection from the proposed method are much larger than those from the conventional uncracked method. To demonstrate the effects of cracking on deflections of walls with different aspect ratios, the following

term, R_{Δ} , is used to express the ratio of deflections for the proposed method, Δ_{CR} , and for the conventional method, Δ_0 .

$$R_{\Delta} = \frac{\Delta_{CR}}{\Delta_0} \quad (6.32)$$

By using this equation, the results of deflections from both methods and the wall aspect ratios are presented in Table 6.1. For selected aspect ratios, the predicted deflections from the proposed method are about three times than those from the conventional method. Because cracked deflections are a direct result of the amount of lateral force (which was arbitrarily chose as 1.5 times the cracking load), the R_{Δ} values shown in Table 6.1 are also somewhat arbitrary. However, they do help illustrate the influence of cracking on deflections.

Consequently, neglecting cracking will result in a significant underestimate lateral deflections for a wall that is loaded past its cracking strength. Thus, the conventional method can not provide reasonable estimates of lateral deflection after cracking. However, it is still a relatively simple procedure for estimating deflections at early loading stages.

CHAPTER 7

CORRELATION BETWEEN PROPOSED METHOD AND EXPERIMENTAL WORK

7.1 Introduction

An analytical methodology for lateral strength and deflection of unreinforced masonry walls has been developed in previous chapters. In order to verify its accuracy and applicability, several tests performed at the University of Illinois at Urbana-Champaign are analyzed in this chapter. Results from test of unreinforced masonry walls under either monotonic or cyclic loading conditions are compared with the analytical numerical values from the proposed methodology.

For monotonic loading, the measured load-deflection relations of five walls tested by Epperson and Abrams (14) are directly compared with those predicted by the proposed method. In the case of cyclic loading, the behavior of three unreinforced masonry walls recently tested by Shari and Abrams (30) are used for the comparison. Based on the results of their experimental work, it is confirmed that the proposed method is applicable to cyclic loading when estimating lateral strength.

Good correlation is demonstrated by the comparisons between the results of experimental and analytical work. It has been shown that the proposed analytical procedure is able to provide a good estimate of lateral strength for a cracked wall subjected either monotonic or cyclic forces. In addition, for the monotonic loading case, the proposed method for estimating lateral deflections of cracked walls worked well for simulating the measured behavior.

7.2 Walls Tested with Monotonically Increasing Loads

7.2.1 Review of Experimental Work

Five unreinforced masonry walls were extracted from an existing building and were loaded with horizontal force to measure their ultimate in-plane shear strengths. The loading condition consisted of a constant vertical compressive stress simulating gravity loads, and an in-plane horizontal lateral force. The test walls were subjected to a different level of vertical stress, ranging from 76 psi to 143 psi (Table 7.1). The length-to-height ratios are very close for five walls from 1.3 to 1.9. The ultimate shear strength of the walls was defined to be the maximum in-plane lateral load divided by the gross cross sectional area.

During each test, it was observed that the initial stiffness of the walls was reduced by flexural cracking at the heel of the wall at moderate levels of horizontal loading. With increasing lateral force, horizontal cracks appeared in the central region of the test walls, which indicated a sliding of the masonry along the bed joints. Stress redistribution resulting from flexural cracking, increased the diagonal compressive stress near the toe of the walls. Finally, diagonal tension cracking occurred which was followed immediately by toe crushing. Failure modes were very similar for all five walls.

Lateral deflections at the top of each wall were measured relative to the test floor. By monitoring both extension and contraction of diagonally oriented displacement transducers, shear deformations were measured. A typical arrangement of displacement transducer is shown in Fig. 7.1. The shear strain was calculated based on the measured extension and contraction along the opposite diagonals. The shear modulus, G , was then calculated by dividing the measured gross shear stress by the calculated shear strain. An initial tangent shear modulus up to the initiation of flexural cracking was cal-

culated to be 195 ksi, and the secant shear modulus at the initiation of diagonal shear cracking was 167 ksi. These values are an average of the five test walls.

7.2.2 Comparison of the Results from Experimental Work and Proposed Method

By using the analytical procedure presented in Chapter 3, lateral strength of the test walls is evaluated. Material properties obtained by testing laboratory samples are used as input parameters. From the analytical results, all walls failed in compression either by diagonal splitting or toe crushing associated with flexural cracking and local sliding. The failure sequence was the same as that observed in each of the experiments. The predicted flexural cracking forces, and the predicted ultimate forces are shown in Table 7.2. As seen from the table, the cracking forces are nominally 60 percent of the ultimate lateral forces, which corroborates the experimental observation. The measured and predicted shear strengths in terms of τ_e and τ_a for all five walls are given in Table 7.3. By comparing both results, it is found that the proposed analytical procedure performs well.

To calculate the deflection by the method presented in Chapter 6, the material parameters that characterize the behavior of these walls need to be defined. The shear modulus and the modulus of elasticity are the necessary parameters. Based on the tests of a series of prisms, the average modulus of elasticity, E equal to 505 ksi is used in the analysis. The shear modulus, G , 167 ksi is considered to be a reasonable value to use, since it was measured after flexural cracking occurred in the walls, and is 0.33 times the assumed value of E .

Force-deflection behavior predicted by the proposed method is correlated with measured behavior in Figs. 7.2 to 7.4. Deflections were calculated by using Eq. (6.28) for various force increments. It is noted that before flexural cracking, the two curves

from calculation and test for each wall are in close agreement, since the proposed method in this range is based on an uncracked wall. After cracking, the two curves for each wall are still in close agreement.

Maximum deflections from experiment and the proposed method are listed in Table 7.4. Since the deflection is calculated for the given loading conditions, the calculated results presented in the table are based on the predicted maximum strength. It is noted that for wall E1 and wall E6, the results from the proposed method are about 40% larger than those from the experiment. The reason is that during the test, the stiffness of the two walls did not decrease rapidly by flexural cracking. This weak part of the correlation is that the maximum lateral deflection was not measured in the laboratory with any great accuracy. Because these tests were done in load control, it was impossible to control displacement for the post-peak region. In spite of the difference between experimental and calculated results, the predictions from the proposed method are generally reasonable and of acceptable accuracy for a few test walls. Therefore, it can be concluded that the proposed method is able to give a good representation of the post-cracking behavior for an unreinforced masonry wall.

7.3 Walls Tested with Cyclic Loads

7.3.1 Behavior of Walls Subjected to Cyclic Forces

In order to study the correlation between lateral capacity estimated by the proposed method and that measured for laboratory specimen, it is necessary to investigate the behavior of unreinforced masonry walls subjected to cyclic loads. If lateral strength and behavior under cyclic loading can be shown to be similar to that under monotonically increasing loads, then the analytical procedure developed in this study may be extended to the cyclic loading case.

Three unreinforced masonry walls were subjected to reversed cyclic lateral deflections. The length-to-height aspect ratio of the three walls were: 2.0, 1.5 and 1.0. The vertical compressive stress applied at the top of walls were ranged from 50 psi to 75 psi. To attempt to observe different failure modes, the wall with an aspect ratio of 2.0 was subjected to a vertical compressive stress of 75 psi, and the other two walls were subjected to 50 psi of lighter vertical stress.

The wall with an aspect ratio of 2.0 was relatively stocky. It failed in shear without flexural cracking. The crack patterns are shown in Fig. 7.5. A first stair-step diagonal crack was noted at a lateral force about 62% of the ultimate load. When the ultimate load was reached, the second diagonal crack was observed. By reversing the lateral force, an identical crack pattern as for the earlier half cycle was observed.

Since the second wall with aspect ratio of 1.5 was less stocky than the first wall, and was subjected to a light amount of vertical compressive stress, a flexural crack along the bottom bed joint was observed initially. Reversing the lateral force resulted in a flexural crack on the opposite side of the wall. The previously opened flexural crack simply closed because of vertical compressive stress. The observed crack pattern is shown in Fig 7.6. The failure of this wall was a result of diagonal tension. The third wall with an aspect ratio of 1.0, and the same vertical compressive stress of 50 psi, was controlled by flexural cracking at the base.

Ultimate lateral strengths in each direction of loading were quite similar. The previously developed crack did not influence the strength for the loading in other direction. From the observation that crack patterns were symmetrical, it can be inferred that the cyclic behavior may be uncoupled into monotonically increasing load components which can be representative of the behavior for the cyclic loading case. This conclusion suggests that the analytical procedure developed in this study for the lateral strength can be used for the cyclic loading case as well.

7.3.2 Comparison of the Lateral Capacity from Experimental Work and Proposed Method

To compare the measured lateral capacity with that predicted by the proposed analytical procedure, mechanical properties of the masonry were obtained based on experimental results. From prism tests, the mean value of compressive strength was 900 psi. The coefficient of cohesion of 100 psi and coefficient of friction of 1.0 were based on the results of in-place shear tests. To consider the flexural tensile strength, the load at which flexural cracking initiates is used to calculate values in accordance with different wall aspect ratios and vertical compressive stresses. As mentioned in the last section, the wall with an aspect ratio of 2.0 failed in shear with no flexural cracking. The flexural tensile strength for this wall is considered to be 150 psi. For the walls with an aspect ratio of 1.5 and 1.0, the flexural tensile strengths are calculated to be 125 psi. Diagonal tension strength is deduced to be 80 psi by measuring the cracking position and calculating the principal diagonal tension stress for the first wall (aspect ratio = 2.0). For the other two walls, the same diagonal tension strength is used. All of these material properties are listed in Table 7.5.

Using these material parameters, lateral capacities are predicted by the proposed analytical procedure. For the wall with an aspect ratio of 2.0, failure is a result of diagonal tension cracking which is the same as that observed in the experiment. The second and third walls fail as a result of flexural cracking. From the experiments, these two walls were governed by flexure with flexural cracking extending over two-thirds of the base. Thus, the behavior from the experiment and the proposed method are similar.

Analytical results are compared with the maximum lateral force of the first quarter cycle for the laboratory specimens. Both results of three test walls are shown in Table 7.6. Measured and predicted lateral forces are in terms of V_e and V_a . It can be seen that

the predicted capacities are about 85% of measured lateral forces. Good agreement is obtained with the experimental results. Thus, the proposed method can be used to estimate the lateral capacity for unreinforced masonry cracked walls subjected to reversed, cyclic loads.

CHAPTER 8

SUMMARY AND CONCLUSIONS

8.1 Summary

An analytical method for estimating lateral strength and deflection of in-plane unreinforced masonry walls has been developed in this study. This method fundamentally differs from the conventional approach in that the post cracked behavior has been considered. The feasibility of this method has been verified by correlation with experimental results. The general applicability of the method is introduced through tabulated values of lateral strength corresponding to various material parameters and wall aspect ratios.

Based on experimental observations discussed in Chapter 1, an analysis method for determining stress fields with considering the cracking effect is developed. All shear transfer across cracked masonry is neglected. By considering masonry to be linear in compression, closed-form expressions are derived for stresses at any location within the plane of a cracked wall. Calculated stress distributions for a sample wall are correlated with the results of finite element analyses.

Expressions for normal and shear stresses including the cracking effect provide the basis for the evaluation of lateral strength. The possible failure modes in an unreinforced masonry wall: flexural cracking, shear sliding, diagonal tension and compression failure including diagonal splitting and toe crushing are discussed and the relevant failure criteria are proposed. Then, an analytical procedure is developed for estimating lateral strength by including all of these failure modes. Using the proposed procedure, summary curves representing the relation between lateral strength and vertical compressive stress are developed.

In order to demonstrate the effects of different material parameters on the shear strength, a parametric study is presented by considering the different values of tensile strength, compressive strength, coefficient of friction, cohesion and diagonal tension strength. From the results of this study, it has been shown that once the specific failure mode resulting in the limit state of a wall is determined, then lateral strength only relies on the material parameter related to this mode.

Based on the analytical procedure, a strength table related to the various material parameters, aspect ratios and vertical compressive stress are presented. This table is convenient for using because it requires but simple input and provides rational results.

A method to calculate lateral deflection by considering the post cracked behavior is developed in this study. According to the assumption that masonry is linear in compression, the shear and flexural deflections constituting the top-deflection are analyzed separately, and then added to give the total deflection. The proposed method is simplified by using shear and flexure amplifying factors. The values of these factors are related directly to the extension of flexural cracking. Since the shear strain varies with the change of the effective area towards the base, the expressions of the factors are complicated. Through a sensitivity study of the relevant parameters, a simple, single diagram is developed for shear and flexure amplifying factors. By using these two factors, lateral deflection can be calculated by using familiar, but modified expression that includes the cracking effect.

With the use of the proposed analytical procedure for strength and deflection, the analytical results for several unreinforced masonry wall element under either monotonic or reversed cyclic loading are compared with the corresponding test data. Good correlation is demonstrated by these comparisons.

8.2 Conclusions

As seen from the comparisons between the analytical and experimental results, the proposed evaluation procedure for lateral strength and deflection performs satisfactorily by considering the post cracked behavior. Stiffness and strength of unreinforced walls under monotonically increasing loads are closely simulated. For the cyclic loading case, the same procedure for lateral strength can be applied because tests have shown that the cyclic behavior can be uncoupled into separate monotonically loading components.

The use of the analytical procedure make it possible to account for the nonlinear lateral behavior of a cracked wall, though a linear stress-strain relation is assumed for compression. The proposed procedure evaluates wall strength based on mechanical properties of masonry at a point. Thus, results from a NDE method such as the in-place shear test may be extrapolated even though a wall is cracked.

Based on the results in this study, the following conclusions can be drawn:

- (1) Predictions of the lateral force-deflection behavior under monotonic loading by the proposed analytical procedure match closely with experimental results.
- (2) The analytical procedure can provide good estimates of cracking development through the loading history.
- (3) By neglecting the shear stress transfer across the cracked masonry, redistributed stresses on the decreasing effective area provide a good correlation with observed phenomenon.
- (4) The strength criteria used in this study are sufficient to represent the possible failure modes. The cracking sequence governed by these criteria is correlated with the results of experimental work.

- (5) Lateral deflection of a cracked wall can be estimated using a conventional linear formula modified with parameters to account for cracking effect.
- (6) Lateral strength of a wall depends on its various material parameters, but the specific failure mode is only related to the relevant strength parameters. Once the specific failure mode is known, the strength evaluation can be made by using the associated failure criterion.

8.3 Recommendations for Further Research

Further extensions of the research are:

- (1) The approach developed in this study should be extended to model load–deflection behavior for cyclic loading. Estimates of lateral strength based on the proposed evaluation procedure need to be confirmed with additional laboratory test data, particularly from walls subjected to reversed cyclic loads.
- (2) The shear stress redistribution after sliding needs to be studied in order to develop a comprehensive expression that includes effects of local sliding.
- (3) The stiffness reduction and the corresponding stress redistribution resulting from the initial diagonal tension cracking should be study further.
- (4) A nondestructive test for measuring true diagonal tension strength needs to be developed so that estimates of lateral capacity can be more rational and accurate.
- (5) By considering post–cracking effects, an analytical procedure for estimating lateral strength of L–shaped and T–shaped walls needs to be developed.

REFERENCES

1. Abrams, D. P., and Xu, W., "Evaluation of In-Plane Shear Resistance of Cracked, Unreinforced Brick Walls", Proceeding of the 9th Intentional Brick/Block Masonry Conference, Vol. 1, pp. 260-267, Berlin, Germany, Oct. 1991.
2. Abrams, D. P. "Strength and Behavior of Unreinforced Masonry Elements", Proceeding of Tenth World Conference on Earthquake Engineering, Madrid, Spain, July, 1992.
3. Abrams, D. P., "Masonry as a Structural Material", ASCE Material Congress, Atlanta, Georgia, Aug. 1992.
4. Abrams, D. P., and Epperson, G. S., "Evaluation of Shear Strength of Unreinforced Brick Walls Based on Nondestructive Measurements", Proc. of Fifth Canadian Masonry Symposium, pp. 817-826, University of British Columbia, June, 1989.
5. Atkinson, R. H., Amadei, B. P., Saeb, S., and Sture, S., "Response of Masonry Bed Joints in Direct Shear", Journal of Structural Engineering, Vol. 115, No. 9, pp. 2276-2296, 1989.
6. "Building Code Requirements for Masonry Structures and Specifications for Masonry Structures", ACI 530-88/ASCE 5-88.
7. Chen, W. F., and Han, D. J., "Plasticity for Structural Engineering" Springer-Verlag, New York, 1988.
8. "Commentary on Buildings Code Requirements for Masonry Structures and Commentary on Specifications for masonry Structures", ACI 530-88/ASCE 5-88.
9. "Commentary to Chapter 24, Masonry of the Uniform Building Code", The Masonry Society, Boulder, Colorado, 1988.
10. Dawe, J. L., and Seah, C. K., "Analysis of Concrete Masonry Infilled Steel Frames Subjected to In-Plane Loads", Proc. of 5th Canadian Masonry Symposium, University of British Columbia, June, 1989.
11. Drysdale, R. G., and Hamid, A. A., "Tension Failure Criteria for Plain Concrete Masonry", Journal of Structural Engineering, Vol. 110, No. 2, pp. 228-244, Feb. 1984.

12. Drysdale, R. G., and Guo, P., "Compressive Strength for Concrete Block Masonry Based on the Properties of Constituent Materials", Proceeding of the 9th International Brick/Block Masonry Conference, Vol. 1, pp. 735-742, Berlin, Germany, Oct. 1991.
13. Dhanasekar, M., Page, A. W., and Kleeman, P. W., "The Failure of Brick Masonry under Biaxial Stresses", Proc. Instn. Civil Engineers, Part 2, pp. 295-313, June, 1985.
14. Epperson, G. S., and Abrams, D. P., "Nondestructive Evaluation of Masonry Buildings", Advanced Construction Technology Center, Report No. 89-26-03, University of Illinois at Urbana-Champaign, October, 1989.
15. Epperson, G. S., and Abrams, D. P., "Evaluating Lateral Strength of Existing Unreinforced Brick Masonry Piers in the Laboratory", Proc. of Fifth North American Masonry Conference, pp. 735-746, University of Illinois at Urbana-Champaign, June, 1990.
16. Essawy, A. S., and Drysdale, R. G., "Macroscopic Failure Criterion for Masonry Assemblages", Proc. of 4th Canadian Masonry Symposium, Vol. 1, pp. 263-277, June 1986.
17. Ganz, H. R. and Thurlimann, B. "Shear Design of Masonry Wall", Proc. of New Analysis Techniques for Structural Masonry, ASCE, 1985.
18. Guggisberg, R., and Thurlimann, B. "Failure Criterion for Laterally Loaded Masonry Walls", Proc. of Fifth North American Masonry Conference, pp. 949-954, University of Illinois at Urbana-Champaign, June, 1990.
19. Hilsdorf, H. K., "An Investigation into the Failure Mechanism of Brick Masonry Loaded in Axial Compression", Designing, Engineering and Constructing with Masonry Products. 1969.
20. Hamid, A. A., and Drysdale, R. G., "Behavior of Brick Masonry Under combined Shear and Compression Loading", Proc. of 2nd Canadian Masonry Symposium, pp. 51-64, Ottawa, Canada, June, 1980.
21. Jolley, R.H. "Shear Strength: A Predictive Technique for Masonry Walls", PhD Dissertation, Brigham Young University, Provo, UT, April 1976.

22. Kingsley, G. R., and Noland, J. " An Overview of Nondestructive Technique for Evaluation of Structural Properties of Brick Masonry ", Proc. of Second Joint UAS-ITALY Workshop, Aug. 1987.
23. Kingsley, G. R., Atkinson, R. H., and Noland J. L., " Nondestructive Evaluation of Masonry Structures Using Sonic Ultrasonic Pulse Velocity Technique ", Proc. of 4th North American Masonry Conference, Vol. 2, Aug. 1987.
24. Kariots, J. C., Ewing, R. D., and Johnson, A. W., " Methodology for Mitigation of Earthquake Hazards in Unreinforced Brick Masonry Buildings ", Proc. of US-PRC Joint Workshop on Seismic Resistance of Masonry Structures, May 1986.
25. Mayes, R. L., and Clough, R. W., " A Literature Survey-Compressive, Tensile, Bond and Shear Strength of Masonry ", No. EERC 75-15, Earthquake Engineering Research Center, University of California, Berkeley, California, June, 1975.
26. McNary, S. W., and Abrams, D. P., " Mechanics of Masonry in Compression ", Journal of Structural Engineering, Vol. 111, No. 4, pp. 857-870, April 1985.
27. Mann, W., and Muller, H., " Failure of Shear - Stressed Masonry - An Enlarged Theory, Tests and Application to Shear Walls ", Proc. of Brit. Ceramic Soc., No. 30, 1982.
28. Meli, R., " Behavior of Masonry Walls Under Lateral Loads ", Proc. of 5th World Conference on Earthquake Engineering, Rome, 1972.
29. Pfeifer, M., " A General Failure Theory for Masonry Walling Subjected to Arbitrary Loading ", Proc. of Fifth North American Masonry Conference Conference, Vol. 2, pp. 455-466, University of Illinois at Urbana-Champaign, June, 1990.
30. Page, A. W., " Finite Element Model for Masonry ", J. Structural Div., ASCE, Vol. 104, No. ST8, 1978.
31. Page, A. W., Samarasinghe, W., and Hendry, A. W., " The In-Plane Failure of Masonry- A Review", Proc. of The British Ceramic Society, Load-Bearing Brickwork (7), Sept. 1982.
32. Page, A.W. "A Parametric Study of the Behavior of Masonry Shear Walls", Proc. of 5th Canadian Masonry Symposium, University of British Columbia, June 1989.
33. Page, A.W., "The Biaxial Compressive Strength of Brick Masonry", Proc. Instn. Civ. Engrs, Part 2, Sept. 1981,

34. Page, A. W., "Influence of Material Properties on the Behavior of Brick Masonry Shear Walls", Proc. of 8th International Brick and Block Masonry Conference, Vol. 1, pp. 528-537, Dublin, Republic of Ireland, Sept. 1988.
35. "Post-Tensioned Masonry Structure", VSL Report Series, 2, Berne, Switzerland, 1990.
36. Riddington, J.R. and Ghazall, M.Z. "Hypothesis for Shear Failure in Masonry Joints", Proc. Instn. Civ. Engrs, Part 2, Mar. 1990.
37. Rouf, M.A. and Sawko, F. "Shear Stress Distribution in Masonry Elements", Proc. Instn. Civ. Engrs, Part 2, Mar. 1985.
38. Rahman, A. M., and Anand, S. C., "A Failure Criterion for Concrete Block-Mortar Joint in Masonry Walls", Proc. of 5th Canadian Masonry Symposium, pp. 79-89, University of British Columbia, June, 1989.
39. Shah, N., and Abrams, D. P., "Cyclic Load Testing of Unreinforced Masonry Walls", Advanced Construction Technology Center, University of Illinois at Urbana-Champaign, 1992.
40. Schneider, R. R., and Dickey, W. L., "Reinforced Masonry Design", Prentice-Hall, Englewood Cliffs, New Jersey, 1987.
41. Stokl, S., Hofmann, P. and Mainz, J. "A Comparative Finite Element Evaluation of Mortar Joint Shear Tests", Masonry International, Vol. 3, No.3, 1990.
42. Schwartz, J. and Thurlimann, B. "Design of Masonry Walls under Normal Force with Swiss STD. SIA V 177/2", Proc. of Fifth North American Masonry Conference, Urbana-Champaign, 1990.
43. Timoshenko, S. P., and Goodier, J. N., "Theory of Elasticity", McGraw-Hill, New York, 1987.
44. U.C.B.C Appendix Chapter 1 "Seismic Strengthening Provisions for Unreinforced Masonry Bearing Wall Buildings", June, 1990.
45. Yokel, F. Y. and Fattal, S. G., "Failure Hypothesis for Masonry Shear Walls", Journal of the Structural Division, Vol. 102, No. ST3, March 1976.

TABLES



Table 6.1 Comparison of Lateral Deflections Calculated by the Proposed Method and Conventional Method

l/h	Δ_{CR} (in)	Δ_0 (in)	R_{Δ}
0.5	0.161	0.058	2.77
1.0	0.125	0.042	2.97
1.5	0.133	0.043	3.09
2.0	0.152	0.048	3.16

Table 7.1 Summary of Wall Test Specimen Subjected to Monotonically Loads

Wall	Wall Area (in ²)	σ_v (psi)	f_t (psi)
E1	1600	126	104
E3	1870	143	62
E5	2170	81	66
E6	2170	76	70
E7	2170	93	54

Table 7.2 Calculated Lateral Capacity of the Test Walls

Wall	Cracking Load V_{CR} (kips)	Maximum Load V_m (kips)	$\frac{V_{CR}}{V_m}$
E1	72	109	0.66
E3	91	165	0.55
E5	91	135	0.67
E6	90	128	0.70
E7	91	153	0.59

Table 7.3 Comparison Between the Predicted and Measured Lateral Strength

Wall	Shear Strength τ_e (psi)	Shear Strength τ_a (psi)	$\frac{\tau_a}{\tau_e}$
E1	75	68	0.91
E3	88	88	1.00
E5	70	62	0.89
E6	69	59	0.86
E7	77	71	0.92

Table 7.4 Comparison Between the Predicted and Measured Maximum Lateral Deflection

Wall	Lateral Deflection Δ_e (in)	Lateral Deflection Δ_a (in)	$\frac{\Delta_a}{\Delta_e}$
E1	0.312	0.214	1.456
E3	0.277	0.291	0.952
E5	0.243	0.284	0.856
E6	0.216	0.157	1.375
E7	0.245	0.274	0.891

Table 7.5 Summary of Wall Test Specimen Subjected to Cyclic Loads

Wall	l/h	σ_v (psi)	f_t (psi)	σ_0 (psi)
1	2.0	75	150	80
2	1.5	50	125	80
3	1.0	50	125	80

Table 7.6 Comparison Between the Predicted and Measured Lateral Capacities

Wall	Shear Capacity V_e (kips)	Shear Capacity V_a (kips)	$\frac{V_a}{V_e}$
1	92	82	0.89
2	43	36	0.84
3	18	16	0.89

FIGURES

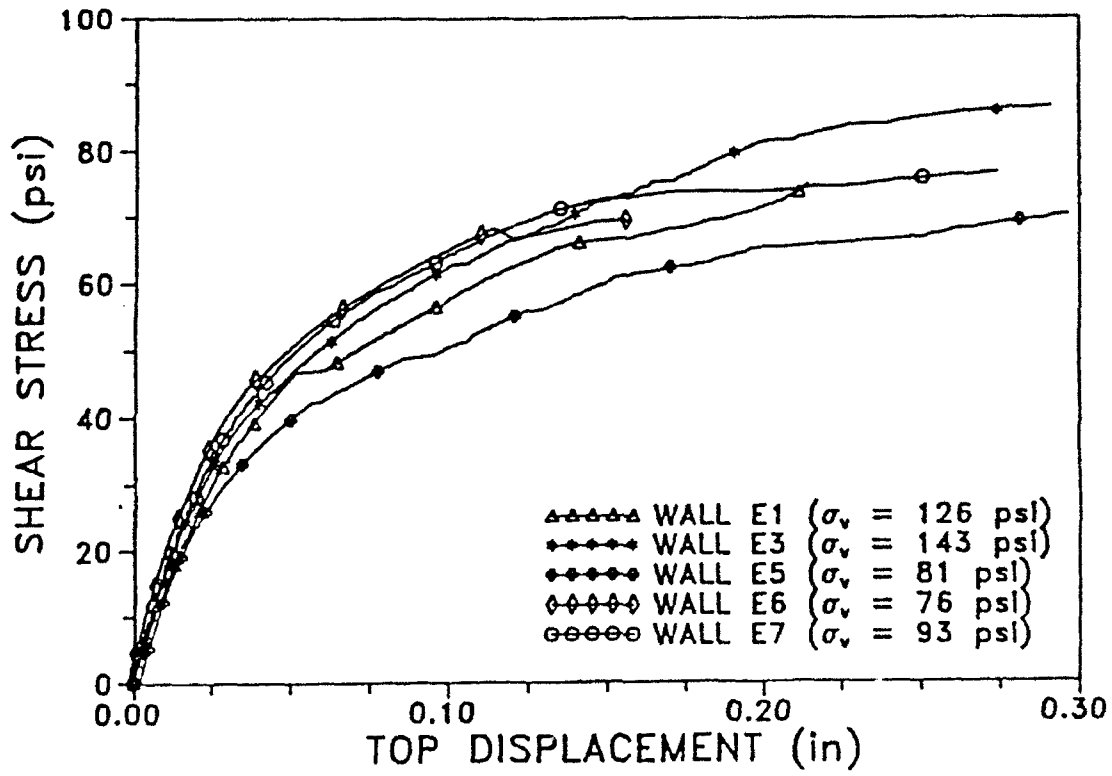


Fig. 1.1 Summary of Measured Top Level Displacement of the Test Walls Versus Shear Stress

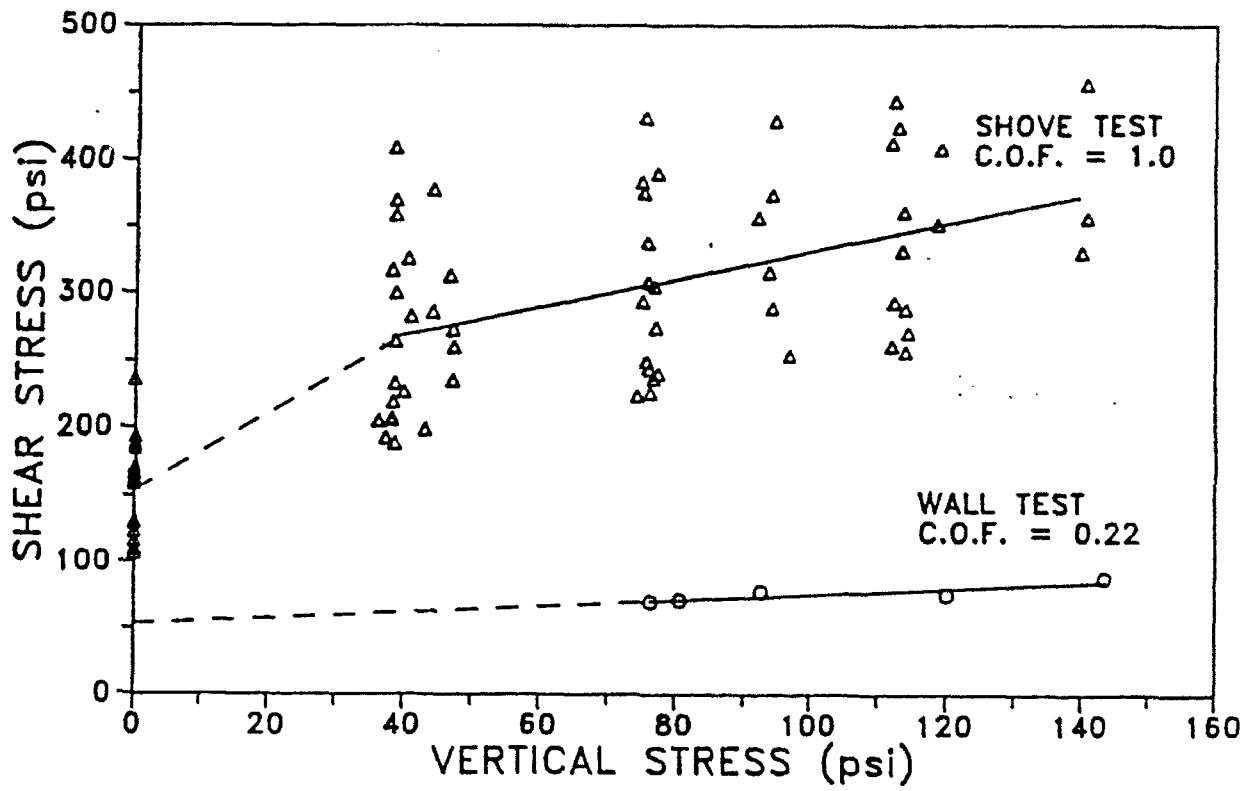


Fig. 1.2 Comparison Between In Situ Shear Strength Estimates and Measured Ultimate Shear Strength of Test Walls

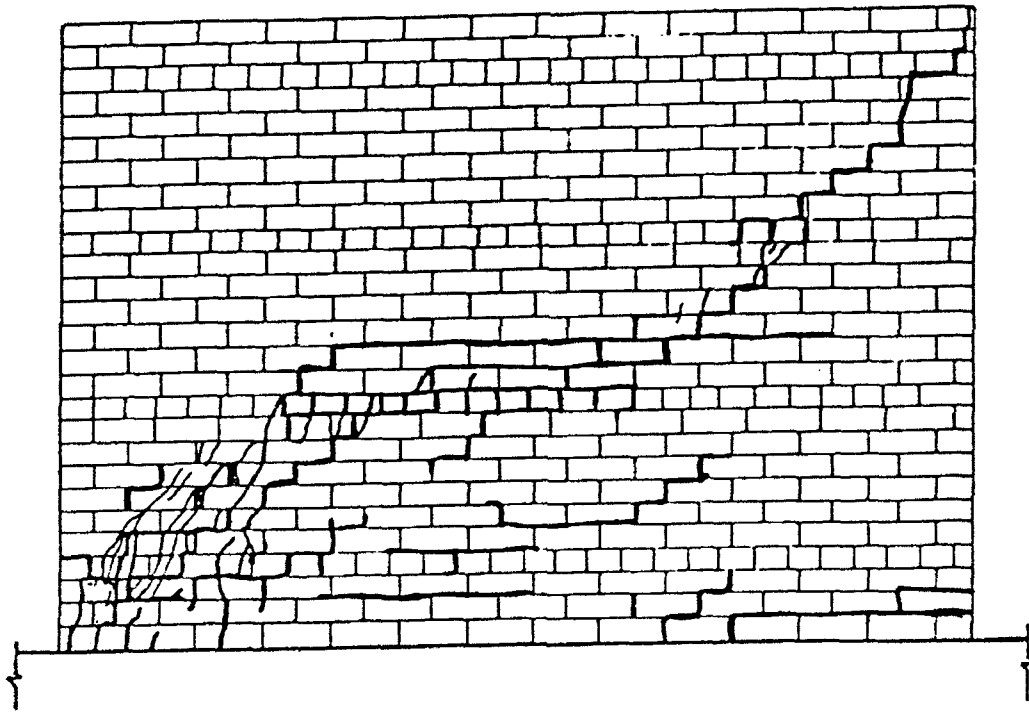


Fig. 1.3 Final Crack Patterns of a Typical Test Wall after Failure

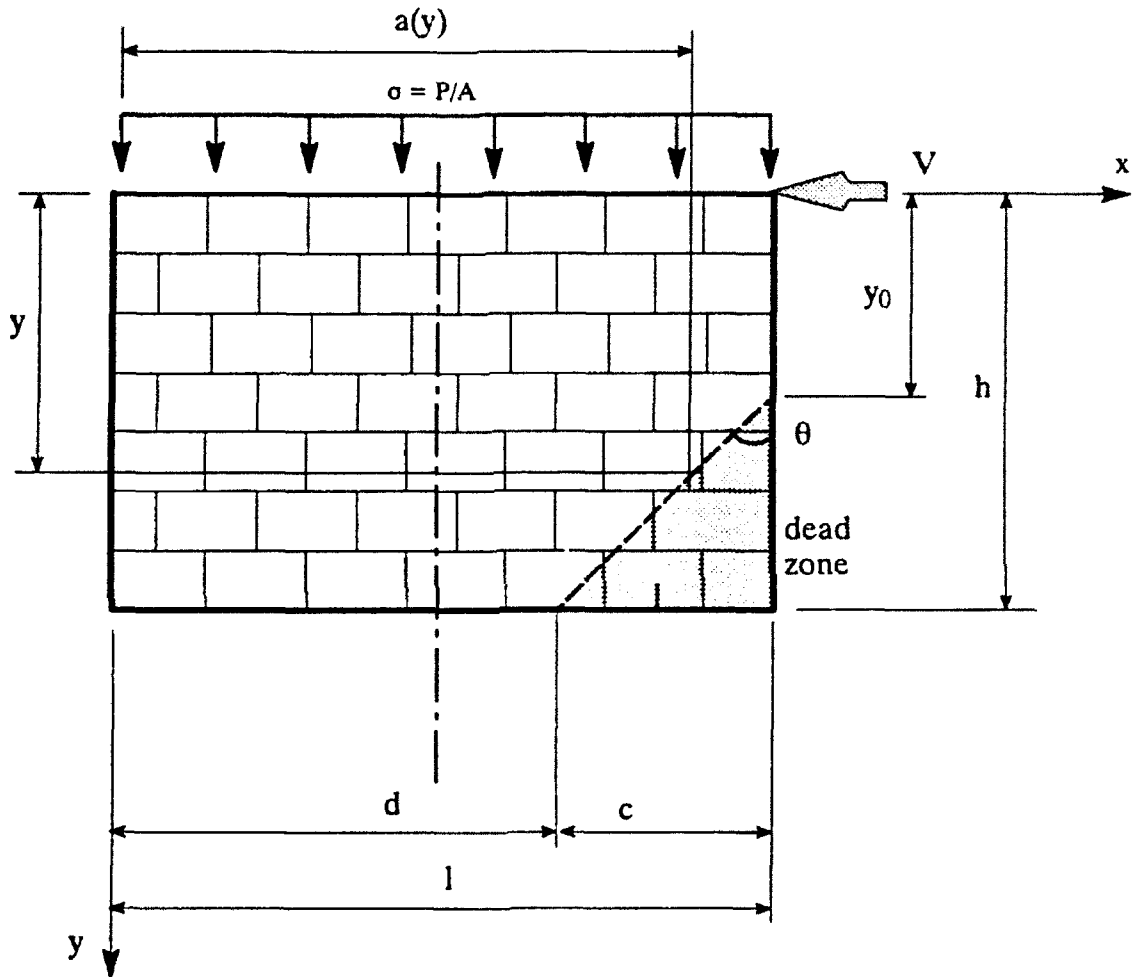


Fig. 2.1 Free Body Diagram of a Wall with "Dead Zone" Resulting from Flexural Tension Cracking

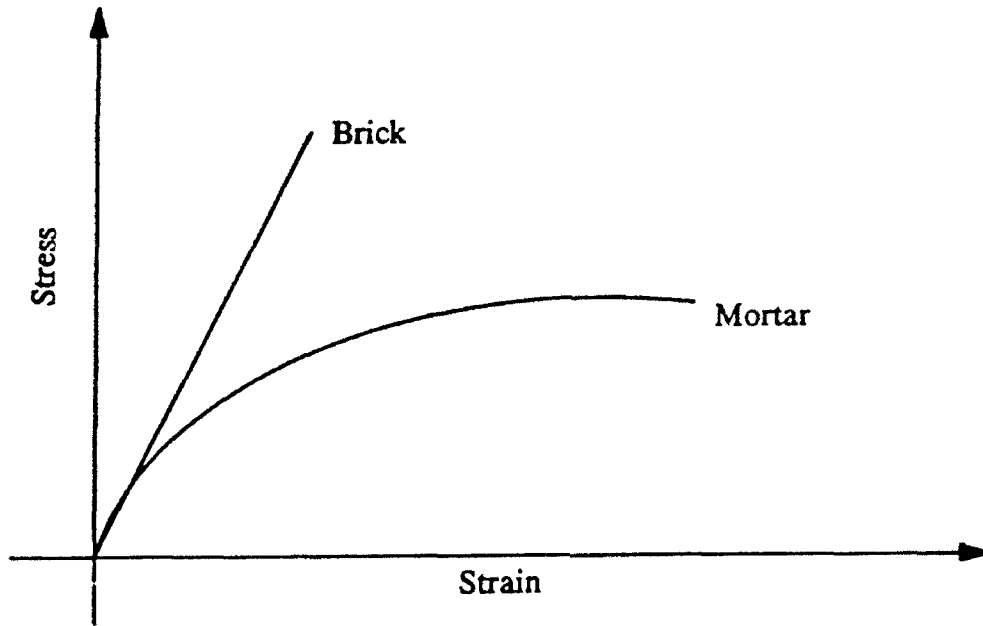


Fig. 2.2 Stress-Strain Relation for Brick and Mortar

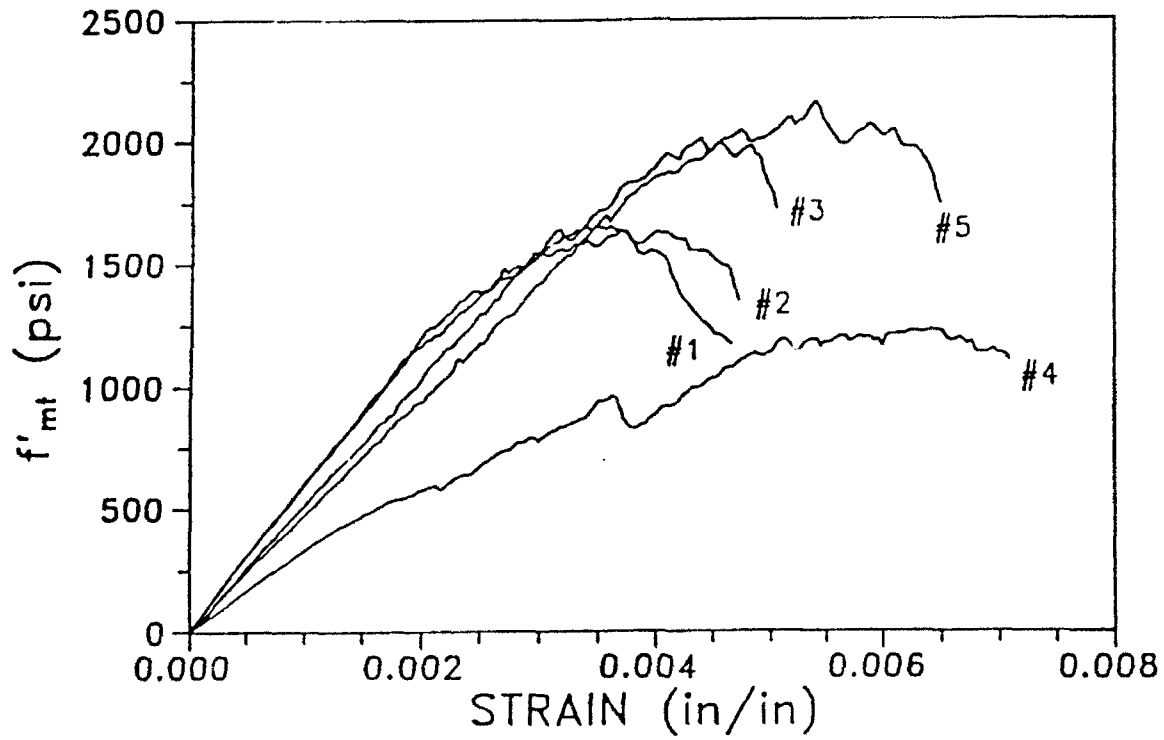


Fig. 2.3 Recorded Stress-Strain Curves for Prisms

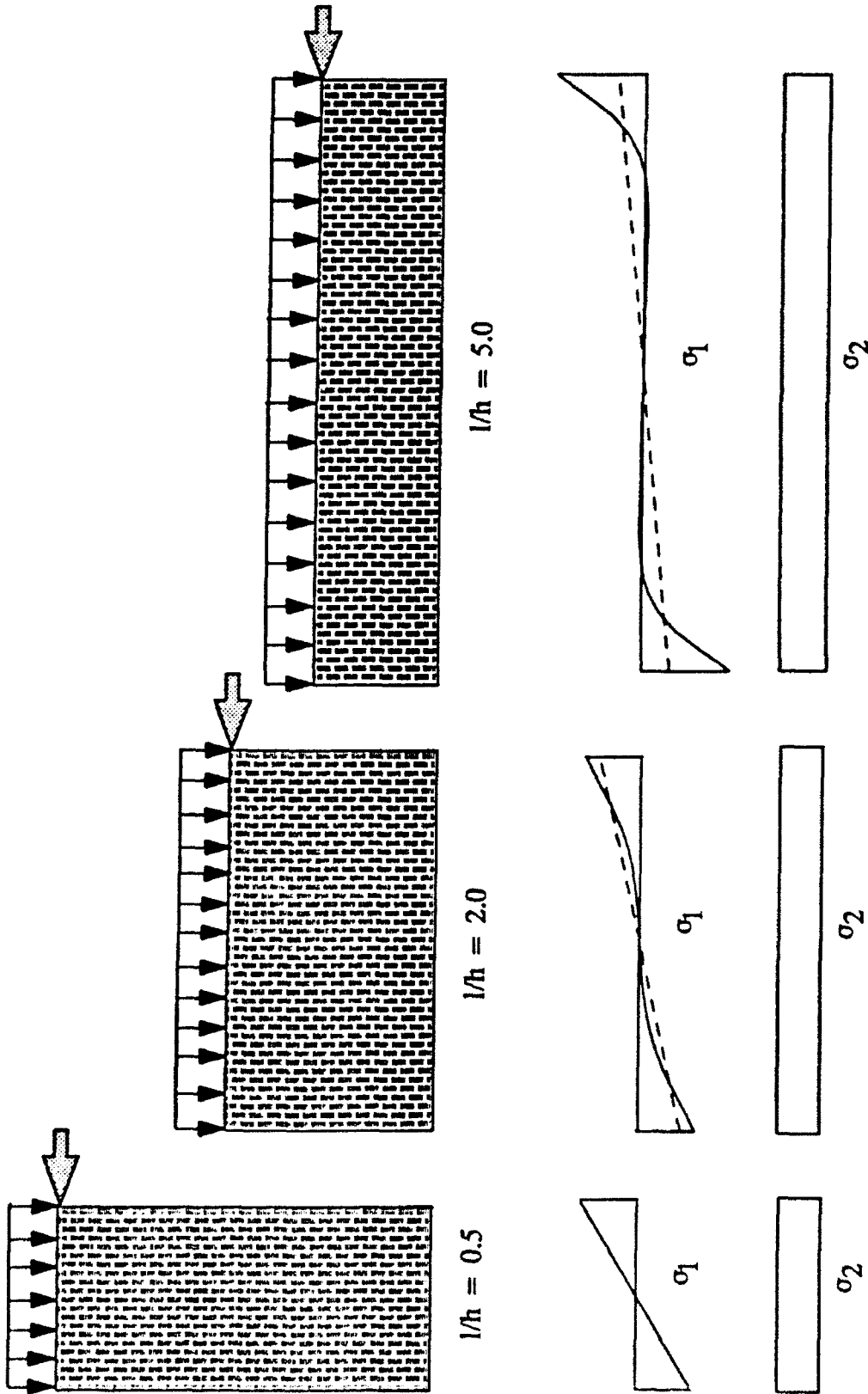


Fig. 2.4 Vertical Stress Distribution at Mid-height of a Wall for Different l/h Ratios

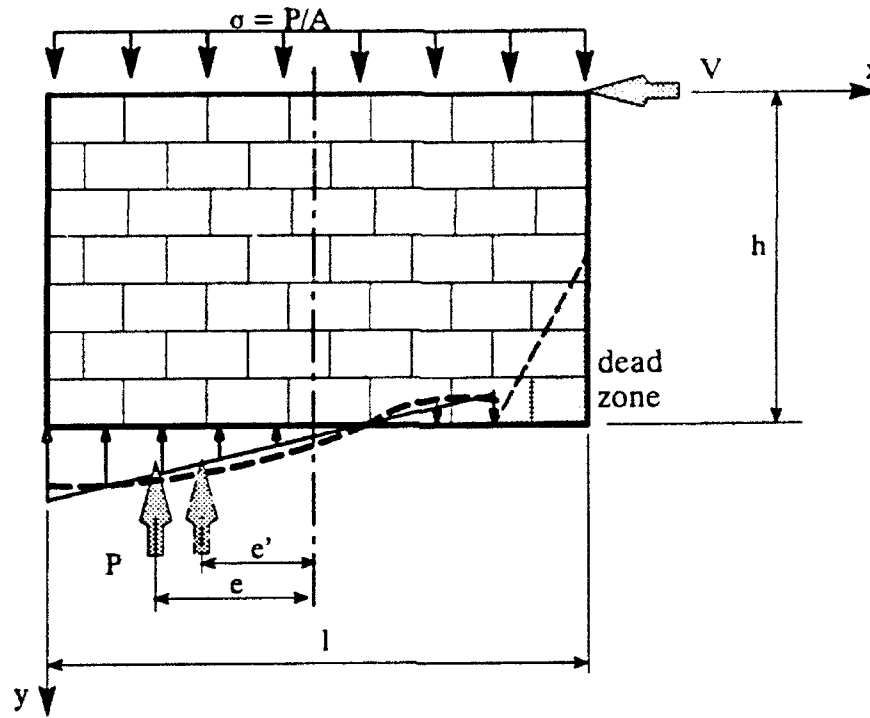


Fig. 2.5 Comparison of Different Vertical Stress Distribution

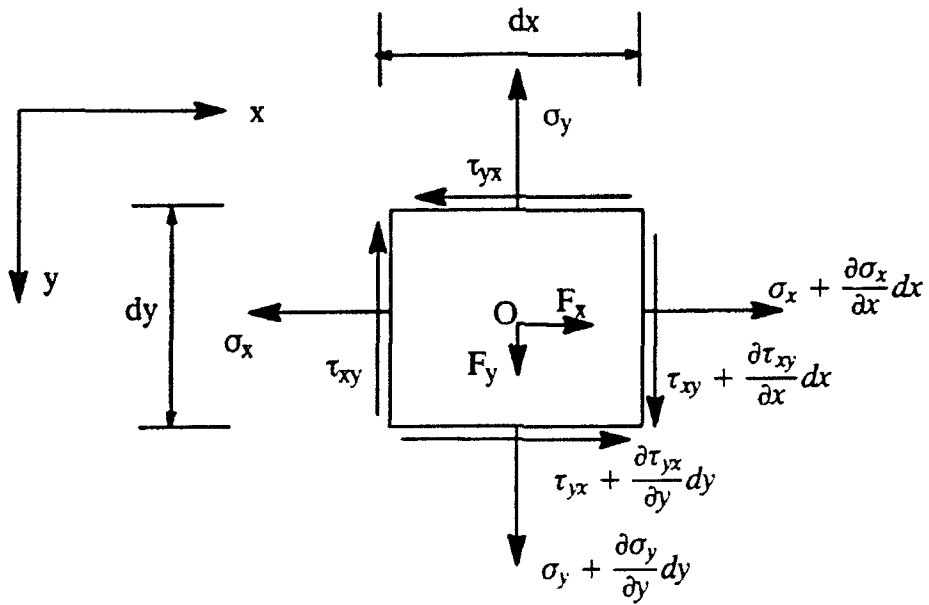


Fig. 2.6 Stress Element

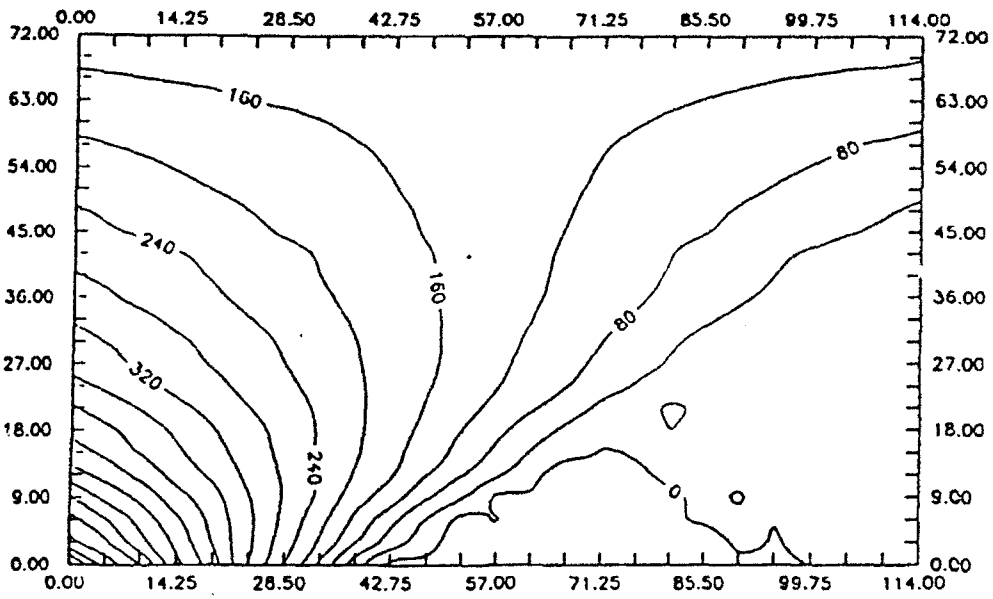


Fig. 2.7 Contours of Vertical Compressive Stress (psi)

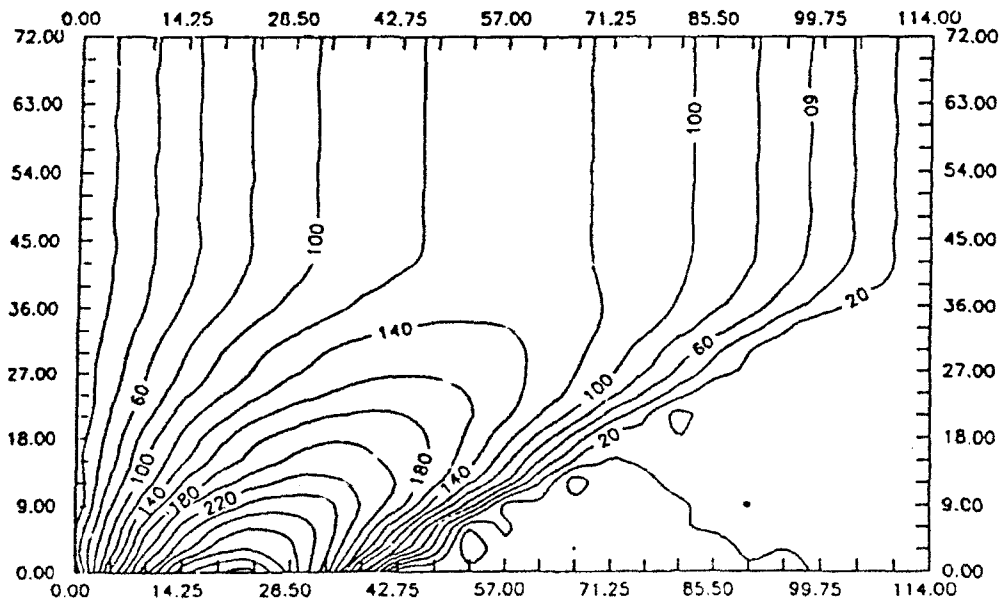


Fig. 2.8 Contours of Shear Stress (psi)

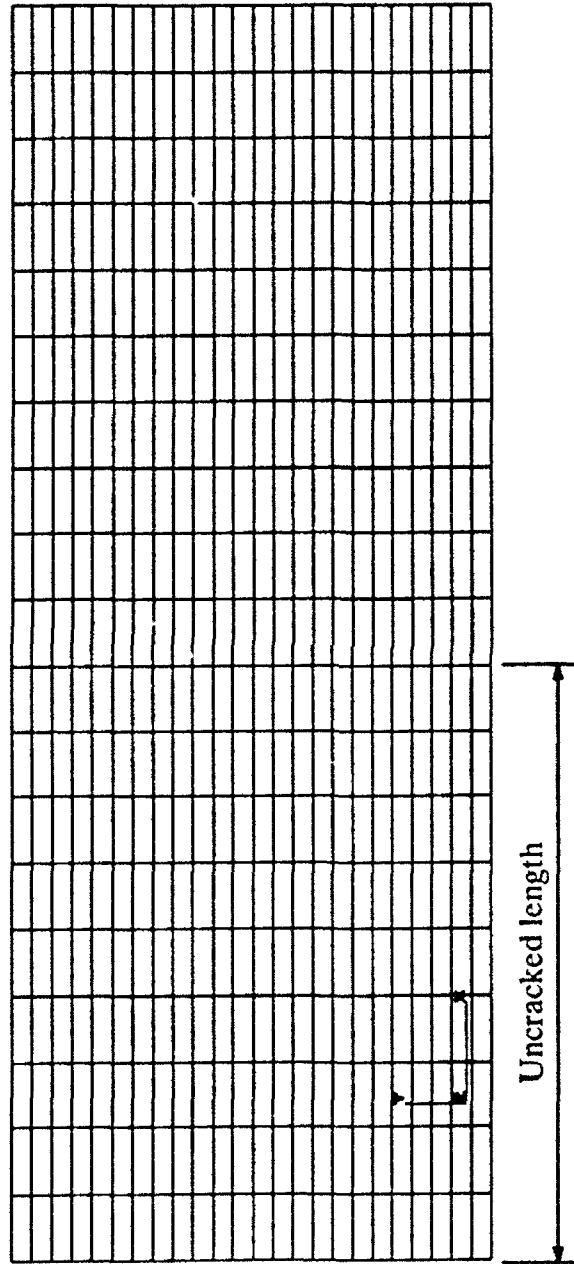


Fig. 2.9 Finite Element Mesh for Stress Analysis

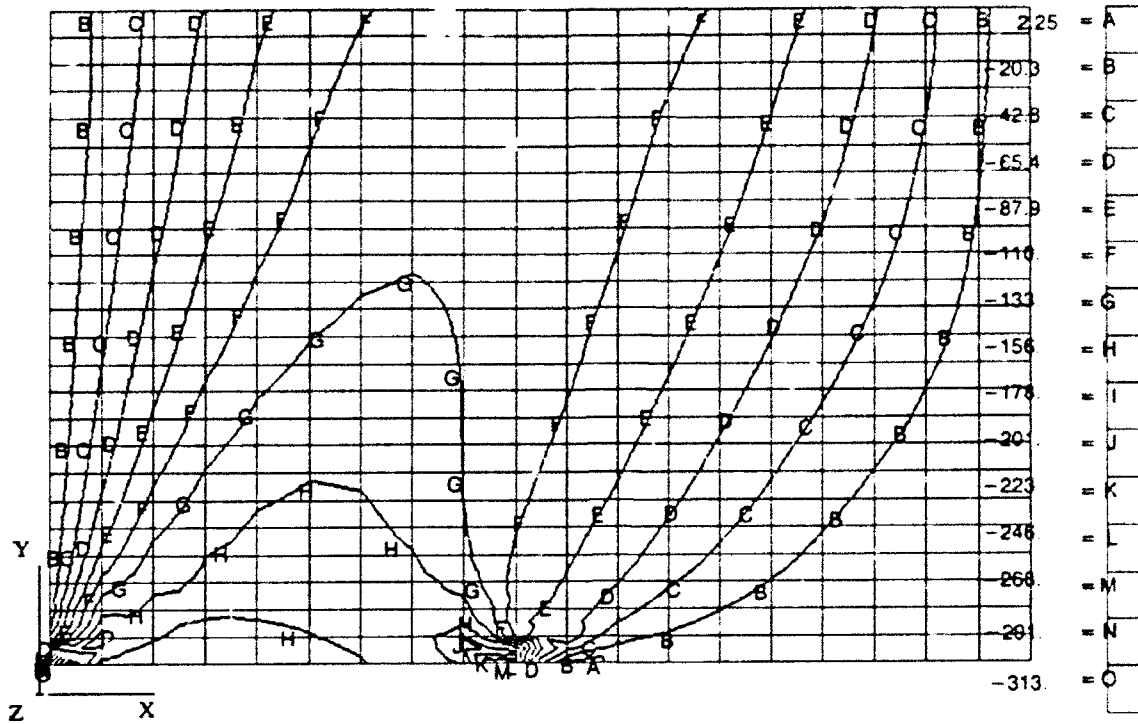


Fig. 2.10 Contours of Shear Stress (psi)

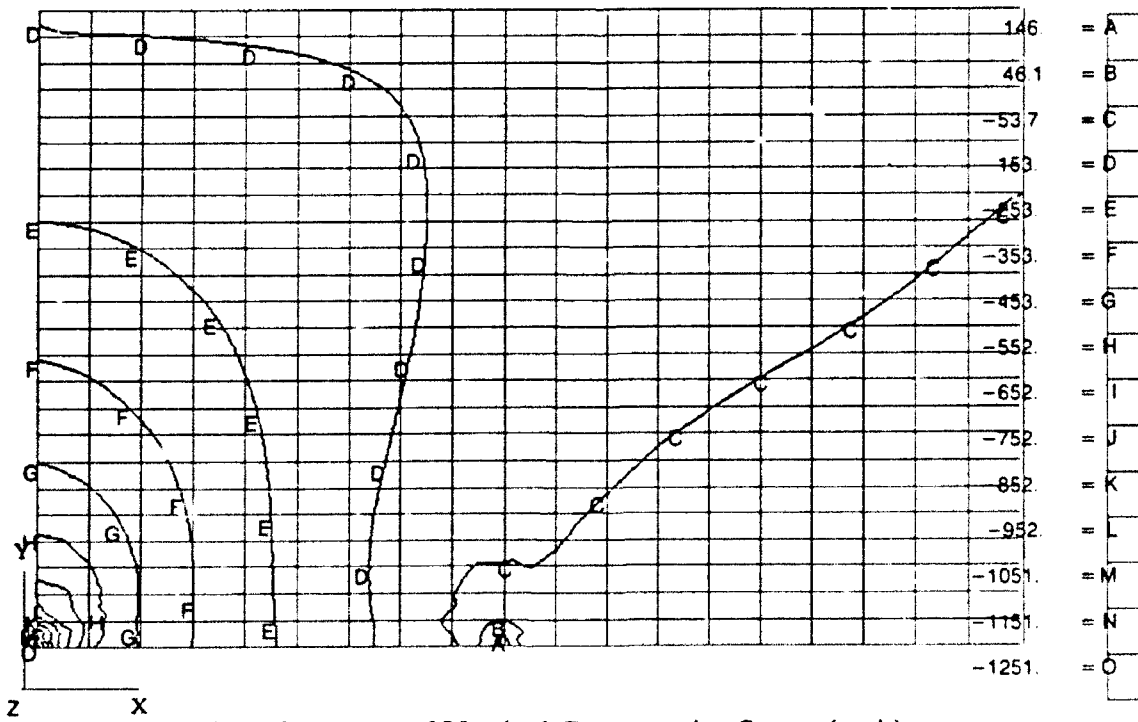


Fig. 2.11 Contours of Vertical Compressive Stress (psi)

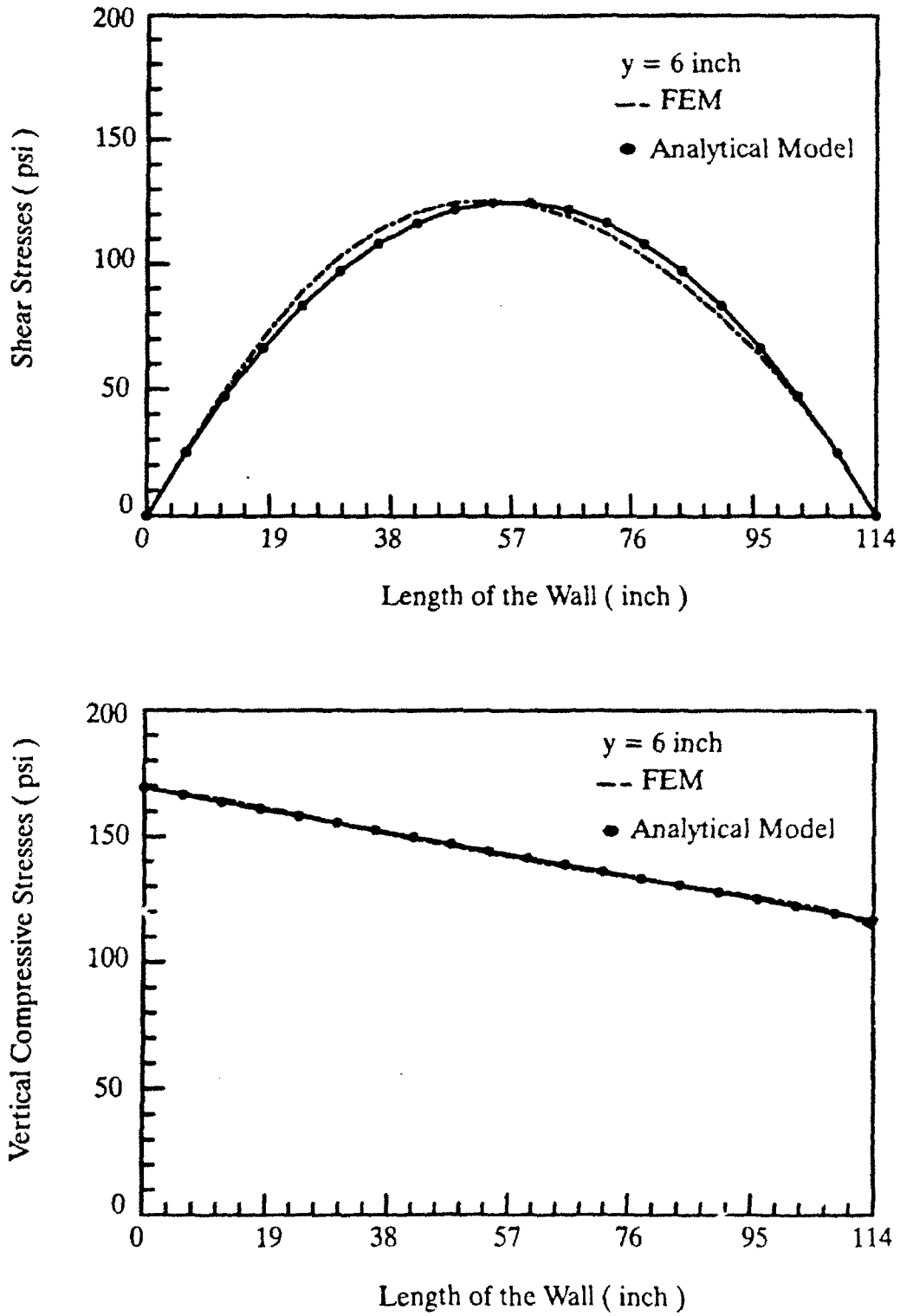


Fig. 2.12 Shear and Vertical Stress Distribution at Given Height of the Wall

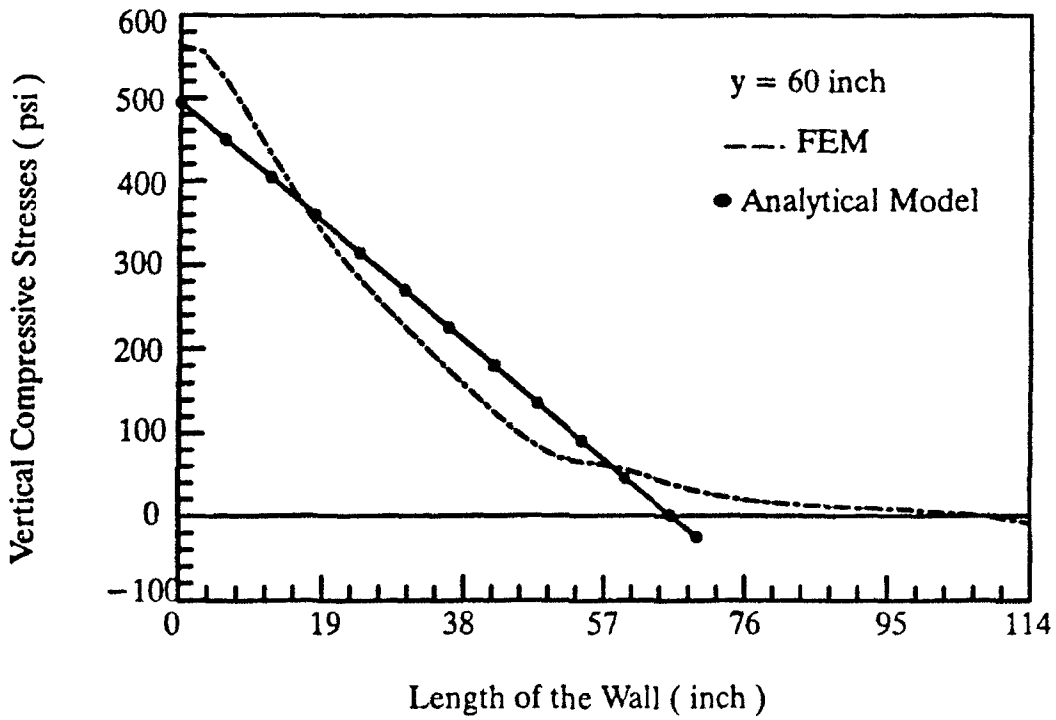
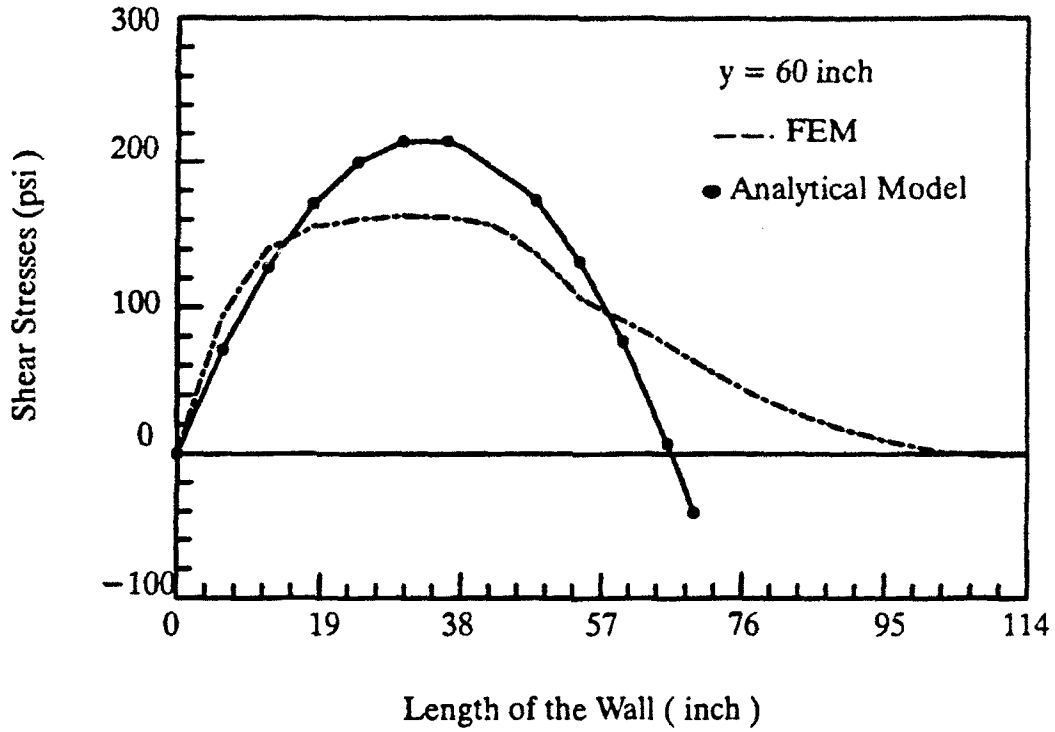
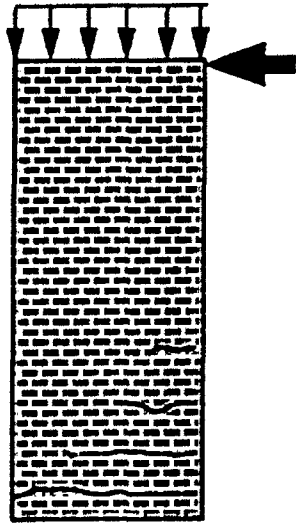
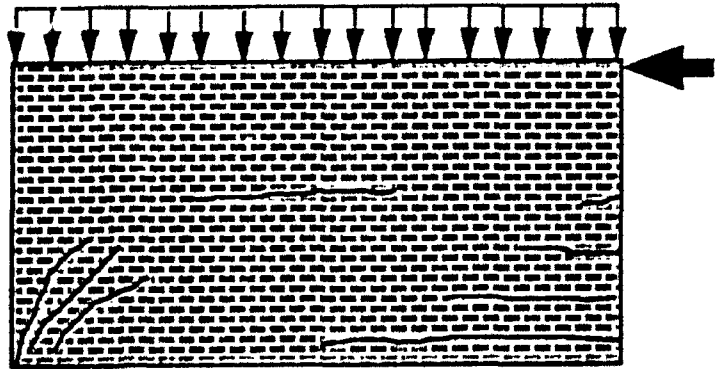


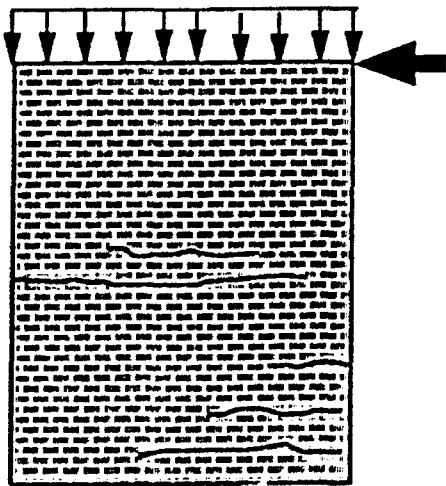
Fig. 2.13 Shear and Vertical Stress Distribution at Given Height of the Wall



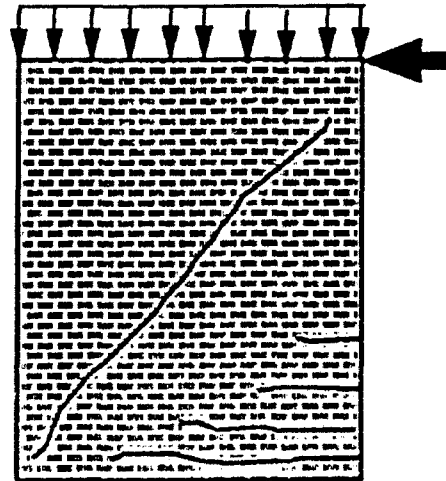
(a)



(b)



(c)



(d)

Fig. 3.1 Failure Modes

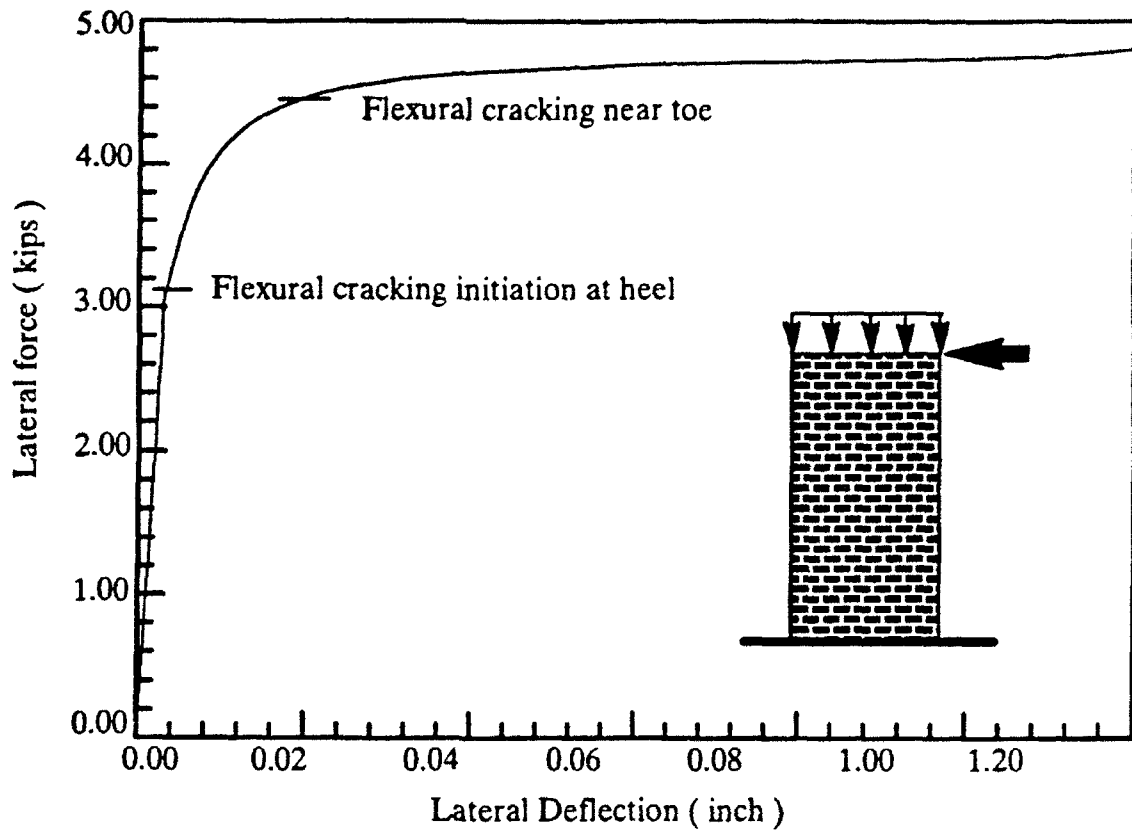


Fig. 3.2 Typical Load-Deflection Relation for Flexural Cracking Failure Mode

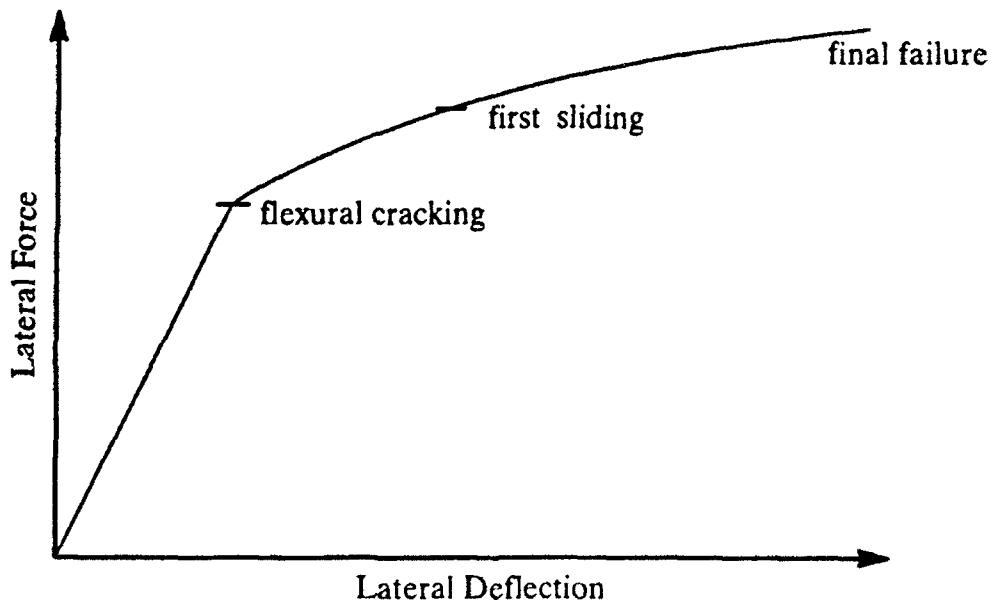


Fig. 3.3 Typical Load-Deflection Behavior for Cracked Wall

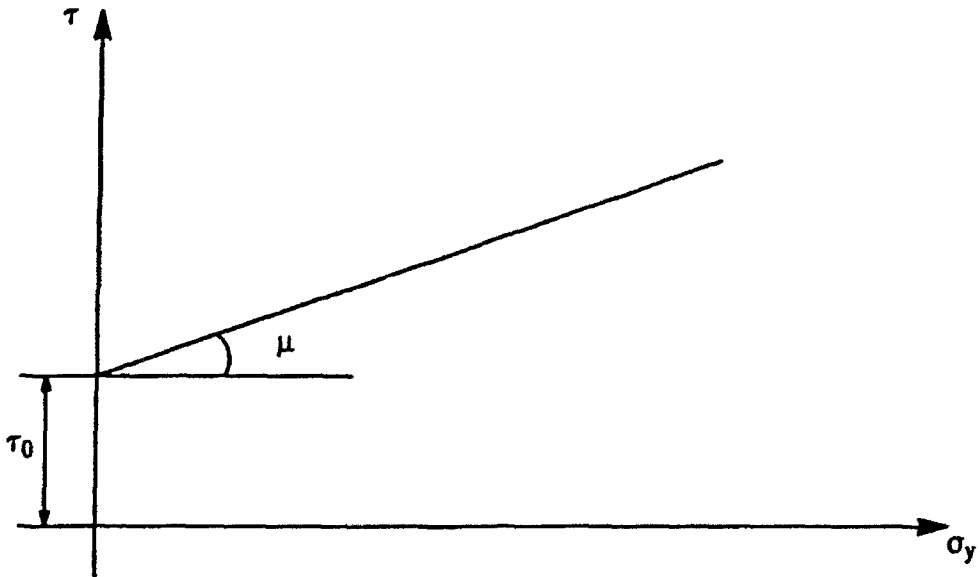


Fig. 3.4 Shear Sliding Failure Criterion

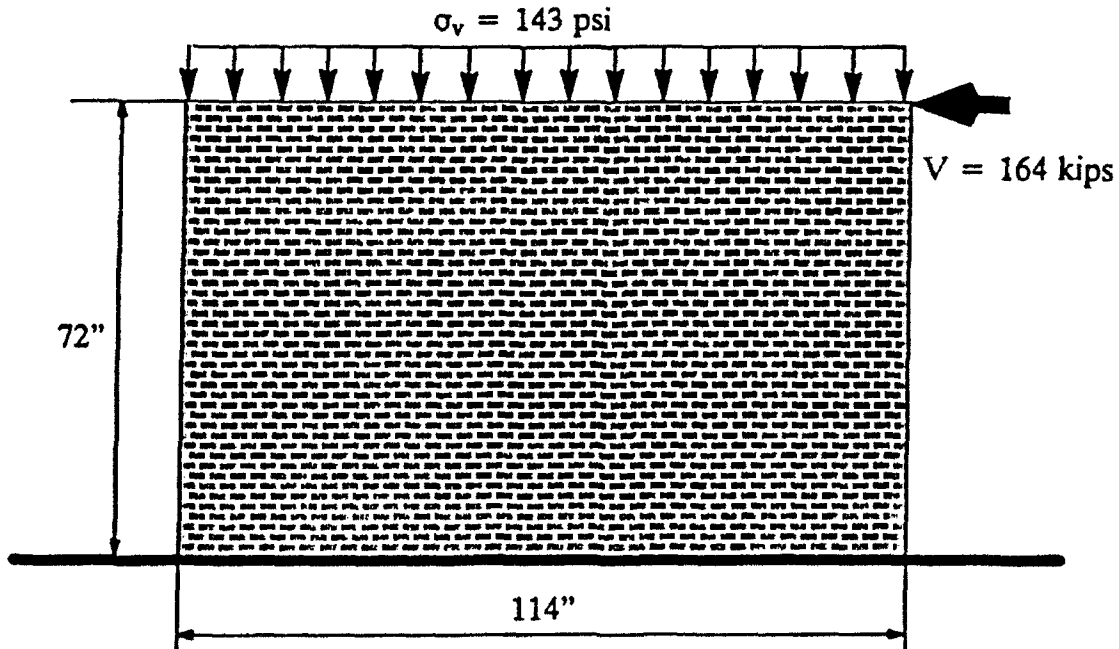


Fig. 3.5 A Sample Wall for Shear Sliding Index

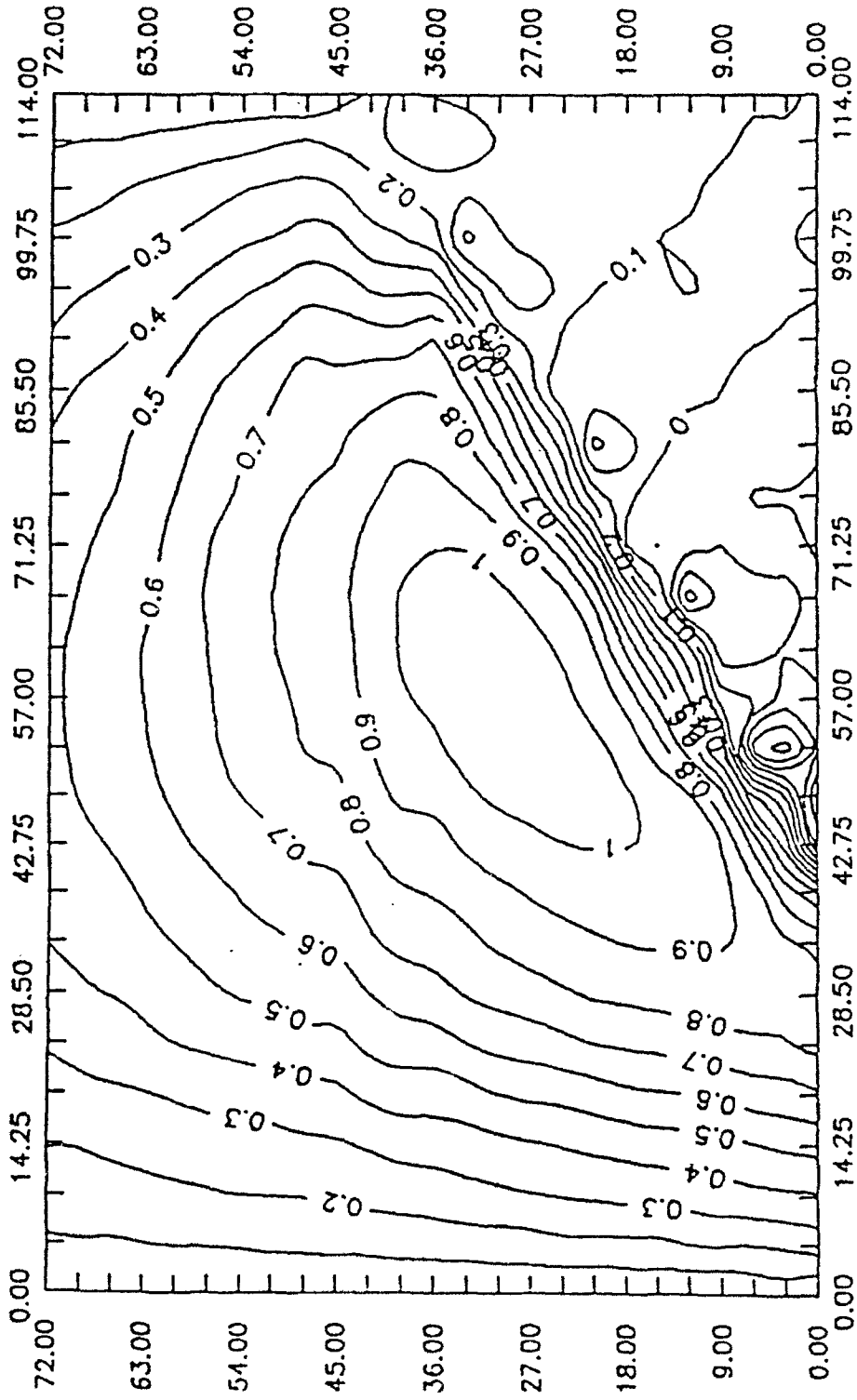
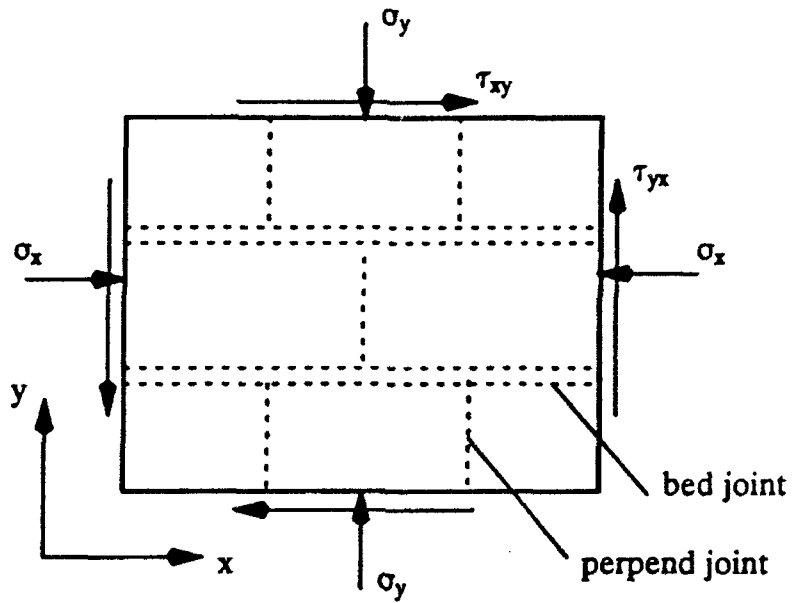
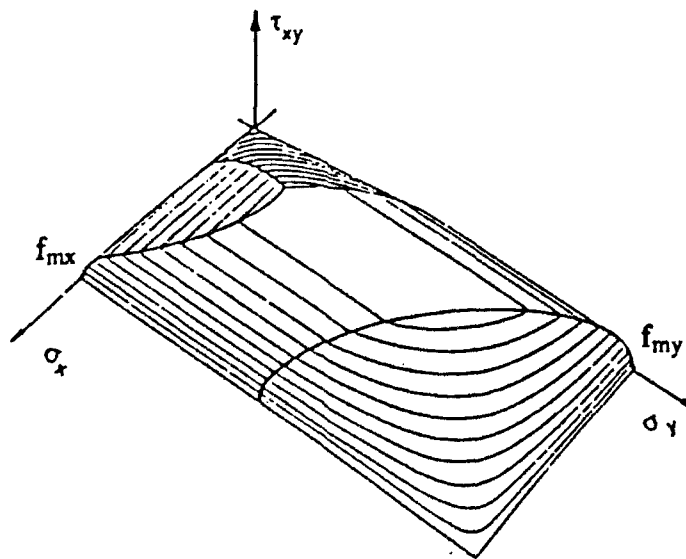


Fig. 3.6 Contour of Shear Sliding Index



(a) Masonry Element and Stresses



(b) Failure Criteria

Fig. 3.7 Masonry Element and Corresponding Failure Criteria

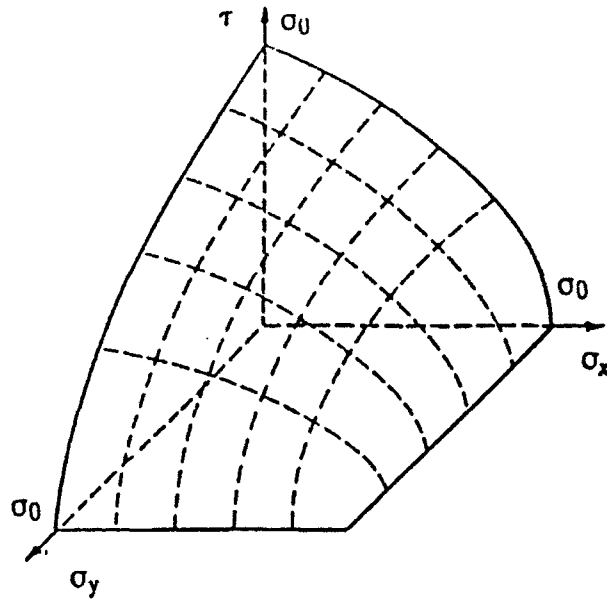


Fig. 3.8 Failure Surface for Diagonal Tension Cracking Mode

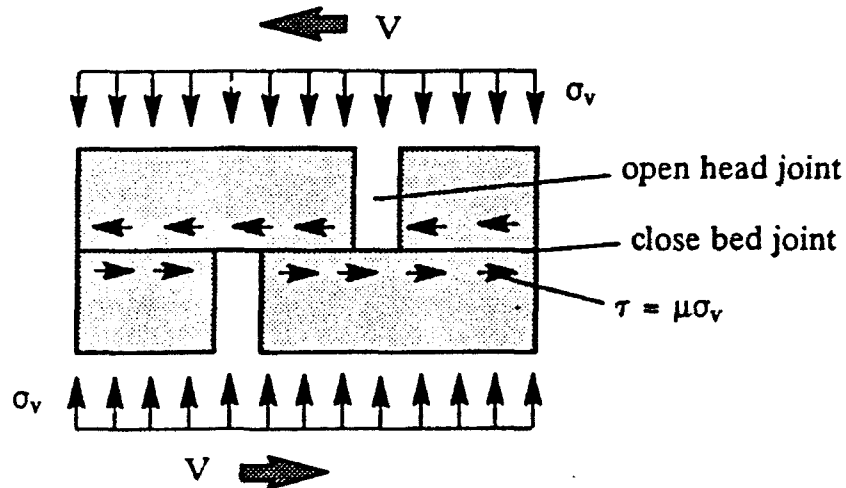


Fig. 3.9 Shear Transfer across Stair-Stepped Crack

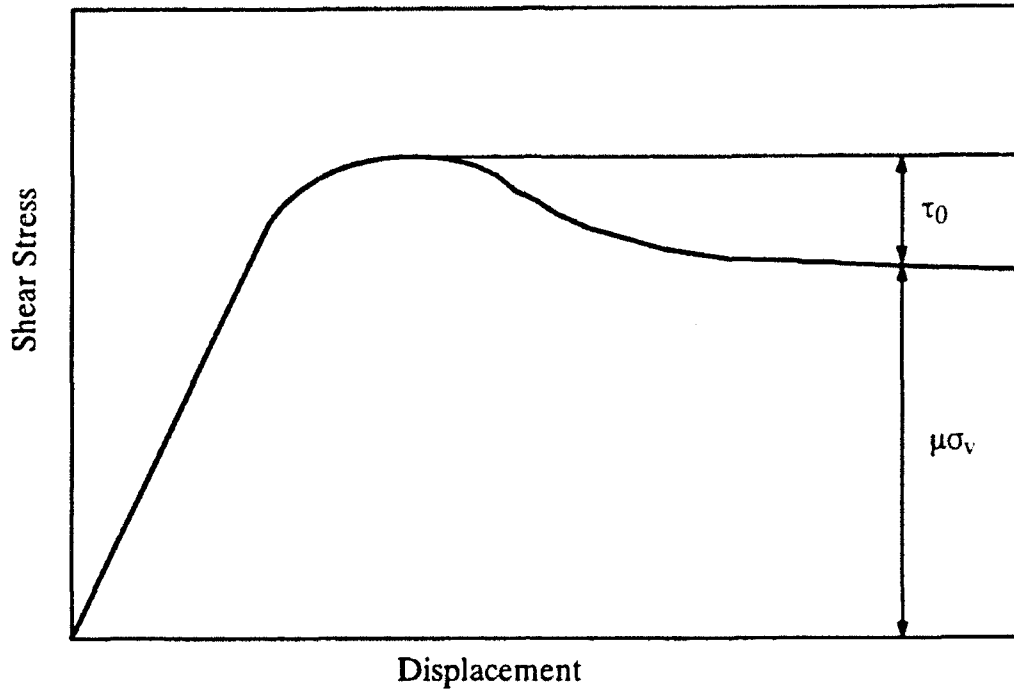


Fig. 3.10 Stress-Strain Relation for Shear after Sliding

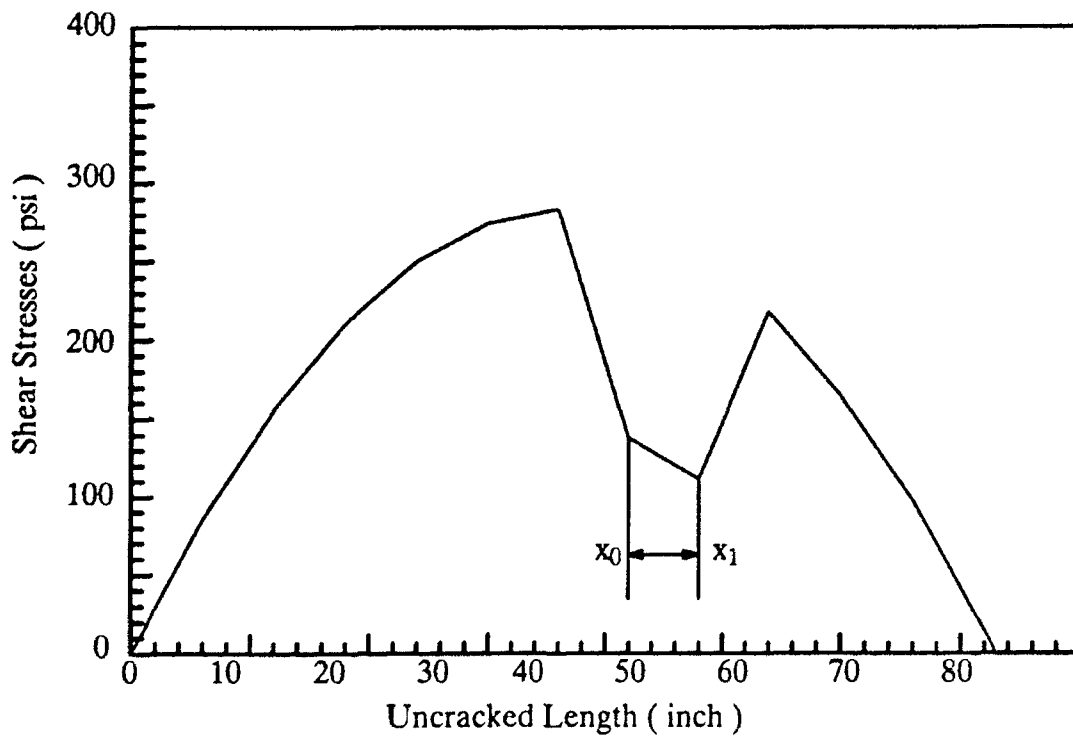


Fig. 3.11 Example of the Shear Stress Distribution after Sliding

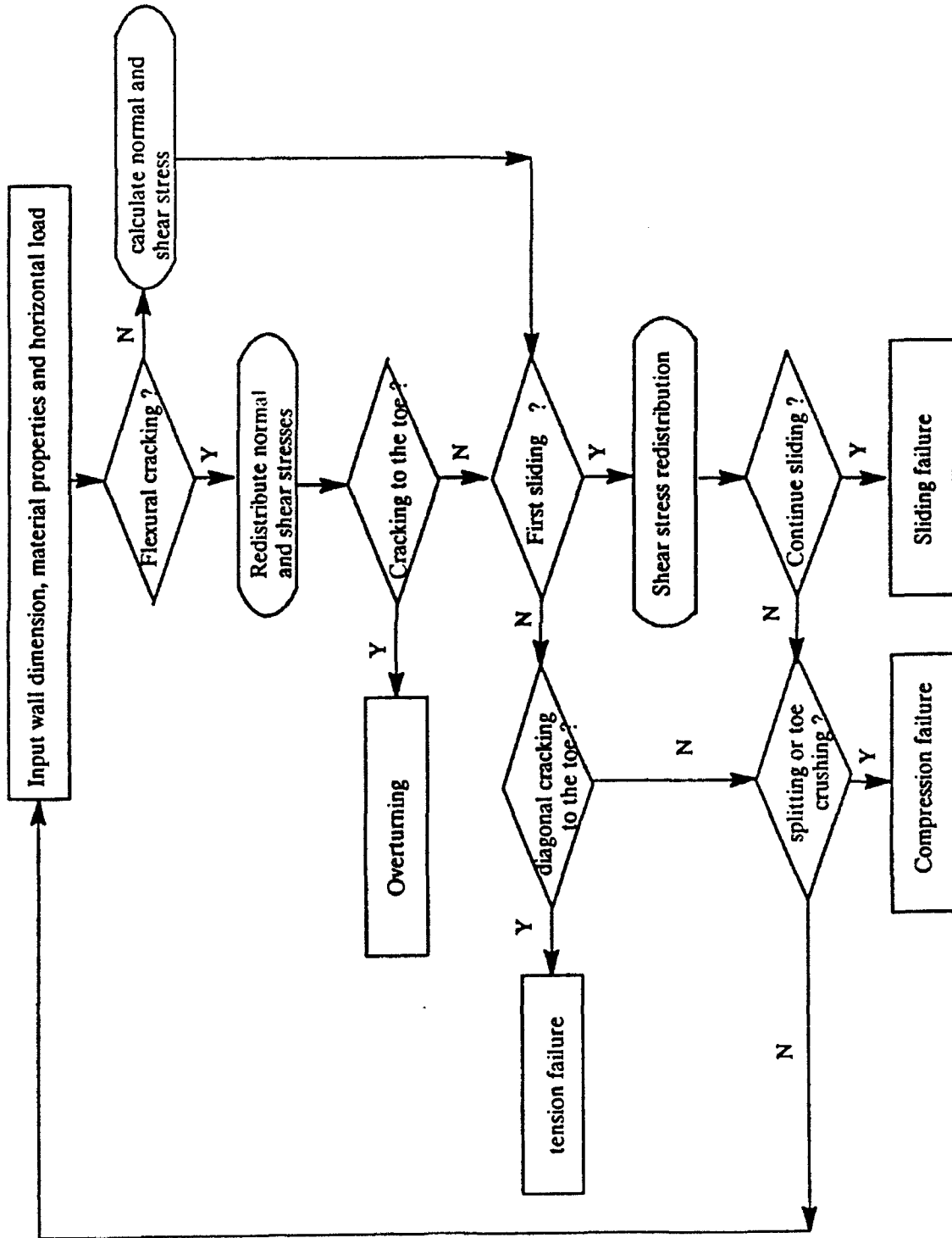


Fig. 3.12 Analytical Procedure for Unreinforced Masonry Cracked Wall

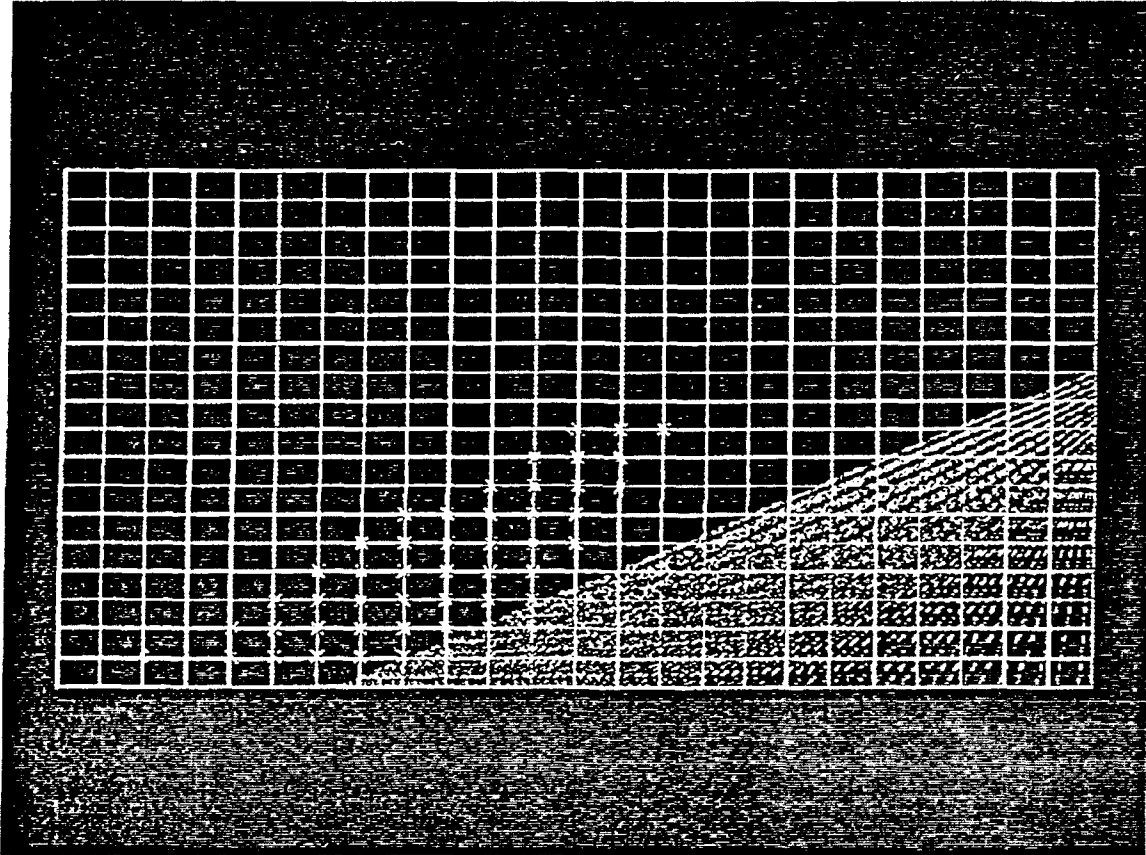


Fig. 3.13 A typical Screen Display of Cracking Development in a Wall

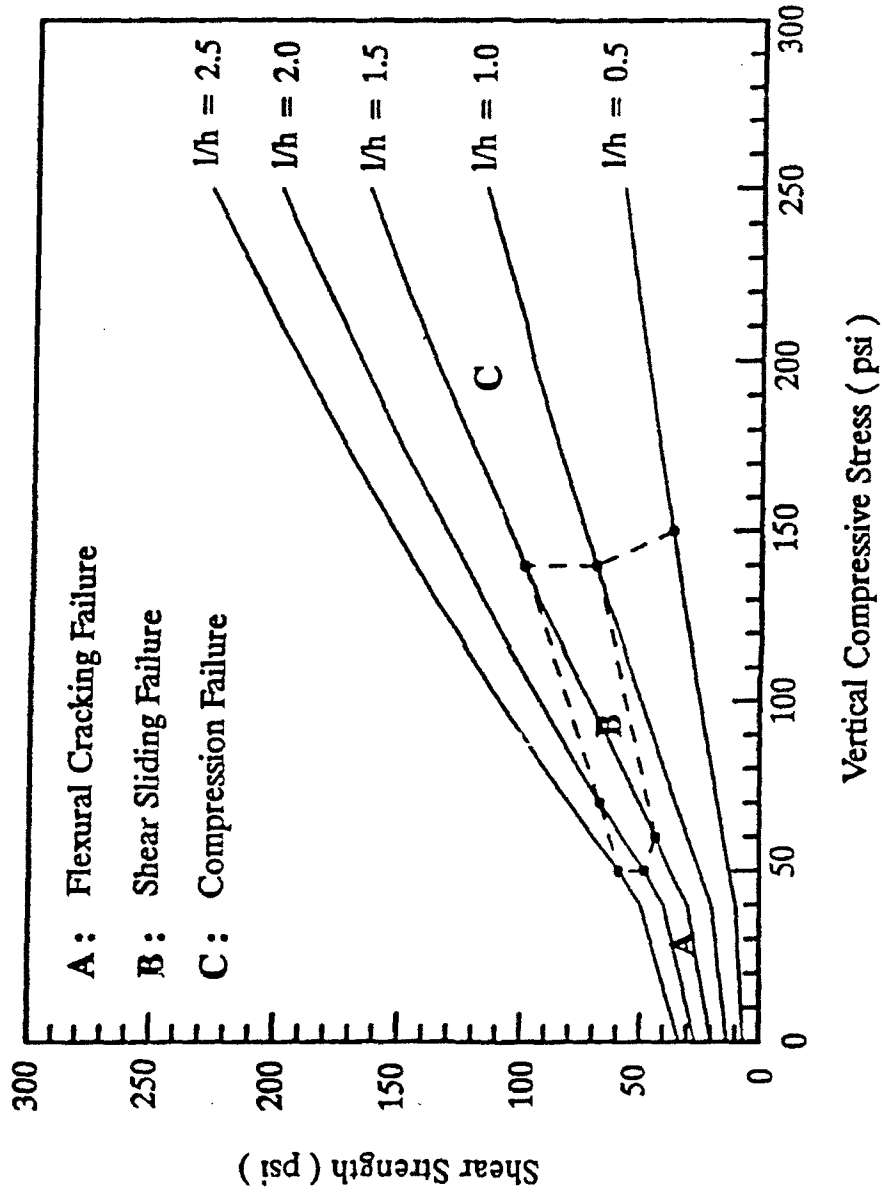


Fig. 3.14 Shear Strength Versus Vertical Compressive Stress for Different l/h Ratios

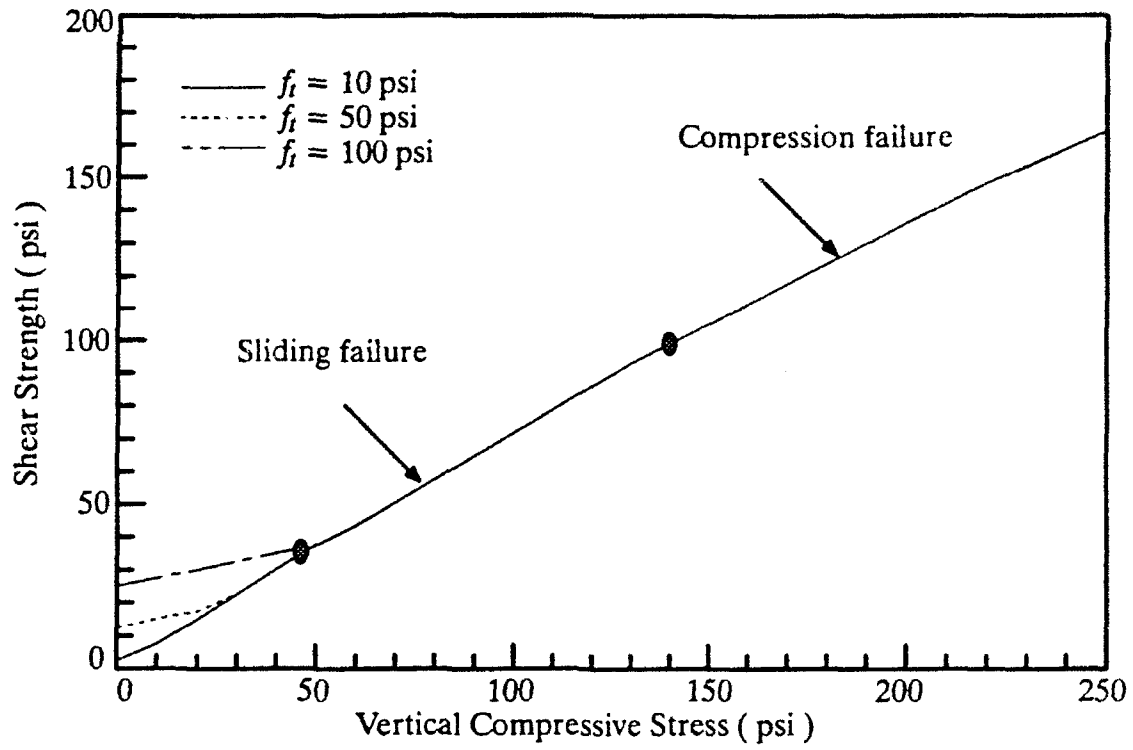


Fig. 4.1 Influence of Flexural Tensile Strength on Shear Strength

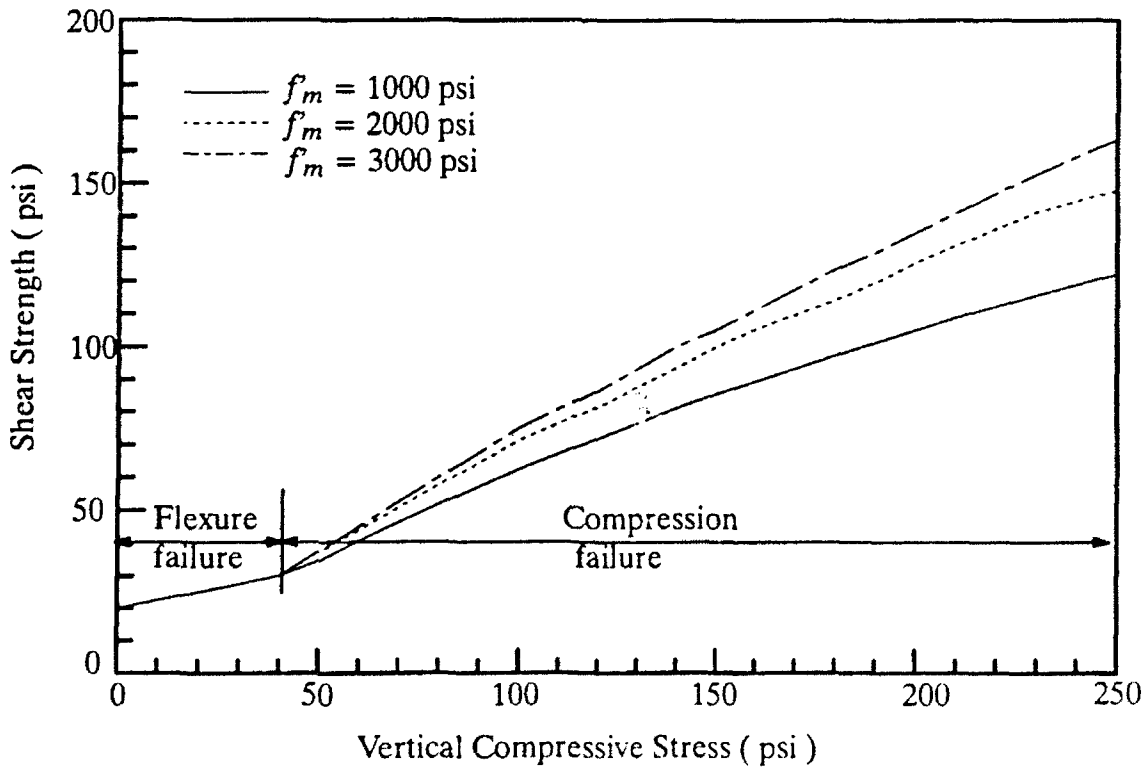


Fig. 4.2 Influence of Compressive Strength on Shear Strength

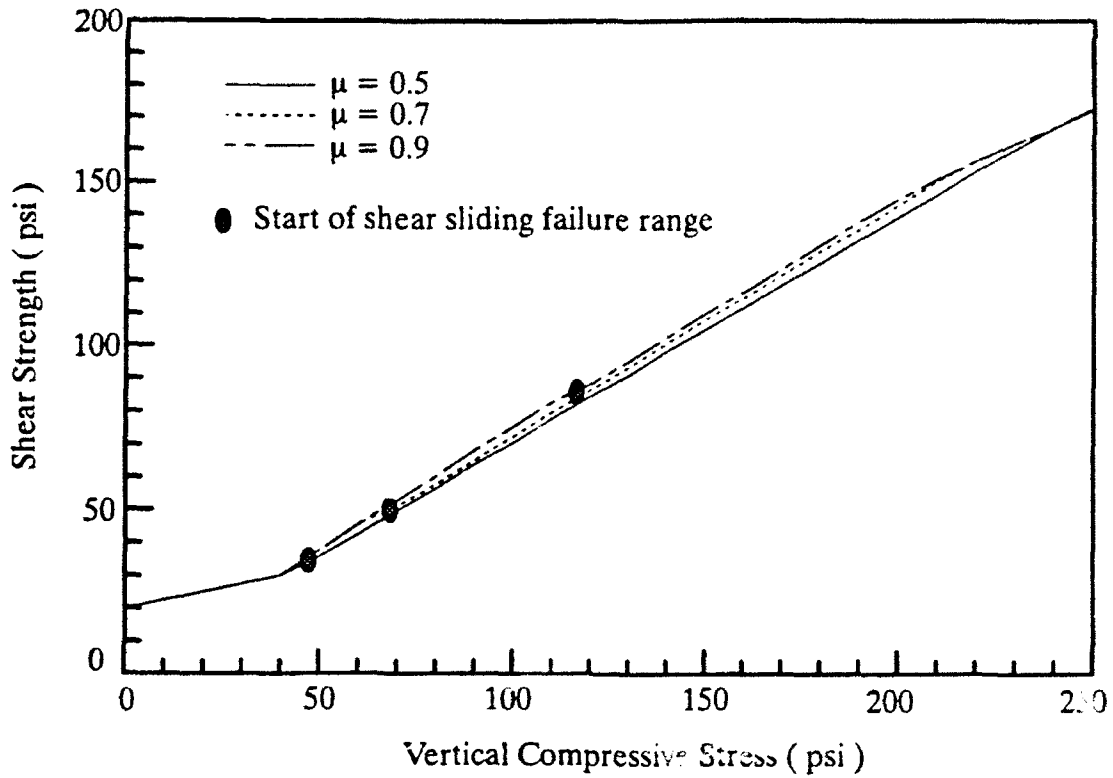


Fig. 4.3 Influence of Frictional Coefficient on Shear Strength

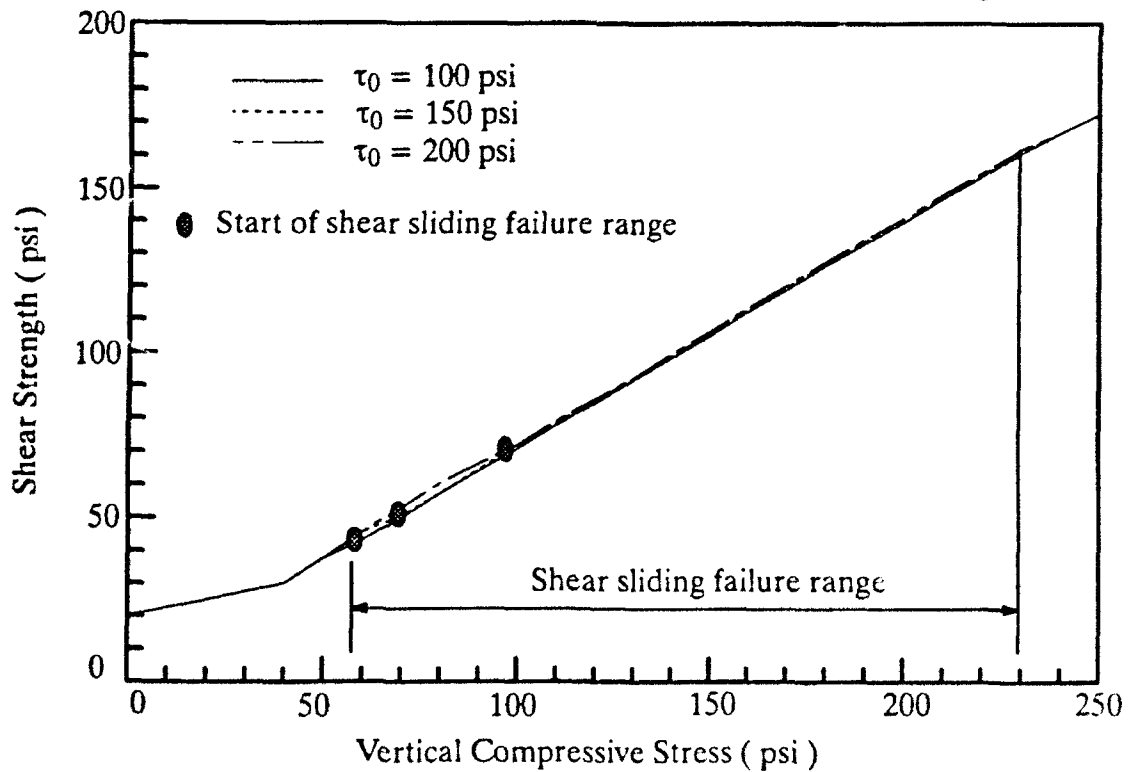


Fig. 4.4 Influence of Cohesion on Shear Strength

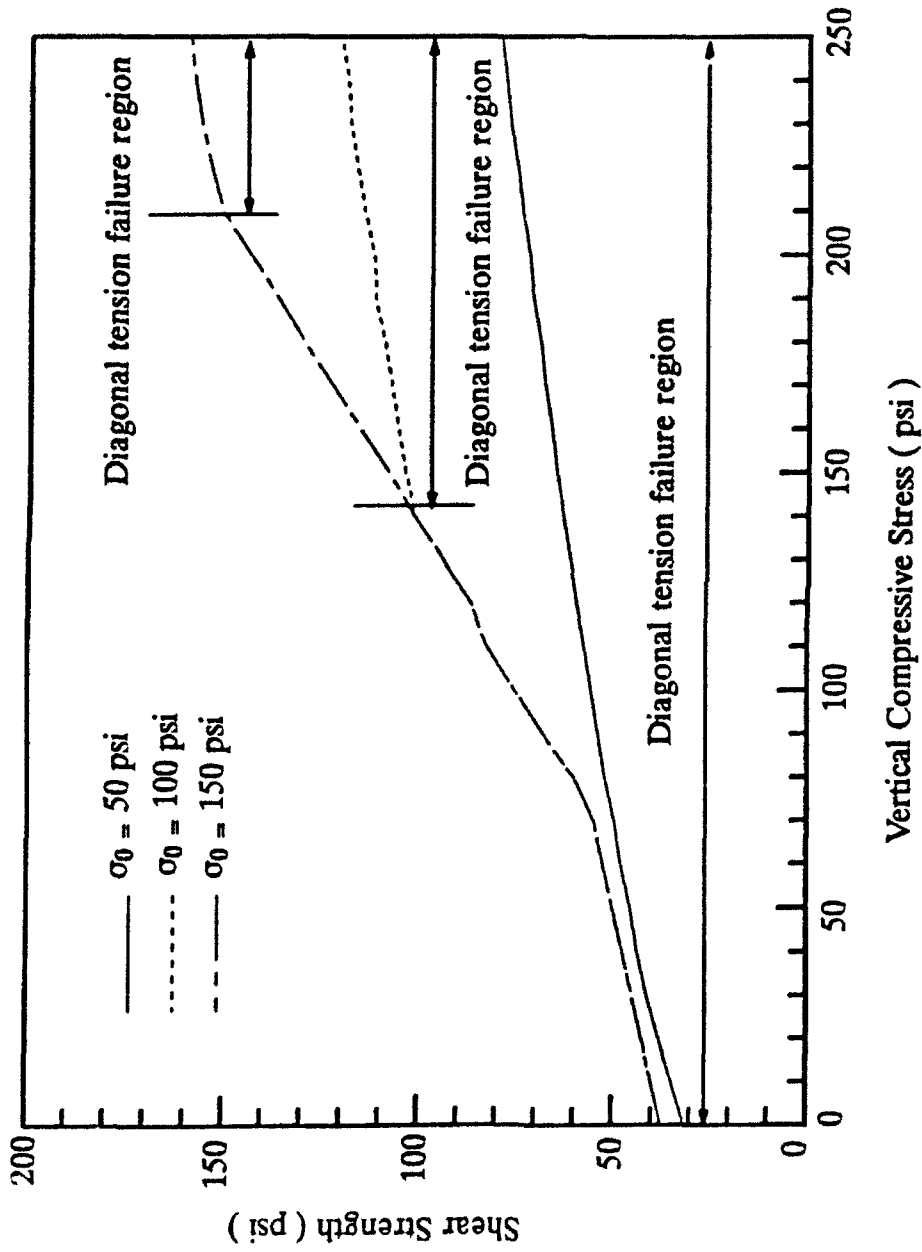


Fig. 4.5 Influence of Diagonal Tension Strength on Shear Strength

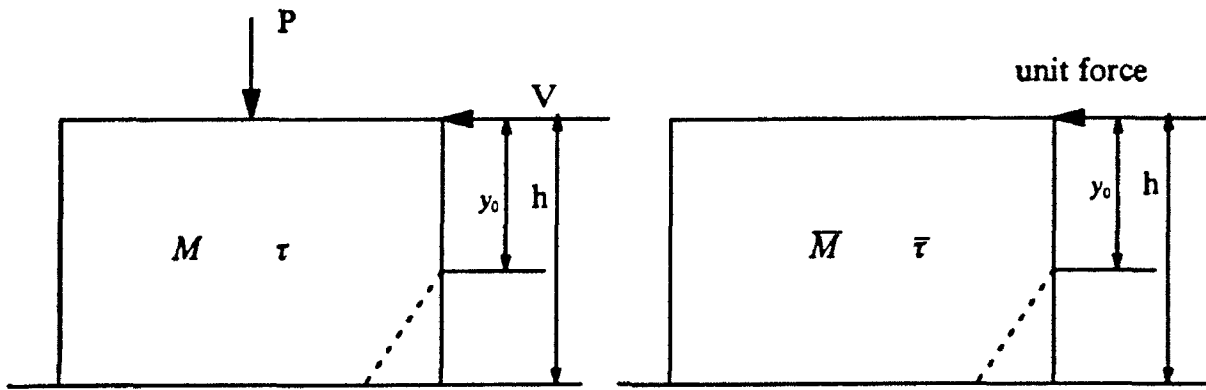


Fig. 6.1(a) Real structure

Fig. 6.1(b) Auxiliary structure

Fig. 6.1 Virtual Work System for Derivation of Displacement Formula

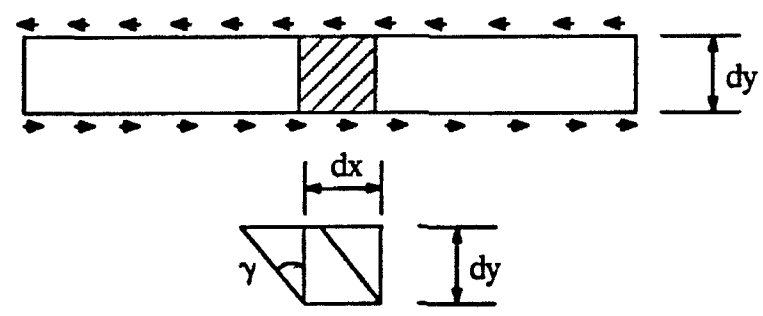


Fig. 6.2 Shear Deformation Diagram

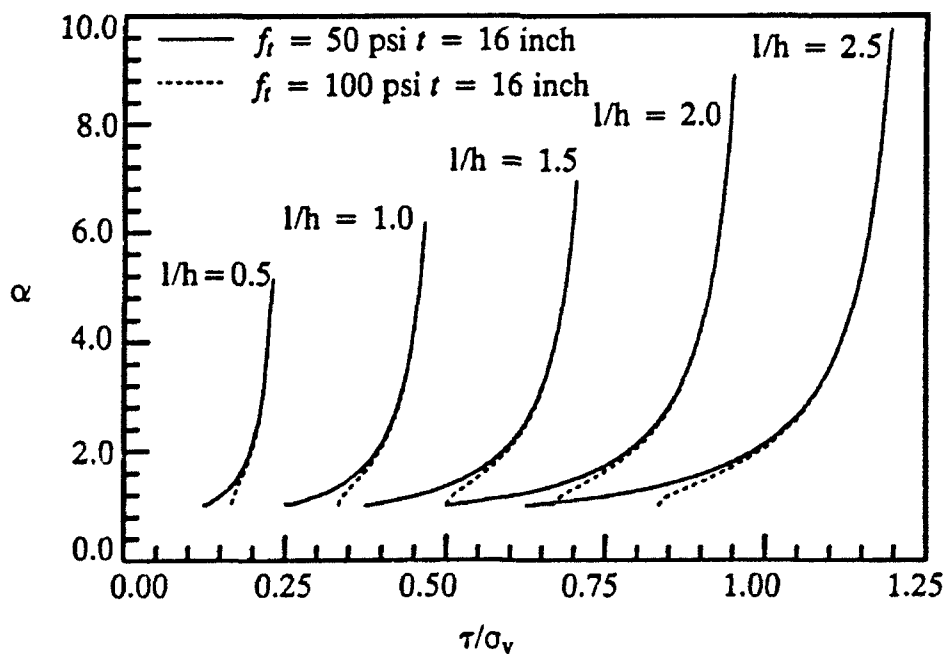
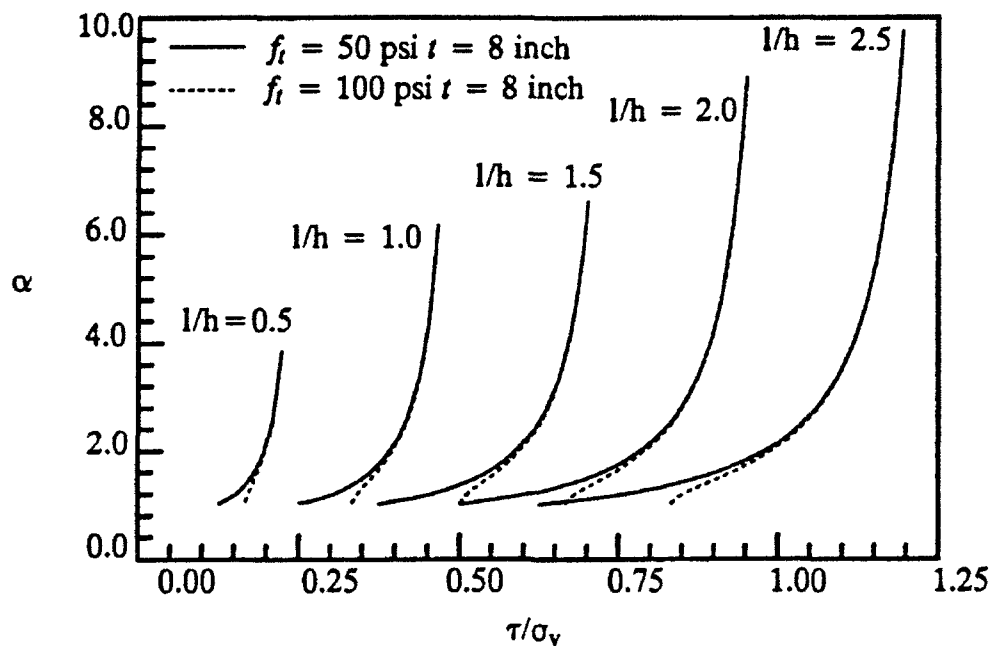


Fig. 6.3 Flexural Deflection Amplifying Factor α vs. Stress Ratio (for Flexural Tensile Strength 50 psi and 100 psi)

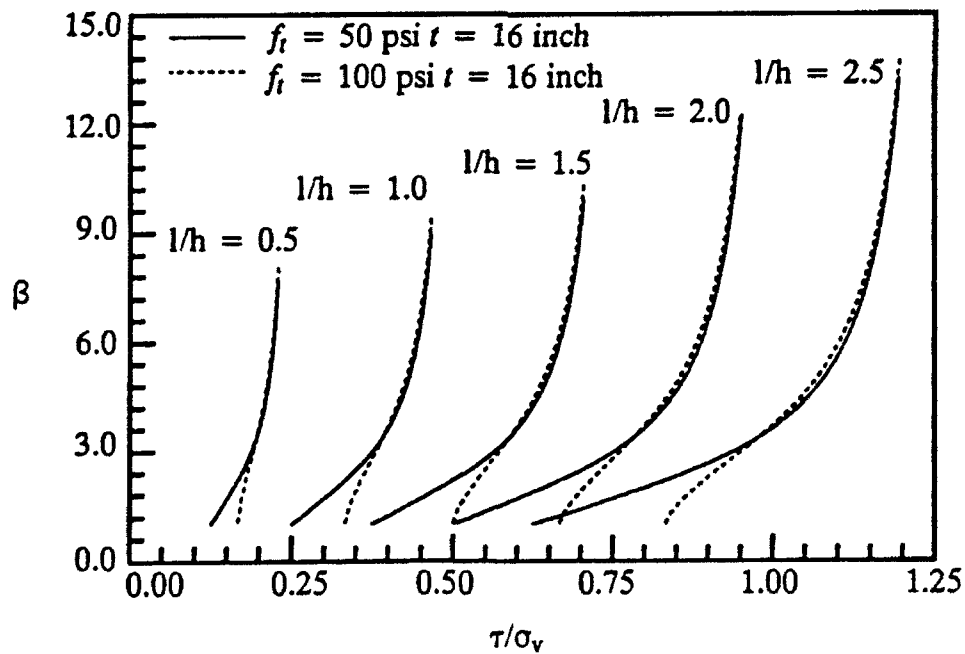
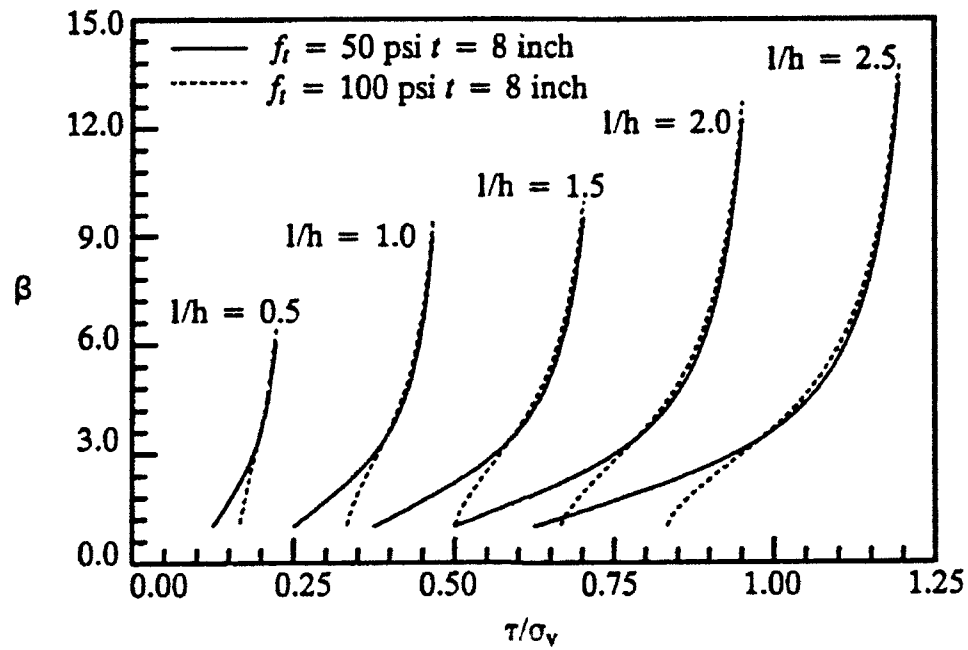


Fig. 6.4 Shear Deflection Amplifying Factor β vs. Stress Ratio (for Flexural Tensile Strength 50 psi and 100 psi)

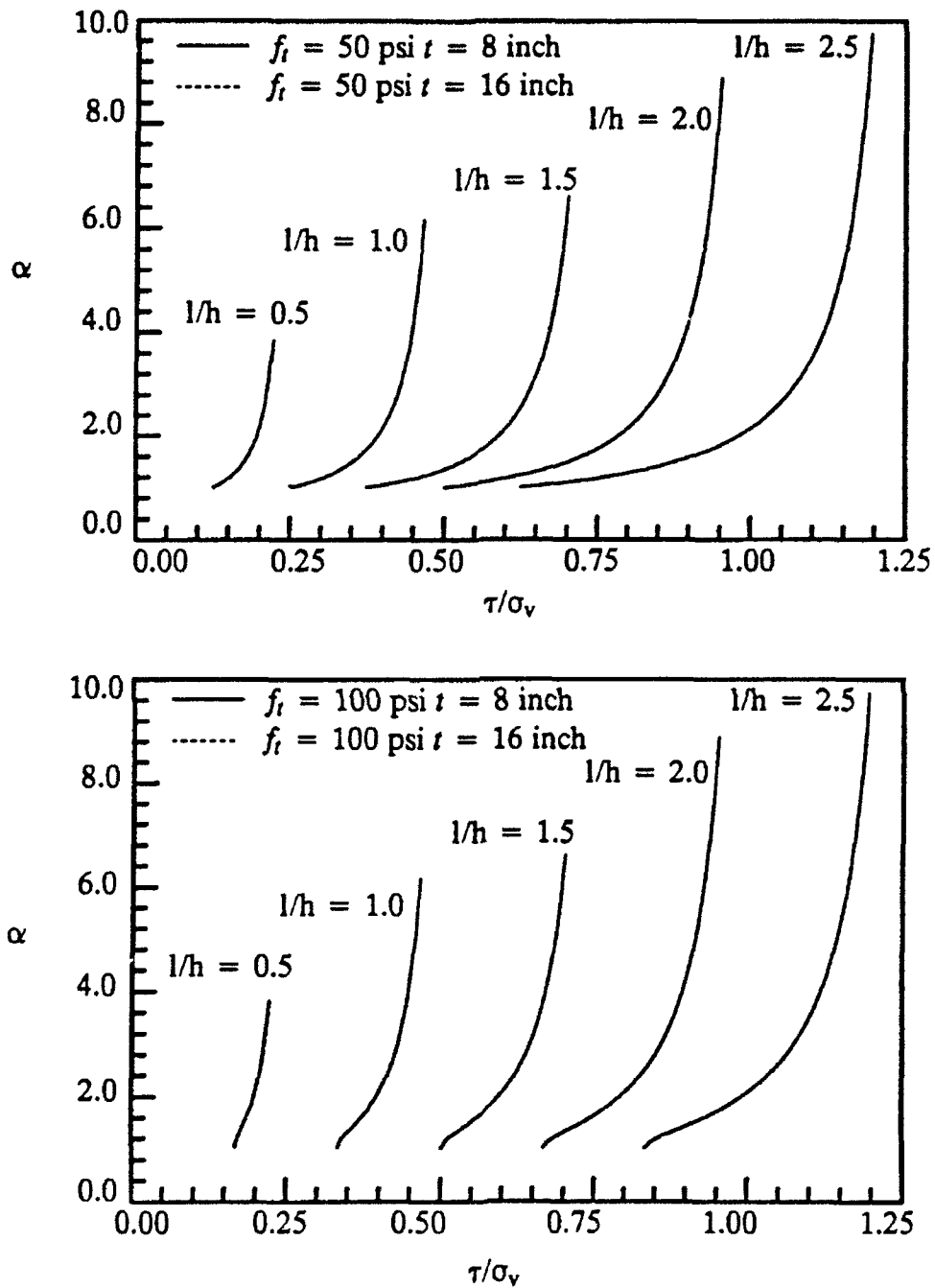


Fig. 6.5 Flexural Deflection Amplifying Factor α vs. Stress Ratio
(for Thickness 8 and 16 inch)

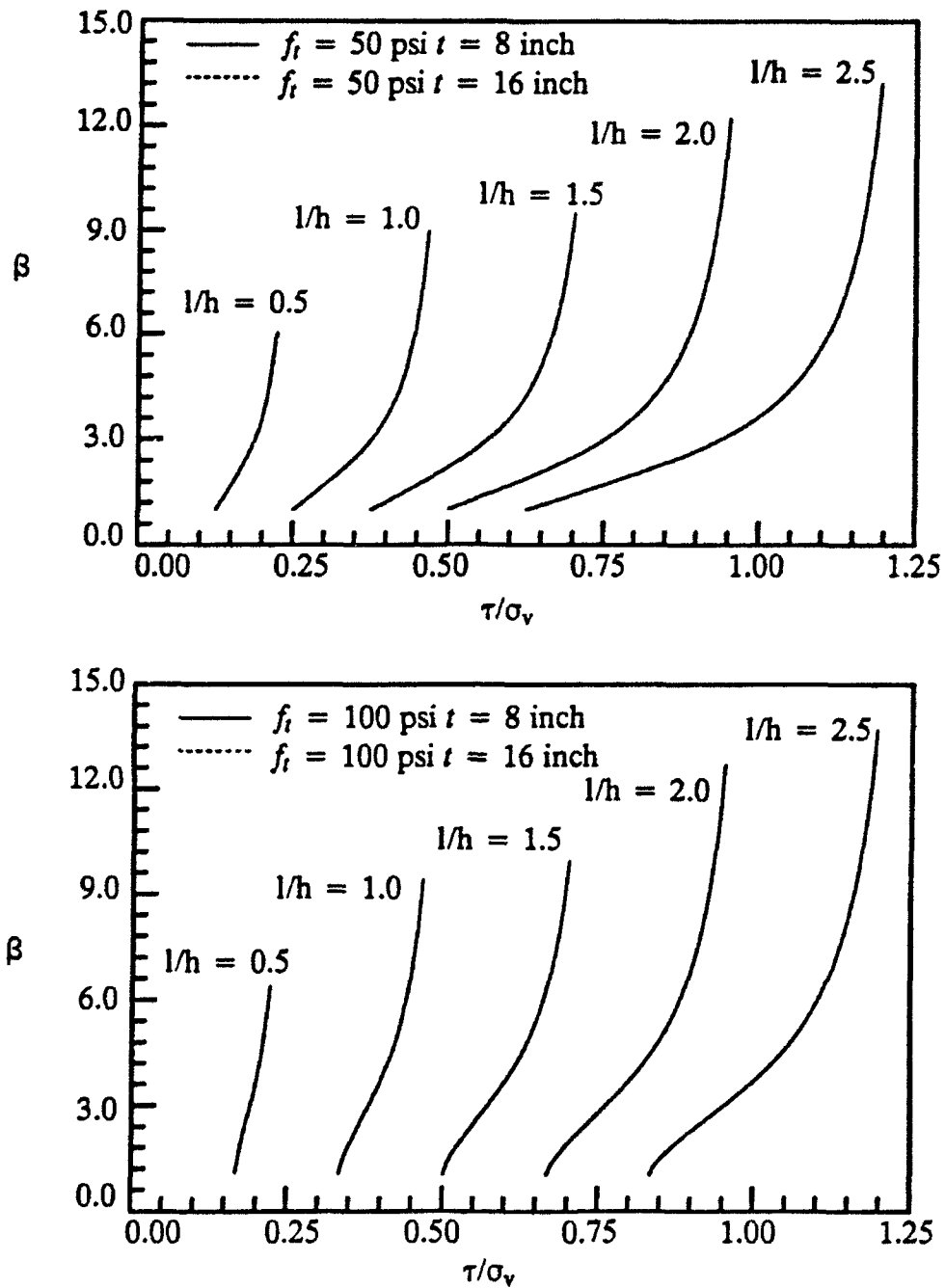


Fig. 6.6 Shear Deflection Amplifying Factor β vs. Stress Ratio
(for Thickness 8 and 16 inch)

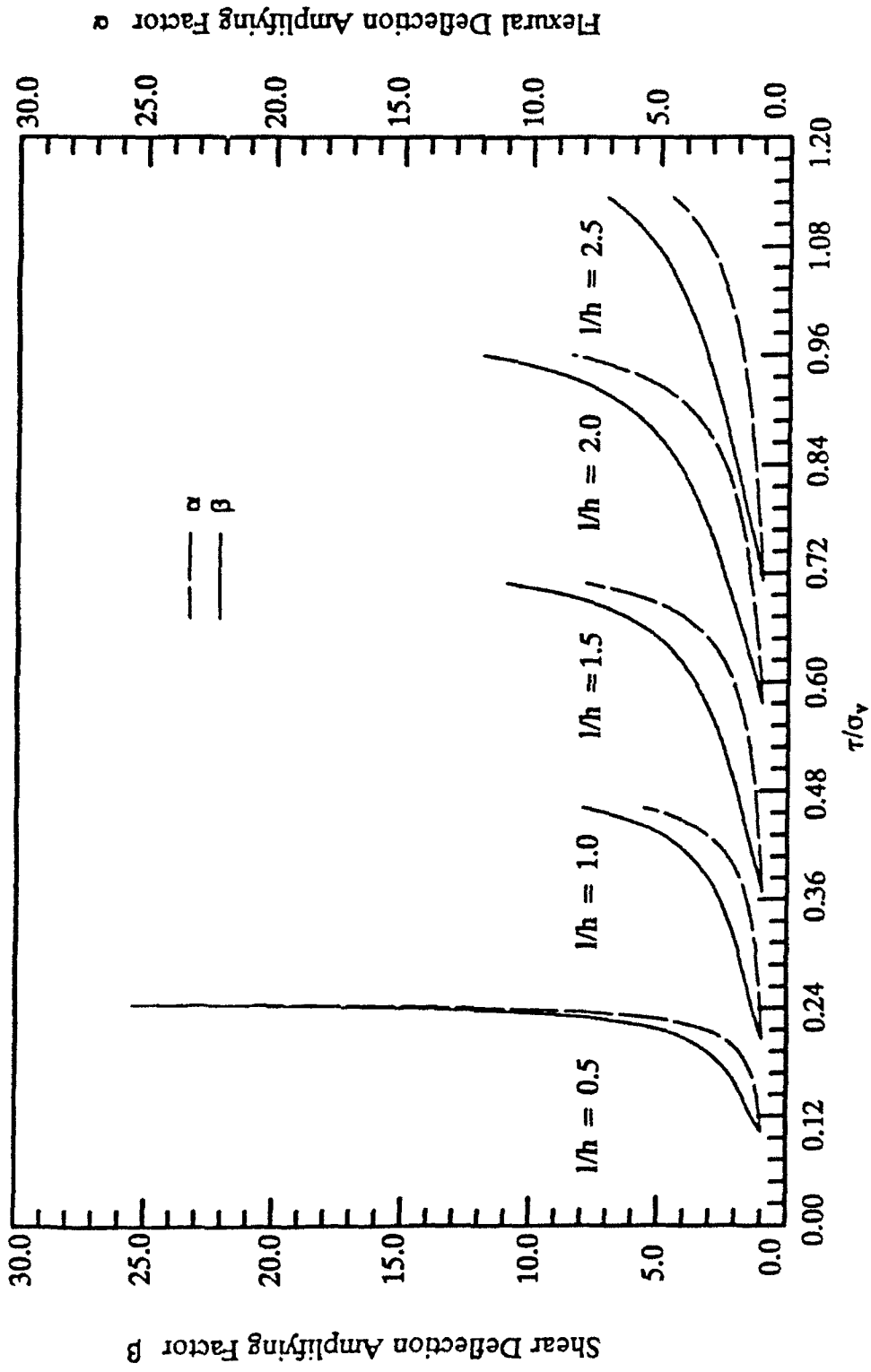


Fig. 6.7 α and β vs. Stress Ratio for Different l/h Ratios

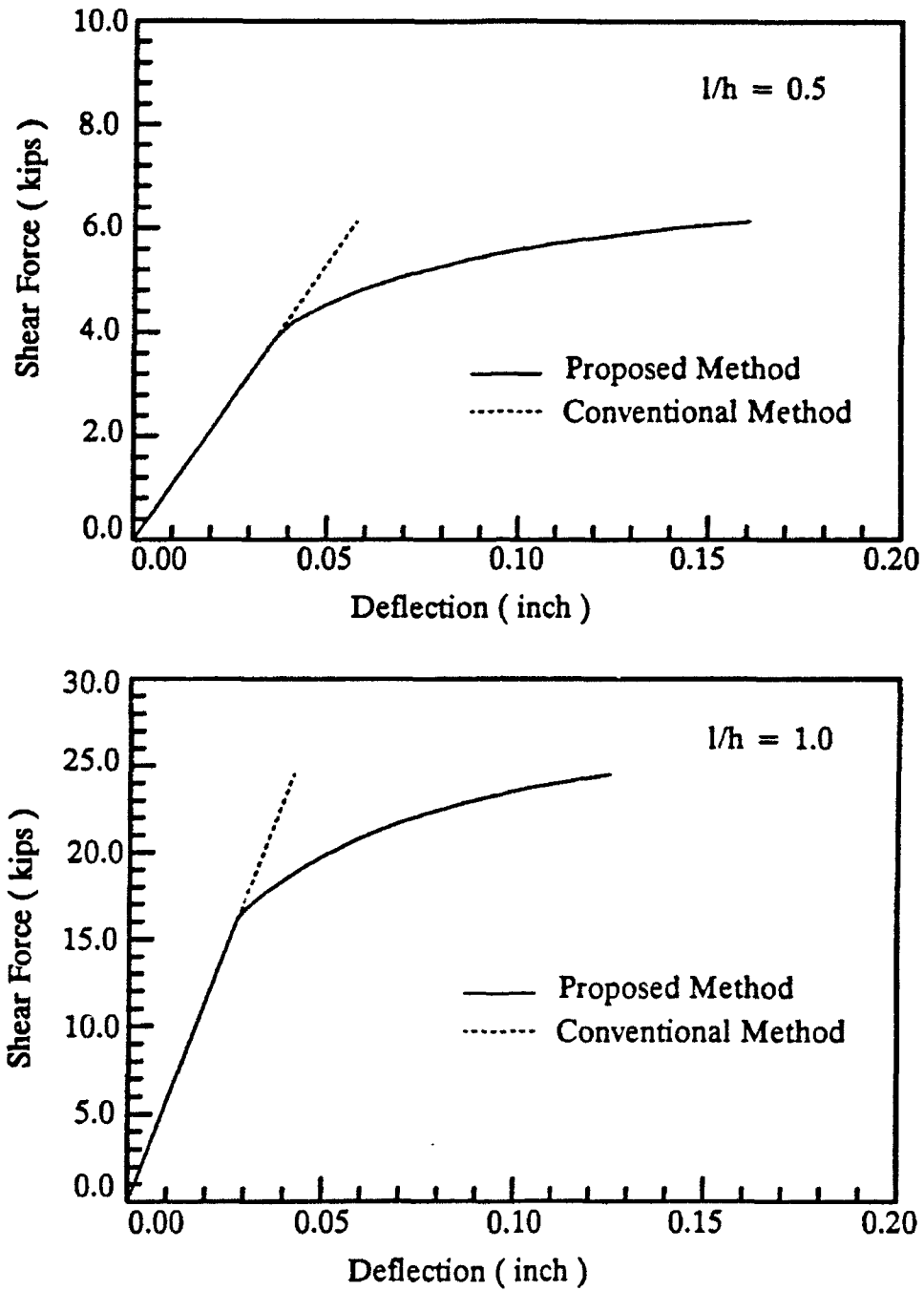


Fig. 6.8 Comparison of Deflections between the Proposed Method and the Conventional Method

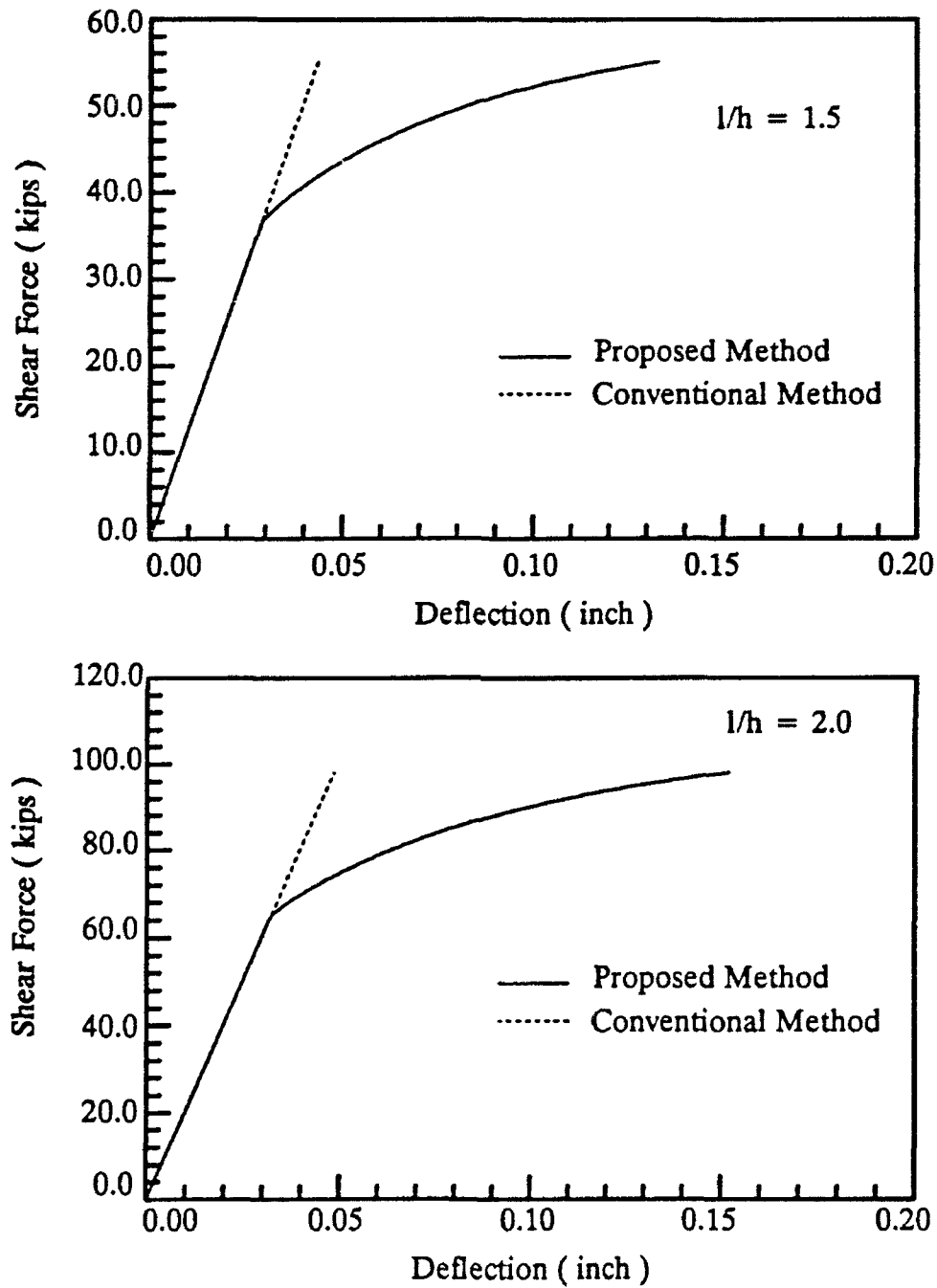


Fig. 6.9 Comparison of Deflections between the Proposed Method and the Conventional Method

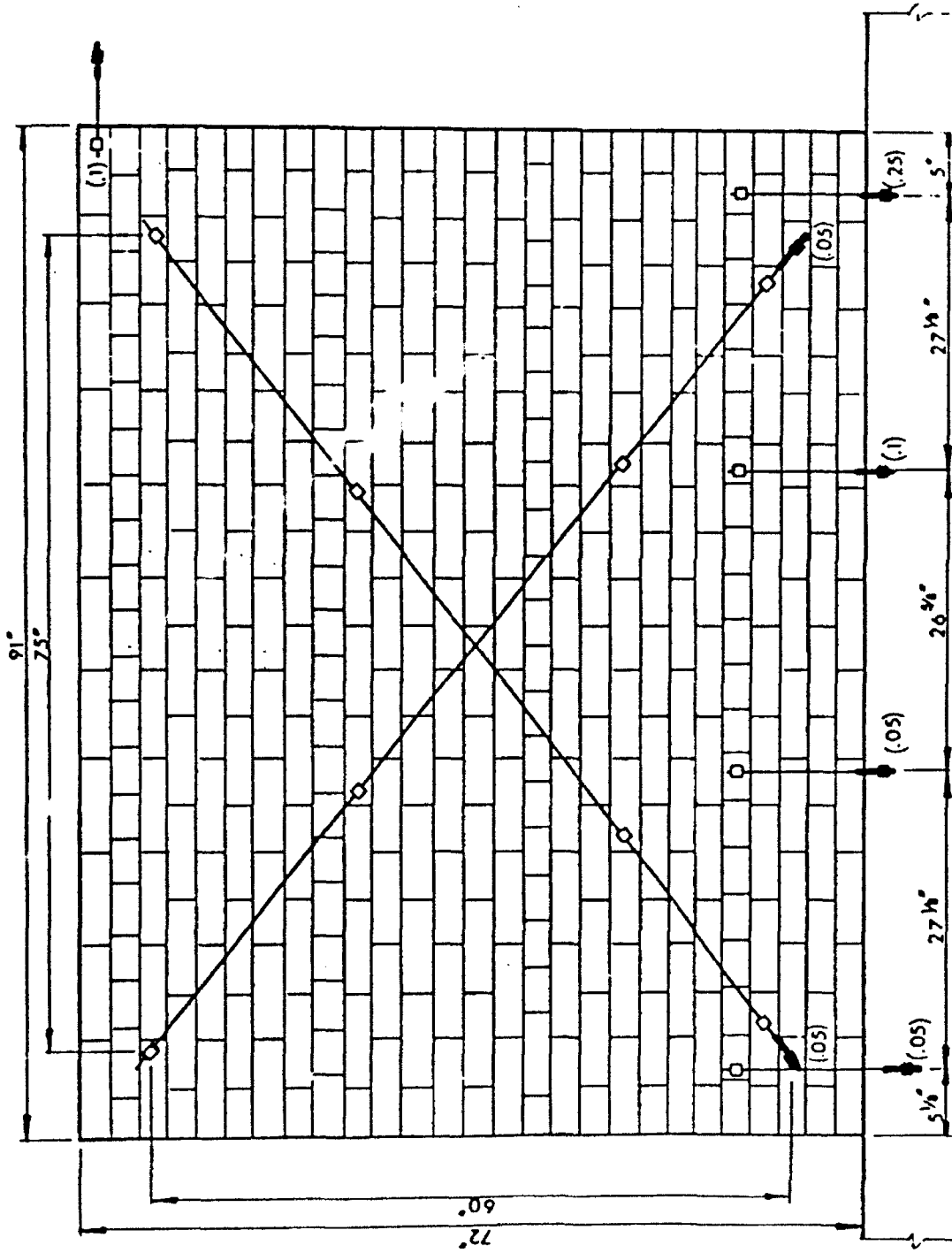


Fig. 7.1 Displacement Transducer Arrangement for Test Walls

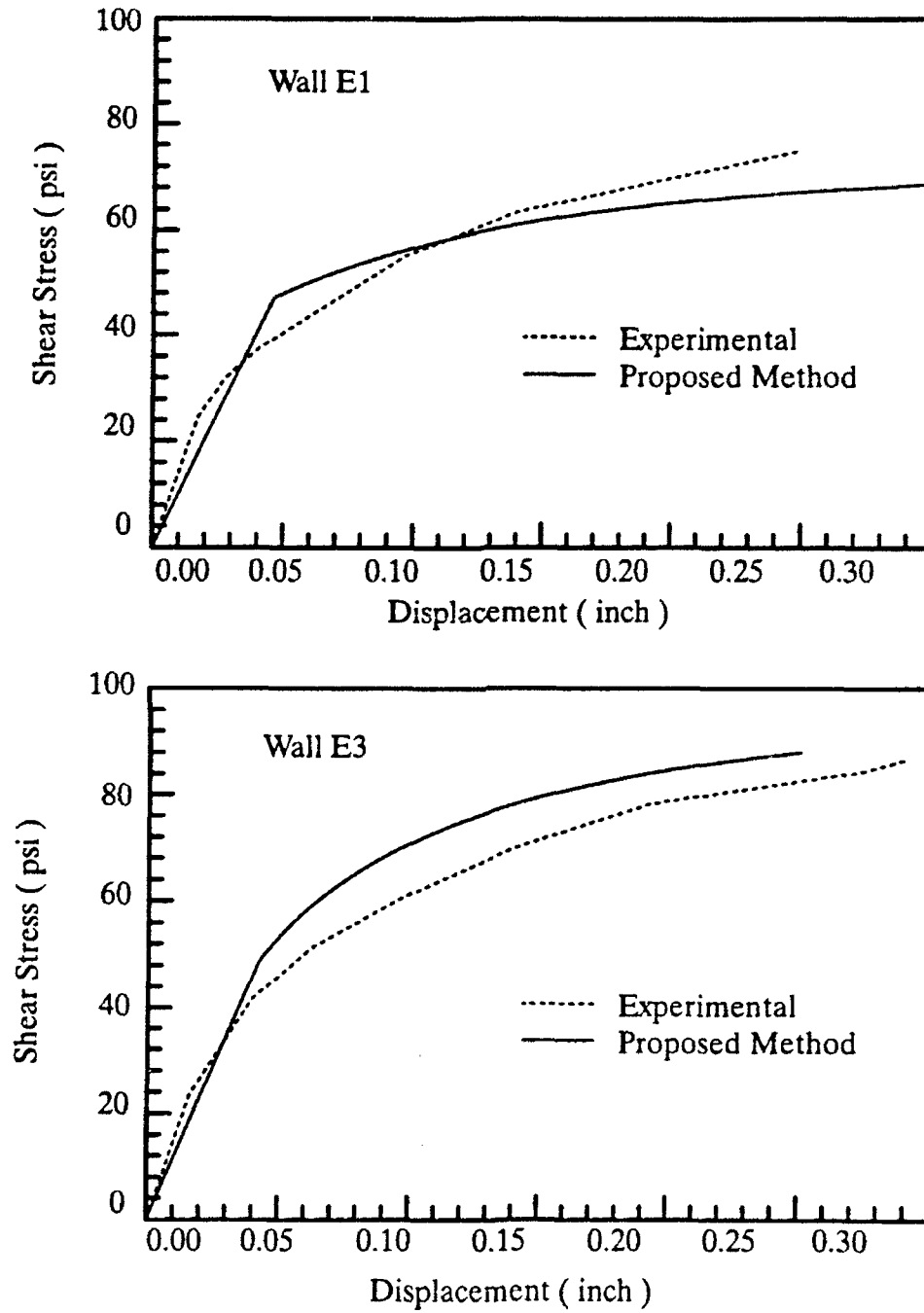


Fig. 7.2 Comparison of the Deflections between the Experimental and the Proposed Method

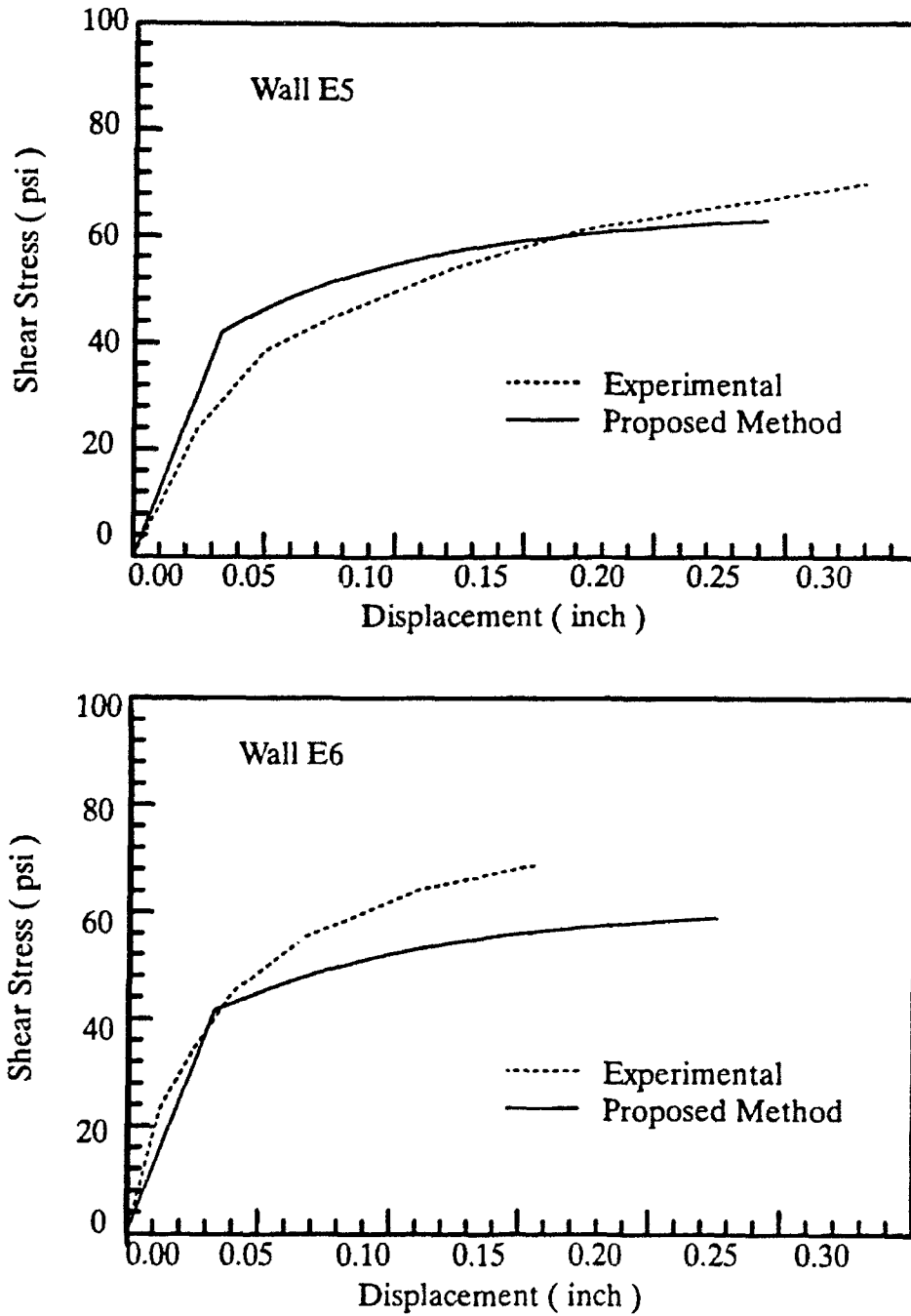


Fig. 7.3 Comparison of the Deflections between the Experimental and the Proposed Method

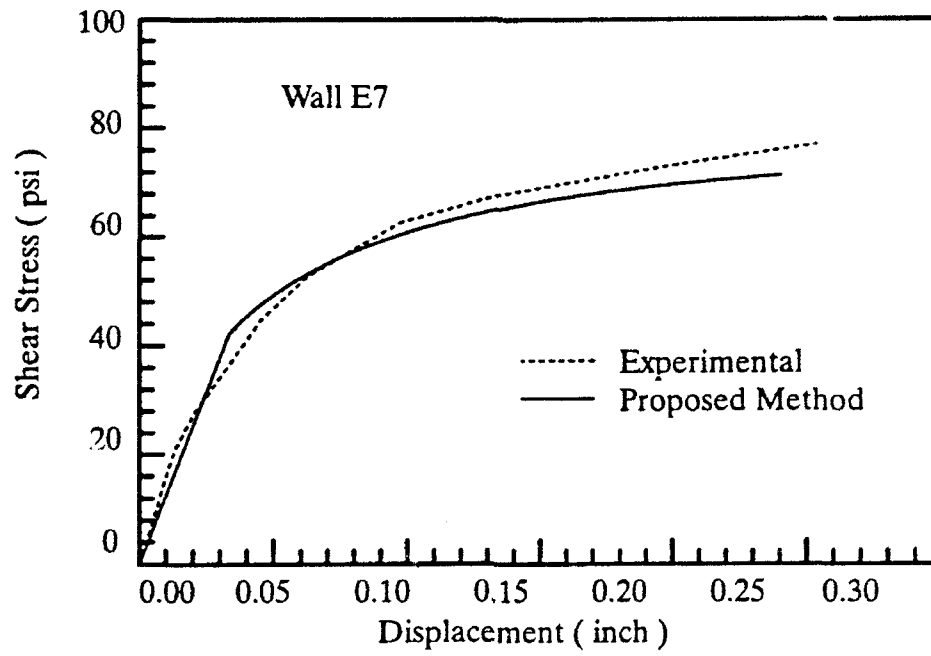


Fig. 7.4 Comparison of the Deflections between the Experimental and the Proposed Method

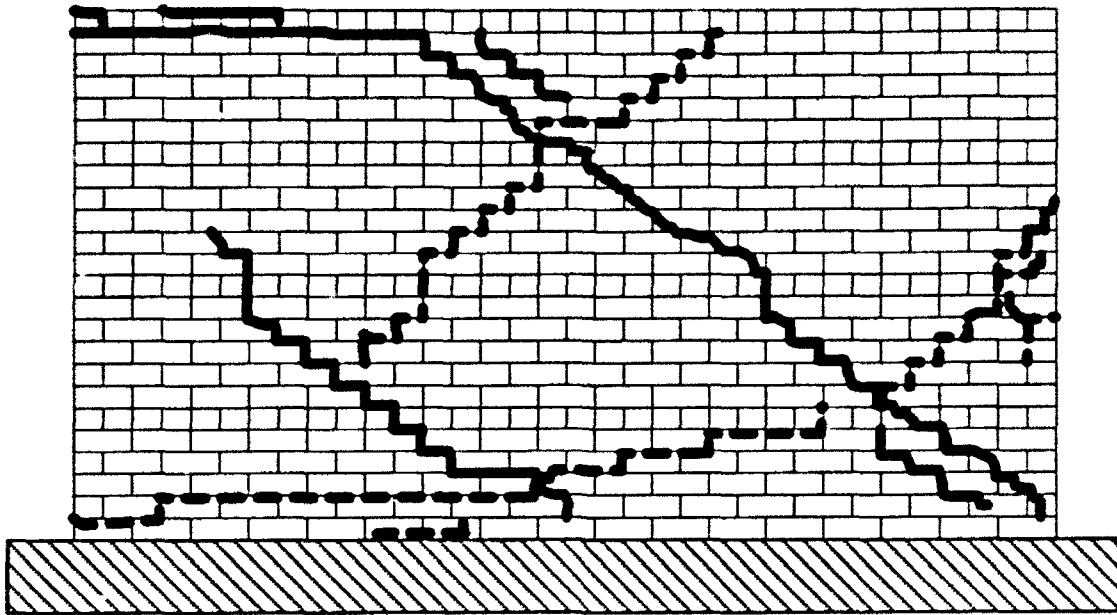


Fig. 7.5 Observed Crack Pattern for Wall 1

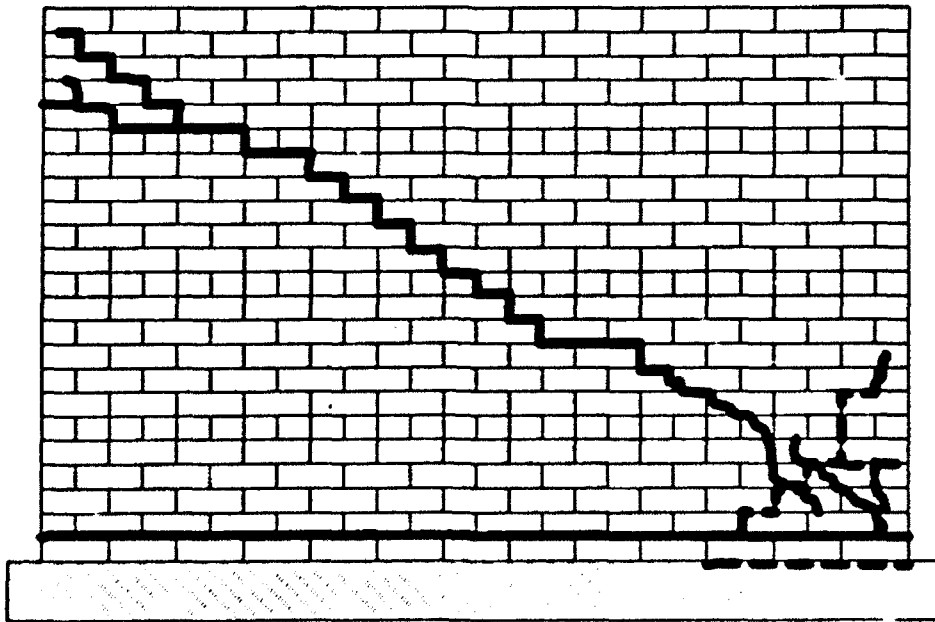


Fig. 7.6 Observed Crack Pattern for Wall 2

APPENDIX A



$\sigma_0 = 50.0\text{psi}$ $\tau_0 = 100.0\text{psi}$ $\mu = 0.4$ $f'_m = 1000.0\text{psi}$

σ_v	50.0	100.0	150.0	200.0	250.0
l/h					
0.5	12.4	23.3	32.0	39.0	44.4
1.0	24.8	46.0	63.7	71.7	78.4
2.0	46.6	57.0	65.8	73.5	80.6
3.0	47.3	58.0	66.7	74.6	81.6
4.0	50.3	58.3	66.7	74.6	81.7
5.0	56.4	62.3	68.8	75.0	81.9

 $f'_m = 2000.0\text{psi}$

σ_v	50.0	100.0	150.0	200.0	250.0
l/h					
0.5	12.7	24.8	36.0	46.2	55.3
1.0	25.1	49.5	64.3	71.7	78.4
2.0	46.6	57.0	65.8	73.5	80.6
3.0	47.3	58.0	66.7	74.6	81.6
4.0	50.3	58.3	66.7	74.6	81.7
5.0	56.4	62.3	68.8	75.0	81.9

 $f'_m = 3000.0\text{psi}$

σ_v	50.0	100.0	150.0	200.0	250.0
l/h					
0.5	12.7	25.1	37.1	48.4	59.0
1.0	25.1	50.1	64.3	71.7	78.4
2.0	46.6	57.0	65.8	73.5	80.6
3.0	47.3	58.0	66.7	74.6	81.6
4.0	50.3	58.3	66.7	74.6	81.7
5.0	56.4	62.3	68.8	75.0	81.9

 $f'_m = 4000.0\text{psi}$

σ_v	50.0	100.0	150.0	200.0	250.0
l/h					
0.5	12.7	25.1	37.5	49.5	60.8
1.0	25.1	50.1	64.3	71.7	78.4
2.0	46.6	57.0	65.8	73.5	80.6
3.0	47.3	58.0	66.7	74.6	81.6
4.0	50.3	58.3	66.7	74.6	81.7
5.0	56.4	62.3	68.8	75.0	81.9

 $f'_m = 5000.0\text{psi}$

σ_v	50.0	100.0	150.0	200.0	250.0
l/h					
0.5	12.7	25.1	37.5	50.2	61.9
1.0	25.1	50.1	64.3	71.7	78.4
2.0	46.6	57.0	65.8	73.5	80.6
3.0	47.3	58.0	66.7	74.6	81.6
4.0	50.3	58.3	66.7	74.6	81.7
5.0	56.4	62.3	68.8	75.0	81.9

 $\sigma_0 = 100.0\text{psi}$ $\tau_0 = 100.0\text{psi}$ $\mu = 0.4$ $f'_m = 1000.0\text{psi}$

σ_v	50.0	100.0	150.0	200.0	250.0
l/h					
0.5	12.4	23.3	32.0	39.0	44.4
1.0	24.8	46.0	63.7	77.7	88.5
2.0	47.0	89.4	104.0	113.9	123.1
3.0	70.7	131.1	105.6	115.6	124.7
4.0	93.8	140.0	160.0	116.5	124.9
5.0	117.2	140.0	160.0	180.0	130.0

 $f'_m = 2000.0\text{psi}$

σ_v	50.0	100.0	150.0	200.0	250.0
l/h					
0.5	12.7	24.8	36.0	46.2	55.3
1.0	25.1	49.5	71.5	90.5	110.3
2.0	47.0	92.5	104.0	113.9	123.1
3.0	70.7	138.6	105.6	115.6	124.7
4.0	93.8	140.0	160.0	116.5	124.9
5.0	117.2	140.0	160.0	180.0	130.0

 $f'_m = 3000.0\text{psi}$

σ_v	50.0	100.0	150.0	200.0	250.0
l/h					
0.5	12.7	25.1	37.1	48.4	59.0
1.0	25.1	50.1	72.1	90.5	112.7
2.0	47.0	92.5	104.0	113.9	123.1
3.0	70.7	138.6	105.6	115.6	124.7
4.0	93.8	140.0	160.0	116.5	124.9
5.0	117.2	140.0	160.0	180.0	130.0

 $f'_m = 4000.0\text{psi}$

σ_v	50.0	100.0	150.0	200.0	250.0
l/h					
0.5	12.7	25.1	37.5	49.5	60.8
1.0	25.1	50.1	72.1	90.5	112.7
2.0	47.0	92.5	104.0	113.9	123.1
3.0	70.7	138.6	105.6	115.6	124.7
4.0	93.8	140.0	160.0	116.5	124.9
5.0	117.2	140.0	160.0	180.0	130.0

 $f'_m = 5000.0\text{psi}$

σ_v	50.0	100.0	150.0	200.0	250.0
l/h					
0.5	12.7	25.1	37.5	50.2	61.9
1.0	25.1	50.1	72.1	90.5	112.7
2.0	47.0	92.5	104.0	113.9	123.1
3.0	70.7	138.6	105.6	115.6	124.7
4.0	93.8	140.0	160.0	116.5	124.9
5.0	117.2	140.0	160.0	180.0	130.0

$\sigma_0=150.0\text{psi}$ $\tau_0=100.0\text{psi}$ $\mu=0.4$ $f'_m=1000.0\text{psi}$

σ_v	50.0	100.0	150.0	200.0	250.0
l/h					
0.5	12.4	23.3	32.0	39.0	44.4
1.0	24.8	46.0	63.7	77.7	88.5
2.0	47.0	89.4	120.4	145.1	163.1
3.0	70.7	131.1	160.0	180.0	200.0
4.0	93.8	140.0	160.0	180.0	200.0
5.0	117.2	140.0	160.0	180.0	200.0

 $f'_m=2000.0\text{psi}$

σ_v	50.0	100.0	150.0	200.0	250.0
l/h					
0.5	12.7	24.8	36.0	46.2	55.3
1.0	25.1	49.5	71.5	90.5	110.3
2.0	47.0	92.5	137.6	178.6	200.0
3.0	70.7	138.6	160.0	180.0	200.0
4.0	93.8	140.0	160.0	180.0	200.0
5.0	117.2	140.0	160.0	180.0	200.0

 $f'_m=3000.0\text{psi}$

σ_v	50.0	100.0	150.0	200.0	250.0
l/h					
0.5	12.7	25.1	37.1	48.4	59.0
1.0	25.1	50.1	72.1	90.5	112.7
2.0	47.0	92.5	137.6	180.0	200.0
3.0	70.7	138.6	160.0	180.0	200.0
4.0	93.8	140.0	160.0	180.0	200.0
5.0	117.2	140.0	160.0	180.0	200.0

 $f'_m=4000.0\text{psi}$

σ_v	50.0	100.0	150.0	200.0	250.0
l/h					
0.5	12.7	25.1	37.5	49.5	60.8
1.0	25.1	50.1	72.1	90.5	112.7
2.0	47.0	92.5	137.6	180.0	200.0
3.0	70.7	138.6	160.0	180.0	200.0
4.0	93.8	140.0	160.0	180.0	200.0
5.0	117.2	140.0	160.0	180.0	200.0

 $f'_m=5000.0\text{psi}$

σ_v	50.0	100.0	150.0	200.0	250.0
l/h					
0.5	12.7	25.1	37.5	50.2	61.9
1.0	25.1	50.1	72.1	90.5	112.7
2.0	47.0	92.5	137.6	180.0	200.0
3.0	70.7	138.6	160.0	180.0	200.0
4.0	93.8	140.0	160.0	180.0	200.0
5.0	117.2	140.0	160.0	180.0	200.0

 $\sigma_0=200.0\text{psi}$ $\tau_0=100.0\text{psi}$ $\mu=0.4$ $f'_m=1000.0\text{psi}$

σ_v	50.0	100.0	150.0	200.0	250.0
l/h					
0.5	12.4	23.3	32.0	39.0	44.4
1.0	24.8	46.0	63.7	77.7	88.5
2.0	47.0	89.4	120.4	145.1	163.1
3.0	70.7	131.1	160.0	180.0	200.0
4.0	93.8	140.0	160.0	180.0	200.0
5.0	117.2	140.0	160.0	180.0	200.0

 $f'_m=2000.0\text{psi}$

σ_v	50.0	100.0	150.0	200.0	250.0
l/h					
0.5	12.7	24.8	36.0	46.2	55.3
1.0	25.1	49.5	71.5	90.5	110.3
2.0	47.0	92.5	137.6	178.6	200.0
3.0	70.7	138.6	160.0	180.0	200.0
4.0	93.8	140.0	160.0	180.0	200.0
5.0	117.2	140.0	160.0	180.0	200.0

 $f'_m=3000.0\text{psi}$

σ_v	50.0	100.0	150.0	200.0	250.0
l/h					
0.5	12.7	25.1	37.1	48.4	59.0
1.0	25.1	50.1	72.1	90.5	112.7
2.0	47.0	92.5	137.6	180.0	200.0
3.0	70.7	138.6	160.0	180.0	200.0
4.0	93.8	140.0	160.0	180.0	200.0
5.0	117.2	140.0	160.0	180.0	200.0

 $f'_m=4000.0\text{psi}$

σ_v	50.0	100.0	150.0	200.0	250.0
l/h					
0.5	12.7	25.1	37.5	49.5	60.8
1.0	25.1	50.1	72.1	90.5	112.7
2.0	47.0	92.5	137.6	180.0	200.0
3.0	70.7	138.6	160.0	180.0	200.0
4.0	93.8	140.0	160.0	180.0	200.0
5.0	117.2	140.0	160.0	180.0	200.0

 $f'_m=5000.0\text{psi}$

σ_v	50.0	100.0	150.0	200.0	250.0
l/h					
0.5	12.7	25.1	37.5	50.2	61.9
1.0	25.1	50.1	72.1	90.5	112.7
2.0	47.0	92.5	137.6	180.0	200.0
3.0	70.7	138.6	160.0	180.0	200.0
4.0	93.8	140.0	160.0	180.0	200.0
5.0	117.2	140.0	160.0	180.0	200.0

$\sigma_0=250.0\text{psi}$ $\tau_0=100.0\text{psi}$ $\mu=0.4$ $f'_m=1000.0\text{psi}$

σ_v	50.0	100.0	150.0	200.0	250.0
l/h					
0.5	12.4	23.3	32.0	39.0	44.4
1.0	24.8	46.0	63.7	77.7	88.5
2.0	47.0	89.4	120.4	145.1	163.1
3.0	70.7	131.1	160.0	180.0	200.0
4.0	93.8	140.0	160.0	180.0	200.0
5.0	117.2	140.0	160.0	180.0	200.0

 $f'_m=2000.0\text{psi}$

σ_v	50.0	100.0	150.0	200.0	250.0
l/h					
0.5	12.7	24.8	36.0	46.2	55.3
1.0	25.1	49.5	71.5	90.5	110.3
2.0	47.0	92.5	137.6	178.6	200.0
3.0	70.7	138.6	160.0	180.0	200.0
4.0	93.8	140.0	160.0	180.0	200.0
5.0	117.2	140.0	160.0	180.0	200.0

 $f'_m=3000.0\text{psi}$

σ_v	50.0	100.0	150.0	200.0	250.0
l/h					
0.5	12.7	25.1	37.1	48.4	59.0
1.0	25.1	50.1	72.1	90.5	112.7
2.0	47.0	92.5	137.6	180.0	200.0
3.0	70.7	138.6	160.0	180.0	200.0
4.0	93.8	140.0	160.0	180.0	200.0
5.0	117.2	140.0	160.0	180.0	200.0

 $f'_m=4000.0\text{psi}$

σ_v	50.0	100.0	150.0	200.0	250.0
l/h					
0.5	12.7	25.1	37.5	49.5	60.8
1.0	25.1	50.1	72.1	90.5	112.7
2.0	47.0	92.5	137.6	180.0	200.0
3.0	70.7	138.6	160.0	180.0	200.0
4.0	93.8	140.0	160.0	180.0	200.0
5.0	117.2	140.0	160.0	180.0	200.0

 $f'_m=5000.0\text{psi}$

σ_v	50.0	100.0	150.0	200.0	250.0
l/h					
0.5	12.7	25.1	37.5	50.2	61.9
1.0	25.1	50.1	72.1	90.5	112.7
2.0	47.0	92.5	137.6	180.0	200.0
3.0	70.7	138.6	160.0	180.0	200.0
4.0	93.8	140.0	160.0	180.0	200.0
5.0	117.2	140.0	160.0	180.0	200.0

 $\sigma_0=50.0\text{psi}$ $\tau_0=200.0\text{psi}$ $\mu=0.4$ $f'_m=1000.0\text{psi}$

σ_v	50.0	100.0	150.0	200.0	250.0
l/h					
0.5	12.4	23.3	32.0	39.0	44.4
1.0	24.8	46.0	63.7	71.7	78.4
2.0	46.6	57.0	65.8	73.5	80.6
3.0	47.3	58.0	66.7	74.6	81.6
4.0	50.3	58.3	66.7	74.6	81.7
5.0	56.4	62.3	68.8	75.0	81.9

 $f'_m=2000.0\text{psi}$

σ_v	50.0	100.0	150.0	200.0	250.0
l/h					
0.5	12.7	24.8	36.0	46.2	55.3
1.0	25.1	49.5	64.3	71.7	78.4
2.0	46.6	57.0	65.8	73.5	80.6
3.0	47.3	58.0	66.7	74.6	81.6
4.0	50.3	58.3	66.7	74.6	81.7
5.0	56.4	62.3	68.8	75.0	81.9

 $f'_m=3000.0\text{psi}$

σ_v	50.0	100.0	150.0	200.0	250.0
l/h					
0.5	12.7	25.1	37.1	48.4	59.0
1.0	25.1	50.1	64.3	71.7	78.4
2.0	46.6	57.0	65.8	73.5	80.6
3.0	47.3	58.0	66.7	74.6	81.6
4.0	50.3	58.3	66.7	74.6	81.7
5.0	56.4	62.3	68.8	75.0	81.9

 $f'_m=4000.0\text{psi}$

σ_v	50.0	100.0	150.0	200.0	250.0
l/h					
0.5	12.7	25.1	37.5	49.5	60.8
1.0	25.1	50.1	64.3	71.7	78.4
2.0	46.6	57.0	65.8	73.5	80.6
3.0	47.3	58.0	66.7	74.6	81.6
4.0	50.3	58.3	66.7	74.6	81.7
5.0	56.4	62.3	68.8	75.0	81.9

 $f'_m=5000.0\text{psi}$

σ_v	50.0	100.0	150.0	200.0	250.0
l/h					
0.5	12.7	25.1	37.5	50.2	61.9
1.0	25.1	50.1	64.3	71.7	78.4
2.0	46.6	57.0	65.8	73.5	80.6
3.0	47.3	58.0	66.7	74.6	81.6
4.0	50.3	58.3	66.7	74.6	81.7
5.0	56.4	62.3	68.8	75.0	81.9

$\sigma_0=100.0\text{psi}$ $\tau_0= 200.0\text{psi}$ $\mu= 0.4$

$\sigma_0=150.0\text{psi}$ $\tau_0= 200.0\text{psi}$ $\mu= 0.4$

$f'_m= 1000.0\text{psi}$

$f'_m= 1000.0\text{psi}$

σ_v	50.0	100.0	150.0	200.0	250.0
l/h					
0.5	12.4	23.3	32.0	39.0	44.4
1.0	24.8	46.0	63.7	77.7	88.5
2.0	48.1	89.4	104.0	113.9	123.1
3.0	71.9	94.3	105.6	115.6	124.7
4.0	91.9	100.6	108.5	116.5	124.9
5.0	104.5	112.5	118.7	124.5	130.0

σ_v	50.0	100.0	150.0	200.0	250.0
l/h					
0.5	12.4	23.3	32.0	39.0	44.4
1.0	24.8	46.0	63.7	77.7	88.5
2.0	48.1	89.4	119.6	142.5	160.7
3.0	71.9	129.5	141.7	152.9	163.5
4.0	95.8	141.3	150.9	157.2	166.1
5.0	119.4	159.1	168.6	172.2	179.5

$f'_m= 2000.0\text{psi}$

$f'_m= 2000.0\text{psi}$

σ_v	50.0	100.0	150.0	200.0	250.0
l/h					
0.5	12.7	24.8	36.0	46.2	55.3
1.0	25.1	49.5	71.5	91.9	110.3
2.0	48.1	93.1	104.0	113.9	123.1
3.0	71.9	94.3	105.6	115.6	124.7
4.0	91.9	100.6	108.5	116.5	124.9
5.0	104.5	112.5	118.7	124.5	130.0

σ_v	50.0	100.0	150.0	200.0	250.0
l/h					
0.5	12.7	24.8	36.0	46.2	55.3
1.0	25.1	49.5	71.5	91.9	110.3
2.0	48.1	94.1	138.0	151.1	161.3
3.0	71.9	129.5	141.7	152.9	163.5
4.0	95.8	141.3	150.9	157.2	166.1
5.0	119.4	159.1	168.6	172.2	179.5

$f'_m= 3000.0\text{psi}$

$f'_m= 3000.0\text{psi}$

σ_v	50.0	100.0	150.0	200.0	250.0
l/h					
0.5	12.7	25.1	37.1	48.4	59.0
1.0	25.1	50.1	74.3	96.5	117.8
2.0	48.1	93.1	104.0	113.9	123.1
3.0	71.9	94.3	105.6	115.6	124.7
4.0	91.9	100.6	108.5	116.5	124.9
5.0	104.5	112.5	118.7	124.5	130.0

σ_v	50.0	100.0	150.0	200.0	250.0
l/h					
0.5	12.7	25.1	37.1	48.4	59.0
1.0	25.1	50.1	74.3	96.5	117.8
2.0	48.1	94.1	139.6	151.1	161.3
3.0	71.9	129.5	141.7	152.9	163.5
4.0	95.8	141.3	150.9	157.2	166.1
5.0	119.4	159.1	168.6	172.2	179.5

$f'_m= 4000.0\text{psi}$

$f'_m= 4000.0\text{psi}$

σ_v	50.0	100.0	150.0	200.0	250.0
l/h					
0.5	12.7	25.1	37.5	49.5	60.8
1.0	25.1	50.1	75.0	98.8	120.9
2.0	48.1	93.1	104.0	113.9	123.1
3.0	71.9	94.3	105.6	115.6	124.7
4.0	91.9	100.6	108.5	116.5	124.9
5.0	104.5	112.5	118.7	124.5	130.0

σ_v	50.0	100.0	150.0	200.0	250.0
l/h					
0.5	12.7	25.1	37.5	49.5	60.8
1.0	25.1	50.1	75.0	98.8	121.4
2.0	48.1	94.1	139.6	151.1	161.3
3.0	71.9	129.5	141.7	152.9	163.5
4.0	95.8	141.3	150.9	157.2	166.1
5.0	119.4	159.1	168.6	172.2	179.5

$f'_m= 5000.0\text{psi}$

$f'_m= 5000.0\text{psi}$

σ_v	50.0	100.0	150.0	200.0	250.0
l/h					
0.5	12.7	25.1	37.5	50.2	61.9
1.0	25.1	50.1	75.0	99.9	120.9
2.0	48.1	93.1	104.0	113.9	123.1
3.0	71.9	94.3	105.6	115.6	124.7
4.0	91.9	100.6	108.5	116.5	124.9
5.0	104.5	112.5	118.7	124.5	130.0

σ_v	50.0	100.0	150.0	200.0	250.0
l/h					
0.5	12.7	25.1	37.5	50.2	61.9
1.0	25.1	50.1	75.0	99.9	123.6
2.0	48.1	94.1	139.6	151.1	161.3
3.0	71.9	129.5	141.7	152.9	163.5
4.0	95.8	141.3	150.9	157.2	166.1
5.0	119.4	159.1	168.6	172.2	179.5

$\sigma_0=200.0\text{psi}$ $\tau_0=200.0\text{psi}$ $\mu=0.4$ $f'_m=1000.0\text{psi}$

σ_v	50.0	100.0	150.0	200.0	250.0
l/h					
0.5	12.4	23.3	32.0	39.0	44.4
1.0	24.8	46.0	63.7	77.7	88.5
2.0	48.1	89.4	119.6	142.5	160.7
3.0	71.9	131.1	176.0	206.6	200.2
4.0	95.8	171.8	227.5	263.5	290.1
5.0	119.4	212.6	260.0	280.0	300.0

 $f'_m=2000.0\text{psi}$

σ_v	50.0	100.0	150.0	200.0	250.0
l/h					
0.5	12.7	24.8	36.0	46.2	55.3
1.0	25.1	49.5	71.5	91.9	110.3
2.0	48.1	94.1	138.0	178.6	199.0
3.0	71.9	141.1	205.1	262.1	200.2
4.0	95.8	187.5	260.0	280.0	300.0
5.0	119.4	234.1	260.0	280.0	300.0

 $f'_m=3000.0\text{psi}$

σ_v	50.0	100.0	150.0	200.0	250.0
l/h					
0.5	12.7	25.1	37.1	48.4	59.0
1.0	25.1	50.1	74.3	96.5	117.8
2.0	48.1	94.1	139.6	184.9	199.0
3.0	71.9	141.1	209.3	277.0	200.2
4.0	95.8	187.5	260.0	280.0	300.0
5.0	119.4	234.1	260.0	280.0	300.0

 $f'_m=4000.0\text{psi}$

σ_v	50.0	100.0	150.0	200.0	250.0
l/h					
0.5	12.7	25.1	37.5	49.5	60.8
1.0	25.1	50.1	75.0	98.8	121.4
2.0	48.1	94.1	139.6	184.9	199.0
3.0	71.9	141.1	209.3	277.0	200.2
4.0	95.8	187.5	260.0	280.0	300.0
5.0	119.4	234.1	260.0	280.0	300.0

 $f'_m=5000.0\text{psi}$

σ_v	50.0	100.0	150.0	200.0	250.0
l/h					
0.5	12.7	25.1	37.5	50.2	61.9
1.0	25.1	50.1	75.0	99.9	123.6
2.0	48.1	94.1	139.6	184.9	199.0
3.0	71.9	141.1	209.3	277.0	200.2
4.0	95.8	187.5	260.0	280.0	300.0
5.0	119.4	234.1	260.0	280.0	300.0

 $\sigma_0=250.0\text{psi}$ $\tau_0=200.0\text{psi}$ $\mu=0.4$ $f'_m=1000.0\text{psi}$

σ_v	50.0	100.0	150.0	200.0	250.0
l/h					
0.5	12.4	23.3	32.0	39.0	44.4
1.0	24.8	46.0	63.7	77.7	88.5
2.0	48.1	89.4	119.6	142.5	160.7
3.0	71.9	131.1	176.0	206.6	224.5
4.0	95.8	171.8	227.5	263.5	290.1
5.0	119.4	212.6	260.0	280.0	300.0

 $f'_m=2000.0\text{psi}$

σ_v	50.0	100.0	150.0	200.0	250.0
l/h					
0.5	12.7	24.8	36.0	46.2	55.3
1.0	25.1	49.5	71.5	91.9	110.3
2.0	48.1	94.1	138.0	178.6	211.5
3.0	71.9	141.1	205.1	262.1	300.0
4.0	95.8	187.5	260.0	280.0	300.0
5.0	119.4	234.1	260.0	280.0	300.0

 $f'_m=3000.0\text{psi}$

σ_v	50.0	100.0	150.0	200.0	250.0
l/h					
0.5	12.7	25.1	37.1	48.4	59.0
1.0	25.1	50.1	74.3	96.5	117.8
2.0	48.1	94.1	139.6	184.9	227.4
3.0	71.9	141.1	209.3	277.0	300.0
4.0	95.8	187.5	260.0	280.0	300.0
5.0	119.4	234.1	260.0	280.0	300.0

 $f'_m=4000.0\text{psi}$

σ_v	50.0	100.0	150.0	200.0	250.0
l/h					
0.5	12.7	25.1	37.5	49.5	60.8
1.0	25.1	50.1	75.0	98.8	121.4
2.0	48.1	94.1	139.6	184.9	230.0
3.0	71.9	141.1	209.3	277.0	300.0
4.0	95.8	187.5	260.0	280.0	300.0
5.0	119.4	234.1	260.0	280.0	300.0

 $f'_m=5000.0\text{psi}$

σ_v	50.0	100.0	150.0	200.0	250.0
l/h					
0.5	12.7	25.1	37.5	50.2	61.9
1.0	25.1	50.1	75.0	99.9	123.6
2.0	48.1	94.1	139.6	184.9	230.0
3.0	71.9	141.1	209.3	277.0	300.0
4.0	95.8	187.5	260.0	280.0	300.0
5.0	119.4	234.1	260.0	280.0	300.0

$\sigma_0=50.0\text{psi}$ $\tau_0=300.0\text{psi}$ $\mu=0.4$ $f'_m=1000.0\text{psi}$

σ_v	50.0	100.0	150.0	200.0	250.0
l/h					
0.5	12.4	23.3	32.0	39.0	44.4
1.0	24.8	46.0	63.7	71.7	78.4
2.0	46.6	57.0	65.8	73.5	80.6
3.0	47.3	58.0	66.7	74.6	81.6
4.0	50.3	58.3	66.7	74.6	81.7
5.0	56.4	62.3	68.8	75.0	81.9

 $f'_m=2000.0\text{psi}$

σ_v	50.0	100.0	150.0	200.0	250.0
l/h					
0.5	12.7	24.8	36.0	46.2	55.3
1.0	25.1	49.5	64.3	71.7	78.4
2.0	46.6	57.0	65.8	73.5	80.6
3.0	47.3	58.0	66.7	74.6	81.6
4.0	50.3	58.3	66.7	74.6	81.7
5.0	56.4	62.3	68.8	75.0	81.9

 $f'_m=3000.0\text{psi}$

σ_v	50.0	100.0	150.0	200.0	250.0
l/h					
0.5	12.7	25.1	37.1	48.4	59.0
1.0	25.1	50.1	64.3	71.7	78.4
2.0	46.6	57.0	65.8	73.5	80.6
3.0	47.3	58.0	66.7	74.6	81.6
4.0	50.3	58.3	66.7	74.6	81.7
5.0	56.4	62.3	68.8	75.0	81.9

 $f'_m=4000.0\text{psi}$

σ_v	50.0	100.0	150.0	200.0	250.0
l/h					
0.5	12.7	25.1	37.5	49.5	60.8
1.0	25.1	50.1	64.3	71.7	78.4
2.0	46.6	57.0	65.8	73.5	80.6
3.0	47.3	58.0	66.7	74.6	81.6
4.0	50.3	58.3	66.7	74.6	81.7
5.0	56.4	62.3	68.8	75.0	81.9

 $f'_m=5000.0\text{psi}$

σ_v	50.0	100.0	150.0	200.0	250.0
l/h					
0.5	12.7	25.1	37.5	50.2	61.9
1.0	25.1	50.1	64.3	71.7	78.4
2.0	46.6	57.0	65.8	73.5	80.6
3.0	47.3	58.0	66.7	74.6	81.6
4.0	50.3	58.3	66.7	74.6	81.7
5.0	56.4	62.3	68.8	75.0	81.9

 $\sigma_0=100.0\text{psi}$ $\tau_0=300.0\text{psi}$ $\mu=0.4$ $f'_m=1000.0\text{psi}$

σ_v	50.0	100.0	150.0	200.0	250.0
l/h					
0.5	12.4	23.3	32.0	39.0	44.4
1.0	24.8	46.0	63.7	77.7	88.5
2.0	49.4	88.7	104.0	113.9	123.1
3.0	72.5	94.3	105.6	115.6	124.7
4.0	91.9	100.6	108.5	116.5	124.9
5.0	104.5	112.5	118.7	124.5	130.0

 $f'_m=2000.0\text{psi}$

σ_v	50.0	100.0	150.0	200.0	250.0
l/h					
0.5	12.7	24.8	36.0	46.2	55.3
1.0	25.1	49.5	71.5	91.9	110.3
2.0	50.1	93.1	104.0	113.9	123.1
3.0	72.8	94.3	105.6	115.6	124.7
4.0	91.9	100.6	108.5	116.5	124.9
5.0	104.5	112.5	118.7	124.5	130.0

 $f'_m=3000.0\text{psi}$

σ_v	50.0	100.0	150.0	200.0	250.0
l/h					
0.5	12.7	25.1	37.1	48.4	59.0
1.0	25.1	50.1	74.3	96.5	117.8
2.0	50.1	93.1	104.0	113.9	123.1
3.0	72.8	94.3	105.6	115.6	124.7
4.0	91.9	100.6	108.5	116.5	124.9
5.0	104.5	112.5	118.7	124.5	130.0

 $f'_m=4000.0\text{psi}$

σ_v	50.0	100.0	150.0	200.0	250.0
l/h					
0.5	12.7	25.1	37.5	49.5	60.8
1.0	25.1	50.1	75.0	98.8	120.9
2.0	50.1	93.1	104.0	113.9	123.1
3.0	72.8	94.3	105.6	115.6	124.7
4.0	91.9	100.6	108.5	116.5	124.9
5.0	104.5	112.5	118.7	124.5	130.0

 $f'_m=5000.0\text{psi}$

σ_v	50.0	100.0	150.0	200.0	250.0
l/h					
0.5	12.7	25.1	37.5	50.2	61.9
1.0	25.1	50.1	75.0	99.9	120.9
2.0	50.1	93.1	104.0	113.9	123.1
3.0	72.8	94.3	105.6	115.6	124.7
4.0	91.9	100.6	108.5	116.5	124.9
5.0	104.5	112.5	118.7	124.5	130.0

$\sigma_0=150.0\text{psi}$ $\tau_0= 300.0\text{psi}$ $\mu= 0.4$

$f'_m= 1000.0\text{psi}$

σ_v	50.0	100.0	150.0	200.0	250.0
l/h					
0.5	12.4	23.3	32.0	39.0	44.4
1.0	24.8	46.0	63.7	77.7	88.5
2.0	49.4	88.7	118.5	141.4	158.5
3.0	72.5	129.5	141.7	152.9	163.5
4.0	96.0	141.3	150.9	157.2	166.1
5.0	119.4	159.1	168.6	172.2	179.5

$f'_m= 2000.0\text{psi}$

σ_v	50.0	100.0	150.0	200.0	250.0
l/h					
0.5	12.7	24.8	36.0	46.2	55.3
1.0	25.1	49.5	71.5	91.9	110.3
2.0	50.1	95.2	138.0	151.1	161.3
3.0	72.8	129.5	141.7	152.9	163.5
4.0	96.9	141.3	150.9	157.2	166.1
5.0	121.2	159.1	168.6	172.2	179.5

$f'_m= 3000.0\text{psi}$

σ_v	50.0	100.0	150.0	200.0	250.0
l/h					
0.5	12.7	25.1	37.1	48.4	59.0
1.0	25.1	50.1	74.3	96.5	117.8
2.0	50.1	95.2	139.7	151.1	161.3
3.0	72.8	129.5	141.7	152.9	163.5
4.0	96.9	141.3	150.9	157.2	166.1
5.0	121.2	159.1	168.6	172.2	179.5

$f'_m= 4000.0\text{psi}$

σ_v	50.0	100.0	150.0	200.0	250.0
l/h					
0.5	12.7	25.1	37.5	49.5	60.8
1.0	25.1	50.1	75.0	98.8	121.4
2.0	50.1	95.2	139.7	151.1	161.3
3.0	72.8	129.5	141.7	152.9	163.5
4.0	96.9	141.3	150.9	157.2	166.1
5.0	121.2	159.1	168.6	172.2	179.5

$f'_m= 5000.0\text{psi}$

σ_v	50.0	100.0	150.0	200.0	250.0
l/h					
0.5	12.7	25.1	37.5	50.2	61.9
1.0	25.1	50.1	75.0	99.9	123.6
2.0	50.1	95.2	139.7	151.1	161.3
3.0	72.8	129.5	141.7	152.9	163.5
4.0	96.9	141.3	150.9	157.2	166.1
5.0	121.2	159.1	168.6	172.2	179.5

$\sigma_0=200.0\text{psi}$ $\tau_0= 300.0\text{psi}$ $\mu= 0.4$

$f'_m= 1000.0\text{psi}$

σ_v	50.0	100.0	150.0	200.0	250.0
l/h					
0.5	12.4	23.3	32.0	39.0	44.4
1.0	24.8	46.0	63.7	77.7	88.5
2.0	49.4	88.7	118.5	141.4	158.5
3.0	72.5	131.1	176.0	188.7	200.2
4.0	96.0	171.8	192.9	201.1	209.1
5.0	119.4	209.0	217.3	224.6	231.2

$f'_m= 2000.0\text{psi}$

σ_v	50.0	100.0	150.0	200.0	250.0
l/h					
0.5	12.7	24.8	36.0	46.2	55.3
1.0	25.1	49.5	71.5	91.9	110.3
2.0	50.1	95.2	138.0	178.6	197.7
3.0	72.8	142.6	177.2	188.7	200.2
4.0	96.9	183.9	192.9	201.1	209.1
5.0	121.2	209.0	217.3	224.6	231.2

$f'_m= 3000.0\text{psi}$

σ_v	50.0	100.0	150.0	200.0	250.0
l/h					
0.5	12.7	25.1	37.1	48.4	59.0
1.0	25.1	50.1	74.3	96.5	117.8
2.0	50.1	95.2	141.1	186.2	197.7
3.0	72.8	142.6	177.2	188.7	200.2
4.0	96.9	183.9	192.9	201.1	209.1
5.0	121.2	209.0	217.3	224.6	231.2

$f'_m= 4000.0\text{psi}$

σ_v	50.0	100.0	150.0	200.0	250.0
l/h					
0.5	12.7	25.1	37.5	49.5	60.8
1.0	25.1	50.1	75.0	98.8	121.4
2.0	50.1	95.2	141.1	186.2	197.7
3.0	72.8	142.6	177.2	188.7	200.2
4.0	96.9	183.9	192.9	201.1	209.1
5.0	121.2	209.0	217.3	224.6	231.2

$f'_m= 5000.0\text{psi}$

σ_v	50.0	100.0	150.0	200.0	250.0
l/h					
0.5	12.7	25.1	37.5	50.2	61.9
1.0	25.1	50.1	75.0	99.9	123.6
2.0	50.1	95.2	141.1	186.2	197.7
3.0	72.8	142.6	177.2	188.7	200.2
4.0	96.9	183.9	192.9	201.1	209.1
5.0	121.2	209.0	217.3	224.6	231.2

$\sigma_0=250.0\text{psi}$ $\tau_0= 300.0\text{psi}$ $\mu= 0.4$

$f'_m= 1000.0\text{psi}$

σ_v	50.0	100.0	150.0	200.0	250.0
l/h					
0.5	12.4	23.3	32.0	39.0	44.4
1.0	24.8	46.0	63.7	77.7	88.5
2.0	49.4	88.7	118.5	141.4	158.5
3.0	72.5	131.1	176.0	206.6	223.6
4.0	96.0	171.8	227.5	238.7	251.4
5.0	119.4	212.6	280.0	324.4	346.6

$f'_m= 2000.0\text{psi}$

σ_v	50.0	100.0	150.0	200.0	250.0
l/h					
0.5	12.7	24.8	36.0	46.2	55.3
1.0	25.1	49.5	71.5	91.9	110.3
2.0	50.1	95.2	138.0	178.6	211.5
3.0	72.8	142.6	205.1	223.9	235.7
4.0	96.9	189.8	230.5	238.7	251.4
5.0	121.2	237.0	339.7	380.0	400.0

$f'_m= 3000.0\text{psi}$

σ_v	50.0	100.0	150.0	200.0	250.0
l/h					
0.5	12.7	25.1	37.1	48.4	59.0
1.0	25.1	50.1	74.3	96.5	117.8
2.0	50.1	95.2	141.1	186.7	227.4
3.0	72.8	142.6	211.5	223.9	235.7
4.0	96.9	189.8	230.5	238.7	251.4
5.0	121.2	237.0	351.0	380.0	400.0

$f'_m= 4000.0\text{psi}$

σ_v	50.0	100.0	150.0	200.0	250.0
l/h					
0.5	12.7	25.1	37.5	49.5	60.8
1.0	25.1	50.1	75.0	98.8	121.4
2.0	50.1	95.2	141.1	186.7	232.0
3.0	72.8	142.6	211.5	223.9	235.7
4.0	96.9	189.8	230.5	238.7	251.4
5.0	121.2	237.0	351.0	380.0	400.0

$f'_m= 5000.0\text{psi}$

σ_v	50.0	100.0	150.0	200.0	250.0
l/h					
0.5	12.7	25.1	37.5	50.2	61.9
1.0	25.1	50.1	75.0	99.9	123.6
2.0	50.1	95.2	141.1	186.7	232.0
3.0	72.8	142.6	211.5	223.9	235.7
4.0	96.9	189.8	230.5	238.7	251.4
5.0	121.2	237.0	351.0	380.0	400.0

$\sigma_0= 50.0\text{psi}$ $\tau_0= 100.0\text{psi}$ $\mu= 0.6$

$f'_m= 1000.0\text{psi}$

σ_v	50.0	100.0	150.0	200.0	250.0
l/h					
0.5	12.4	23.3	32.0	39.0	44.4
1.0	24.8	46.0	63.7	71.7	78.4
2.0	46.6	57.0	65.8	73.5	80.6
3.0	47.3	58.0	66.7	74.6	81.6
4.0	50.3	58.3	66.7	74.6	81.7
5.0	56.4	62.3	68.8	75.0	81.9

$f'_m= 2000.0\text{psi}$

σ_v	50.0	100.0	150.0	200.0	250.0
l/h					
0.5	12.7	24.8	36.0	46.2	55.3
1.0	25.1	49.5	64.3	71.7	78.4
2.0	46.6	57.0	65.8	73.5	80.6
3.0	47.3	58.0	66.7	74.6	81.6
4.0	50.3	58.3	66.7	74.6	81.7
5.0	56.4	62.3	68.8	75.0	81.9

$f'_m= 3000.0\text{psi}$

σ_v	50.0	100.0	150.0	200.0	250.0
l/h					
0.5	12.7	25.1	37.1	48.4	59.0
1.0	25.1	50.1	64.3	71.7	78.4
2.0	46.6	57.0	65.8	73.5	80.6
3.0	47.3	58.0	66.7	74.6	81.6
4.0	50.3	58.3	66.7	74.6	81.7
5.0	56.4	62.3	68.8	75.0	81.9

$f'_m= 4000.0\text{psi}$

σ_v	50.0	100.0	150.0	200.0	250.0
l/h					
0.5	12.7	25.1	37.5	49.5	60.8
1.0	25.1	50.1	64.3	71.7	78.4
2.0	46.6	57.0	65.8	73.5	80.6
3.0	47.3	58.0	66.7	74.6	81.6
4.0	50.3	58.3	66.7	74.6	81.7
5.0	56.4	62.3	68.8	75.0	81.9

$f'_m= 5000.0\text{psi}$

σ_v	50.0	100.0	150.0	200.0	250.0
l/h					
0.5	12.7	25.1	37.5	50.2	61.9
1.0	25.1	50.1	64.3	71.7	78.4
2.0	46.6	57.0	65.8	73.5	80.6
3.0	47.3	58.0	66.7	74.6	81.6
4.0	50.3	58.3	66.7	74.6	81.7
5.0	56.4	62.3	68.8	75.0	81.9

$\sigma_0=100.0\text{psi}$ $\tau_0=100.0\text{psi}$ $\mu=0.6$ $f'_m=1000.0\text{psi}$

σ_v	50.0	100.0	150.0	200.0	250.0
l/h					
0.5	12.4	23.3	32.0	39.0	44.4
1.0	24.8	46.0	63.7	77.7	88.5
2.0	48.2	89.7	104.0	113.9	123.1
3.0	72.5	94.3	105.6	115.6	124.7
4.0	96.0	100.6	108.5	116.5	124.9
5.0	119.4	160.0	118.7	124.5	130.0

 $f'_m=2000.0\text{psi}$

σ_v	50.0	100.0	150.0	200.0	250.0
l/h					
0.5	12.7	24.8	36.0	46.2	55.3
1.0	25.1	49.5	71.5	91.9	110.3
2.0	48.2	93.1	104.0	113.9	123.1
3.0	72.5	94.3	105.6	115.6	124.7
4.0	96.5	100.6	108.5	116.5	124.9
5.0	120.5	160.0	118.7	124.5	130.0

 $f'_m=3000.0\text{psi}$

σ_v	50.0	100.0	150.0	200.0	250.0
l/h					
0.5	12.7	25.1	37.1	48.4	59.0
1.0	25.1	50.1	74.3	96.5	117.8
2.0	48.2	93.1	104.0	113.9	123.1
3.0	72.5	94.3	105.6	115.6	124.7
4.0	96.5	100.6	108.5	116.5	124.9
5.0	120.5	160.0	118.7	124.5	130.0

 $f'_m=4000.0\text{psi}$

σ_v	50.0	100.0	150.0	200.0	250.0
l/h					
0.5	12.7	25.1	37.5	49.5	60.8
1.0	25.1	50.1	75.0	98.8	120.9
2.0	48.2	93.1	104.0	113.9	123.1
3.0	72.5	94.3	105.6	115.6	124.7
4.0	96.5	100.6	108.5	116.5	124.9
5.0	120.5	160.0	118.7	124.5	130.0

 $f'_m=5000.0\text{psi}$

σ_v	50.0	100.0	150.0	200.0	250.0
l/h					
0.5	12.7	25.1	37.5	50.2	61.9
1.0	25.1	50.1	75.0	99.9	120.9
2.0	48.2	93.1	104.0	113.9	123.1
3.0	72.5	94.3	105.6	115.6	124.7
4.0	96.5	100.6	108.5	116.5	124.9
5.0	120.5	160.0	118.7	124.5	130.0

 $\sigma_0=150.0\text{psi}$ $\tau_0=100.0\text{psi}$ $\mu=0.6$ $f'_m=1000.0\text{psi}$

σ_v	50.0	100.0	150.0	200.0	250.0
l/h					
0.5	12.4	23.3	32.0	39.0	44.4
1.0	24.8	46.0	63.7	77.7	88.5
2.0	48.2	89.7	120.5	144.1	162.2
3.0	72.5	131.1	176.0	206.6	163.5
4.0	96.0	160.0	190.0	220.0	166.1
5.0	119.4	160.0	190.0	220.0	250.0

 $f'_m=2000.0\text{psi}$

σ_v	50.0	100.0	150.0	200.0	250.0
l/h					
0.5	12.7	24.8	36.0	46.2	55.3
1.0	25.1	49.5	71.5	91.9	110.3
2.0	48.2	95.4	138.1	179.5	162.2
3.0	72.5	143.5	190.0	220.0	163.5
4.0	96.5	160.0	190.0	220.0	166.1
5.0	120.5	160.0	190.0	220.0	250.0

 $f'_m=3000.0\text{psi}$

σ_v	50.0	100.0	150.0	200.0	250.0
l/h					
0.5	12.7	25.1	37.1	48.4	59.0
1.0	25.1	50.1	74.3	96.5	117.8
2.0	48.2	95.4	142.6	188.3	162.2
3.0	72.5	143.5	190.0	220.0	163.5
4.0	96.5	160.0	190.0	220.0	166.1
5.0	120.5	160.0	190.0	220.0	250.0

 $f'_m=4000.0\text{psi}$

σ_v	50.0	100.0	150.0	200.0	250.0
l/h					
0.5	12.7	25.1	37.5	49.5	60.8
1.0	25.1	50.1	75.0	98.8	121.4
2.0	48.2	95.4	142.6	189.8	162.2
3.0	72.5	143.5	190.0	220.0	163.5
4.0	96.5	160.0	190.0	220.0	166.1
5.0	120.5	160.0	190.0	220.0	250.0

 $f'_m=5000.0\text{psi}$

σ_v	50.0	100.0	150.0	200.0	250.0
l/h					
0.5	12.7	25.1	37.5	50.2	61.9
1.0	25.1	50.1	75.0	99.9	123.6
2.0	48.2	95.4	142.6	189.8	162.2
3.0	72.5	143.5	190.0	220.0	163.5
4.0	96.5	160.0	190.0	220.0	166.1
5.0	120.5	160.0	190.0	220.0	250.0

$\sigma_0=200.0\text{psi}$ $\tau_0=100.0\text{psi}$ $\mu=0.6$ $f'_m=1000.0\text{psi}$

σ_v	50.0	100.0	150.0	200.0	250.0
l/h					
0.5	12.4	23.3	32.0	39.0	44.4
1.0	24.8	46.0	63.7	77.7	88.5
2.0	48.2	89.7	120.5	144.1	162.3
3.0	72.5	131.1	176.0	206.6	228.4
4.0	96.0	160.0	190.0	220.0	250.0
5.0	119.4	160.0	190.0	220.0	250.0

 $f'_m=2000.0\text{psi}$

σ_v	50.0	100.0	150.0	200.0	250.0
l/h					
0.5	12.7	24.8	36.0	46.2	55.3
1.0	25.1	49.5	71.5	91.9	110.3
2.0	48.2	95.4	138.1	179.5	211.5
3.0	72.5	143.5	190.0	220.0	250.0
4.0	96.5	160.0	190.0	220.0	250.0
5.0	120.5	160.0	190.0	220.0	250.0

 $f'_m=3000.0\text{psi}$

σ_v	50.0	100.0	150.0	200.0	250.0
l/h					
0.5	12.7	25.1	37.1	48.4	59.0
1.0	25.1	50.1	74.3	96.5	117.8
2.0	48.2	95.4	142.6	188.3	228.2
3.0	72.5	143.5	190.0	220.0	250.0
4.0	96.5	160.0	190.0	220.0	250.0
5.0	120.5	160.0	190.0	220.0	250.0

 $f'_m=4000.0\text{psi}$

σ_v	50.0	100.0	150.0	200.0	250.0
l/h					
0.5	12.7	25.1	37.5	49.5	60.8
1.0	25.1	50.1	75.0	98.8	121.4
2.0	48.2	95.4	142.6	189.8	236.8
3.0	72.5	143.5	190.0	220.0	250.0
4.0	96.5	160.0	190.0	220.0	250.0
5.0	120.5	160.0	190.0	220.0	250.0

 $f'_m=5000.0\text{psi}$

σ_v	50.0	100.0	150.0	200.0	250.0
l/h					
0.5	12.7	25.1	37.5	50.2	61.9
1.0	25.1	50.1	75.0	99.9	123.6
2.0	48.2	95.4	142.6	189.8	236.8
3.0	72.5	143.5	190.0	220.0	250.0
4.0	96.5	160.0	190.0	220.0	250.0
5.0	120.5	160.0	190.0	220.0	250.0

 $\sigma_0=250.0\text{psi}$ $\tau_0=100.0\text{psi}$ $\mu=0.6$ $f'_m=1000.0\text{psi}$

σ_v	50.0	100.0	150.0	200.0	250.0
l/h					
0.5	12.4	23.3	32.0	39.0	44.4
1.0	24.8	46.0	63.7	77.7	88.5
2.0	48.2	89.7	120.5	144.1	162.3
3.0	72.5	131.1	176.0	206.6	228.4
4.0	96.0	160.0	190.0	220.0	250.0
5.0	119.4	160.0	190.0	220.0	250.0

 $f'_m=2000.0\text{psi}$

σ_v	50.0	100.0	150.0	200.0	250.0
l/h					
0.5	12.7	24.8	36.0	46.2	55.3
1.0	25.1	49.5	71.5	91.9	110.3
2.0	48.2	95.4	138.1	179.5	211.5
3.0	72.5	143.5	190.0	220.0	250.0
4.0	96.5	160.0	190.0	220.0	250.0
5.0	120.5	160.0	190.0	220.0	250.0

 $f'_m=3000.0\text{psi}$

σ_v	50.0	100.0	150.0	200.0	250.0
l/h					
0.5	12.7	25.1	37.1	48.4	59.0
1.0	25.1	50.1	74.3	96.5	117.8
2.0	48.2	95.4	142.6	188.3	228.2
3.0	72.5	143.5	190.0	220.0	250.0
4.0	96.5	160.0	190.0	220.0	250.0
5.0	120.5	160.0	190.0	220.0	250.0

 $f'_m=4000.0\text{psi}$

σ_v	50.0	100.0	150.0	200.0	250.0
l/h					
0.5	12.7	25.1	37.5	49.5	60.8
1.0	25.1	50.1	75.0	98.8	121.4
2.0	48.2	95.4	142.6	189.8	236.8
3.0	72.5	143.5	190.0	220.0	250.0
4.0	96.5	160.0	190.0	220.0	250.0
5.0	120.5	160.0	190.0	220.0	250.0

 $f'_m=5000.0\text{psi}$

σ_v	50.0	100.0	150.0	200.0	250.0
l/h					
0.5	12.7	25.1	37.5	50.2	61.9
1.0	25.1	50.1	75.0	99.9	123.6
2.0	48.2	95.4	142.6	189.8	236.8
3.0	72.5	143.5	190.0	220.0	250.0
4.0	96.5	160.0	190.0	220.0	250.0
5.0	120.5	160.0	190.0	220.0	250.0

$\sigma_0=50.0\text{psi}$ $\tau_0=200.0\text{psi}$ $\mu=0.6$ $f'_m=1000.0\text{psi}$

σ_v	50.0	100.0	150.0	200.0	250.0
l/h					
0.5	12.4	23.3	32.0	39.0	44.4
1.0	24.8	46.0	63.7	71.7	78.4
2.0	46.6	57.0	65.8	73.5	80.6
3.0	47.3	58.0	66.7	74.6	81.6
4.0	50.3	58.3	66.7	74.6	81.7
5.0	56.4	62.3	68.8	75.0	81.9

 $f'_m=2000.0\text{psi}$

σ_v	50.0	100.0	150.0	200.0	250.0
l/h					
0.5	12.7	24.8	36.0	46.2	55.3
1.0	25.1	49.5	64.3	71.7	78.4
2.0	46.6	57.0	65.8	73.5	80.6
3.0	47.3	58.0	66.7	74.6	81.6
4.0	50.3	58.3	66.7	74.6	81.7
5.0	56.4	62.3	68.8	75.0	81.9

 $f'_m=3000.0\text{psi}$

σ_v	50.0	100.0	150.0	200.0	250.0
l/h					
0.5	12.7	25.1	37.1	48.4	59.0
1.0	25.1	50.1	64.3	71.7	78.4
2.0	46.6	57.0	65.8	73.5	80.6
3.0	47.3	58.0	66.7	74.6	81.6
4.0	50.3	58.3	66.7	74.6	81.7
5.0	56.4	62.3	68.8	75.0	81.9

 $f'_m=4000.0\text{psi}$

σ_v	50.0	100.0	150.0	200.0	250.0
l/h					
0.5	12.7	25.1	37.5	49.5	60.8
1.0	25.1	50.1	64.3	71.7	78.4
2.0	46.6	57.0	65.8	73.5	80.6
3.0	47.3	58.0	66.7	74.6	81.6
4.0	50.3	58.3	66.7	74.6	81.7
5.0	56.4	62.3	68.8	75.0	81.9

 $f'_m=5000.0\text{psi}$

σ_v	50.0	100.0	150.0	200.0	250.0
l/h					
0.5	12.7	25.1	37.5	50.2	61.9
1.0	25.1	50.1	64.3	71.7	78.4
2.0	46.6	57.0	65.8	73.5	80.6
3.0	47.3	58.0	66.7	74.6	81.6
4.0	50.3	58.3	66.7	74.6	81.7
5.0	56.4	62.3	68.8	75.0	81.9

 $\sigma_0=100.0\text{psi}$ $\tau_0=200.0\text{psi}$ $\mu=0.6$ $f'_m=1000.0\text{psi}$

σ_v	50.0	100.0	150.0	200.0	250.0
l/h					
0.5	12.4	23.3	32.0	39.0	44.4
1.0	24.8	46.0	63.7	77.7	88.5
2.0	48.8	89.1	104.0	113.9	123.1
3.0	72.5	94.3	105.6	115.6	124.7
4.0	91.9	100.6	108.5	116.5	124.9
5.0	104.5	112.5	118.7	124.5	130.0

 $f'_m=2000.0\text{psi}$

σ_v	50.0	100.0	150.0	200.0	250.0
l/h					
0.5	12.7	24.8	36.0	46.2	55.3
1.0	25.1	49.5	71.5	91.9	110.3
2.0	48.8	93.1	104.0	113.9	123.1
3.0	73.4	94.3	105.6	115.6	124.7
4.0	91.9	100.6	108.5	116.5	124.9
5.0	104.5	112.5	118.7	124.5	130.0

 $f'_m=3000.0\text{psi}$

σ_v	50.0	100.0	150.0	200.0	250.0
l/h					
0.5	12.7	25.1	37.1	48.4	59.0
1.0	25.1	50.1	74.3	96.5	117.8
2.0	48.8	93.1	104.0	113.9	123.1
3.0	73.4	94.3	105.6	115.6	124.7
4.0	91.9	100.6	108.5	116.5	124.9
5.0	104.5	112.5	118.7	124.5	130.0

 $f'_m=4000.0\text{psi}$

σ_v	50.0	100.0	150.0	200.0	250.0
l/h					
0.5	12.7	25.1	37.5	49.5	60.8
1.0	25.1	50.1	75.0	98.8	120.9
2.0	48.8	93.1	104.0	113.9	123.1
3.0	73.4	94.3	105.6	115.6	124.7
4.0	91.9	100.6	108.5	116.5	124.9
5.0	104.5	112.5	118.7	124.5	130.0

 $f'_m=5000.0\text{psi}$

σ_v	50.0	100.0	150.0	200.0	250.0
l/h					
0.5	12.7	25.1	37.5	50.2	61.9
1.0	25.1	50.1	75.0	99.9	120.9
2.0	48.8	93.1	104.0	113.9	123.1
3.0	73.4	94.3	105.6	115.6	124.7
4.0	91.9	100.6	108.5	116.5	124.9
5.0	104.5	112.5	118.7	124.5	130.0

$\sigma_0=150.0\text{psi}$ $\tau_0=200.0\text{psi}$ $\mu=0.6$ $f'_m=1000.0\text{psi}$

σ_v	50.0	100.0	150.0	200.0	250.0
l/h					
0.5	12.4	23.3	32.0	39.0	44.4
1.0	24.8	46.0	63.7	77.7	88.5
2.0	48.8	89.1	119.1	141.6	158.5
3.0	72.5	129.5	141.7	152.9	163.5
4.0	96.0	141.3	150.9	157.2	166.1
5.0	119.4	159.1	168.6	172.2	179.5

 $f'_m=2000.0\text{psi}$

σ_v	50.0	100.0	150.0	200.0	250.0
l/h					
0.5	12.7	24.8	36.0	46.2	55.3
1.0	25.1	49.5	71.5	91.9	110.3
2.0	48.8	96.3	138.1	151.1	161.3
3.0	73.4	129.5	141.7	152.9	163.5
4.0	97.6	141.3	150.9	157.2	166.1
5.0	122.0	159.1	168.6	172.2	179.5

 $f'_m=3000.0\text{psi}$

σ_v	50.0	100.0	150.0	200.0	250.0
l/h					
0.5	12.7	25.1	37.1	48.4	59.0
1.0	25.1	50.1	74.3	96.5	117.8
2.0	48.8	96.3	139.7	151.1	161.3
3.0	73.4	129.5	141.7	152.9	163.5
4.0	97.6	141.3	150.9	157.2	166.1
5.0	122.0	159.1	168.6	172.2	179.5

 $f'_m=4000.0\text{psi}$

σ_v	50.0	100.0	150.0	200.0	250.0
l/h					
0.5	12.7	25.1	37.5	49.5	60.8
1.0	25.1	50.1	75.0	98.8	121.4
2.0	48.8	96.3	139.7	151.1	161.3
3.0	73.4	129.5	141.7	152.9	163.5
4.0	97.6	141.3	150.9	157.2	166.1
5.0	122.0	159.1	168.6	172.2	179.5

 $f'_m=5000.0\text{psi}$

σ_v	50.0	100.0	150.0	200.0	250.0
l/h					
0.5	12.7	25.1	37.5	50.2	61.9
1.0	25.1	50.1	75.0	99.9	123.6
2.0	48.8	96.3	139.7	151.1	161.3
3.0	73.4	129.5	141.7	152.9	163.5
4.0	97.6	141.3	150.9	157.2	166.1
5.0	122.0	159.1	168.6	172.2	179.5

 $\sigma_0=200.0\text{psi}$ $\tau_0=200.0\text{psi}$ $\mu=0.6$ $f'_m=1000.0\text{psi}$

σ_v	50.0	100.0	150.0	200.0	250.0
l/h					
0.5	12.4	23.3	32.0	39.0	44.4
1.0	24.8	46.0	63.7	77.7	88.5
2.0	48.8	89.1	119.1	141.6	158.5
3.0	72.5	131.1	176.0	188.7	200.2
4.0	96.0	171.8	192.9	201.1	209.1
5.0	119.4	212.6	280.0	320.0	231.2

 $f'_m=2000.0\text{psi}$

σ_v	50.0	100.0	150.0	200.0	250.0
l/h					
0.5	12.7	24.8	36.0	46.2	55.3
1.0	25.1	49.5	71.5	91.9	110.3
2.0	48.8	96.3	138.1	179.5	197.7
3.0	73.4	144.7	177.2	188.7	200.2
4.0	97.6	191.8	192.9	201.1	209.1
5.0	122.0	238.8	290.0	320.0	231.2

 $f'_m=3000.0\text{psi}$

σ_v	50.0	100.0	150.0	200.0	250.0
l/h					
0.5	12.7	25.1	37.1	48.4	59.0
1.0	25.1	50.1	74.3	96.5	117.8
2.0	48.8	96.3	143.6	186.2	197.7
3.0	73.4	144.7	177.2	188.7	200.2
4.0	97.6	192.7	192.9	201.1	209.1
5.0	122.0	240.6	290.0	320.0	231.2

 $f'_m=4000.0\text{psi}$

σ_v	50.0	100.0	150.0	200.0	250.0
l/h					
0.5	12.7	25.1	37.5	49.5	60.8
1.0	25.1	50.1	75.0	98.8	121.4
2.0	48.8	96.3	143.6	186.2	197.7
3.0	73.4	144.7	177.2	188.7	200.2
4.0	97.6	192.7	192.9	201.1	209.1
5.0	122.0	240.6	290.0	320.0	231.2

 $f'_m=5000.0\text{psi}$

σ_v	50.0	100.0	150.0	200.0	250.0
l/h					
0.5	12.7	25.1	37.5	50.2	61.9
1.0	25.1	50.1	75.0	99.9	123.6
2.0	48.8	96.3	143.6	186.2	197.7
3.0	73.4	144.7	177.2	188.7	200.2
4.0	97.6	192.7	192.9	201.1	209.1
5.0	122.0	240.6	290.0	320.0	231.2

$\sigma_0=250.0\text{psi}$ $\tau_0=200.0\text{psi}$ $\mu=0.6$ $f'_m=1000.0\text{psi}$

σ_v	50.0	100.0	150.0	200.0	250.0
l/h					
0.5	12.4	23.3	32.0	39.0	44.4
1.0	24.8	46.0	63.7	77.7	88.5
2.0	48.8	89.1	119.1	141.6	158.5
3.0	72.5	131.1	176.0	206.6	223.6
4.0	96.0	171.8	227.5	264.2	290.1
5.0	119.4	212.6	280.0	320.0	349.5

 $f'_m=2000.0\text{psi}$

σ_v	50.0	100.0	150.0	200.0	250.0
l/h					
0.5	12.7	24.8	36.0	46.2	55.3
1.0	25.1	49.5	71.5	91.9	110.3
2.0	48.8	96.3	138.1	179.5	211.5
3.0	73.4	144.7	206.0	262.1	305.5
4.0	97.6	191.8	273.3	320.0	350.0
5.0	122.0	238.8	290.0	320.0	350.0

 $f'_m=3000.0\text{psi}$

σ_v	50.0	100.0	150.0	200.0	250.0
l/h					
0.5	12.7	25.1	37.1	48.4	59.0
1.0	25.1	50.1	74.3	96.5	117.8
2.0	48.8	96.3	143.6	188.3	228.2
3.0	73.4	144.7	216.0	277.6	340.1
4.0	97.6	192.7	287.6	320.0	350.0
5.0	122.0	240.6	290.0	320.0	350.0

 $f'_m=4000.0\text{psi}$

σ_v	50.0	100.0	150.0	200.0	250.0
l/h					
0.5	12.7	25.1	37.5	49.5	60.8
1.0	25.1	50.1	75.0	98.8	121.4
2.0	48.8	96.3	143.6	190.8	238.0
3.0	73.4	144.7	216.0	287.0	350.0
4.0	97.6	192.7	287.6	320.0	350.0
5.0	122.0	240.6	290.0	320.0	350.0

 $f'_m=5000.0\text{psi}$

σ_v	50.0	100.0	150.0	200.0	250.0
l/h					
0.5	12.7	25.1	37.5	50.2	61.9
1.0	25.1	50.1	75.0	99.9	123.6
2.0	48.8	96.3	143.6	190.8	238.0
3.0	73.4	144.7	216.0	287.0	350.0
4.0	97.6	192.7	287.6	320.0	350.0
5.0	122.0	240.6	290.0	320.0	350.0

 $\sigma_0=50.0\text{psi}$ $\tau_0=300.0\text{psi}$ $\mu=0.6$ $f'_m=1000.0\text{psi}$

σ_v	50.0	100.0	150.0	200.0	250.0
l/h					
0.5	12.4	23.3	32.0	39.0	44.4
1.0	24.8	46.0	63.7	71.7	78.4
2.0	46.6	57.0	65.8	73.5	80.6
3.0	47.3	58.0	66.7	74.6	81.6
4.0	50.3	58.3	66.7	74.6	81.7
5.0	56.4	62.3	68.8	75.0	81.9

 $f'_m=2000.0\text{psi}$

σ_v	50.0	100.0	150.0	200.0	250.0
l/h					
0.5	12.7	24.8	36.0	46.2	55.3
1.0	25.1	49.5	64.3	71.7	78.4
2.0	46.6	57.0	65.8	73.5	80.6
3.0	47.3	58.0	66.7	74.6	81.6
4.0	50.3	58.3	66.7	74.6	81.7
5.0	56.4	62.3	68.8	75.0	81.9

 $f'_m=3000.0\text{psi}$

σ_v	50.0	100.0	150.0	200.0	250.0
l/h					
0.5	12.7	25.1	37.1	48.4	59.0
1.0	25.1	50.1	64.3	71.7	78.4
2.0	46.6	57.0	65.8	73.5	80.6
3.0	47.3	58.0	66.7	74.6	81.6
4.0	50.3	58.3	66.7	74.6	81.7
5.0	56.4	62.3	68.8	75.0	81.9

 $f'_m=4000.0\text{psi}$

σ_v	50.0	100.0	150.0	200.0	250.0
l/h					
0.5	12.7	25.1	37.5	49.5	60.8
1.0	25.1	50.1	64.3	71.7	78.4
2.0	46.6	57.0	65.8	73.5	80.6
3.0	47.3	58.0	66.7	74.6	81.6
4.0	50.3	58.3	66.7	74.6	81.7
5.0	56.4	62.3	68.8	75.0	81.9

 $f'_m=5000.0\text{psi}$

σ_v	50.0	100.0	150.0	200.0	250.0
l/h					
0.5	12.7	25.1	37.5	50.2	61.9
1.0	25.1	50.1	64.3	71.7	78.4
2.0	46.6	57.0	65.8	73.5	80.6
3.0	47.3	58.0	66.7	74.6	81.6
4.0	50.3	58.3	66.7	74.6	81.7
5.0	56.4	62.3	68.8	75.0	81.9

$\sigma_0=100.0\text{psi}$ $\tau_0=300.0\text{psi}$ $\mu=0.6$ $f'_m=1000.0\text{psi}$

σ_v	50.0	100.0	150.0	200.0	250.0
l/h					
0.5	12.4	23.3	32.0	39.0	44.4
1.0	24.8	46.0	63.7	77.7	88.5
2.0	49.4	88.4	104.0	113.9	123.1
3.0	72.5	94.3	105.6	115.6	124.7
4.0	91.9	100.6	108.5	116.5	124.9
5.0	104.5	112.5	118.7	124.5	130.0

 $f'_m=2000.0\text{psi}$

σ_v	50.0	100.0	150.0	200.0	250.0
l/h					
0.5	12.7	24.8	36.0	46.2	55.3
1.0	25.1	49.5	71.5	91.9	110.3
2.0	50.1	93.1	104.0	113.9	123.1
3.0	74.0	94.3	105.6	115.6	124.7
4.0	91.9	100.6	108.5	116.5	124.9
5.0	104.5	112.5	118.7	124.5	130.0

 $f'_m=3000.0\text{psi}$

σ_v	50.0	100.0	150.0	200.0	250.0
l/h					
0.5	12.7	25.1	37.1	48.4	59.0
1.0	25.1	50.1	74.3	96.5	117.8
2.0	50.1	93.1	104.0	113.9	123.1
3.0	74.0	94.3	105.6	115.6	124.7
4.0	91.9	100.6	108.5	116.5	124.9
5.0	104.5	112.5	118.7	124.5	130.0

 $f'_m=4000.0\text{psi}$

σ_v	50.0	100.0	150.0	200.0	250.0
l/h					
0.5	12.7	25.1	37.5	49.5	60.8
1.0	25.1	50.1	75.0	98.8	120.9
2.0	50.1	93.1	104.0	113.9	123.1
3.0	74.0	94.3	105.6	115.6	124.7
4.0	91.9	100.6	108.5	116.5	124.9
5.0	104.5	112.5	118.7	124.5	130.0

 $f'_m=5000.0\text{psi}$

σ_v	50.0	100.0	150.0	200.0	250.0
l/h					
0.5	12.7	25.1	37.5	50.2	61.9
1.0	25.1	50.1	75.0	99.9	120.9
2.0	50.1	93.1	104.0	113.9	123.1
3.0	74.0	94.3	105.6	115.6	124.7
4.0	91.9	100.6	108.5	116.5	124.9
5.0	104.5	112.5	118.7	124.5	130.0

 $c_v=150.0\text{psi}$ $\tau_0=300.0\text{psi}$ $\mu=0.6$ $f'_m=1000.0\text{psi}$

σ_v	50.0	100.0	150.0	200.0	250.0
l/h					
0.5	12.4	23.3	32.0	39.0	44.4
1.0	24.8	46.0	63.7	77.7	88.5
2.0	49.4	88.4	118.1	141.4	158.5
3.0	72.5	129.5	141.7	152.9	163.5
4.0	96.0	141.3	150.9	157.2	166.1
5.0	119.4	159.1	168.6	172.2	179.5

 $f'_m=2000.0\text{psi}$

σ_v	50.0	100.0	150.0	200.0	250.0
l/h					
0.5	12.7	24.8	36.0	46.2	55.3
1.0	25.1	49.5	71.5	91.9	110.3
2.0	50.1	96.9	138.1	151.1	161.3
3.0	74.0	129.5	141.7	152.9	163.5
4.0	98.3	141.3	150.9	157.2	166.1
5.0	122.7	159.1	168.6	172.2	179.5

 $f'_m=3000.0\text{psi}$

σ_v	50.0	100.0	150.0	200.0	250.0
l/h					
0.5	12.7	25.1	37.1	48.4	59.0
1.0	25.1	50.1	74.3	96.5	117.8
2.0	50.1	96.9	139.7	151.1	161.3
3.0	74.0	129.5	141.7	152.9	163.5
4.0	98.3	141.3	150.9	157.2	166.1
5.0	122.7	159.1	168.6	172.2	179.5

 $f'_m=4000.0\text{psi}$

σ_v	50.0	100.0	150.0	200.0	250.0
l/h					
0.5	12.7	25.1	37.5	49.5	60.8
1.0	25.1	50.1	75.0	98.8	121.4
2.0	50.1	96.9	139.7	151.1	161.3
3.0	74.0	129.5	141.7	152.9	163.5
4.0	98.3	141.3	150.9	157.2	166.1
5.0	122.7	159.1	168.6	172.2	179.5

 $f'_m=5000.0\text{psi}$

σ_v	50.0	100.0	150.0	200.0	250.0
l/h					
0.5	12.7	25.1	37.5	50.2	61.9
1.0	25.1	50.1	75.0	99.9	123.6
2.0	50.1	96.9	139.7	151.1	161.3
3.0	74.0	129.5	141.7	152.9	163.5
4.0	98.3	141.3	150.9	157.2	166.1
5.0	122.7	159.1	168.6	172.2	179.5

$\sigma_0=200.0\text{psi}$ $\tau_0=300.0\text{psi}$ $\mu=0.6$ $f'_m=1000.0\text{psi}$

σ_v	50.0	100.0	150.0	200.0	250.0
l/h					
0.5	12.4	23.3	32.0	39.0	44.4
1.0	24.8	46.0	63.7	77.7	88.5
2.0	49.4	88.4	118.1	141.4	158.5
3.0	72.5	131.1	176.0	188.7	200.2
4.0	96.0	171.8	192.9	201.1	209.1
5.0	119.4	209.0	217.3	224.6	231.2

 $f'_m=2000.0\text{psi}$

σ_v	50.0	100.0	150.0	200.0	250.0
l/h					
0.5	12.7	24.8	36.0	46.2	55.3
1.0	25.1	49.5	71.5	91.9	110.3
2.0	50.1	96.9	138.1	178.2	197.7
3.0	74.0	145.0	177.2	188.7	200.2
4.0	98.3	183.9	192.9	201.1	209.1
5.0	122.7	209.0	217.3	224.6	231.2

 $f'_m=3000.0\text{psi}$

σ_v	50.0	100.0	150.0	200.0	250.0
l/h					
0.5	12.7	25.1	37.1	48.4	59.0
1.0	25.1	50.1	74.3	96.5	117.8
2.0	50.1	96.9	144.4	186.2	197.7
3.0	74.0	145.6	177.2	188.7	200.2
4.0	98.3	183.9	192.9	201.1	209.1
5.0	122.7	209.0	217.3	224.6	231.2

 $f'_m=4000.0\text{psi}$

σ_v	50.0	100.0	150.0	200.0	250.0
l/h					
0.5	12.7	25.1	37.5	49.5	60.8
1.0	25.1	50.1	75.0	98.8	121.4
2.0	50.1	96.9	144.4	186.2	197.7
3.0	74.0	145.6	177.2	188.7	200.2
4.0	98.3	183.9	192.9	201.1	209.1
5.0	122.7	209.0	217.3	224.6	231.2

 $f'_m=5000.0\text{psi}$

σ_v	50.0	100.0	150.0	200.0	250.0
l/h					
0.5	12.7	25.1	37.5	50.2	61.9
1.0	25.1	50.1	75.0	99.9	123.6
2.0	50.1	96.9	144.4	186.2	197.7
3.0	74.0	145.6	177.2	188.7	200.2
4.0	98.3	183.9	192.9	201.1	209.1
5.0	122.7	209.0	217.3	224.6	231.2

 $\sigma_0=250.0\text{psi}$ $\tau_0=300.0\text{psi}$ $\mu=0.6$ $f'_m=1000.0\text{psi}$

σ_v	50.0	100.0	150.0	200.0	250.0
l/h					
0.5	12.4	23.3	32.0	39.0	44.4
1.0	24.8	46.0	63.7	77.7	88.5
2.0	49.4	88.4	118.1	141.4	158.5
3.0	72.5	131.1	176.0	206.6	223.6
4.0	96.0	171.8	227.5	238.7	251.4
5.0	119.4	212.6	259.6	266.5	280.7

 $f'_m=2000.0\text{psi}$

σ_v	50.0	100.0	150.0	200.0	250.0
l/h					
0.5	12.7	24.8	36.0	46.2	55.3
1.0	25.1	49.5	71.5	91.9	110.3
2.0	50.1	96.9	138.1	178.2	211.5
3.0	74.0	145.0	206.0	223.9	235.7
4.0	98.3	191.8	230.5	238.7	251.4
5.0	122.7	238.8	259.6	266.5	280.7

 $f'_m=3000.0\text{psi}$

σ_v	50.0	100.0	150.0	200.0	250.0
l/h					
0.5	12.7	25.1	37.1	48.4	59.0
1.0	25.1	50.1	74.3	96.5	117.8
2.0	50.1	96.9	144.4	188.3	228.2
3.0	74.0	145.6	211.8	223.9	235.7
4.0	98.3	194.1	230.5	238.7	251.4
5.0	122.7	242.5	259.6	266.5	280.7

 $f'_m=4000.0\text{psi}$

σ_v	50.0	100.0	150.0	200.0	250.0
l/h					
0.5	12.7	25.1	37.5	49.5	60.8
1.0	25.1	50.1	75.0	98.8	121.4
2.0	50.1	96.9	144.4	191.7	232.7
3.0	74.0	145.6	211.8	223.9	235.7
4.0	98.3	194.1	230.5	238.7	251.4
5.0	122.7	242.5	259.6	266.5	280.7

 $f'_m=5000.0\text{psi}$

σ_v	50.0	100.0	150.0	200.0	250.0
l/h					
0.5	12.7	25.1	37.5	50.2	61.9
1.0	25.1	50.1	75.0	99.9	123.6
2.0	50.1	96.9	144.4	191.7	232.7
3.0	74.0	145.6	211.8	223.9	235.7
4.0	98.3	194.1	230.5	238.7	251.4
5.0	122.7	242.5	259.6	266.5	280.7

$\sigma_0=50.0\text{psi}$ $\tau_0=100.0\text{psi}$ $\mu=0.8$ $f'_m=1000.0\text{psi}$

σ_v	50.0	100.0	150.0	200.0	250.0
l/h					
0.5	12.4	23.3	32.0	39.0	44.4
1.0	24.8	46.0	63.7	71.7	78.4
2.0	46.6	57.0	65.8	73.5	80.6
3.0	47.3	58.0	66.7	74.6	81.6
4.0	50.3	58.3	66.7	74.6	81.7
5.0	56.4	62.3	68.8	75.0	81.9

 $f'_m=2000.0\text{psi}$

σ_v	50.0	100.0	150.0	200.0	250.0
l/h					
0.5	12.7	24.8	36.0	46.2	55.3
1.0	25.1	49.5	64.3	71.7	78.4
2.0	46.6	57.0	65.8	73.5	80.6
3.0	47.3	58.0	66.7	74.6	81.6
4.0	50.3	58.3	66.7	74.6	81.7
5.0	56.4	62.3	68.8	75.0	81.9

 $f'_m=3000.0\text{psi}$

σ_v	50.0	100.0	150.0	200.0	250.0
l/h					
0.5	12.7	25.1	37.1	48.4	59.0
1.0	25.1	50.1	64.3	71.7	78.4
2.0	46.6	57.0	65.8	73.5	80.6
3.0	47.3	58.0	66.7	74.6	81.6
4.0	50.3	58.3	66.7	74.6	81.7
5.0	56.4	62.3	68.8	75.0	81.9

 $f'_m=4000.0\text{psi}$

σ_v	50.0	100.0	150.0	200.0	250.0
l/h					
0.5	12.7	25.1	37.5	49.5	60.8
1.0	25.1	50.1	64.3	71.7	78.4
2.0	46.6	57.0	65.8	73.5	80.6
3.0	47.3	58.0	66.7	74.6	81.6
4.0	50.3	58.3	66.7	74.6	81.7
5.0	56.4	62.3	68.8	75.0	81.9

 $f'_m=5000.0\text{psi}$

σ_v	50.0	100.0	150.0	200.0	250.0
l/h					
0.5	12.7	25.1	37.5	50.2	61.9
1.0	25.1	50.1	64.3	71.7	78.4
2.0	46.6	57.0	65.8	73.5	80.6
3.0	47.3	58.0	66.7	74.6	81.6
4.0	50.3	58.3	66.7	74.6	81.7
5.0	56.4	62.3	68.8	75.0	81.9

 $\sigma_0=100.0\text{psi}$ $\tau_0=100.0\text{psi}$ $\mu=0.8$ $f'_m=1000.0\text{psi}$

σ_v	50.0	100.0	150.0	200.0	250.0
l/h					
0.5	12.4	23.3	32.0	39.0	44.4
1.0	24.8	46.0	63.7	77.7	88.5
2.0	48.9	89.4	104.0	113.9	123.1
3.0	72.5	94.3	105.6	115.6	124.7
4.0	91.9	100.6	108.5	116.5	124.9
5.0	119.4	112.5	118.7	124.5	130.0

 $f'_m=2000.0\text{psi}$

σ_v	50.0	100.0	150.0	200.0	250.0
l/h					
0.5	12.7	24.8	36.0	46.2	55.3
1.0	25.1	49.5	71.5	91.9	110.3
2.0	48.9	93.1	104.0	113.9	123.1
3.0	73.7	94.3	105.6	115.6	124.7
4.0	91.9	100.6	108.5	116.5	124.9
5.0	122.7	112.5	118.7	124.5	130.0

 $f'_m=3000.0\text{psi}$

σ_v	50.0	100.0	150.0	200.0	250.0
l/h					
0.5	12.7	25.1	37.1	48.4	59.0
1.0	25.1	50.1	74.3	96.5	117.8
2.0	48.9	93.1	104.0	113.9	123.1
3.0	73.7	94.3	105.6	115.6	124.7
4.0	91.9	100.6	108.5	116.5	124.9
5.0	122.7	112.5	118.7	124.5	130.0

 $f'_m=4000.0\text{psi}$

σ_v	50.0	100.0	150.0	200.0	250.0
l/h					
0.5	12.7	25.1	37.5	49.5	60.8
1.0	25.1	50.1	75.0	98.8	120.9
2.0	48.9	93.1	104.0	113.9	123.1
3.0	73.7	94.3	105.6	115.6	124.7
4.0	91.9	100.6	108.5	116.5	124.9
5.0	122.7	112.5	118.7	124.5	130.0

 $f'_m=5000.0\text{psi}$

σ_v	50.0	100.0	150.0	200.0	250.0
l/h					
0.5	12.7	25.1	37.5	50.2	61.9
1.0	25.1	50.1	75.0	99.9	120.9
2.0	48.9	93.1	104.0	113.9	123.1
3.0	73.7	94.3	105.6	115.6	124.7
4.0	91.9	100.6	108.5	116.5	124.9
5.0	122.7	112.5	118.7	124.5	130.0

$\sigma_0=150.0\text{psi}$ $\tau_0=100.0\text{psi}$ $\mu=0.8$ $f'_m=1000.0\text{psi}$

σ_v	50.0	100.0	150.0	200.0	250.0
l/h					
0.5	12.4	23.3	32.0	39.0	44.4
1.0	24.8	46.0	63.7	77.7	88.5
2.0	48.9	89.4	120.1	143.7	160.1
3.0	72.5	131.1	141.7	152.9	163.5
4.0	96.0	171.8	220.0	157.2	166.1
5.0	119.4	180.0	220.0	172.2	179.5

 $f'_m=2000.0\text{psi}$

σ_v	50.0	100.0	150.0	200.0	250.0
l/h					
0.5	12.7	24.8	36.0	46.2	55.3
1.0	25.1	49.5	71.5	91.9	110.3
2.0	48.9	97.2	138.5	151.1	161.3
3.0	73.7	145.0	141.7	152.9	163.5
4.0	98.3	180.0	220.0	157.2	166.1
5.0	122.7	180.0	220.0	172.2	179.5

 $f'_m=3000.0\text{psi}$

σ_v	50.0	100.0	150.0	200.0	250.0
l/h					
0.5	12.7	25.1	37.1	48.4	59.0
1.0	25.1	50.1	74.3	96.5	117.8
2.0	48.9	97.2	140.2	151.1	161.3
3.0	73.7	146.5	141.7	152.9	163.5
4.0	98.3	180.0	220.0	157.2	166.1
5.0	122.7	180.0	220.0	172.2	179.5

 $f'_m=4000.0\text{psi}$

σ_v	50.0	100.0	150.0	200.0	250.0
l/h					
0.5	12.7	25.1	37.5	49.5	60.8
1.0	25.1	50.1	75.0	98.8	121.4
2.0	48.9	97.2	140.2	151.1	161.3
3.0	73.7	146.5	141.7	152.9	163.5
4.0	98.3	180.0	220.0	157.2	166.1
5.0	122.7	180.0	220.0	172.2	179.5

 $f'_m=5000.0\text{psi}$

σ_v	50.0	100.0	150.0	200.0	250.0
l/h					
0.5	12.7	25.1	37.5	50.2	61.9
1.0	25.1	50.1	75.0	99.9	123.6
2.0	48.9	97.2	140.2	151.1	161.3
3.0	73.7	146.5	141.7	152.9	163.5
4.0	98.3	180.0	220.0	157.2	166.1
5.0	122.7	180.0	220.0	172.2	179.5

 $\sigma_0=200.0\text{psi}$ $\tau_0=100.0\text{psi}$ $\mu=0.8$ $f'_m=1000.0\text{psi}$

σ_v	50.0	100.0	150.0	200.0	250.0
l/h					
0.5	12.4	23.3	32.0	39.0	44.4
1.0	24.8	46.0	63.7	77.7	88.5
2.0	48.9	89.4	120.1	143.7	160.1
3.0	72.5	131.1	176.0	206.6	200.2
4.0	96.0	171.8	220.0	260.0	290.1
5.0	119.4	180.0	220.0	260.0	300.0

 $f'_m=2000.0\text{psi}$

σ_v	50.0	100.0	150.0	200.0	250.0
l/h					
0.5	12.7	24.8	36.0	46.2	55.3
1.0	25.1	49.5	71.5	91.9	110.3
2.0	48.9	97.2	138.5	178.7	200.1
3.0	73.7	145.0	205.7	260.0	200.2
4.0	98.3	180.0	220.0	260.0	300.0
5.0	122.7	180.0	220.0	260.0	300.0

 $f'_m=3000.0\text{psi}$

σ_v	50.0	100.0	150.0	200.0	250.0
l/h					
0.5	12.7	25.1	37.1	48.4	59.0
1.0	25.1	50.1	74.3	96.5	117.8
2.0	48.9	97.2	145.4	188.3	200.1
3.0	73.7	146.5	217.5	260.0	200.2
4.0	98.3	180.0	220.0	260.0	300.0
5.0	122.7	180.0	220.0	260.0	300.0

 $f'_m=4000.0\text{psi}$

σ_v	50.0	100.0	150.0	200.0	250.0
l/h					
0.5	12.7	25.1	37.5	49.5	60.8
1.0	25.1	50.1	75.0	98.8	121.4
2.0	48.9	97.2	145.4	193.7	200.1
3.0	73.7	146.5	219.4	260.0	200.2
4.0	98.3	180.0	220.0	260.0	300.0
5.0	122.7	180.0	220.0	260.0	300.0

 $f'_m=5000.0\text{psi}$

σ_v	50.0	100.0	150.0	200.0	250.0
l/h					
0.5	12.7	25.1	37.5	50.2	61.9
1.0	25.1	50.1	75.0	99.9	123.6
2.0	48.9	97.2	145.4	193.7	200.1
3.0	73.7	146.5	219.4	260.0	200.2
4.0	98.3	180.0	220.0	260.0	300.0
5.0	122.7	180.0	220.0	260.0	300.0

$\sigma_0=250.0\text{psi}$ $\tau_0=100.0\text{psi}$ $\mu=0.8$ $f'_m=1000.0\text{psi}$

σ_v	50.0	100.0	150.0	200.0	250.0
l/h					
0.5	12.4	23.3	32.0	39.0	44.4
1.0	24.8	46.0	63.7	77.7	88.5
2.0	48.9	89.4	120.1	143.7	160.1
3.0	72.5	131.1	176.0	206.6	226.3
4.0	96.0	171.8	220.0	260.0	290.1
5.0	119.4	180.0	220.0	260.0	300.0

 $f'_m=2000.0\text{psi}$

σ_v	50.0	100.0	150.0	200.0	250.0
l/h					
0.5	12.7	24.8	36.0	46.2	55.3
1.0	25.1	49.5	71.5	91.9	110.3
2.0	48.9	97.2	138.5	178.7	211.5
3.0	73.7	145.0	205.7	260.0	300.0
4.0	98.3	180.0	220.0	260.0	300.0
5.0	122.7	180.0	220.0	260.0	300.0

 $f'_m=3000.0\text{psi}$

σ_v	50.0	100.0	150.0	200.0	250.0
l/h					
0.5	12.7	25.1	37.1	48.4	59.0
1.0	25.1	50.1	74.3	96.5	117.8
2.0	48.9	97.2	145.4	188.3	229.0
3.0	73.7	146.5	217.5	260.0	300.0
4.0	98.3	180.0	220.0	260.0	300.0
5.0	122.7	180.0	220.0	260.0	300.0

 $f'_m=4000.0\text{psi}$

σ_v	50.0	100.0	150.0	200.0	250.0
l/h					
0.5	12.7	25.1	37.5	49.5	60.8
1.0	25.1	50.1	75.0	98.8	121.4
2.0	48.9	97.2	145.4	193.7	238.2
3.0	73.7	146.5	219.4	260.0	300.0
4.0	98.3	180.0	220.0	260.0	300.0
5.0	122.7	180.0	220.0	260.0	300.0

 $f'_m=5000.0\text{psi}$

σ_v	50.0	100.0	150.0	200.0	250.0
l/h					
0.5	12.7	25.1	37.5	50.2	61.9
1.0	25.1	50.1	75.0	99.9	123.6
2.0	48.9	97.2	145.4	193.7	241.9
3.0	73.7	146.5	219.4	260.0	300.0
4.0	98.3	180.0	220.0	260.0	300.0
5.0	122.7	180.0	220.0	260.0	300.0

 $\sigma_0=50.0\text{psi}$ $\tau_0=200.0\text{psi}$ $\mu=0.8$ $f'_m=1000.0\text{psi}$

σ_v	50.0	100.0	150.0	200.0	250.0
l/h					
0.5	12.4	23.3	32.0	39.0	44.4
1.0	24.8	46.0	63.7	71.7	78.4
2.0	46.6	57.0	65.8	73.5	80.6
3.0	47.3	58.0	66.7	74.6	81.6
4.0	50.3	58.3	66.7	74.6	81.7
5.0	56.4	62.3	68.8	75.0	81.9

 $f'_m=2000.0\text{psi}$

σ_v	50.0	100.0	150.0	200.0	250.0
l/h					
0.5	12.7	24.8	36.0	46.2	55.3
1.0	25.1	49.5	64.3	71.7	78.4
2.0	46.6	57.0	65.8	73.5	80.6
3.0	47.3	58.0	66.7	74.6	81.6
4.0	50.3	58.3	66.7	74.6	81.7
5.0	56.4	62.3	68.8	75.0	81.9

 $f'_m=3000.0\text{psi}$

σ_v	50.0	100.0	150.0	200.0	250.0
l/h					
0.5	12.7	25.1	37.1	48.4	59.0
1.0	25.1	50.1	64.3	71.7	78.4
2.0	46.6	57.0	65.8	73.5	80.6
3.0	47.3	58.0	66.7	74.6	81.6
4.0	50.3	58.3	66.7	74.6	81.7
5.0	56.4	62.3	68.8	75.0	81.9

 $f'_m=4000.0\text{psi}$

σ_v	50.0	100.0	150.0	200.0	250.0
l/h					
0.5	12.7	25.1	37.5	49.5	60.8
1.0	25.1	50.1	64.3	71.7	78.4
2.0	46.6	57.0	65.8	73.5	80.6
3.0	47.3	58.0	66.7	74.6	81.6
4.0	50.3	58.3	66.7	74.6	81.7
5.0	56.4	62.3	68.8	75.0	81.9

 $f'_m=5000.0\text{psi}$

σ_v	50.0	100.0	150.0	200.0	250.0
l/h					
0.5	12.7	25.1	37.5	50.2	61.9
1.0	25.1	50.1	64.3	71.7	78.4
2.0	46.6	57.0	65.8	73.5	80.6
3.0	47.3	58.0	66.7	74.6	81.6
4.0	50.3	58.3	66.7	74.6	81.7
5.0	56.4	62.3	68.8	75.0	81.9

$\sigma_0=100.0\text{psi}$ $\tau_0=200.0\text{psi}$ $\mu=0.8$ $f'_m=1000.0\text{psi}$

σ_v	50.0	100.0	150.0	200.0	250.0
l/h					
0.5	12.4	23.3	32.0	39.0	44.4
1.0	24.8	46.0	63.7	77.7	88.5
2.0	49.4	88.7	104.0	113.9	123.1
3.0	72.5	94.3	105.6	115.6	124.7
4.0	91.9	100.6	108.5	116.5	124.9
5.0	104.5	112.5	118.7	124.5	130.0

 $f'_m=2000.0\text{psi}$

σ_v	50.0	100.0	150.0	200.0	250.0
l/h					
0.5	12.7	24.8	36.0	46.2	55.3
1.0	25.1	49.5	71.5	91.9	110.3
2.0	50.1	93.1	104.0	113.9	123.1
3.0	74.3	94.3	105.6	115.6	124.7
4.0	91.9	100.6	108.5	116.5	124.9
5.0	104.5	112.5	118.7	124.5	130.0

 $f'_m=3000.0\text{psi}$

σ_v	50.0	100.0	150.0	200.0	250.0
l/h					
0.5	12.7	25.1	37.1	48.4	59.0
1.0	25.1	50.1	74.3	96.5	117.8
2.0	50.1	93.1	104.0	113.9	123.1
3.0	74.3	94.3	105.6	115.6	124.7
4.0	91.9	100.6	108.5	116.5	124.9
5.0	104.5	112.5	118.7	124.5	130.0

 $f'_m=4000.0\text{psi}$

σ_v	50.0	100.0	150.0	200.0	250.0
l/h					
0.5	12.7	25.1	37.5	49.5	60.8
1.0	25.1	50.1	75.0	98.8	120.9
2.0	50.1	93.1	104.0	113.9	123.1
3.0	74.3	94.3	105.6	115.6	124.7
4.0	91.9	100.6	108.5	116.5	124.9
5.0	104.5	112.5	118.7	124.5	130.0

 $f'_m=5000.0\text{psi}$

σ_v	50.0	100.0	150.0	200.0	250.0
l/h					
0.5	12.7	25.1	37.5	50.2	61.9
1.0	25.1	50.1	75.0	99.9	120.9
2.0	50.1	93.1	104.0	113.9	123.1
3.0	74.3	94.3	105.6	115.6	124.7
4.0	91.9	100.6	108.5	116.5	124.9
5.0	104.5	112.5	118.7	124.5	130.0

 $\sigma_0=150.0\text{psi}$ $\tau_0=200.0\text{psi}$ $\mu=0.8$ $f'_m=1000.0\text{psi}$

σ_v	50.0	100.0	150.0	200.0	250.0
l/h					
0.5	12.4	23.3	32.0	39.0	44.4
1.0	24.8	46.0	63.7	77.7	88.5
2.0	49.4	88.7	118.1	141.4	158.5
3.0	72.5	129.5	141.7	152.9	163.5
4.0	96.0	141.3	150.9	157.2	166.1
5.0	119.4	159.1	168.6	172.2	179.5

 $f'_m=2000.0\text{psi}$

σ_v	50.0	100.0	150.0	200.0	250.0
l/h					
0.5	12.7	24.8	36.0	46.2	55.3
1.0	25.1	49.5	71.5	91.9	110.3
2.0	50.1	97.8	138.0	151.1	161.3
3.0	74.3	129.5	141.7	152.9	163.5
4.0	99.0	141.3	150.9	157.2	166.1
5.0	123.8	159.1	168.6	172.2	179.5

 $f'_m=3000.0\text{psi}$

σ_v	50.0	100.0	150.0	200.0	250.0
l/h					
0.5	12.7	25.1	37.1	48.4	59.0
1.0	25.1	50.1	74.3	96.5	117.8
2.0	50.1	97.8	139.7	151.1	161.3
3.0	74.3	129.5	141.7	152.9	163.5
4.0	99.0	141.3	150.9	157.2	166.1
5.0	123.8	159.1	168.6	172.2	179.5

 $f'_m=4000.0\text{psi}$

σ_v	50.0	100.0	150.0	200.0	250.0
l/h					
0.5	12.7	25.1	37.5	49.5	60.8
1.0	25.1	50.1	75.0	98.8	121.4
2.0	50.1	97.8	139.7	151.1	161.3
3.0	74.3	129.5	141.7	152.9	163.5
4.0	99.0	141.3	150.9	157.2	166.1
5.0	123.8	159.1	168.6	172.2	179.5

 $f'_m=5000.0\text{psi}$

σ_v	50.0	100.0	150.0	200.0	250.0
l/h					
0.5	12.7	25.1	37.5	50.2	61.9
1.0	25.1	50.1	75.0	99.9	123.6
2.0	50.1	97.8	139.7	151.1	161.3
3.0	74.3	129.5	141.7	152.9	163.5
4.0	99.0	141.3	150.9	157.2	166.1
5.0	123.8	159.1	168.6	172.2	179.5

$\sigma_0=200.0\text{psi}$ $\tau_0=200.0\text{psi}$ $\mu=0.8$ $f'_m=1000.0\text{psi}$

σ_v	50.0	100.0	150.0	200.0	250.0
l/h					
0.5	12.4	23.3	32.0	39.0	44.4
1.0	24.8	46.0	63.7	77.7	88.5
2.0	49.4	88.7	118.1	141.4	158.5
3.0	72.5	131.1	176.0	188.7	200.2
4.0	96.0	171.8	192.9	201.1	209.1
5.0	119.4	212.6	280.0	224.6	231.2

 $f'_m=2000.0\text{psi}$

σ_v	50.0	100.0	150.0	200.0	250.0
l/h					
0.5	12.7	24.8	36.0	46.2	55.3
1.0	25.1	49.5	71.5	91.9	110.3
2.0	50.1	97.8	138.0	178.7	197.7
3.0	74.3	145.0	177.2	188.7	200.2
4.0	99.0	183.9	192.9	201.1	209.1
5.0	123.8	238.8	320.0	224.6	231.2

 $f'_m=3000.0\text{psi}$

σ_v	50.0	100.0	150.0	200.0	250.0
l/h					
0.5	12.7	25.1	37.1	48.4	59.0
1.0	25.1	50.1	74.3	96.5	117.8
2.0	50.1	97.8	146.1	186.2	197.7
3.0	74.3	147.1	177.2	188.7	200.2
4.0	99.0	183.9	192.9	201.1	209.1
5.0	123.8	245.4	320.0	224.6	231.2

 $f'_m=4000.0\text{psi}$

σ_v	50.0	100.0	150.0	200.0	250.0
l/h					
0.5	12.7	25.1	37.5	49.5	60.8
1.0	25.1	50.1	75.0	98.8	121.4
2.0	50.1	97.8	146.1	186.2	197.7
3.0	74.3	147.1	177.2	188.7	200.2
4.0	99.0	183.9	192.9	201.1	209.1
5.0	123.8	245.4	320.0	224.6	231.2

 $f'_m=5000.0\text{psi}$

σ_v	50.0	100.0	150.0	200.0	250.0
l/h					
0.5	12.7	25.1	37.5	50.2	61.9
1.0	25.1	50.1	75.0	99.9	123.6
2.0	50.1	97.8	146.1	186.2	197.7
3.0	74.3	147.1	177.2	188.7	200.2
4.0	99.0	183.9	192.9	201.1	209.1
5.0	123.8	245.4	320.0	224.6	231.2

 $\sigma_0=250.0\text{psi}$ $\tau_0=200.0\text{psi}$ $\mu=0.8$ $f'_m=1000.0\text{psi}$

σ_v	50.0	100.0	150.0	200.0	250.0
l/h					
0.5	12.4	23.3	32.0	39.0	44.4
1.0	24.8	46.0	63.7	77.7	88.5
2.0	49.4	88.7	118.1	141.4	158.5
3.0	72.5	131.1	176.0	206.6	223.6
4.0	96.0	171.8	227.5	238.7	251.4
5.0	119.4	212.6	280.0	329.1	349.5

 $f'_m=2000.0\text{psi}$

σ_v	50.0	100.0	150.0	200.0	250.0
l/h					
0.5	12.7	24.8	36.0	46.2	55.3
1.0	25.1	49.5	71.5	91.9	110.3
2.0	50.1	97.8	138.0	178.7	211.5
3.0	74.3	145.0	205.7	223.9	235.7
4.0	99.0	191.8	273.3	238.7	251.4
5.0	123.8	238.8	320.0	360.0	400.0

 $f'_m=3000.0\text{psi}$

σ_v	50.0	100.0	150.0	200.0	250.0
l/h					
0.5	12.7	25.1	37.1	48.4	59.0
1.0	25.1	50.1	74.3	96.5	117.8
2.0	50.1	97.8	146.1	188.3	227.2
3.0	74.3	147.1	211.8	223.9	235.7
4.0	99.0	196.4	287.6	238.7	251.4
5.0	123.8	245.4	320.0	360.0	400.0

 $f'_m=4000.0\text{psi}$

σ_v	50.0	100.0	150.0	200.0	250.0
l/h					
0.5	12.7	25.1	37.5	49.5	60.8
1.0	25.1	50.1	75.0	98.8	121.4
2.0	50.1	97.8	146.1	194.3	232.7
3.0	74.3	147.1	211.8	223.9	235.7
4.0	99.0	196.4	293.5	238.7	251.4
5.0	123.8	245.4	320.0	360.0	400.0

 $f'_m=5000.0\text{psi}$

σ_v	50.0	100.0	150.0	200.0	250.0
l/h					
0.5	12.7	25.1	37.5	50.2	61.9
1.0	25.1	50.1	75.0	99.9	123.6
2.0	50.1	97.8	146.1	194.3	232.7
3.0	74.3	147.1	211.8	223.9	235.7
4.0	99.0	196.4	293.5	238.7	251.4
5.0	123.8	245.4	320.0	360.0	400.0

$\sigma_0=50.0\text{psi}$ $\tau_0=300.0\text{psi}$ $\mu=0.8$ $f'_m=1000.0\text{psi}$

α_v	50.0	100.0	150.0	200.0	250.0
l/h					
0.5	12.4	23.3	32.0	39.0	44.4
1.0	24.8	46.0	63.7	71.7	78.4
2.0	46.6	57.0	65.8	73.5	80.6
3.0	47.3	58.0	66.7	74.6	81.6
4.0	50.3	58.3	66.7	74.6	81.7
5.0	56.4	62.3	68.8	75.0	81.9

 $f'_m=2000.0\text{psi}$

α_v	50.0	100.0	150.0	200.0	250.0
l/h					
0.5	12.7	24.8	36.0	46.2	55.3
1.0	25.1	49.5	64.3	71.7	78.4
2.0	46.6	57.0	65.8	73.5	80.6
3.0	47.3	58.0	66.7	74.6	81.6
4.0	50.3	58.3	66.7	74.6	81.7
5.0	56.4	62.3	68.8	75.0	81.9

 $f'_m=3000.0\text{psi}$

α_v	50.0	100.0	150.0	200.0	250.0
l/h					
0.5	12.7	25.1	37.1	48.4	59.0
1.0	25.1	50.1	64.3	71.7	78.4
2.0	46.6	57.0	65.8	73.5	80.6
3.0	47.3	58.0	66.7	74.6	81.6
4.0	50.3	58.3	66.7	74.6	81.7
5.0	56.4	62.3	68.8	75.0	81.9

 $f'_m=4000.0\text{psi}$

α_v	50.0	100.0	150.0	200.0	250.0
l/h					
0.5	12.7	25.1	37.5	49.5	60.8
1.0	25.1	50.1	64.3	71.7	78.4
2.0	46.6	57.0	65.8	73.5	80.6
3.0	47.3	58.0	66.7	74.6	81.6
4.0	50.3	58.3	66.7	74.6	81.7
5.0	56.4	62.3	68.8	75.0	81.9

 $f'_m=5000.0\text{psi}$

α_v	50.0	100.0	150.0	200.0	250.0
l/h					
0.5	12.7	25.1	37.5	50.2	61.9
1.0	25.1	50.1	64.3	71.7	78.4
2.0	46.6	57.0	65.8	73.5	80.6
3.0	47.3	58.0	66.7	74.6	81.6
4.0	50.3	58.3	66.7	74.6	81.7
5.0	56.4	62.3	68.8	75.0	81.9

 $\sigma_0=100.0\text{psi}$ $\tau_0=300.0\text{psi}$ $\mu=0.8$ $f'_m=1000.0\text{psi}$

α_v	50.0	100.0	150.0	200.0	250.0
l/h					
0.5	12.4	23.3	32.0	39.0	44.4
1.0	24.8	46.0	63.7	77.7	88.5
2.0	49.4	88.4	104.0	113.9	123.1
3.0	72.5	94.3	105.6	115.6	124.7
4.0	91.9	100.6	108.5	116.5	124.9
5.0	104.5	112.5	118.7	124.5	130.0

 $f'_m=2000.0\text{psi}$

α_v	50.0	100.0	150.0	200.0	250.0
l/h					
0.5	12.7	24.8	36.0	46.2	55.3
1.0	25.1	49.5	71.5	91.9	110.3
2.0	50.1	93.1	104.0	113.9	123.1
3.0	74.6	94.3	105.6	115.6	124.7
4.0	91.9	100.6	108.5	116.5	124.9
5.0	104.5	112.5	118.7	124.5	130.0

 $f'_m=3000.0\text{psi}$

α_v	50.0	100.0	150.0	200.0	250.0
l/h					
0.5	12.7	25.1	37.1	48.4	59.0
1.0	25.1	50.1	74.3	96.5	117.8
2.0	50.1	93.1	104.0	113.9	123.1
3.0	74.6	94.3	105.6	115.6	124.7
4.0	91.9	100.6	108.5	116.5	124.9
5.0	104.5	112.5	118.7	124.5	130.0

 $f'_m=4000.0\text{psi}$

α_v	50.0	100.0	150.0	200.0	250.0
l/h					
0.5	12.7	25.1	37.5	49.5	60.8
1.0	25.1	50.1	75.0	98.8	120.9
2.0	50.1	93.1	104.0	113.9	123.1
3.0	74.6	94.3	105.6	115.6	124.7
4.0	91.9	100.6	108.5	116.5	124.9
5.0	104.5	112.5	118.7	124.5	130.0

 $f'_m=5000.0\text{psi}$

α_v	50.0	100.0	150.0	200.0	250.0
l/h					
0.5	12.7	25.1	37.5	50.2	61.9
1.0	25.1	50.1	75.0	99.9	120.9
2.0	50.1	93.1	104.0	113.9	123.1
3.0	74.6	94.3	105.6	115.6	124.7
4.0	91.9	100.6	108.5	116.5	124.9
5.0	104.5	112.5	118.7	124.5	130.0

$\sigma_0=150.0\text{psi}$ $\tau_0=300.0\text{psi}$ $\mu=0.8$ $f'_m=1000.0\text{psi}$

σ_v	50.0	100.0	150.0	200.0	250.0
l/h					
0.5	12.4	23.3	32.0	39.0	44.4
1.0	24.8	46.0	63.7	77.7	88.5
2.0	49.4	88.4	118.1	141.4	153.5
3.0	72.5	129.5	141.7	152.9	163.5
4.0	96.0	141.3	150.9	157.2	166.1
5.0	119.4	159.1	168.6	172.2	179.5

 $f'_m=2000.0\text{psi}$

σ_v	50.0	100.0	150.0	200.0	250.0
l/h					
0.5	12.7	24.8	36.0	46.2	55.3
1.0	25.1	49.5	71.5	91.9	110.3
2.0	50.1	98.2	138.0	151.1	161.3
3.0	74.6	129.5	141.7	152.9	163.5
4.0	99.4	141.3	150.9	157.2	166.1
5.0	124.1	159.1	168.6	172.2	179.5

 $f'_m=3000.0\text{psi}$

σ_v	50.0	100.0	150.0	200.0	250.0
l/h					
0.5	12.7	25.1	37.1	48.4	59.0
1.0	25.1	50.1	74.3	96.5	117.8
2.0	50.1	98.2	139.7	151.1	161.3
3.0	74.6	129.5	141.7	152.9	163.5
4.0	99.4	141.3	150.9	157.2	166.1
5.0	124.1	159.1	168.6	172.2	179.5

 $f'_m=4000.0\text{psi}$

σ_v	50.0	100.0	150.0	200.0	250.0
l/h					
0.5	12.7	25.1	37.5	49.5	60.8
1.0	25.1	50.1	75.0	98.8	121.4
2.0	50.1	98.2	139.7	151.1	161.3
3.0	74.6	129.5	141.7	152.9	163.5
4.0	99.4	141.3	150.9	157.2	166.1
5.0	124.1	159.1	168.6	172.2	179.5

 $f'_m=5000.0\text{psi}$

σ_v	50.0	100.0	150.0	200.0	250.0
l/h					
0.5	12.7	25.1	37.5	50.2	61.9
1.0	25.1	50.1	75.0	99.9	123.6
2.0	50.1	98.2	139.7	151.1	161.3
3.0	74.6	129.5	141.7	152.9	163.5
4.0	99.4	141.3	150.9	157.2	166.1
5.0	124.1	159.1	168.6	172.2	179.5

 $\sigma_0=200.0\text{psi}$ $\tau_0=300.0\text{psi}$ $\mu=0.8$ $f'_m=1000.0\text{psi}$

σ_v	50.0	100.0	150.0	200.0	250.0
l/h					
0.5	12.4	23.3	32.0	39.0	44.4
1.0	24.8	46.0	63.7	77.7	88.5
2.0	49.4	88.4	118.1	141.4	158.5
3.0	72.5	131.1	175.7	188.7	200.2
4.0	96.0	171.8	192.9	201.1	209.1
5.0	119.4	209.0	217.3	224.6	231.2

 $f'_m=2000.0\text{psi}$

σ_v	50.0	100.0	150.0	200.0	250.0
l/h					
0.5	12.7	24.8	36.0	46.2	55.3
1.0	25.1	49.5	71.5	91.9	110.3
2.0	50.1	98.2	138.0	178.7	197.7
3.0	74.6	145.0	177.2	188.7	200.2
4.0	99.4	183.9	192.9	201.1	209.1
5.0	124.1	209.0	217.3	224.6	231.2

 $f'_m=3000.0\text{psi}$

σ_v	50.0	100.0	150.0	200.0	250.0
l/h					
0.5	12.7	25.1	37.1	48.4	59.0
1.0	25.1	50.1	74.3	96.5	117.8
2.0	50.1	98.2	146.5	186.2	197.7
3.0	74.6	147.8	177.2	188.7	200.2
4.0	99.4	183.9	192.9	201.1	209.1
5.0	124.1	209.0	217.3	224.6	231.2

 $f'_m=4000.0\text{psi}$

σ_v	50.0	100.0	150.0	200.0	250.0
l/h					
0.5	12.7	25.1	37.5	49.5	60.8
1.0	25.1	50.1	75.0	98.8	121.4
2.0	50.1	98.2	146.5	186.2	197.7
3.0	74.6	147.8	177.2	188.7	200.2
4.0	99.4	183.9	192.9	201.1	209.1
5.0	124.1	209.0	217.3	224.6	231.2

 $f'_m=5000.0\text{psi}$

σ_v	50.0	100.0	150.0	200.0	250.0
l/h					
0.5	12.7	25.1	37.5	50.2	61.9
1.0	25.1	50.1	75.0	99.9	123.6
2.0	50.1	98.2	146.5	186.2	197.7
3.0	74.6	147.8	177.2	188.7	200.2
4.0	99.4	183.9	192.9	201.1	209.1
5.0	124.1	209.0	217.3	224.6	231.2

$\sigma_0=250.0\text{psi}$ $\tau_0=300.0\text{psi}$ $\mu=0.8$ $f'_m=1000.0\text{psi}$

σ_v	50.0	100.0	150.0	200.0	250.0
l/h					
0.5	12.4	23.3	32.0	39.0	44.4
1.0	24.8	46.0	63.7	77.7	88.5
2.0	49.4	88.4	118.1	141.4	158.5
3.0	72.5	131.1	175.7	206.3	223.6
4.0	96.0	171.8	227.5	238.7	251.4
5.0	119.4	212.6	259.6	266.5	280.7

 $f'_m=2000.0\text{psi}$

σ_v	50.0	100.0	150.0	200.0	250.0
l/h					
0.5	12.7	24.8	36.0	46.2	55.3
1.0	25.1	49.5	71.5	91.9	110.3
2.0	50.1	98.2	138.0	178.7	211.5
3.0	74.6	145.0	205.7	223.9	235.7
4.0	99.4	191.8	230.5	238.7	251.4
5.0	124.1	238.8	259.6	266.5	280.7

 $f'_m=3000.0\text{psi}$

σ_v	50.0	100.0	150.0	200.0	250.0
l/h					
0.5	12.7	25.1	37.1	48.4	59.0
1.0	25.1	50.1	74.3	96.5	117.8
2.0	50.1	98.2	146.5	188.3	227.2
3.0	74.6	147.8	211.8	223.9	235.7
4.0	99.4	197.1	230.5	238.7	251.4
5.0	124.1	246.1	259.6	266.5	280.7

 $f'_m=4000.0\text{psi}$

σ_v	50.0	100.0	150.0	200.0	250.0
l/h					
0.5	12.7	25.1	37.5	49.5	60.8
1.0	25.1	50.1	75.0	98.8	121.4
2.0	50.1	98.2	146.5	194.9	232.7
3.0	74.6	147.8	211.8	223.9	235.7
4.0	99.4	197.1	230.5	238.7	251.4
5.0	124.1	246.1	259.6	266.5	280.7

 $f'_m=5000.0\text{psi}$

σ_v	50.0	100.0	150.0	200.0	250.0
l/h					
0.5	12.7	25.1	37.5	50.2	61.9
1.0	25.1	50.1	75.0	99.9	123.6
2.0	50.1	98.2	146.5	194.9	232.7
3.0	74.6	147.8	211.8	223.9	235.7
4.0	99.4	197.1	230.5	238.7	251.4
5.0	124.1	246.1	259.6	266.5	280.7

 $\sigma_0=50.0\text{psi}$ $\tau_0=100.0\text{psi}$ $\mu=1.0$ $f'_m=1000.0\text{psi}$

σ_v	50.0	100.0	150.0	200.0	250.0
l/h					
0.5	12.4	23.3	32.0	39.0	44.4
1.0	24.8	46.0	63.7	71.7	78.4
2.0	46.6	57.0	65.8	73.5	80.6
3.0	47.3	58.0	66.7	74.6	81.6
4.0	50.3	58.3	66.7	74.6	81.7
5.0	56.4	62.3	68.8	75.0	81.9

 $f'_m=2000.0\text{psi}$

σ_v	50.0	100.0	150.0	200.0	250.0
l/h					
0.5	12.7	24.8	36.0	46.2	55.3
1.0	25.1	49.5	64.3	71.7	78.4
2.0	46.6	57.0	65.8	73.5	80.6
3.0	47.3	58.0	66.7	74.6	81.6
4.0	50.3	58.3	66.7	74.6	81.7
5.0	56.4	62.3	68.8	75.0	81.9

 $f'_m=3000.0\text{psi}$

σ_v	50.0	100.0	150.0	200.0	250.0
l/h					
0.5	12.7	25.1	37.1	48.4	59.0
1.0	25.1	50.1	64.3	71.7	78.4
2.0	46.6	57.0	65.8	73.5	80.6
3.0	47.3	58.0	66.7	74.6	81.6
4.0	50.3	58.3	66.7	74.6	81.7
5.0	56.4	62.3	68.8	75.0	81.9

 $f'_m=4000.0\text{psi}$

σ_v	50.0	100.0	150.0	200.0	250.0
l/h					
0.5	12.7	25.1	37.5	49.5	60.8
1.0	25.1	50.1	64.3	71.7	78.4
2.0	46.6	57.0	65.8	73.5	80.6
3.0	47.3	58.0	66.7	74.6	81.6
4.0	50.3	58.3	66.7	74.6	81.7
5.0	56.4	62.3	68.8	75.0	81.9

 $f'_m=5000.0\text{psi}$

σ_v	50.0	100.0	150.0	200.0	250.0
l/h					
0.5	12.7	25.1	37.5	50.2	61.9
1.0	25.1	50.1	64.3	71.7	78.4
2.0	46.6	57.0	65.8	73.5	80.6
3.0	47.3	58.0	66.7	74.6	81.6
4.0	50.3	58.3	66.7	74.6	81.7
5.0	56.4	62.3	68.8	75.0	81.9

$\sigma_0=100.0\text{psi}$ $\tau_0=100.0\text{psi}$ $\mu=1.0$ $f'_m=1000.0\text{psi}$

σ_v	50.0	100.0	150.0	200.0	250.0
l/h					
0.5	12.4	23.3	32.0	39.0	44.4
1.0	24.8	46.0	63.7	77.7	88.5
2.0	49.4	88.9	104.0	113.9	123.1
3.0	72.5	94.3	105.6	115.6	124.7
4.0	91.9	100.6	108.5	116.5	124.9
5.0	119.4	112.5	118.7	124.5	130.0

 $f'_m=2000.0\text{psi}$

σ_v	50.0	100.0	150.0	200.0	250.0
l/h					
0.5	12.7	24.8	36.0	46.2	55.3
1.0	25.1	49.5	71.5	91.9	110.3
2.0	49.4	93.1	104.0	113.9	123.1
3.0	74.3	94.3	105.6	115.6	124.7
4.0	91.9	100.6	108.5	116.5	124.9
5.0	124.5	112.5	118.7	124.5	130.0

 $f'_m=3000.0\text{psi}$

σ_v	50.0	100.0	150.0	200.0	250.0
l/h					
0.5	12.7	25.1	37.1	48.4	59.0
1.0	25.1	50.1	74.3	96.5	117.8
2.0	49.4	93.1	104.0	113.9	123.1
3.0	74.3	94.3	105.6	115.6	124.7
4.0	91.9	100.6	108.5	116.5	124.9
5.0	124.5	112.5	118.7	124.5	130.0

 $f'_m=4000.0\text{psi}$

σ_v	50.0	100.0	150.0	200.0	250.0
l/h					
0.5	12.7	25.1	37.5	49.5	60.8
1.0	25.1	50.1	75.0	98.8	120.9
2.0	49.4	93.1	104.0	113.9	123.1
3.0	74.3	94.3	105.6	115.6	124.7
4.0	91.9	100.6	108.5	116.5	124.9
5.0	124.5	112.5	118.7	124.5	130.0

 $f'_m=5000.0\text{psi}$

σ_v	50.0	100.0	150.0	200.0	250.0
l/h					
0.5	12.7	25.1	37.5	50.2	61.9
1.0	25.1	50.1	75.0	99.9	120.9
2.0	49.4	93.1	104.0	113.9	123.1
3.0	74.3	94.3	105.6	115.6	124.7
4.0	91.9	100.6	108.5	116.5	124.9
5.0	124.5	12.5	118.7	124.5	130.0

 $\sigma_0=150.0\text{psi}$ $\tau_0=100.0\text{psi}$ $\mu=1.0$ $f'_m=1000.0\text{psi}$

σ_v	50.0	100.0	150.0	200.0	250.0
l/h					
0.5	12.4	23.3	32.0	39.0	44.4
1.0	24.8	46.0	63.7	77.7	88.5
2.0	49.4	88.9	119.4	141.6	158.5
3.0	72.5	129.5	141.7	152.9	163.5
4.0	96.0	171.8	150.9	157.2	166.1
5.0	119.4	200.0	250.0	172.2	179.5

 $f'_m=2000.0\text{psi}$

σ_v	50.0	100.0	150.0	200.0	250.0
l/h					
0.5	12.7	24.8	36.0	46.2	55.3
1.0	25.1	49.5	71.5	91.9	110.3
2.0	49.4	98.4	138.0	151.1	161.3
3.0	74.3	129.5	141.7	152.9	163.5
4.0	99.4	191.8	150.9	157.2	166.1
5.0	124.5	200.0	250.0	172.2	179.5

 $f'_m=3000.0\text{psi}$

σ_v	50.0	100.0	150.0	200.0	250.0
l/h					
0.5	12.7	25.1	37.1	48.4	59.0
1.0	25.1	50.1	74.3	96.5	117.8
2.0	49.4	98.4	139.7	151.1	161.3
3.0	74.3	129.5	141.7	152.9	163.5
4.0	99.4	198.2	150.9	157.2	166.1
5.0	124.5	200.0	250.0	172.2	179.5

 $f'_m=4000.0\text{psi}$

σ_v	50.0	100.0	150.0	200.0	250.0
l/h					
0.5	12.7	25.1	37.5	49.5	60.8
1.0	25.1	50.1	75.0	98.8	121.4
2.0	49.4	98.4	139.7	151.1	161.3
3.0	74.3	129.5	141.7	152.9	163.5
4.0	99.4	198.2	150.9	157.2	166.1
5.0	124.5	200.0	250.0	172.2	179.5

 $f'_m=5000.0\text{psi}$

σ_v	50.0	100.0	150.0	200.0	250.0
l/h					
0.5	12.7	25.1	37.5	50.2	61.9
1.0	25.1	50.1	75.0	99.9	123.6
2.0	49.4	98.4	139.7	151.1	161.3
3.0	74.3	129.5	141.7	152.9	163.5
4.0	99.4	198.2	150.9	157.2	166.1
5.0	124.5	200.0	250.0	172.2	179.5

$\sigma_0=200.0\text{psi}$ $\tau_0=100.0\text{psi}$ $\mu=1.0$ $f'_m=1000.0\text{psi}$

σ_v	50.0	100.0	150.0	200.0	250.0
l/h					
0.5	12.4	23.3	32.0	39.0	44.4
1.0	24.8	46.0	63.7	77.7	88.5
2.0	49.4	88.9	119.4	141.6	158.5
3.0	72.5	131.1	176.0	188.7	200.2
4.0	96.0	171.8	227.5	266.0	209.1
5.0	119.4	200.0	250.0	300.0	231.2

 $f'_m=2000.0\text{psi}$

σ_v	50.0	100.0	150.0	200.0	250.0
l/h					
0.5	12.7	24.8	36.0	46.2	55.3
1.0	25.1	49.5	71.5	91.9	110.3
2.0	49.4	98.4	138.0	179.1	197.7
3.0	74.3	145.0	206.0	188.7	200.2
4.0	99.4	191.8	250.0	300.0	209.1
5.0	124.5	200.0	250.0	300.0	231.2

 $f'_m=3000.0\text{psi}$

σ_v	50.0	100.0	150.0	200.0	250.0
l/h					
0.5	12.7	25.1	37.1	48.4	59.0
1.0	25.1	50.1	74.3	96.5	117.8
2.0	49.4	98.4	147.3	187.4	197.7
3.0	74.3	148.4	217.5	188.7	200.2
4.0	99.4	198.2	250.0	300.0	209.1
5.0	124.5	200.0	250.0	300.0	231.2

 $f'_m=4000.0\text{psi}$

σ_v	50.0	100.0	150.0	200.0	250.0
l/h					
0.5	12.7	25.1	37.5	49.5	60.8
1.0	25.1	50.1	75.0	98.8	121.4
2.0	49.4	98.4	147.3	187.4	197.7
3.0	74.3	148.4	222.4	188.7	200.2
4.0	99.4	198.2	250.0	300.0	209.1
5.0	124.5	200.0	250.0	300.0	231.2

 $f'_m=5000.0\text{psi}$

σ_v	50.0	100.0	150.0	200.0	250.0
l/h					
0.5	12.7	25.1	37.5	50.2	61.9
1.0	25.1	50.1	75.0	99.9	123.6
2.0	49.4	98.4	147.3	187.4	197.7
3.0	74.3	148.4	222.4	188.7	200.2
4.0	99.4	198.2	250.0	300.0	209.1
5.0	124.5	200.0	250.0	300.0	231.2

 $\sigma_0=250.0\text{psi}$ $\tau_0=100.0\text{psi}$ $\mu=1.0$ $f'_m=1000.0\text{psi}$

σ_v	50.0	100.0	150.0	200.0	250.0
l/h					
0.5	12.4	23.3	32.0	39.0	44.4
1.0	24.8	46.0	63.7	77.7	88.5
2.0	49.4	88.9	119.4	141.6	158.5
3.0	72.5	131.1	176.0	206.6	225.1
4.0	96.0	171.8	227.5	266.0	290.1
5.0	119.4	200.0	250.0	300.0	350.0

 $f'_m=2000.0\text{psi}$

σ_v	50.0	100.0	150.0	200.0	250.0
l/h					
0.5	12.7	24.8	36.0	46.2	55.3
1.0	25.1	49.5	71.5	91.9	110.3
2.0	49.4	98.4	138.0	179.1	211.5
3.0	74.3	145.0	206.0	262.1	307.0
4.0	99.4	191.8	250.0	300.0	350.0
5.0	124.5	200.0	250.0	300.0	350.0

 $f'_m=3000.0\text{psi}$

σ_v	50.0	100.0	150.0	200.0	250.0
l/h					
0.5	12.7	25.1	37.1	48.4	59.0
1.0	25.1	50.1	74.3	96.5	117.8
2.0	49.4	98.4	147.3	188.3	227.5
3.0	74.3	148.4	217.5	277.6	340.4
4.0	99.4	198.2	250.0	300.0	350.0
5.0	124.5	200.0	250.0	300.0	350.0

 $f'_m=4000.0\text{psi}$

σ_v	50.0	100.0	150.0	200.0	250.0
l/h					
0.5	12.7	25.1	37.5	49.5	60.8
1.0	25.1	50.1	75.0	98.8	121.4
2.0	49.4	98.4	147.3	196.2	238.2
3.0	74.3	148.4	222.4	290.0	350.0
4.0	99.4	198.2	250.0	300.0	350.0
5.0	124.5	200.0	250.0	300.0	350.0

 $f'_m=5000.0\text{psi}$

σ_v	50.0	100.0	150.0	200.0	250.0
l/h					
0.5	12.7	25.1	37.5	50.2	61.9
1.0	25.1	50.1	75.0	99.9	123.6
2.0	49.4	98.4	147.3	196.2	245.2
3.0	74.3	148.4	222.4	296.1	350.0
4.0	99.4	198.2	250.0	300.0	350.0
5.0	124.5	200.0	250.0	300.0	350.0

$\sigma_0= 50.0\text{psi}$ $\tau_0= 200.0\text{psi}$ $\mu= 1.0$

$f'_m= 1000.0\text{psi}$

σ_v	50.0	100.0	150.0	200.0	250.0
l/h					
0.5	12.4	23.3	32.0	39.0	44.4
1.0	24.8	46.0	63.7	71.7	78.4
2.0	46.6	57.0	65.8	73.5	80.6
3.0	47.3	58.0	66.7	74.6	81.6
4.0	50.3	58.3	66.7	74.6	81.7
5.0	56.4	62.3	68.8	75.0	81.9

$f'_m= 2000.0\text{psi}$

σ_v	50.0	100.0	150.0	200.0	250.0
l/h					
0.5	12.7	24.8	36.0	46.2	55.3
1.0	25.1	49.5	64.3	71.7	78.4
2.0	46.6	57.0	65.8	73.5	80.6
3.0	47.3	58.0	66.7	74.6	81.6
4.0	50.3	58.3	66.7	74.6	81.7
5.0	56.4	62.3	68.8	75.0	81.9

$f'_m= 3000.0\text{psi}$

σ_v	50.0	100.0	150.0	200.0	250.0
l/h					
0.5	12.7	25.1	37.1	48.4	59.0
1.0	25.1	50.1	64.3	71.7	78.4
2.0	46.6	57.0	65.8	73.5	80.6
3.0	47.3	58.0	66.7	74.6	81.6
4.0	50.3	58.3	66.7	74.6	81.7
5.0	56.4	62.3	68.8	75.0	81.9

$f'_m= 4000.0\text{psi}$

σ_v	50.0	100.0	150.0	200.0	250.0
l/h					
0.5	12.7	25.1	37.5	49.5	60.8
1.0	25.1	50.1	64.3	71.7	78.4
2.0	46.6	57.0	65.8	73.5	80.6
3.0	47.3	58.0	66.7	74.6	81.6
4.0	50.3	58.3	66.7	74.6	81.7
5.0	56.4	62.3	68.8	75.0	81.9

$f'_m= 5000.0\text{psi}$

σ_v	50.0	100.0	150.0	200.0	250.0
l/h					
0.5	12.7	25.1	37.5	50.2	61.9
1.0	25.1	50.1	64.3	71.7	78.4
2.0	46.6	57.0	65.8	73.5	80.6
3.0	47.3	58.0	66.7	74.6	81.6
4.0	50.3	58.3	66.7	74.6	81.7
5.0	56.4	62.3	68.8	75.0	81.9

$\sigma_0=100.0\text{psi}$ $\tau_0= 200.0\text{psi}$ $\mu= 1.0$

$f'_m= 1000.0\text{psi}$

σ_v	50.0	100.0	150.0	200.0	250.0
l/h					
0.5	12.4	23.3	32.0	39.0	44.4
1.0	24.8	46.0	63.7	77.7	88.5
2.0	49.4	88.4	104.0	113.9	123.1
3.0	72.5	94.3	105.6	115.6	124.7
4.0	91.9	100.6	108.5	116.5	124.9
5.0	104.5	112.5	118.7	124.5	130.0

$f'_m= 2000.0\text{psi}$

σ_v	50.0	100.0	150.0	200.0	250.0
l/h					
0.5	12.7	24.8	36.0	46.2	55.3
1.0	25.1	49.5	71.5	91.9	110.3
2.0	50.1	93.1	104.0	113.9	123.1
3.0	74.9	94.3	105.6	115.6	124.7
4.0	91.9	100.6	108.5	116.5	124.9
5.0	104.5	112.5	118.7	124.5	130.0

$f'_m= 3000.0\text{psi}$

σ_v	50.0	100.0	150.0	200.0	250.0
l/h					
0.5	12.7	25.1	37.1	48.4	59.0
1.0	25.1	50.1	74.3	96.5	117.8
2.0	50.1	93.1	104.0	113.9	123.1
3.0	74.9	94.3	105.6	115.6	124.7
4.0	91.9	100.6	108.5	116.5	124.9
5.0	104.5	112.5	118.7	124.5	130.0

$f'_m= 4000.0\text{psi}$

σ_v	50.0	100.0	150.0	200.0	250.0
l/h					
0.5	12.7	25.1	37.5	49.5	60.8
1.0	25.1	50.1	75.0	98.8	120.9
2.0	50.1	93.1	104.0	113.9	123.1
3.0	74.9	94.3	105.6	115.6	124.7
4.0	91.9	100.6	108.5	116.5	124.9
5.0	104.5	112.5	118.7	124.5	130.0

$f'_m= 5000.0\text{psi}$

σ_v	50.0	100.0	150.0	200.0	250.0
l/h					
0.5	12.7	25.1	37.5	50.2	61.9
1.0	25.1	50.1	75.0	99.9	120.9
2.0	50.1	93.1	104.0	113.9	123.1
3.0	74.9	94.3	105.6	115.6	124.7
4.0	91.9	100.6	108.5	116.5	124.9
5.0	104.5	112.5	118.7	124.5	130.0

$\sigma_0=150.0\text{psi}$ $\tau_0=200.0\text{psi}$ $\mu=1.0$ $f'_m=1000.0\text{psi}$

σ_v	50.0	100.0	150.0	200.0	250.0
l/h					
0.5	12.4	23.3	32.0	39.0	44.4
1.0	24.8	46.0	63.7	77.7	88.5
2.0	49.4	88.4	118.1	141.4	158.5
3.0	72.5	129.5	141.7	152.9	163.5
4.0	96.0	141.3	150.9	157.2	166.1
5.0	119.4	159.1	168.6	172.2	179.5

 $f'_m=2000.0\text{psi}$

σ_v	50.0	100.0	150.0	200.0	250.0
l/h					
0.5	12.7	24.8	36.0	46.2	55.3
1.0	25.1	49.5	71.5	91.9	110.3
2.0	50.1	98.8	138.0	151.1	161.3
3.0	74.9	129.5	141.7	152.9	163.5
4.0	99.9	141.3	150.9	157.2	166.1
5.0	124.9	159.1	168.6	172.2	179.5

 $f'_m=3000.0\text{psi}$

σ_v	50.0	100.0	150.0	200.0	250.0
l/h					
0.5	12.7	25.1	37.1	48.4	59.0
1.0	25.1	50.1	74.3	96.5	117.8
2.0	50.1	98.8	139.7	151.1	161.3
3.0	74.9	129.5	141.7	152.9	163.5
4.0	99.9	141.3	150.9	157.2	166.1
5.0	124.9	159.1	168.6	172.2	179.5

 $f'_m=4000.0\text{psi}$

σ_v	50.0	100.0	150.0	200.0	250.0
l/h					
0.5	12.7	25.1	37.5	49.5	60.8
1.0	25.1	50.1	75.0	98.8	121.4
2.0	50.1	98.8	139.7	151.1	161.3
3.0	74.9	129.5	141.7	152.9	163.5
4.0	99.9	141.3	150.9	157.2	166.1
5.0	124.9	159.1	168.6	172.2	179.5

 $f'_m=5000.0\text{psi}$

σ_v	50.0	100.0	150.0	200.0	250.0
l/h					
0.5	12.7	25.1	37.5	50.2	61.9
1.0	25.1	50.1	75.0	99.9	123.6
2.0	50.1	98.8	139.7	151.1	161.3
3.0	74.9	129.5	141.7	152.9	163.5
4.0	99.9	141.3	150.9	157.2	166.1
5.0	124.9	159.1	168.6	172.2	179.5

 $\sigma_0=200.0\text{psi}$ $\tau_0=200.0\text{psi}$ $\mu=1.0$ $f'_m=1000.0\text{psi}$

σ_v	50.0	100.0	150.0	200.0	250.0
l/h					
0.5	12.4	23.3	32.0	39.0	44.4
1.0	24.8	46.0	63.7	77.7	88.5
2.0	49.4	88.4	118.1	141.4	158.5
3.0	72.5	131.1	176.0	188.7	200.2
4.0	96.0	171.8	192.9	201.1	209.1
5.0	119.4	212.6	217.3	224.6	231.2

 $f'_m=2000.0\text{psi}$

σ_v	50.0	100.0	150.0	200.0	250.0
l/h					
0.5	12.7	24.8	36.0	46.2	55.3
1.0	25.1	49.5	71.5	91.9	110.3
2.0	50.1	98.8	138.0	177.8	197.7
3.0	74.9	145.0	177.2	188.7	200.2
4.0	99.9	183.9	192.9	201.1	209.1
5.0	124.9	238.8	217.3	224.6	231.2

 $f'_m=3000.0\text{psi}$

σ_v	50.0	100.0	150.0	200.0	250.0
l/h					
0.5	12.7	25.1	37.1	48.4	59.0
1.0	25.1	50.1	74.3	96.5	117.8
2.0	50.1	98.8	147.7	186.2	197.7
3.0	74.9	148.7	177.2	188.7	200.2
4.0	99.9	183.9	192.9	201.1	209.1
5.0	124.9	248.6	217.3	224.6	231.2

 $f'_m=4000.0\text{psi}$

σ_v	50.0	100.0	150.0	200.0	250.0
l/h					
0.5	12.7	25.1	37.5	49.5	60.8
1.0	25.1	50.1	75.0	98.8	121.4
2.0	50.1	98.8	147.7	186.2	197.7
3.0	74.9	148.7	177.2	188.7	200.2
4.0	99.9	183.9	192.9	201.1	209.1
5.0	124.9	248.6	217.3	224.6	231.2

 $f'_m=5000.0\text{psi}$

σ_v	50.0	100.0	150.0	200.0	250.0
l/h					
0.5	12.7	25.1	37.5	50.2	61.9
1.0	25.1	50.1	75.0	99.9	123.6
2.0	50.1	98.8	147.7	186.2	197.7
3.0	74.9	148.7	177.2	188.7	200.2
4.0	99.9	183.9	192.9	201.1	209.1
5.0	124.9	248.6	217.3	224.6	231.2

$\sigma_0=250.0\text{psi}$ $\tau_0=200.0\text{psi}$ $\mu=1.0$ $f'_m=1000.0\text{psi}$

σ_v	50.0	100.0	150.0	200.0	250.0
l/h					
0.5	12.4	23.3	32.0	39.0	44.4
1.0	24.8	46.0	63.7	77.7	88.5
2.0	49.4	88.4	118.1	141.4	158.5
3.0	72.5	131.1	176.0	206.6	223.6
4.0	96.0	171.8	227.5	238.7	251.4
5.0	119.4	212.6	280.0	266.5	280.7

 $f'_m=2000.0\text{psi}$

σ_v	50.0	100.0	150.0	200.0	250.0
l/h					
0.5	12.7	24.8	36.0	46.2	55.3
1.0	25.1	49.5	71.5	91.9	110.3
2.0	50.1	98.8	138.0	177.8	211.5
3.0	74.9	145.0	206.0	223.9	235.7
4.0	99.9	191.8	230.5	238.7	251.4
5.0	124.9	238.8	341.5	266.5	280.7

 $f'_m=3000.0\text{psi}$

σ_v	50.0	100.0	150.0	200.0	250.0
l/h					
0.5	12.7	25.1	37.1	48.4	59.0
1.0	25.1	50.1	74.3	96.5	117.8
2.0	50.1	98.8	147.7	188.3	227.5
3.0	74.9	148.7	211.8	223.9	235.7
4.0	99.9	198.6	230.5	238.7	251.4
5.0	124.9	248.6	350.0	266.5	280.7

 $f'_m=4000.0\text{psi}$

σ_v	50.0	100.0	150.0	200.0	250.0
l/h					
0.5	12.7	25.1	37.5	49.5	60.8
1.0	25.1	50.1	75.0	98.8	121.4
2.0	50.1	98.8	147.7	196.7	232.7
3.0	74.9	148.7	211.8	223.9	235.7
4.0	99.9	198.6	230.5	238.7	251.4
5.0	124.9	248.6	350.0	266.5	280.7

 $f'_m=5000.0\text{psi}$

σ_v	50.0	100.0	150.0	200.0	250.0
l/h					
0.5	12.7	25.1	37.5	50.2	61.9
1.0	25.1	50.1	75.0	99.9	123.6
2.0	50.1	98.8	147.7	196.7	232.7
3.0	74.9	148.7	211.8	223.9	235.7
4.0	99.9	198.6	230.5	238.7	251.4
5.0	124.9	248.6	350.0	266.5	280.7

 $\sigma_0=50.0\text{psi}$ $\tau_0=300.0\text{psi}$ $\mu=1.0$ $f'_m=1000.0\text{psi}$

σ_v	50.0	100.0	150.0	200.0	250.0
l/h					
0.5	12.4	23.3	32.0	39.0	44.4
1.0	24.8	46.0	63.7	71.7	78.4
2.0	46.6	57.0	65.8	73.5	80.6
3.0	47.3	58.0	66.7	74.6	81.6
4.0	50.3	58.3	66.7	74.6	81.7
5.0	56.4	62.3	68.8	75.0	81.9

 $f'_m=2000.0\text{psi}$

σ_v	50.0	100.0	150.0	200.0	250.0
l/h					
0.5	12.7	24.8	36.0	46.2	55.3
1.0	25.1	49.5	64.3	71.7	78.4
2.0	46.6	57.0	65.8	73.5	80.6
3.0	47.3	58.0	66.7	74.6	81.6
4.0	50.3	58.3	66.7	74.6	81.7
5.0	56.4	62.3	68.8	75.0	81.9

 $f'_m=3000.0\text{psi}$

σ_v	50.0	100.0	150.0	200.0	250.0
l/h					
0.5	12.7	25.1	37.1	48.4	59.0
1.0	25.1	50.1	64.3	71.7	78.4
2.0	46.6	57.0	65.8	73.5	80.6
3.0	47.3	58.0	66.7	74.6	81.6
4.0	50.3	58.3	66.7	74.6	81.7
5.0	56.4	62.3	68.8	75.0	81.9

 $f'_m=4000.0\text{psi}$

σ_v	50.0	100.0	150.0	200.0	250.0
l/h					
0.5	12.7	25.1	37.5	49.5	60.8
1.0	25.1	50.1	64.3	71.7	78.4
2.0	46.6	57.0	65.8	73.5	80.6
3.0	47.3	58.0	66.7	74.6	81.6
4.0	50.3	58.3	66.7	74.6	81.7
5.0	56.4	62.3	68.8	75.0	81.9

 $f'_m=5000.0\text{psi}$

σ_v	50.0	100.0	150.0	200.0	250.0
l/h					
0.5	12.7	25.1	37.5	50.2	61.9
1.0	25.1	50.1	64.3	71.7	78.4
2.0	46.6	57.0	65.8	73.5	80.6
3.0	47.3	58.0	66.7	74.6	81.6
4.0	50.3	58.3	66.7	74.6	81.7
5.0	56.4	62.3	68.8	75.0	81.9

$\sigma_0=100.0\text{psi}$ $\tau_0=300.0\text{psi}$ $\mu=1.0$

$f'_m=1000.0\text{psi}$

σ_v	50.0	100.0	150.0	200.0	250.0
l/h					
0.5	12.4	23.3	32.0	39.0	44.4
1.0	24.8	46.0	63.7	77.7	88.5
2.0	49.4	88.4	104.0	113.9	123.1
3.0	72.5	94.3	105.6	115.6	124.7
4.0	91.9	100.6	108.5	116.5	124.9
5.0	104.5	112.5	118.7	124.5	130.0

$f'_m=2000.0\text{psi}$

σ_v	50.0	100.0	150.0	200.0	250.0
l/h					
0.5	12.7	24.8	36.0	46.2	55.3
1.0	25.1	49.5	71.5	91.9	110.3
2.0	50.1	93.1	104.0	113.9	123.1
3.0	75.2	94.3	105.6	115.6	124.7
4.0	91.9	100.6	108.5	116.5	124.9
5.0	104.5	112.5	118.7	124.5	130.0

$f'_m=3000.0\text{psi}$

σ_v	50.0	100.0	150.0	200.0	250.0
l/h					
0.5	12.7	25.1	37.1	48.4	59.0
1.0	25.1	50.1	74.3	96.5	117.8
2.0	50.1	93.1	104.0	113.9	123.1
3.0	75.2	94.3	105.6	115.6	124.7
4.0	91.9	100.6	108.5	116.5	124.9
5.0	104.5	112.5	118.7	124.5	130.0

$f'_m=4000.0\text{psi}$

σ_v	50.0	100.0	150.0	200.0	250.0
l/h					
0.5	12.7	25.1	37.5	49.5	60.8
1.0	25.1	50.1	75.0	98.8	120.9
2.0	50.1	93.1	104.0	113.9	123.1
3.0	75.2	94.3	105.6	115.6	124.7
4.0	91.9	100.6	108.5	116.5	124.9
5.0	104.5	112.5	118.7	124.5	130.0

$f'_m=5000.0\text{psi}$

σ_v	50.0	100.0	150.0	200.0	250.0
l/h					
0.5	12.7	25.1	37.5	50.2	61.9
1.0	25.1	50.1	75.0	99.9	120.9
2.0	50.1	93.1	104.0	112.9	123.1
3.0	75.2	94.3	105.6	115.6	124.7
4.0	91.9	100.6	108.5	116.5	124.9
5.0	104.5	112.5	118.7	124.5	130.0

$\sigma_0=150.0\text{psi}$ $\tau_0=300.0\text{psi}$ $\mu=1.0$

$f'_m=1000.0\text{psi}$

σ_v	50.0	100.0	150.0	200.0	250.0
l/h					
0.5	12.4	23.3	32.0	39.0	44.4
1.0	24.8	46.0	63.7	77.7	88.5
2.0	49.4	88.4	118.1	141.4	158.5
3.0	72.5	129.5	141.7	152.9	163.5
4.0	96.0	141.3	150.9	157.2	166.1
5.0	119.4	159.1	168.6	172.2	179.5

$f'_m=2000.0\text{psi}$

σ_v	50.0	100.0	150.0	200.0	250.0
l/h					
0.5	12.7	24.8	36.0	46.2	55.3
1.0	25.1	49.5	71.5	91.9	110.3
2.0	50.1	98.8	138.0	151.1	161.3
3.0	75.2	129.5	141.7	152.9	163.5
4.0	100.1	141.3	150.9	157.2	166.1
5.0	125.2	159.1	168.6	172.2	179.5

$f'_m=3000.0\text{psi}$

σ_v	50.0	100.0	150.0	200.0	250.0
l/h					
0.5	12.7	25.1	37.1	48.4	59.0
1.0	25.1	50.1	74.3	96.5	117.8
2.0	50.1	100.0	139.7	151.1	161.3
3.0	75.2	129.5	141.7	152.9	163.5
4.0	100.1	141.3	150.9	157.2	166.1
5.0	125.2	159.1	168.6	172.2	179.5

$f'_m=4000.0\text{psi}$

σ_v	50.0	100.0	150.0	200.0	250.0
l/h					
0.5	12.7	25.1	37.5	49.5	60.8
1.0	25.1	50.1	75.0	98.8	121.4
2.0	50.1	100.0	139.7	151.1	161.3
3.0	75.2	129.5	141.7	152.9	163.5
4.0	100.1	141.3	150.9	157.2	166.1
5.0	125.2	159.1	168.6	172.2	179.5

$f'_m=5000.0\text{psi}$

σ_v	50.0	100.0	150.0	200.0	250.0
l/h					
0.5	12.7	25.1	37.5	50.2	61.9
1.0	25.1	50.1	75.0	99.9	123.6
2.0	50.1	100.0	139.7	151.1	161.3
3.0	75.2	129.5	141.7	152.9	163.5
4.0	100.1	141.3	150.9	157.2	166.1
5.0	125.2	159.1	168.6	172.2	179.5

$\alpha_0=200.0\text{psi}$ $\tau_0=300.0\text{psi}$ $\mu=1.0$ $f'_m=1000.0\text{psi}$

σ_v	50.0	100.0	150.0	200.0	250.0
l/h					
0.5	12.4	23.3	32.0	39.0	44.4
1.0	24.8	46.0	63.7	77.7	88.5
2.0	49.4	88.4	118.1	141.4	158.5
3.0	72.5	131.1	174.8	188.7	200.2
4.0	96.0	171.8	192.9	201.1	209.1
5.0	119.4	209.0	217.3	224.6	231.2

 $f'_m=2000.0\text{psi}$

σ_v	50.0	100.0	150.0	200.0	250.0
l/h					
0.5	12.7	24.8	36.0	46.2	55.3
1.0	25.1	49.5	71.5	91.9	110.3
2.0	50.1	98.8	138.0	177.6	197.7
3.0	75.2	145.0	177.2	188.7	200.2
4.0	100.1	183.9	192.9	201.1	209.1
5.0	125.2	209.0	217.3	224.6	231.2

 $f'_m=3000.0\text{psi}$

σ_v	50.0	100.0	150.0	200.0	250.0
l/h					
0.5	12.7	25.1	37.1	48.4	59.0
1.0	25.1	50.1	74.3	96.5	117.8
2.0	50.1	100.0	148.1	186.2	197.7
3.0	75.2	149.3	177.2	188.7	200.2
4.0	100.1	183.9	192.9	201.1	209.1
5.0	125.2	209.0	217.3	224.6	231.2

 $f'_m=4000.0\text{psi}$

σ_v	50.0	100.0	150.0	200.0	250.0
l/h					
0.5	12.7	25.1	37.5	49.5	60.8
1.0	25.1	50.1	75.0	98.8	121.4
2.0	50.1	100.0	148.1	186.2	197.7
3.0	75.2	149.3	177.2	188.7	200.2
4.0	100.1	183.9	192.9	201.1	209.1
5.0	125.2	209.0	217.3	224.6	231.2

 $f'_m=5000.0\text{psi}$

σ_v	50.0	100.0	150.0	200.0	250.0
l/h					
0.5	12.7	25.1	37.5	50.2	61.9
1.0	25.1	50.1	75.0	99.9	123.6
2.0	50.1	100.0	148.1	186.2	197.7
3.0	75.2	149.3	177.2	188.7	200.2
4.0	100.1	183.9	192.9	201.1	209.1
5.0	125.2	209.0	217.3	224.6	231.2

 $\alpha_0=250.0\text{psi}$ $\tau_0=300.0\text{psi}$ $\mu=1.0$ $f'_m=1000.0\text{psi}$

σ_v	50.0	100.0	150.0	200.0	250.0
l/h					
0.5	12.4	23.3	32.0	39.0	44.4
1.0	24.8	46.0	63.7	77.7	88.5
2.0	49.4	88.4	118.1	141.4	158.5
3.0	72.5	131.1	174.8	205.7	223.6
4.0	96.0	171.8	227.5	238.7	251.4
5.0	119.4	212.6	259.6	266.5	280.7

 $f'_m=2000.0\text{psi}$

σ_v	50.0	100.0	150.0	200.0	250.0
l/h					
0.5	12.7	24.8	36.0	46.2	55.3
1.0	25.1	49.5	71.5	91.9	110.3
2.0	50.1	98.8	138.0	177.6	211.5
3.0	75.2	145.0	206.0	223.9	235.7
4.0	100.1	191.8	230.5	238.7	251.4
5.0	125.2	238.8	259.6	266.5	280.7

 $f'_m=3000.0\text{psi}$

σ_v	50.0	100.0	150.0	200.0	250.0
l/h					
0.5	12.7	25.1	37.1	48.4	59.0
1.0	25.1	50.1	74.3	96.5	117.8
2.0	50.1	100.0	148.1	188.3	227.5
3.0	75.2	149.3	211.8	223.9	235.7
4.0	100.1	199.1	230.5	238.7	251.4
5.0	125.2	249.0	259.6	266.5	280.7

 $f'_m=4000.0\text{psi}$

σ_v	50.0	100.0	150.0	200.0	250.0
l/h					
0.5	12.7	25.1	37.5	49.5	60.8
1.0	25.1	50.1	75.0	98.8	121.4
2.0	50.1	100.0	148.1	197.1	232.7
3.0	75.2	149.3	211.8	223.9	235.7
4.0	100.1	199.1	230.5	238.7	251.4
5.0	125.2	249.0	259.6	266.5	280.7

 $f'_m=5000.0\text{psi}$

σ_v	50.0	100.0	150.0	200.0	250.0
l/h					
0.5	12.7	25.1	37.5	50.2	61.9
1.0	25.1	50.1	75.0	99.9	123.6
2.0	50.1	100.0	148.1	197.1	232.7
3.0	75.2	149.3	211.8	223.9	235.7
4.0	100.1	199.1	230.5	238.7	251.4
5.0	125.2	249.0	259.6	266.5	280.7

APPENDIX B

C PROGRAM LATS

C

C THIS PROGRAM IS TO BE USED TO ANALYZE THE STRESS
 C DISTRIBUTION AND CALCULATE THE LATERAL STRENGTH
 C THAT IS LIMITED BY THE FLEXURE CRACKING, SLIDING,
 C DIAGONAL TENSION AND COMPRESSIVE SPLITTING

C

C

C *****

C * *

C * *

C * **

C * * *

C * * *

C *****

C

C

C

C NOTATION OF VARIABLES

C

C V = LATERAL FORCE

C SEGM = VERTICAL COMPRESSIVE STRESS

C L = LENGTH OF A WALL

C H = HEIGHT OF A WALL

C T = THICKNESS OF A WALL

C TS = SHEAR STRESS

C XS = NORMAL STRESS IN PARALLEL BED JOINT DIRECTION

C YS = NORMAL STRESS IN PERPENDICULAR BED JOINT DIRECTION

C VMAX = ULTIMATE LATERAL LOAD

C FR = FLEXURAL TENSILE STRENGTH

C FM = COMPRESSIVE STRENGTH PERPENDICULAR TO BED JOINT

C T0 = COHESION IN BED JOINT

C U = COEFFICIENT OF FRICTION IN BED JOINT

C S0 = DIAGONAL TENSILE STRENGTH

C BETA = RATIO OF THE COMPRESSIVE STRENGTH IN X AND Y DIRECTION

C DLTV = INCREMENT OF LATERAL FORCE

C

C

INCLUDE 'FGRAPH.FI'

INCLUDE 'FGRAPH.FD'

LOGICAL FOURCOLORS

EXTERNAL FOURCOLORS

```

IF ( FOURCOLORS() ) THEN
  CALL ANALYSIS()
ELSE
  WRITE (*,*) ' THIS PROGRAM REQUIRES A CGA, EGA, OR',
+           ' VGA GRAPHICS CARD.'
END IF
END

SUBROUTINE ANALYSIS()
INCLUDE 'FGRAPH.FD'
COMMON/BLOCK1/T0,U,YS,XS,TS,X,Y,H,V,L,P,T,FM,BETA,YSTART,S0,Z0,
*YSTEP,XEND,XSTEP,A,S,SLIDST,SLIDEN,SLIDS(40000,3),IS,KF,SEGM,D,
*SDZC(2,2),SUBL
INTEGER XSTEP,YSTEP
REAL L

RECORD /VIDEOCONFIG/ SCREEN
COMMON/BLOCK2/SCREEN,XWIDTH,YHEIGHT,X0,Y0,XPLUS,YPLUS

INTEGER X0,Y0,XPLUS,YPLUS,XWIDTH, YHEIGHT, DUMMY

PRINT *, 'PLEASE INPUT L,H,T,T0,U,FR,FM,BETA,DLTV,S0,SEGM'
READ(*,*) L,H,T,T0,U,FR,FM,BETA,DLTV,S0,SEGM
WRITE(6,1)
1 FORMAT(/,2X,'THE INPUT LIST CONTAINS' /)
WRITE(6,2) L,H,T
2 FORMAT(' L=',F7.3,2X,' H=',F6.3,2X,' T=',F6.3)
WRITE(6,3)T0,U
3 FORMAT(' T0=',F6.2, 2X,' U=',F6.3)
WRITE(6,4)FR,FM,BETA,S0
4 FORMAT(' FR=',F6.1,2X,' FM=',F8.2,2X,' BETA=',F6.3,2X,' S0=',F6.2)
WRITE(6,5)SEGM
5 FORMAT(' SEGM=',F6.2//)
KF = 0
VV =100.0

CALL CLEARSCREEN( $GCLEARSCREEN )
XWIDTH = SCREEN.NUMXPIXELS
YHEIGHT = SCREEN.NUMYPIXELS
XSTEP = 6
YSTEP = -4
C
C INCREASE VERTICAL STRESS TO GET DIFFERENT FAILURE LOAD
C
V = VV
P = SEGM * L * T
SUBL = L

```

```

CALL CLEARSCREEN( $GCLEARSCREEN )
CALL SETVIEWPORT( 0, 0, XWIDTH - 1, YHEIGHT - 1 )
DUMMY = SETWINDOW( .FALSE., 1, 1, XWIDTH - 2, YHEIGHT - 2 )
CALL GRIDSHAPE( )
CALL MMAIN (FR,DLTV)
KF = 0
CALL PLOTSIGNAL( )
DUMMY = SETVIDEOMODE( $DEFAULTMODE )
END

```

```

SUBROUTINE MMAIN (FR,DLTV)

```

```

C -----
C THIS SUBROUTINE CALCULATE THE STRESS DISTRIBUTION AND CHECK
C THE DIFFERENT FAILURE CRITERIA
C -----

```

```

COMMON/BLOCK1/T0,U,YS,XS,TS,X,Y,H,V,L,P,T,FM,BETA,YSTART,S0,Z0,
*YSTEP,XEND,XSTEP,A,S,SLIDST,SLIDEN,SLIDS(40000,3),IS,KF,SEGM,D,
*SDZC(2,2),SUBL
INTEGER XSTEP,YSTEP
REAL L

```

```

C
C CALCULATE FLEXURAL CRACKING LOAD
C

```

```

V0 = (P/(L*T) + FR) * (L*L*T/(6*H))

```

```

C
C INITIATE SLIDING RECORD MATRIX
C

```

```

WHO = 0.0
DOLD = L
IS = 0
DO 20 I = 1,40000
DO 10 J = 1,3
SLIDS(IJ) = 0.0

```

```

10 CONTINUE
20 CONTINUE

```

```

C
C INITIATE DIAGONAL CRACKING RECORD MATRIX
C

```

```

DO 40 I = 1,2
DO 30 J = 1,2
SDZC(IJ) = 0.0
30 CONTINUE
40 CONTINUE

```

```

ZS = H
DS = L

```

```

D = L
VUL = T0 + U * SEGM
1000 CONTINUE
C
C CALCULATE THE EXTENSION OF DIAGONAL TENSION CRACK
C
IF (SDZC(1,1) .GT. 0.0 .AND. SDZC(2,1) .GT. 0.0) THEN
  SA = TAN(SDZC(2,1) * 3.1415629 / 180.0)
  ZS = (SDZC(1,1) - L) * SA + SDZC(1,2)
  DS1 = SDZC(1,1) + (SDZC(1,2) - H) / SA
  IF (ZS .LE. 0) THEN
    ZS = 0.0
    TMPL = SDZC(1,1) + SDZC(1,2) / SA
  END IF
  IF (DS1 .LT. DS) THEN
    DS = DS1
    CALL DRAWLINE(DS,ZS,TMPL)
  END IF
C
C CHECK DIAGONAL TENSION CRACKING FAILURE CRITERIA
C
IF (DS1 .LT. 2 * XSTEP) THEN
  WRITE(6,60)
60  FORMAT(1X,'DIAGONAL TENSION FAILURE',/)
  WRITE (6,70)
  V = V - DLTV
  TAU = V/(L*T)
  WRITE (6,80) V,TAU,SEGM,DS,ZS,SUBL
  KF = 2
  RETURN
  END IF
70  FORMAT (4X,'VMAX',12X,'TAU',12X,'SEGM',10X,'DS',10X,'ZS',10X,
*      'SUBL')
80  FORMAT (11,6F12.4,/)
  END IF
C
C CHECK IF BOTTOM CRACKED BY FLEXURE
C
CALL FLEX(V0,FR,DLTV,DF)
IF (KF .GT. 0) THEN
  RETURN
  END IF
C
C CHECK WHETHER 'DEAD ZONE' CAUSED BY FLEXURE
C
IF (DF .LT. L) THEN

```

```

      Z0 = P*L/(6*V)
      D = DF
ELSE
C
C IF WITHOUT 'DEAD ZONE', STRESSES DISTRIBUTED
C ON WHOLE SECTION OF A WALL.
C
      D = L
      S = 0.0
      A = L
      YSTART = H
      YSTEP = -4
      XEND = L
      XSTEP = 6
      DO 45 I = 1,2
      DO 35 J = 1,2
        SDZC(I,J) = 0.0
35 CONTINUE
45 CONTINUE
      KF = 0
      A = L
      CALL STRESS1
      IF (KF .GT. 0) THEN
        RETURN
      END IF
      TAUT = V / (L * T)
      IF (TAUT .GE. VUL) THEN
        TAU = VUL
        WRITE (6,62)
62  FORMAT(1X,'SLIDING FAILURE AT TOP')
        WRITE (6,70)
        WRITE (6,80) V,TAU,SEGM,DS,ZS,SUBL
        KF = 2
        RETURN
      END IF
      V = V + DLTV
      GO TO 1000
    END IF
C
C IF 'DEAD ZONE' HAS FORMED, STRESSES DISTRIBUTED ON DECREASED
C SECTION OF A WALL.
C
      CALL DRAWFD()
      S = (SUBL - D) / (H - Z0)
      KF = 0
      CALL STREDIS

```

```

IF (KF .GT. 0) THEN
  RETURN
END IF
C
C IF LATERAL LOAD INCREASE TO CERTAIN DEFINED VALUE WITHOUT
C FAILURE FORCED TO STOP OTHERWISE INCREASE LATERAL LOAD
C AGAIN AND REPEAT PREVIOUS PROCEDURE.
C
TAUT = V / (L * T)
IF (TAUT .GE. VUL) THEN
  TAU = VUL
  WRITE (6,62)
  WRITE (6,70)
  WRITE (6,80) V,TAU,SEGM,DS,ZS,SUBL
  KF = 2
  RETURN
END IF
V = V + DLTV
GO TO 1000
WRITE (6,100) Z0,Y,X,TS,YS,XS
KF = 4
100 FORMAT (1X,6F10.5)
RETURN
END

SUBROUTINE FLEX(V0,FR,DLTV,DF)
C
C CHECK FLEXURE FAILURE
C
COMMON/BLOCK1/T0,U,YS,XS,TS,X,Y,H,V,L,P,T,FM,BETA,YSTART,S0,Z0,
*YSTEP,XEND,XSTEP,A,S,SLIDST,SLIDEN,SLIDS(40000,3),IS,KF,SEGM,D,
*SDZC(2,2),SUBL
INTEGER XSTEP,YSTEP
REAL L
C
C CHECK BOTTOM UNCRACKED LENGTH
C
IF (V .LT. V0) THEN
  DF = L
ELSE IF (V .EQ. V0) THEN
  DF = P/(FR*T) + SQRT(P*P/((FR*T)**2)-(3*P*L - 6*H*V)/(FR*T))
ELSE
  DF = P/(FR*T) - SQRT(P*P/((FR*T)**2)-(3*P*L - 6*H*V)/(FR*T))
ENDIF
C
C IF UNCRACKED LENGTH IS LESS THAN ZERO WITH A LOAD INCREMENT

```

C HIGHER THAN CRACKING LOAD, USE CRACKING LOAD AS MAXIMUM LOAD.

C

IF (DF .LT. 0.0 .AND. V - DLTV .LE. V0) THEN

V = V0

END IF

C

C CHECK FLEXURAL CRACKING FAILURE CRITERIA

C

IF (DF .LT. 0.1) THEN

KF = 1

WRITE (6,*) 'FLEXURAL CRACKING FAILURE'

WRITE (6,15)

TAU = V/(L*T)

WRITE (6,25) V,TAU,SEGM,DF

15 FORMAT (4X,'VMAX',10X,'TAU',10X,'SEGM',10X,'DF')

25 FORMAT (1X,6F12.4)

ENDIF

RETURN

END

SUBROUTINE STREDIS

C

C THIS SUBROUTINE REDISTRIBUTES STRESSES BASED ON THE
C FORMATION OF 'DEAD ZONE'

C

COMMON/BLOCK1/T0,U,YS,XS,TS,X,Y,H,V,L,P,T,FM,BETA,YSTART,S0,Z0,

*YSTEP,XEND,XSTEP,A,S,SLIDST,SLIDEN,SLIDS(40000,3),IS,KF,SEGM,D,

*SDZC(2,2),SUBL

INTEGER XSTEP,YSTEP

REAL L

YSTEP = -4

YSTART = H

XSTEP = 6

CALL STRESS2

IF (KF .GT. 0) THEN

RETURN

ENDIF

IF (Z0 .GE. - YSTEP) THEN

N = INT (Z0/(- YSTEP))

YSTART = N*(- YSTEP)

A = L

CALL STRESS1

END IF

RETURN

END

SUBROUTINE STRESS1

```

C
C -----
C THIS SUBROUTINE ANALYSIS THE STRESS FIELD BEFORE THE
C FLEXTURE CRACKING OR THE SHEAR DIAGONAL CRACKING
C OCCUR.
C -----
COMMON/BLOCK1/T0,U,YS,XS,TS,X,Y,H,V,L,P,T,FM,BETA,YSTART,S0,Z0,
*YSTEP,XEND,XSTEP,A,S,SLIDST,SLIDEN,SLIDS(40000,3),IS,KF,SEGM,D,
*SDZC(2,2),SUBL
INTEGER XSTEP,YSTEP
REAL L

SI = L**3 * T / 12.0
C
C CHECK IF SLIDING OCCURED BEFORE
C
DO 20 Y = YSTART,0,YSTEP
ISOLD = IS
DO 5 I = 1,IS,1
IF (Y .EQ. SLIDS(I,1))THEN
CALL MODEL2(I)
IF (KF .GT. 0)THEN
RETURN
ENDIF
GOTO 20
ENDIF
5 CONTINUE
SLIDST = -1.0
SLIDEN = -1.0
C
C CALCULATE STRESSES AT ANY GIVEN HEIGHT
C
DO 10 X = 0,XEND,XSTEP
YS = P / (L*T) + V*Y*(L/2 - X) / SI
TS = V*((L/2)**2 - (X-L/2)**2)/(2*SI)
XS = 0.0
C
C CHECK IF THERE IS DIAGONAL CHECKING
C
CALL SHEARD
IF (KF .GT. 0) THEN
RETURN
ENDIF
C
C CHECK IF THERE IS SLIDING
C

```

```

CALL CHECK1
IF (KF .GT. 0) THEN
  RETURN
ENDIF
IF (IS .GT. ISOLD) GOTO 20
10 CONTINUE
20 CONTINUE
RETURN
END

SUBROUTINE STRESS2
C -----
C THIS SUBROUTINE ANALYSIS THE STRESS FIELD AFTER THE
C FLEXTURE CRACKING.
C -----
COMMON/BLOCK1/T0,U,YS,XS,TS,X,Y,H,V,L,P,T,FM,BETA,YSTART,S0,Z0,
*YSTEP,XEND,XSTEP,A,S,SLIDST,SLIDEN,SLIDS(40000,3),IS,KF,SEGM,D,
*SDZC(2,2),SUBL
INTEGER XSTEP,YSTEP
REAL L

Y = YSTART
2000 CONTINUE

ISOLD = IS
IF (Y .LT. Z0) THEN
  Y = Z0
ENDIF

C
C CALCULATE UNCRACKED LENGTH AT ANY GIVEN HEIGHT
C
A1 = (Y-Z0)*S
A = SUBL - A1
XEND = A

C
C CHECK IF SLIDING HAPPENED BEFORE
C
DO 5 I = 1,IS,1
  IF (Y .EQ. SLIDS(I,1)) THEN
    CALL MODEL2(I)
    IF (KF .GT. 0) THEN
      RETURN
    ENDIF
    GOTO 60
  ENDIF
5 CONTINUE
SLIDST = -1.0

```

```

SLIDEN = -1.0
C
C CALCULATE STRESSES FOR ANY GIVEN HEIGHT
C
DO 50 X = 0,XEND,XSTEP
  F = T*A**3 / 12.0
  W = V*Y - P*A1/2.0
  B = V*A + 2.0*W*S - P*S*A/3.0
  C = V - P*S/2.0 + 3.0*S*W/A
  B1 = 4.0*S*V - 5.0*P*S*S/3.0 + 6.0*S*S*W/A
  B2 = 6.0*S*(V-P*S/2.0)/A + 12.0*S*S*W/(A*A)
  TS = (X*B-X**2*C)/(2*F)
C
C NEGLECT NEGATIVE SHEAR STRESS
C
  IF (TS .LT. 0) THEN
    TS = 0
  ENDIF
  YS = P/(A*T) + (W/F)*(A/2 - X)
  IF (Y .EQ. Z0) THEN
    XS = 0
  ELSE
    XS = (X*X*B1/2.0 - (X**3)*B2/3.0)/(2.0*F)
C
C NEGLECT NEGATIVE NORMAL STRESS IN PARALLEL BED JOINT DIRECTION
C
  IF (XS .LT. 0) THEN
    XS = 0
  ENDIF
ENDIF
C
C CHECK IF THERE IS DIAGONAL CRACKING
C
  CALL SHEARD
  IF (KF .GT. 0) THEN
    RETURN
  ENDIF
C
C CHECK IF THERE IS SLIDING
C
  CALL CHECK1
  IF (KF .GT. 0) THEN
    RETURN
  ENDIF
  IF (IS .GT. ISOLD) GOTO 60
50 CONTINUE

```

```

C
C  CALCULATE EDGE POINT STRESSES
C
  IF (X-XSTEP .LT. XEND) THEN
    TS = (A*B-A**2*C)/(2*F)
    IF (TS .LT. 0) THEN
      TS = 0
    ENDIF
    YS = P/(A*T) + (W/F)*(A/2 - A)
    XS = (A*A*B1/2.0-(A**3)*B2/3.0)/(2.0*F)
    IF (XS .LT. 0) THEN
      XS = 0
    ENDIF
    CALL SHEARD
    IF (KF .GT. 0) THEN
      RETURN
    ENDIF
    CALL CHECK1
    IF (KF .GT. 0) THEN
      RETURN
    ENDIF
  ENDIF
60 Y = Y + YSTEP
  IF (Y .LT. Z0 .OR. Y .LT. 0) THEN
    RETURN
  ELSE
    GOTO 2000
  END IF
  RETURN
END

SUBROUTINE CHECK1
C
C  _____
C  THIS SUBROUTINE CHECK THE SLIDING CRITERIA AFTER THE
C  FLEXURAL CRACKING.
C  _____
COMMON/BLOCK1/T0,U,YS,XS,TS,X,Y,H,V,L,P,T,FM,BETA,YSTART,S0,Z0,
*YSTEP,XEND,XSTEP,A,S,SLIDST,SLIDEN,SLIDS(40000,3),JS,KF,SEGM,D,
*SDZC(2,2),SUBL
INTEGER XSTEP,YSTEP
REAL L
C
C  SLIDING HAPPENING ON THE BOTTOM LINE (Y = H) IS NEGLECTED.
C
  IF (Y .EQ. H .OR. YS .LT. 0) RETURN

```

```

C
C CHECK SLIDING CRITERIA FIRST
C
SLIPF = (T0+U*YS)
TS1 = TS
C
C IF NOT THE SLIDING POINT THEN CALCULATE THE SLIDING LENGTH
C AT THIS HEIGHT, AND STORE CORDINATES INTO ARRAY SLIDS.
C IF THERE IS SLIDING ON THIS LEVEL CALL MODEL 2 TO GET SHEAR
C STRESS REDISTRIBUTION.
C
IF (TS1 .LT. SLIPF) THEN
  SLIDL = SLIDEN - SLIDST
  IF (SLIDL .GT. 0) THEN
    IS = IS + 1
    SLIDS(IS,1) = Y
    SLIDS(IS,2) = SLIDST
    SLIDS(IS,3) = SLIDEN
    CALL MODEL2(IS)
C
C IF SLIDING FAILURE (FROM SUB CHECK2), RETURN AND STOP
C
  IF (KF .GT. 0) THEN
    RETURN
  ENDIF
C
C IF THERE IS NO SLIDING ON THIS LEVEL, CHECK DIAGONAL SPLITTING
C CRITERIA.
C
  ELSE
    CALL SPLIT
C
C IF DIAGONAL SPLITTING FAILURE (FROM SUB SPLIT), RETURN AND STOP
C
  IF (KF .GT. 0) THEN
    RETURN
  ENDIF
ENDIF
C
C IF SLIDING HAPPENS AT THIS POINT, REDIFINE SLIDING START AND END
C POINTS.
C
ELSE
  IF (SLIDST .LT. 0) THEN
    SLIDST = X
    SLIDEN = X

```

```

ELSE
  SLIDEN = X
ENDIF
CALL DRAWCROSS()
ENDIF
RETURN
END

```

```

SUBROUTINE MODEL2(I)

```

```

C _____
C
C THIS SUBROUTIN ANALYSIS THE SHEAR STRESS REDISTRUBITION
C AFTER SLIDING.
C _____
COMMON/BLOCK1/T0,U,YS,XS,TS,X,Y0,H,V,L,P,T,FM,BETA,YSTART,S0,Z0,
*YSTEP,XEND,XSTEP,A,S,X0,X1,SLIDS(40000,3),IS,KF,SEGM,D,
*SDZC(2,2),SUBL
INTEGER XSTEP,YSTEP
REAL L
LOGICAL SLCHANG
C
C DEFINE SLIDING LENGTH
C
X0 = SLIDS(I,2)
IF (SLIDS(I,3) .GT. A) THEN
  X1 = A
  SLIDS(I,3) = A
ELSE
  X1 = SLIDS(I,3)
ENDIF

SLCHANG = .TRUE.
DO WHILE (SLCHANG)
  SLCHANG = .FALSE.
  SM = A**3*T/12.0
  A1 = L - A
  W = V*Y0 - P*A1/2.0
C
C CALCULATE THE LOAD RESISTED BY SLIDING PART
C
IF (X1 .EQ. A) THEN
  YS0 = P/(A*T) + (W/SM) * (A/2 - X0)
  SUBV = T*U*YS0*(A - X0)/2
ELSE
  SUBV = U * T * ((X1-X0)*(P/(A*T)+W*A/(SM*2))-
* W*(X1*X1-X0*X0)/(2*SM))

```

```

      ENDIF
C
C REDISTRIBUTE SHEAR STRESS
C
      V1 = V - SUBV
      X = 0.0
      XEND = A
      SLIDENOLD = X1
      DO WHILE (X .LE. A .AND. .NOT. SLCHANG)
      YS = P/(A*T) + (W/SM)*(A/2-X)
      IF (A .LT. L) THEN
        B1 = 4.0*S*V - 5.0*P*S*S/3.0 + 6.0*S*S*W/A
        B2 = 6.0*S*(V-P*S/2.0)/A + 12.0*S*S*W/(A*A)
        XS = (X*X*B1/2.0-(X**3)*B2/3.0)/(2.0*SM)
        IF (XS .LT. 0) THEN
          XS = 0
        ENDIF
      ELSE
        XS = 0
      ENDIF
C
C IF END SLIDING POINT IS EDGE POINT, SHEAR STRESS DISTRIBUTED IN
C STRAIGHT LINE
C
      IF (X .GE. X0 .AND. X .LE. X1) THEN
        IF (X1 .EQ. A) THEN
          TS = U*YS0 - U*YS0*(X - X0)/(X1 - X0)
        ELSE
C
C FOR SLIDING PART, SHEAR STRESS EQUAL TO FRICTION COMPONENT
C
          TS = U*YS
        ENDIF
        IF (TS .LT. 0) THEN
          TS = 0.0
        ENDIF
      ELSE IF (A .LT. L) THEN
C
C FOR UNSLIDING PART, SHEAR STRESS DISTRIBUTED AS BEFORE
C
        B = V1*A + 2.0*W*S - P*S*A/3.0
        C = V1 - P*S/2.0 + 3.0*S*W/A
        TS = (X*B-X**2*C)/(2*SM)
        IF (TS .LT. 0) THEN
          TS = 0.0
        ENDIF
      ENDIF

```

```

      ELSE
      TS = V1*((L/2)**2 - (X-L/2)**2)/(2*SM)
      ENDIF
C
C CHECK IF CONTINUE SLIDING
C
      CALL CHECK2 (SLCHANG, SLIDENOLD,I)
      IF (KF .GT. 0) THEN
      RETURN
      ENDIF
      X = X + XSTEP
      END DO
END DO
RETURN
END

SUBROUTINE CHECK2(SLCHANG, SLIDENOLD,I)
C
C
C THIS SUBROUTINE CHECK FURTHER SLIDING AFTER SHEAR STRESS
C REDISTRIBUTION.
C
COMMON/BLOCK1/T0,U,YS,XS,TS,X,Y0,H,V,L,P,T,FM,BETA,YSTART,S0,Z0,
*YSTEP,XEND,XSTEP,A,S,SLIDST,SLIDEN,SLIDS(40000,3),IS,KF,SEGM,D,
*SDZC(2,2),SUBL
INTEGER XSTEP,YSTEP
REAL L
LOGICAL SLCHANG
C
C CHECK SLIDING CRITERIA
C
      SLIPF = (T0+U*YS)
      TS1 = TS
      IF (TS1 .LT. SLIPF .OR. YS .LT. 0) THEN
      IF (SLIDENOLD .LT. SLIDEN)THEN
      SLCHANG = .TRUE.
      ELSE
C
C IF NO CONTINUE SLIDING CHECK DIAGONAL COMPRESSION
C
      CALL SPLIT
      IF (KF .GT. 0) THEN
      RETURN
      ENDIF
      ENDIF

```

```

ELSE IF (X .LE. XSTEP) THEN
  KF = 1
  CALL DRAWCROSS()
  PRINT *, 'SLIDING FAILURE'
  WRITE (6,10)
  TAU = V/(L*T)
  WRITE (6,20)V,X,Y0,TAU,SEGM,D
10  FORMAT (4X,'VMAX',12X,'X',12X,'Y',10X,'TAU',10X,'SEGM',5X,'D')
20  FORMAT (1X,6F12.4)
  RETURN
C
C IF CONTINUE SLIDING BUT NOT PROPGRATE TO THE EDGE OF THE WALL
C
ELSE IF (X .LT. SLIDST) THEN
  SLIDST = X
  SLIDS (1,2) = X
  SLCHANG = .TRUE.
  CALL DRAWCROSS()
  CALL SPLIT
  IF (KF .GT. 0) THEN
    RETURN
  ENDIF
ELSE IF (X .GT. SLIDEN)THEN
  SLIDEN = X
  SLIDS (1,3) = X
  CALL DRAWCROSS()
  CALL SPLIT
  IF (KF .GT. 0) THEN
    RETURN
  ENDIF
ENDIF
RETURN
END

```

SUBROUTINE SPLIT

```

C _____
C
C THIS SUBROUTINE CHECK THE DIAGONAL SPLITTING FAILURE
C CRITERIA.
C _____
COMMON/BLOCK1/T0,U,YS,XS,TS,X,Y,H,V,L,P,T,FM,BETA,YSTART,S0,Z0,
*YSTEP,XEND,XSTEP,A,S,SLIDST,SLIDEN,SLIDS(40000,3),IS,KF,SEGM,D,
*SDZC(2,2),SUBL
INTEGER XSTEP,YSTEP
REAL L

```

C

C CHECK DIAGONAL SPLITTING FAILURE CRITERIA

C

CM = (1-BETA)*FM

IF (YS .LT. CM) RETURN

CL = TS*TS

CR1 = (FM - YS)*(BETA*FM - XS)

IF (CL .LE. CR1 .OR. Y .EQ. H) THEN

RETURN

ELSE IF (X .EQ. 0.0 .AND. YS .GE. FM) THEN

KF = 1

CALL PLOT CIRCLE()

PRINT *, 'TOE CRUSHION'

WRITE (6,10)

TAU = V/(L*T)

WRITE (6,20) V,X,Y,TAU,SEGM,D

ELSE

KF = 1

CALL PLOT CIRCLE()

PRINT *, 'DIAGONAL SPLITTING FAILURE'

WRITE (6,10)

TAU = V/(L*T)

WRITE (6,20) V,X,Y,TAU,SEGM,D

10 FORMAT (4X,'VMAX',12X,'X',12X,'Y',10X,'TAU',10X,'SEGM',5X,'D')

20 FORMAT (1X,6F12.4)

RETURN

ENDIF

RETURN

END

SUBROUTINE SHEARD

C

C

C CHECK SHEAR DIAGONAL TENSION FAILURES

C

COMMON/BLOCK1/T0,U,YS,XS,TS,X,Y,H,V,L,P,T,FM,BETA,YSTART,S0,Z0,

*YSTEP,XEND,XSTEP,A,S,SLIDST,SLIDEN,SLIDS(40000.3),IS,KF,SEGM,D,

*SDZC(2.2),SUBL

INTEGER XSTEP,YSTEP

REAL L,LH

C

C CHECK SHEAR DIAGONAL TENSION FAILURE

C

C KF = -2, DIAGONAL SPLITTING FAILURE

C

IF (Y .EQ. H) RETURN

```
LH = -(XS + YS)/2.0 + SQRT((XS - YS)*(XS - YS)/4.0 + TS*TS)
```

```
RH = S0
```

```
IF (LH .GT. RH) THEN
```

```
C
```

```
C SPLITTING FAILURE ANGLE SHOULD BE AROUND 20 TO 70 DEGREES
```

```
C
```

```
XY = ABS(XS - YS)
```

```
IF (XY .LT. 0.0001) RETURN
```

```
IF (YS .LT. 0) THEN
```

```
ANGLE = 2 * TS / (XS - YS)
```

```
ELSE
```

```
ANGLE = 2 * TS / (YS - XS)
```

```
END IF
```

```
ANGLE = ATAN(ANGLE) * 180.0 / (3.1415629 * 2.0)
```

```
ANGLE = ABS(ANGLE)
```

```
IF (ANGLE .GE. 20 .AND. ANGLE .LE. 70) THEN
```

```
CALL PLOTSQUARE()
```

```
IF (SDZC(1,1) .EQ. 0.0) THEN
```

```
SDZC(1,1) = X
```

```
SDZC(1,2) = Y
```

```
SDZC(2,1) = ANGLE
```

```
KF = -2
```

```
ELSE
```

```
SA = TAN(SDZC(2,1) * 3.1415629 / 180.0)
```

```
DSO = SDZC(1,1) + (SDZC(1,2) - H) / SA
```

```
SA = TAN(ANGLE * 3.1415629 / 180.0)
```

```
DSN = X + (Y - H) / SA
```

```
IF (DSN .LT. DSO) THEN
```

```
SDZC(1,1) = X
```

```
SDZC(1,2) = Y
```

```
SDZC(2,1) = ANGLE
```

```
KF = -2
```

```
END IF
```

```
END IF
```

```
END IF
```

```
END IF
```

```
RETURN
```

```
END
```

```
C ADDITIONAL FUNCTIONS FOR PLOTTING DEFINED BELOW
```

```
LOGICAL FUNCTION FOURCOLORS()
```

```
INCLUDE 'FGRAPH.FD'
```

```
INTEGER XWIDTH, YHEIGHT, DUMMY,X0,Y0,XPLUS,YPLUS
```

```
RECORD /VIDEOCONFIG/ SCREEN
```

```

COMMON/BLOCK2/SCREEN,XWIDTH,YHEIGHT,X0,Y0,XPLUS,YPLUS
C
C SET TO MAXIMUM NUMBER OF AVAILABLE COLORS.
C
CALL GETVIDEOCONFIG( SCREEN )
SELECT CASE( SCREEN.ADAPTER )
CASE( $CGA, $OCGA )
DUMMY = SETVIDEOMODE( $MRES4COLOR )
CASE( $EGA, $OEGA )
DUMMY = SETVIDEOMODE( $ERESCOLOR )
CASE( $VGA, $OVGA )
DUMMY = SETVIDEOMODE( $VRES16COLOR )
CASE DEFAULT
DUMMY = 0
END SELECT

CALL GETVIDEOCONFIG( SCREEN )
FOURCOLORS = .TRUE.
IF( DUMMY .EQ. 0 ) FOURCOLORS = .FALSE.
END

C THIS SUBROUTINE PLOTS THE GRID OF THE WALL

SUBROUTINE GRIDSHAPE()

INCLUDE 'FGRAPH.FD'

COMMON/BLOCK1/T0,U,YS,XS,TS,X,Y,H,V,L,P,T,FM,BETA,YSTART,S0,Z0,
*YSTEP,XEND,XSTEP,A,S,SLIDST,SLIDEN,SLIDS(40000.3),IS,KF,SEGM,D,
*SDZC(2,2),SUBL
INTEGER XSTEP,YSTEP
REAL L

RECORD /VIDEOCONFIG/ SCREEN
COMMON/BLOCK2/SCREEN,XWIDTH,YHEIGHT,X0,Y0,XPLUS,YPLUS

INTEGER NUML,NUMH,XL,YH,YHALF,XHALF,
* XPLUS, YPLUS,XC,YC,J,X0,Y0,
* XWIDTH, YHEIGHT, DUMMY
RECORD /WXYCOORD/ WXY
C
DUMMY = SETCOLOR( 7 )
NUML = INT(L)
NUMH = INT(H)
R1 = (XWIDTH * 1.0) / (YHEIGHT * 1.0)
R2 = L / H
IF (R1 .LE. R2) THEN

```

```

        XL = XWIDTH - 40
        RATIO = XL / NUML
        YH = NUMH * RATIO
    ELSE
        YH = YHEIGHT - 80
        RATIO = YH / NUMH
        XL = NUML * RATIO
    END IF
C
C   PLOT THE GRID
C
    XPLUS = XSTEP * RATIO
    YPLUS = IABS(YSTEP) * RATIO
    J = NUML / XSTEP + 1
    K = NUMH / IABS(YSTEP) + 1
    XL = XPLUS * (J - 1)
    XHALF = XL / 2
    YH = YPLUS * (K - 1)
    YHALF = YH / 2
    X0 = XWIDTH / 2 - XHALF
    XC = X0 - XPLUS
    DO I = 1, J
        XC = XC + XPLUS
        DUMMY = SETCOLOR(7)
        CALL MOVETO_W(XC, YHEIGHT / 2 - YHALF, WXY)
        DUMMY = LINETO_W(XC, YHEIGHT / 2 + YHALF)
    END DO
    Y0 = YHEIGHT / 2 - YHALF
    YC = Y0 - YPLUS
    DO I = 1, K
        YC = YC + YPLUS
        DUMMY = SETCOLOR(7)
        CALL MOVETO_W(XWIDTH / 2 - XHALF, YC, WXY)
        DUMMY = LINETO_W(XWIDTH / 2 + XHALF, YC)
    END DO
END

SUBROUTINE DRAWCROSS()
INCLUDE 'FGRAPH.FD'

COMMON/BLOCK1/T0,U,YS,XS,TS,X,Y,H,V,L,P,T,FM,BETA,YSTART,S0,Z0,
*YSTEP,XEND,XSTEP,A,S,SLIDST,SLIDEN,SLIDS(40000,3),IS,KF,SEGM,D,
*SDZC(2,2),SUBL
INTEGER XSTEP,YSTEP
REAL L

```

```

RECORD /VIDEOCONFIG/ SCREEN
COMMON/BLOCK2/SCREEN,XWIDTH,YHEIGHT,X0,Y0,XPLUS,YPLUS

```

```

INTEGER DUMMY,XWIDTH,YHEIGHT, XC, YC,X0,Y0,XPLUS,YPLUS

```

```

C

```

```

C DRAW CROSS.

```

```

C

```

```

DUMMY = SETCOLOR( 14 )
XC = X0 + INT(X) * XPLUS / XSTEP - 3
I = Y0 + INT(Y) * YPLUS / IABS(YSTEP) - 3
J = Y0 + INT(Y) * YPLUS / IABS(YSTEP) + 3
DO YC = I, J

```

```

    DUMMY = SETPIXEL( XC, YC )

```

```

    XC = XC + 1

```

```

END DO

```

```

XC = X0 + INT(X) * XPLUS / XSTEP - 3

```

```

I = Y0 + INT(Y) * YPLUS / IABS(YSTEP) + 3

```

```

J = Y0 + INT(Y) * YPLUS / IABS(YSTEP) - 3

```

```

DO YC = I, J, -1

```

```

    DUMMY = SETPIXEL( XC, YC )

```

```

    XC = XC + 1

```

```

END DO

```

```

END

```

```

C

```

```

SUBROUTINE PLOTSQUARE()

```

```

INCLUDE 'FGRAPH.FD'

```

```

COMMON/BLOCK1/T0,U,YS,XS,TS,X,Y,H,V,L,P,T,FM,BETA,YSTART,S0,Z0,

```

```

*YSTEP,XEND,XSTEP,A,S,SLIDST,SLIDEN,SLIDS(40000,3),IS,KF,SEGM,D,

```

```

*SDZC(2,2),SUBL

```

```

INTEGER XSTEP,YSTEP

```

```

REAL L

```

```

RECORD /VIDEOCONFIG/ SCREEN

```

```

COMMON/BLOCK2/SCREEN,XWIDTH,YHEIGHT,X0,Y0,XPLUS,YPLUS

```

```

INTEGER DUMMY, XWIDTH,YHEIGHT,XC, YC,X0,Y0,XPLUS,YPLUS

```

```

C

```

```

C DRAW SQUARE.

```

```

C

```

```

L DUMMY = SETCOLOR( 10 )

```

```

CALL SETLINESTYLE(-1)

```

```

XC = X0 + INT(X) * XPLUS / XSTEP

```

```

YC = Y0 + INT(Y) * YPLUS / IABS(YSTEP)

```

```

DUMMY = RECTANGLE( $GBORDER, XC - 3, YC - 2, XC + 3, YC + 2 )

```

```

END

```

```

C

```

```

SUBROUTINE PLOTCIRCLE()
INCLUDE 'FGRAPH.FD'

```

```

COMMON/BLOCK1/T0,U,YS,XS,TS,X,Y,H,V,L,P,T,FM,BETA,YSTART,S0,Z0,
*YSTEP,XEND,XSTEP,A,S,SLIDST,SLIDEN,SLIDS(40000,3),IS,KF,SEGM,D,
*SDZC(2,2),SUBL
REAL L

```

```

RECORD /VIDEOCONFIG/ SCREEN
COMMON/BLOCK2/SCREEN,XWIDTH,YHEIGHT,X0,Y0,XPLUS,YPLUS

```

```

INTEGER DUMMY,XWIDTH,YHEIGHT,X0,Y0,XSTEP,YSTEP
INTEGER XC,YC,XPLUS,YPLUS

```

```

C
C DRAW CIRCLE.
C

```

```

DUMMY = SETCOLOR( 12 )
CALL SETLINESTYLE(-1)
XC = X0 + INT(X) * XPLUS / XSTEP
YC = Y0 + INT(Y) * YPLUS / IABS(YSTEP)
DUMMY = ELLIPSE( $GBORDER, XC - 2, YC - 3, XC + 2, YC + 3 )
END

```

```

SUBROUTINE DRAWFD()
INCLUDE 'FGRAPH.FD'

```

```

COMMON/BLOCK1/T0,U,YS,XS,TS,X,Y,H,V,L,P,T,FM,BETA,YSTART,S0,Z0,
*YSTEP,XEND,XSTEP,A,S,SLIDST,SLIDEN,SLIDS(40000,3),IS,KF,SEGM,D,
*SDZC(2,2),SUBL
REAL L

```

```

RECORD /VIDEOCONFIG/ SCREEN
RECORD /WXYCOORD/ WXY
COMMON/BLOCK2/SCREEN,XWIDTH,YHEIGHT,X0,Y0,XPLUS,YPLUS

```

```

INTEGER DUMMY,XWIDTH,YHEIGHT,X0,Y0,XSTEP,YSTEP
INTEGER XC,YC,XPLUS,YPLUS

```

```

C
C DRAW LINE
C

```

```

DUMMY = SETCOLOR( 11 )
CALL SETLINESTYLE( #AA3C )
IF (D .LE. 0) THEN
  DD = 0.0
ELSE
  DD = D
END IF

```

```

XC = INT(X0 + DD * XPLUS / XSTEP)
YC = Y0 + INT(H) * YPLUS / IABS(YSTEP)
CALL MOVETO_W(XC, YC, WXY )
IF (Z0 .LE. 0.0) THEN
  XC = INT(X0 + SUBL * XPLUS / XSTEP)
  YC = Y0
ELSE
  XC = INT(X0 + L * XPLUS / XSTEP)
  YC = Y0 + INT(Z0) * YPLUS / IABS(YSTEP)
END IF
DUMMY = LINETO_W(XC , YC)
END

```

```

SUBROUTINE DRAWLINE(DS,ZS,TMPL)
INCLUDE 'FGRAPH.FD'

```

```

COMMON/BLOCK1/T0,U,YS,XS,TS,X,Y,H,V,L,P,T,FM,BETA,YSTART,S0,Z0,
*YSTEP,XEND,XSTEP,A,S,SLIDST,SLIDEN,SLIDS(40000,3),IS,KF,SEGM,D,
*SDZC(2,2),SUBL
REAL L

```

```

RECORD /VIDEOCONFIG/ SCREEN
RECORD /WXYCOORD/ WXY
COMMON/BLOCK2/SCREEN,XWIDTH,YHEIGHT,X0,Y0,XPLUS,YPLUS

```

```

INTEGER DUMMY,XWIDTH,YHEIGHT,X0,Y0,XSTEP,YSTEP
INTEGER XC,YC,XPLUS,YPLUS

```

C
C
C

```

DRAW LINE

```

```

DUMMY = SETCOLOR( 11 )
CALL SETLINESTYLE( #AA3C )
IF (DS .LE. 0) THEN
  DD = 0.0
ELSE
  DD = DS
END IF
XC = INT(X0 + DD * XPLUS / XSTEP)
YC = Y0 + INT(H) * YPLUS / IABS(YSTEP)
CALL MOVETO_W(XC, YC, WXY )
IF (ZS .LE. 0.0) THEN
  XC = INT(X0 + TMPL * XPLUS / XSTEP)
  YC = Y0
ELSE
  XC = INT(X0 + L * XPLUS / XSTEP)
  YC = Y0 + INT(ZS) * YPLUS / IABS(YSTEP)
END IF

```

```
DUMMY = LINETO_W(XC , YC)  
END
```

```
SUBROUTINE PLOTSIGNAL()  
INCLUDE 'FGRAPH.FD'
```

```
RECORD /VIDEOCONFIG/ SCREEN  
COMMON/BLOCK2/SCREEN,XWIDTH,YHEIGHT,X0,Y0,XPLUS,YPLUS
```

```
INTEGER DUMMY,XWIDTH,YHEIGHT,X0,Y0,XPLUS,YPLUS
```

```
C
```

```
C DRAW CIRCLE.
```

```
C
```

```
DUMMY = SETCOLOR( 15 )
```

```
DUMMY = ELLIPSE( $GFILLINTERIOR, 3, 3, 7, 7 )
```

```
READ (*,*)
```

```
END
```